Process models for the continuous manufacturing of tablets via direct compression

Dissertation

zur

Erlangung des Doktorgrades (Dr. rer. nat.)

der

Mathematisch-Naturwissenschaftlichen Fakultät

der

Rheinischen Friedrich-Wilhelms-Universität Bonn

vorgelegt von

Marius Johannes Kreiser

aus

Rastatt

Bonn 2022

Angefertigt mit Genehmigung der Mathematisch-Naturwissenschaftlichen Fakultät der
Rheinischen Friedrich-Wilhelms-Universität Bonn

Promotionskommission:

Erstgutachter: Prof. Dr. Karl Gerhard Wagner
Zweitgutachter: Prof. Dr. Alf Lamprecht
Fachnahes Mitglied: Prof. Dr. Michael Gütschow
Fachfremdes Mitglied: Prof. Dr. Andreas Schieber

Tag der Promotion: 05.12.2022
Erscheinungsjahr: 2022

Danksagung

Die vorliegende Arbeit entstand im Zeitraum von August 2019 bis Juli 2022 in Kooperation zwischen dem Institut für Pharmazeutische Technologie und Biopharmazie der Rheinischen Friedrich-Wilhelms-Universität Bonn und der Produkt- und Prozessentwicklung der Pfizer Manufacturing Deutschland GmbH, Freiburg. An dieser Stelle richte ich meinen Dank an Hr. Dr. Axel Knoch, Hr. Dr. Clemens Stief und Hr. Dr. Christoph Wabel, die die Kooperation seitens Pfizer ermöglichten.

Besonderer Dank gilt meinem Doktorvater Herrn Prof. Dr. Karl G. Wagner. Vielen Dank für deine Bereitschaft zu dieser Kooperation, die konstruktiven Diskussionen, die geholfen haben, die Masse an generierten Daten sinnvoll zu strukturieren und für die wissenschaftliche Begleitung in den letzten 3 Jahren.
Herrn Prof. Dr. Alf Lamprecht danke ich herzlich für die Übernahme des Zweitgutachtens. Darüber hinaus danke ich Herrn Prof. Dr. Michael Gütschow und Herrn Prof. Dr. Andreas Schieber für die Bereitschaft als Mitglieder der Prüfungskommission zu fungieren.

Herr Dr. Wabel wirkte in den letzten Jahren als mein Betreuer und Mentor bei Pfizer. Vielen Dank für Ihre offene und interessierte Art, sodass wir bereits im Jahr 2014, bei meiner Famulatur, das Thema duale Doktorarbeit anschneiden konnten. An dieser Stelle möchte ich mich für Ihren Einsatz rund um meine Promotion bedanken, sowohl administrativer als auch fachlicher Art. Unser stetiger Austausch über die PCMM hat mir immer wieder neue Denkanstöße und alternative Blickwinkel auf die technologischen Fragestellungen auf den Weg mitgegeben.

Ein weiteres Dankeschön möchte ich meinen Pfizer Kollegen in Freiburg (Andreas Butsky, Yannik Hohenberger, Dominik Jager, Thierry Lemoine, Matthias Danner, Anas Husain und Marcin Pawliczek) zusprechen, die mich fachlich und operativ bei meinen Versuchsansätzen unterstützt haben. Vielen Dank für euer tatkräftiges und engagiertes Zutun bei meinen Versuchen und Analysen. Ihr habt maßgeblich zum Erfolg dieser Arbeit beigetragen. I would also like to thank the Pfizer colleagues in Groton and Sandwich for their constructive discussions about the PCMM and the detailed reviews of my work.

Auch gilt mein Dank meinen ehemaligen Kommilitonen Manuel Bunk und Patrick Knoll, die bereits im Pharmaziestudium immer unterstützend an meiner Seite standen. Vielen Dank für den stetigen Austausch über unseren jeweiligen Promotionsstand im Botanischen Garten.

Zu guter Letzt danke ich meiner Familie. Nur durch euch war mein bisheriger Werdegang möglich. Ihr habt mir immer den Rücken freigehalten und wart jederzeit zur Stelle. Mein besonderer Dank gilt meiner Frau Elina. Du hast mich in den letzten 10 Jahren in allen Lebenslagen begleitet, unterstützt und motiviert. Durch dich weiß ich, dass alles möglich ist!

TABLE OF CONTENT

1 Abbreviations ..... - 1 -

2 Introduction and Theoretical Background ..... - 3 -

2.1 Continuous Manufacturing of Solid Oral Dosage Forms using the “PCMM” ..... - 3 -

3 Aims and Scope ..... - 12 -

4 Materials and Methods ..... - 14 -

4.1 Materials ..... - 14 -

4.2 Tableting ..... - 14 -

4.3 Blend Potency measured by NIR ..... - 15 -

4.4 Freeman Powder Rheometer FT4 ..... - 16 -

4.5 Particle Size Distribution ..... - 18 -

4.6 k-fold Cross-Validation ..... - 18 -

4.7 Software ..... - 19 -

5 A Screening to Evaluate the Impact of Screw Pitch, Refill Level, Top up Volume and Gearbox on the Feed Performance ..... - 21 -

5.1 Introduction ..... - 21 -

5.2 Aims and Scope ..... - 21 -

5.3 Materials ..... - 22 -

5.4 DoE Settings ..... - 22 -

5.5 Results and Discussion ..... - 23 -

5.6 Conclusion ..... - 31 -

6 Developing a Method to Predict the Feed Factor Curve Based on Material Attributes, Screw Pitch and Feeder Throughput ..... - 32 -

6.1 Introduction ..... - 32 -

6.2 Aims and Scope ..... - 32 -

6.3 Materials ..... - 32 -

6.4 Feed Factor Calibration ..... - 33 -

6.5 Results and Discussion ..... - 34 -

6.6 Conclusion ..... - 39 -

7 Impact of Vertical Blender Unit Parameters on Subsequent Process Parameters and Tablet Properties in a Continuous Direct Compression Line ..... - 40 -
7.1 Introduction ..... - 40 -
7.2 Aims and Scope ..... - 40 -
7.3 Materials ..... - 41 -
7.4 DoE Settings ..... - 41 -
7.5 Results and Discussion ..... - 43 -
7.6 Sweet Spot ..... - 69 -
7.7 Conclusion ..... - 70 -
8 Verification of the Derived Process Model Using Alternative Raw Materials ..... - 71 -
8.1 Introduction ..... - 71 -
8.2 Aims and Scope ..... - 72 -
8.3 Materials ..... - 72 -
8.4 DoE Settings ..... - 73 -
8.5 Results and Discussion ..... - 75 -
8.6 Conclusion ..... - 97 -
9 Impact of Impeller Speed, Throughput and Drug Load on Continuous Process Parameters, Material Attributes of the Blend and Blend Uniformity ..... - 99 -
9.1 Introduction ..... - 99 -
9.2 Aims and Scope ..... - 99 -
9.3 Materials ..... - 100 -
9.4 DoE Settings ..... - 100 -
9.5 Results and Discussion ..... - 102 -
9.6 Conclusion ..... - 119 -
10 Development of a Simplified Model Based on Raw Material Densities, Drug Load and Mixing Parameters ..... - 120 -
10.1 Introduction ..... - 120 -
10.2 Aims and Scope ..... - 121 -
10.3 Materials ..... - 121 -
10.4 DoE Settings and Model Building ..... - 121 -

10.5 Results and Discussion ..... - 122 -
10.6 Conclusion ..... - 140 -
11 Summary and Outlook ..... - 142 -
12 Publication ..... - 146 -
13 References ..... - 147 -
A Appendix ..... - 153 -
A.1 Chapter 6 ..... - 153 -
A.2 Chapter 7 ..... - 171 -
A.3 Chapter 10 ..... - 173 -

1 Abbreviations

API	active pharmaceutical ingredient
BCH	bottom main compression height
BFE	basic flow energy
CBD	conditioned bulk density
CM	continuous manufacturing
CMT	continuous mixing technology
Comp	compressibility at 15 kPa (normal stress)
CP	compression pressure
CU	content uniformity
DC	direct compression
DCP	dicalcium phosphate
DL	drug load
DoE	design of experiments
EF	ejection force
Eq.	equation
EV	exit valve opening width
EV SD	exit valve opening width standard deviation
F1	formulation 1
F2	formulation 2
F3	formulation 3
F4	formulation 4
FD	fill depth
FFc	flow function coefficient
FRI	flow rate index
GB	gearbox type
HUM	hold up mass
IMP	impeller speed
LiW	loss in weight
MBM	mass balance model
MCC	microcrystalline cellulose
MgSt	magnesium stearate
MLR	multiple linear regression
MRT	mean residence time
NIR	near infrared
OOS	out of specification

PCMM	portable, continuous, modular & miniature
PID	proportional–integral–derivative
PLS	partial least square
PV	process value
RL	refill level
RMSE	root mean square error
RSD	relative standard deviation
RTD	residence time distribution
ScP	screw pitch
SD	standard deviation
SE	specific energy
SEM	scanning electron microscopy
SI	stability index
SiO_2	colloidal silicon dioxide
SNV	standard normal variate
SP	setpoint
TBP	total blade passes
THR	throughput
T_L	torque lower impeller
T_L SD	torque lower impeller standard deviation
TS	tablet tensile strength
TT	tablet thickness
TU	top up volume
TW	tablet weight

2 Introduction and Theoretical Background

Continuous manufacturing (CM) of solid oral dosage forms has received more and more attention in recent years. Due to the multitude of advantages, a paradigm shift was initiated regarding the CM of tablets. Smaller equipment and fewer process steps increase productivity, enhance efficiency, and reduce the amount of required material in the development stages of a product. An easy scale-up reduces development time, and hence, fast response to market needs can be assured and associated costs can be minimized. Due to the connected process units, more thorough control of the individual process states is enabled, where real-time monitoring, for example, by a soft sensor is already established (Badman and Trout, 2014; Burcham et al., 2018; Cogoni, 2021; Fisher, 2022; Fonteyne et al., 2014; Kamyar, 2021; Lee et al., 2015; Leuenberger, 2001; Roggo et al., 2020). However, a broad understanding of the entire process chain is required to exploit these benefits. That includes the function of the machine itself, the dependencies and relationships between the parameters of each unit and the impact of the material attributes.

2.1 Continuous Manufacturing of Solid Oral Dosage Forms using the “PCMM”

The PCMM (portable, continuous, modular and miniature) installed at the Pfizer sites in Freiburg, Germany and Groton, CT, USA consists of GEA Compact Feeders, a vertical continuous blender (CMT – continuous mixing technology), a MODUL™ P tablet press equipped with an NIR (near infrared) probe installed in the feed frame and an at-line automatic tablet testing system to analyze tablet properties such as thickness, weight and crushing strength (Figure 1). Next to the benefits of continuous manufacturing, the modular setup allows an eased transfer amongst various production sites as the setup could be more easily cloned from the pilot plant or launch site (Blackwood et al., 2019). Besides the machine, the recipe with all the parameter settings is included.

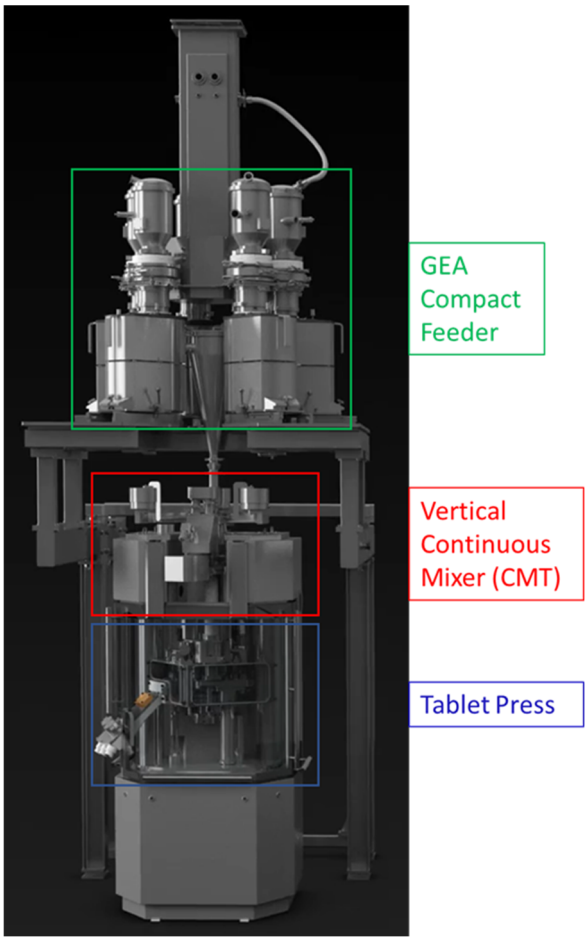

Figure 1 Overview of the direct compression line used for this work.

2.1.1 GEA Compact Feeder

For each raw material, the powder is transferred from a polyethylene bag via a top-up valve into an agitated hopper, where co-rotating screws supply the powder by the loss in weight (LiW) principle at a composition-related feed rate. A proportional–integral–derivative (PID) - control loop is in place to maintain a consistent powder flow. The continuous process demands a periodical hopper refill triggered by a defined refill level, performed by a rotating volumetric refill device with flexible volume inserts (Bostijn et al., 2019; Hsiao et al., 2020; Nowak, 2016). Since feeding is the first step within a continuous process, it is consequently one of the first critical control elements besides the material attributes. Accurate feeding is substantial for the quality of a continuous process to avoid deviations regarding the quality of blend and content uniformity (CU) of the tablets (Engisch and Muzzio, 2015a; Gao et al., 2011a; Hanson, 2018; Tahir et al., 2020; Toson et al., 2018). To provide low variability in feed rate, the optimal feeder design and the corresponding parameter settings such as refill level (RL), top up volume (TU), screw pitch (ScP), feed factor array (governing dosing in volumetric mode during e.g. refill or other disturbances of the weighing cells) and gearbox type (GB) (Figure 2) should be individually adjusted based on composition, throughput and powder attributes. For example,

an incompatible combination of GB, ScP, THR, and material attributes can cause the range of rotation speed of the screws to be too small at the used GB to maintain the feed rate. In this case, the required screw speed cannot be reached to transfer the correct amount of powder because the servo motor within the GB operates at its maximum (Engisch and Muzzio, 2015b, 2015a, 2012; Escotet-Espinoza et al., 2018a; Hopkins, 2006; Nowak, 2016; Tahir et al., 2020; Toson et al., 2018; Wang et al., 2017; Yadav et al., 2019).

Several feeders supply each raw material separately and the powder falls through the conical-shaped inlet hopper into the continuous vertical mixer.

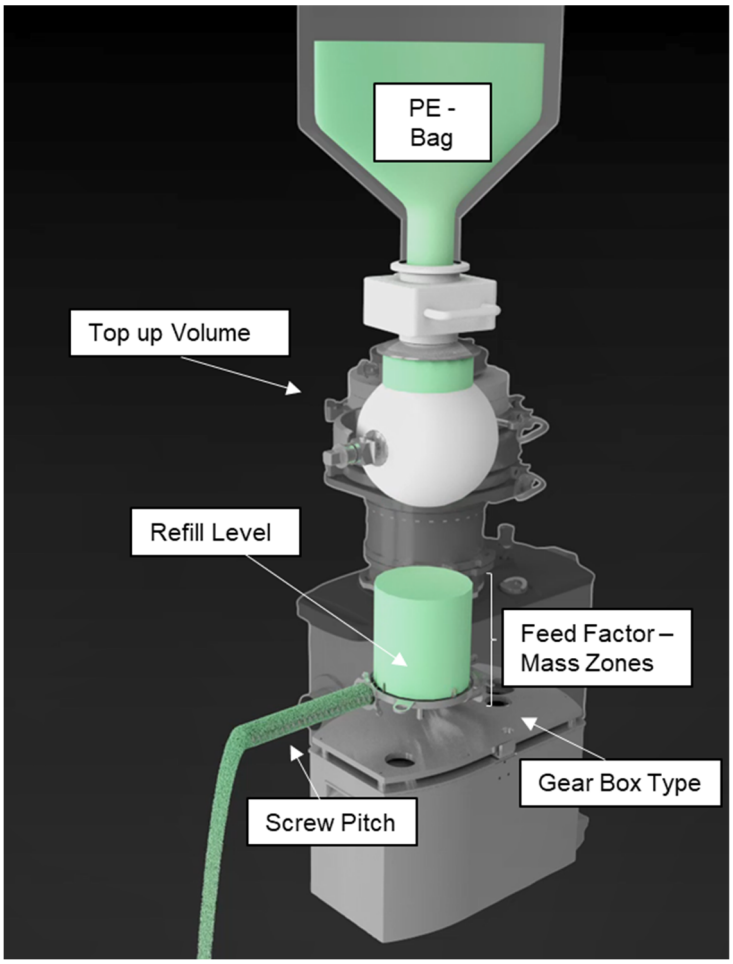

Figure 2 Overview of a GEA Compact Feeder and corresponding adjustment options.

2.1.1.1 **Feed Factor**

The feed factor (FF) is calculated in equation (eq.) (1) and reveals the amount of powder delivered per screw revolution (Tahir et al., 2020). It mainly depends on the screw pitch and the material attributes (Bostijn et al., 2019; Snick, 2017a).

$$FF\ \left[\frac{g}{rev}\right] = \frac{feed\ rate\ \left[\frac{g}{min}\right]}{screw\ speed\ [\mathrm{rpm}]} \tag{1}$$

If the feeder hopper is completely filled, the mass of the powder causes a gradual consolidation of the powder within the hopper. Therefore, the powder at the bottom of the hopper is compacted, dependent on the filling level. This subsequent density gradient within the feeder hopper can hence be reflected in the FF.

The feeder hopper is theoretically split into 10 mass zones. Each zone depends on the mass pressure on top of it and is therefore compacted accordingly so that a corresponding FF can be obtained (Figure 3). The FF in the array is updated in real time as soon as the lower boundary of the mass zone has been crossed. The FFs in the array are used if the system switches from gravimetric mode (LiW) into volumetric mode, e.g. during a refill, when the weighing cells cannot measure precisely anymore, where the screw speed is calculated based on the feed rate set point (SP) and the appropriate FF in the array.

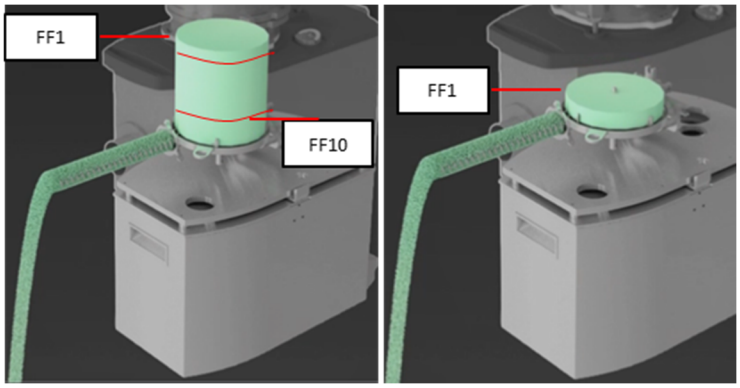

Figure 3 The mass zone of FF10 is more consolidated due to the mass pressure of the powder within the hopper and therefore shows the highest value. Since no further powder in the hopper can consolidate mass zone 1 (FF1), the least amount of powder is delivered per screw revolution.

2.1.1.2 **Feed Factor Calibration**

The feed factor calibration can be carried out to obtain the feed factors used for the FF array in the recipe. Therefore, the corresponding raw material is entirely filled in the feeder hopper. Using a fixed feeder throughput, the screw speed is adjusted automatically according to the material attributes as the hopper empties. The corresponding FF are calculated based on feed rate and screw speed as shown in eq. (1). For the FF array in the recipe, an FF for each mass zone is calculated internally.

2.1.2 **Continuous Mixing Technology**

Unlike other pharmaceutical manufacturers, the PCMM uses a continuous vertical blender. It comprises two regions: the upper delumping and the lower mixing region (Figure 4). In both, the impellers can be adjusted independently regarding speed, direction and vertical position, i.e. the gap between impeller and conical sieve. In the delumping region, a downstream sieve (d = 2.1 mm) is set to delump possible agglomerates. The powder leaves the upper part and

arrives in the conical mixing region, where a second impeller is mounted. The whole setup of the CMT is attached to load cells which monitor the weight of the powder within the mixer. This hold up mass (HUM) is defined in the recipe and determines the mass, which is mixed in the CMT continuously throughout the process.

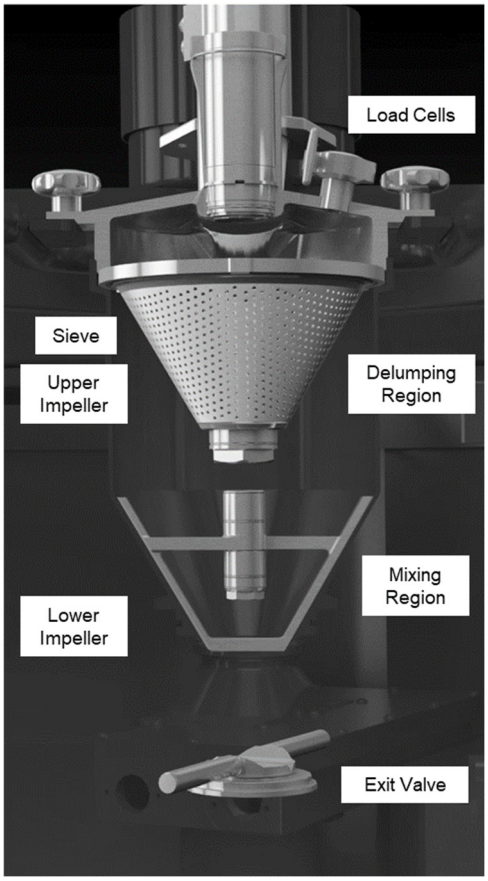

Figure 4 Overview of the CMT. The view of the upper impeller is obstructed by the sieve.

Other researchers focus on a horizontal continuous mixer, where the HUM is considered a function of flow rate and impeller speed and cannot be set individually (Gao et al., 2011b; Marikh et al., 2008). In contrast, the HUM in a continuous vertical mixer remains constant and various shear rates (impeller speeds) can be applied despite a constant residence time distribution (RTD) (Toson et al., 2018). As in this case, the continuous direct compression (DC) line includes only one mixing step for all mixture components, including the lubricant. An impact, especially on lubricant sensitive mixtures as well as on the blend uniformity of the mixture and subsequently content uniformity of the tablets, can be expected (Lee et al., 2021; Mehrotra et al., 2007; Swaminathan and Kildsig, 2002).

The exit valve is located at the bottom of the CMT. Utilizing a PID - control loop, the exit valve opening width is adjusted automatically based on the current HUM value to keep the CMT mass constant. The controlled exit valve ensures that the same amount of mass entering the CMT simultaneously leaves the CMT ($mass_{in}$ = $mass_{out}$). Feed fluctuations of each feeder and the respective variability in the mass flow can be balanced that way. Smaller exit valve opening

widths are recommended so newly entering raw materials can be appropriately mixed with the blend already present in the blender. Otherwise, unmixed or poorly mixed material can pass by and leave the CMT without being blended, causing content uniformity variability (Toson et al., 2018). To control the blend uniformity, the mass balance model (MBM) is used, where data regarding the feed rates of each raw material and the HUM is used to calculate the concentration of each ingredient within the CMT in real-time.

A particle's mean residence time (MRT, eq. (2)) can be calculated based on the overall throughput and the HUM. It reflects the mixing period of that particle within the CMT (Toson et al., 2018).

$$MRT\ [min] = \frac{HUM\ [kg]}{THR\ \left[\frac{kg}{h}\right]} * 60\frac{min}{h} \tag{2}$$

The total blade passes (TBP, eq. (3)) reveal how often the impeller, on average, passes a particle and shows the intensity of the shear transmitted to the powder. With an increasing number of revolutions and increased shear, a lubricant like magnesium stearate (MgSt) can be incorporated to a greater extent into the blend or even filmed onto the particles, potentially resulting in decreasing tensile strength (TS) of tablets.

$$TBP = MRT\ [min] * IMP\ [rpm] \tag{3}$$

Therefore, particular attention is paid to the single mixing step in the CMT, where the lubricant is incorporated right from the start with the remaining raw materials, potentially resulting in a narrow process window between a homogeneous and an overlubricated blend. Hence, it is required to set a suitable combination for HUM and IMP to ensure that TS and disintegration, as well as dissolution time, are within specification (Johansson, 1984; Ketterhagen et al., 2018; Kushner, 2012; Kushner and Moore, 2010; Kushner and Schlack, 2014; Portillo et al., 2008; Wang et al., 2010). Thresholds regarding HUM and IMP are beside the MBM part of the control strategy of the CMT. If the process values (PV) exceed the specific limits, an alarm occurs and the process stops. Furthermore, variations in HUM and IMP could also impact the exit valve opening width and, subsequently, the mixing quality.

2.1.3 **Tablet Press**

After the powder exits the CMT, it travels through the feed chute into the feed frame, where the powder is held up and fed into the Courtoy Tablet Press. Position sensors in the feed chute measure the filling levels. Using an internal feedback loop, the turret speed of the tablet press is controlled according to the filling levels preventing powder from backing up or the tablet press from running empty. An increasing feed chute level increases the tablet press's turret speed, i.e. increased powder demand, and vice versa.

The NIR probe in the feed frame is the first chemometric measurement in the process and, therefore, part of the control strategy. It is essential to understand the impact of upstream settings and process states on the conformity of potency as predicted by the NIR model.
The NIR probe measures a defined volume of the powder. The corresponding spectra are used to predict the active pharmaceutical ingredient (API) content. If inhomogeneity of the blend or variability in the upstream process units occurs, it can consequently be detected by NIR and is seen as a disturbance in the blend potency measured by NIR inside the feed frame (Vanarase et al., 2010).
Depending on the chosen control strategy, the impacted tablets can be diverted into the waste channel if the signals exceed the specification limits. As soon the signals are within specification limits again, the diverter switches back to the good product channel after a defined lead-lag time (De Leersnyder et al., 2018; Peeters et al., 2021; Van Hauwermeiren et al., 2021).
In general, the tablet press runs with a control mode (mode 2: displacement control and dual control force) enabled, where the tablet weight control is based on the pre-compression displacement. For that, the pre-compression roller is set in a guiding position, where an air cushion causes the exerted force. By means of the pre-compression height, the pre-compression rollers are positioned in a way that the displacement (within the air cushion) of the top pre-compression roller is between 0.1 mm and 0.5 mm. Assuming a constant powder density, the tablet weight is equivalent to the amount of powder in the die. I.e., tablet weight is directly proportional to the height of the powder within the die, which is measured by the displacement. Therefore, variations of the die filling can be detected by changes in the displacement and if displacement tolerance limits are exceeded the fill depth (FD) is adjusted, accordingly.
The bottom main compression height (BCH) controls the thickness and compression pressure and, therefore, the crushing strength of the tablets. An internal control loop, namely a force loop, monitors whether the values are within the tolerance limits by measuring the main compression pressure and the main compression height. If the limits exceed these tolerances, the control loop adjusts the bottom main compression height to bring the compression pressure or the thickness of the tablets back within their limits (“GEA Operating and Maintenance Manual for a ‘Modul P,’” 2018). At the end of the tablet press, the tablets can be directed into the good channel, diverted into the waste channel or directed to the automated tablet testing system, where at-line measurements regarding tablet properties can be performed in containment.

2.1.4 **Process Control of the Continuous Direct Compression Line**

As already mentioned in the respective text passages above, the following elements can be monitored or controlled to ensure a robust process. The PCMM utilizes a multi-element integrated control strategy, which means the quality of the drug product is not dependent on any one element, but on many elements working together:

1. Material attributes: If a material property of an ingoing raw material is identified to impact the processing or final drug product quality attributes, a control on the raw material property can be specified. For example, particle size controls are often placed around the ingoing API material. This can allow for more processing consistency batch to batch or can help control downstream drug product quality (ICH, 2009).
2. Feeder process parameters: Maintaining a constant feed rate is achieved by a PID control loop based on the LiW principle for each individual feeder. Feed rate alarm limits are set to ensure the feeder remains at or near target setpoint. For example, some feeder alarm limits control the amplitude of a feed rate deviation for a duration of time the deviation can occur (Blackwood et al., 2019; Meier et al., 2016).
3. Mixer process parameters: To maintain consistent TBP, HUM and IMP should be maintained constant. Therefore, alarm limits for HUM and IMP are defined in the recipe and ensure these process parameters remain at or near target setpoint.
4. Mass balance model: The MBM uses real-time feeding data for each component and convolutes it over an RTD to predict the concentration of each component at the outlet of the CMT. Alarm limits are set on each component to ensure they stay at or near target concentration in the blend (Lee et al., 2021).
5. NIR Controls: A NIR probe measures spectra of the blend in the feed frame. Using internal calculations, the API concentration is predicted based on the wavelength and the intensity of the corresponding spectra. OOS values cause a diversion to the waste channel at the end of the tablet press.
6. Tablet core attributes: To ensure that weight, hardness or thickness meet specification, the tablet cores can be analyzed in containment by the automatic tablet testing system.

2.1.5 **The Transition from Batch to Continuous Manufacturing**

To transfer a process from batch to continuous, it needs to be ensured that all steps of a batch process are adopted. For that, Figure 5 shows the process steps which were considered in the development of the PCMM.

The GEA Compact Feeder includes weighing the material, which ensures a composition-related powder supply, and an optional outlet screen at the end of the barrel to avoid accumulation and bearding of the raw material. This setup replaces the traditional weighing and sieving steps with one feeding unit.

The CMT is composed of two regions, where the upper delumping region is equipped with an impeller and a sieve to deagglomerate powder accumulations and ensure a specific range of particle size within the blender. In the lower region, the actual blending occurs through a conical-shaped hopper design and another impeller. Unlike the batch process, there is only one blending step, where the raw materials and the API are mixed simultaneously with the lubricant. I.e., a sieving and at least two blending steps are combined in the CMT.

To replace numerous HPLC measurements, a NIR probe in the feed frame measures the API content of the blend and the tablets, respectively, in real time.

To avoid additional capacities regarding operators and laboratory equipment, the at-line automated tablet testing system periodically measures the tablets' hardness, thickness, and weight. The data can be obtained considerably faster through the connection to the tablet press.

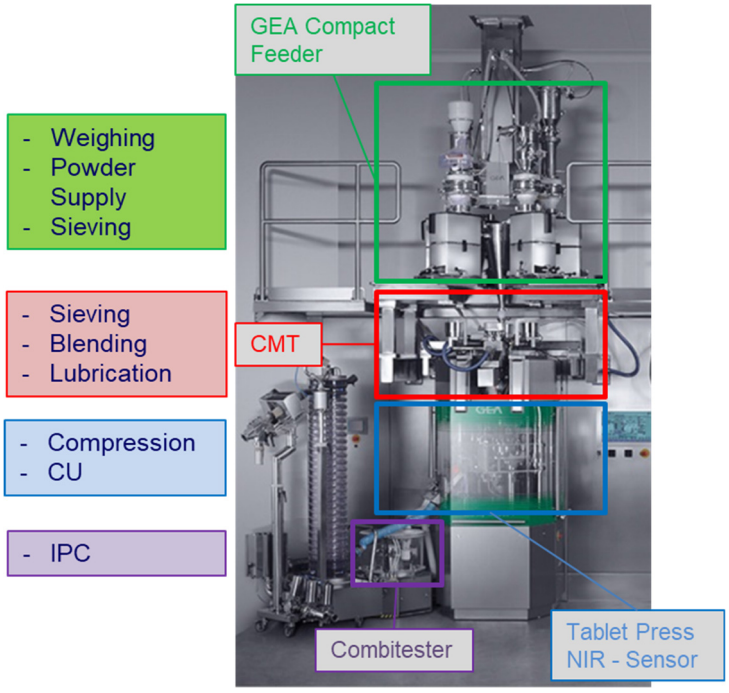

Figure 5 Overview of the batch process steps which are incorporated in the process units of the continuous, direct compression line.

3 Aims and Scope

The CM is a more cost and time-efficient method to produce tablets than the usual batch process (Fisher, 2022). Several manufacturing steps, which require different process rooms and numerous qualified operators and fitters, are combined into one manufacturing line. Therefore, this fusion of process units creates new parameter dependencies that need to be examined in detail. To obtain an overview of process behavior and parameter relationships regarding feeder, vertical blender, tablet press, tablet properties and the set-up which impacts these different process states, this work investigated the following topics:

1. During the development of the appropriate feeder set-up, the correct combination of screw pitch (ScP), gearbox type (GB), top up volume (TU) and refill level (RL) needs to be chosen to ensure a consistent feed rate. Therefore, three designs of experiments (DoE) were carried out to identify the significant parameters to reduce variability in feed rate. Furthermore, the impact on FF, Screw Speed and the corresponding relative standard deviation (RSD) was investigated. To reduce variabilities during a refill, the deviation of feed rate, FF and screw speed before and after a refill was assessed. Moreover, it was evaluated if normalization of FF by ScP is applicable (chapter 5).

2. In a pharmaceutical production, specifications regarding material attributes ensure a consistent powder quality. Nevertheless, the specification latitude allows for lot-to-lot variability, which may impact the process behavior. In this context, density variation likely results in a changed feed factor (FF) curve between two refills, which may affect, for example, the refill strategy. Moreover, the ScP might be switched due to feed performance enhancement, which changes the FF accordingly. To comprehend to what extent the FF curve is influenced by lot-to-lot variability and feeder settings, a method was developed to predict the FF curve during a complete hopper dispensing based on conditioned bulk density (CBD), compressibility (Comp), throughput (THR) and ScP (chapter 6).

3. The vertical blender is the heart of the continuous direct compression line, where HUM and IMP can be individually set. In this context, the overall mass throughput must be considered an additional CMT parameter. Different combinations of the three parameters result in different MRTs and TBP, influence the lubrication of the blend and impact the downstream process parameters. To comprehend the impact of the CMT parameters, a DoE was designed to investigate correlations and connections between the CMT settings and the downstream process and, moreover, between the individual

process states along the continuous process. For this investigation, the DoE was carried out with two different formulations (chapters 7 and 8).

4. During the early stages of development, the final drug load is mostly not yet determined. Therefore, the evaluation of the process window, in which the PCMM can perform appropriately, was performed employing an additional DoE, where THR, IMP and drug load (DL) were set as input parameters. Besides the uniformity of the MBM and potency measured by NIR, the impact on several continuous process parameters could be assessed based on the composition and CMT parameter changes (chapter 9).

5. As the impact of lot-to-lot variability was already investigated in chapter 6, this consideration was expanded from the impact on the FF to the influence on the entire continuous process. Therefore, the data of chapters 7 and 9 were combined and a new model was built. Since the basic formulation was the same and only composition changes were made, a theoretical “input density“ could be calculated. I.e., the impact on the continuous process could be evaluated based on the raw material attributes and the CMT parameters THR, HUM and IMP. Regarding the tensile strength, the compression pressure was used as an additional factor (chapter 10).

4 Materials and Methods

4.1 Materials

Table 1 Overview of the used materials in this work.

Name	Tradename	Supplier
Agglomerated alpha-Lactose Monohydrate	Tablettose® 80	MEGGLE GmbH & Co. KG, Wasserburg, Germany
Dicalcium Phosphate (DCP)	A-Tab®	Innophos, Chicago Heights, IL, USA
Colloidal Silicon Dioxide (SiO_2)	Aerosil ® 200	Evonik Operations GmbH, Essen, Germany
Magnesium stearate (MgSt)	Magnesium Stearate HyQual®	Mallinckrodt Pharmaceuticals, St.Louis, MO, USA
Microcrystalline Cellulose (MCC)	Avicel PH® 102	FMC, Cork, Ireland
Saccharin Sodium Monohydrate	Saccharin Sodium Monohydrate	JMC, Ulsan, South Korea
Sodium Starch Glycolate (SSG)	Glycolys®	Roquette Frères, Lestrem, France
Sodium Stearyl Fumarate (SSF)	PRUV®	JRS Pharma GmbH & Co. KG, Rosenberg, Germany
Spray Dried Mannitol	Pearlitol® 100 SD	Roquette Frères, Lestrem, France
Tricalciumcitrat (TCC)	Tricalciumcitrat TB	Jungbunzlauer GmbH, Ladenburg, Germany

The used formulations are shown in the individual chapters.

4.2 Tableting

A MODUL™ P tablet press (GEA Pharma Systems, Courtoy™, Halle, Belgium) was implemented at the end of the continuous manufacturing line. For the trials in chapters 7, 8, 9 and 10, Mode 2 (displacement control and dual control force) was selected, where the tablet weight control is based on pre-compression displacement measurements, adjusting the fill depth accordingly (Peeters, 2014).
Convex, round tablets with 11 mm diameter and 1.12 mm cup height were manufactured.

The target tablet weight was 600 mg, tablet crushing strength and tablet thickness were tested periodically in the middle of each steady-state using the automated at-line tablet tester, UTS IP65i (Kraemer Elektronik GmbH, Darmstadt, Germany). The feed chute level was controlled to a constant level at 40 % and the paddle speed remained steady at 45 or 40 rpm. Turret speed set-points and speed tolerances of the tablet press were adapted to the respective mass throughputs (11 rpm $\pm$ 2.2 rpm; 21 rpm $\pm$ 4.2 rpm and 32 rpm $\pm$ 6.4 rpm).

4.2.1 **Tensile Strength**

The tensile strength of the convex, round tablets was calculated based on the following equation (Pitt et al., 1988):

$$Tensile\ Strength = \frac{10P_S}{\pi D^2}\left(2.84\frac{t}{D} - 0.126\frac{t}{W} + 3.15\frac{W}{D} + 0.01\right)^{-1} \quad (4)$$

Where P_s=tablet core crushing strength, D=tablet core diameter, t=tablet core thickness and W=cylinder length. Tablet crushing strength was measured using the combitester (see 4.2.2), which is directly connected to the continuous manufacturing line.

4.2.2 **Automated Tablet Testing System**

To analyze tablet properties such as tablet hardness, weight and thickness, the at-line automatic tablet testing system UTS IP65i (Kraemer Elektronik GmbH, Darmstadt, Germany), referred to as combitester in this work, was used, which is directly connected to the PCMM. Tablet samples can be withdrawn automatically in a periodical frequency or manually requested samples can be measured anytime during the process. The combitester was used to measure all tablet properties mentioned in this work.

4.3 **Blend Potency measured by NIR**

To analyze the impact of the CMT settings on the blend potency in chapters 7, 9 and 10, a NIR spectrometer (SentroProbe DR LS NIR 170C ATEX, Sentronic, Germany) was installed in the feed frame with an insertion depth of 1 mm. Using PharmaMV 5.3 (Perceptive Engineering, UK) a spectrum was recorded every 4 seconds. Approximately 150 - 200 mg of the blend was measured during one measurement cycle. The collected data were preprocessed, applying the savitzky golay filter first and then the standard normalize variate method (SNV). After that, the data were processed by a partial least square (PLS) regression model. The integration time was 9 ms, 133 average scans.

4.4 Freeman Powder Rheometer FT4

The FT4 Powder Rheometer (Freeman Technology Inc., Worcestershire, UK) is used to characterize flow properties of powders and granulates. 3 Methods (Stability and Variable Flow Rate, Powder Compressibility and Shear Cell) were used to analyze the raw materials and the impact of CMT parameters on the flowability of the resulting blends.

4.4.1 Stability and Variable Flow Rate

A cylindrical 25 mm x 25 ml split vessel was used. After an initial condition cycle, the powder was split to obtain a defined amount of powder to ensure reproducible measurements. The actual testing consists of seven alternating conditioning and test cycles where the blade is inserted in the powder bed and moved downwards with a rotational blade tip speed of 100 mm/s to remove history and operator influence. Subsequently, 4 cycles with decreasing blade tip speed (100 mm/s, 70 mm/s, 40 mm/s and 10 m/s) were performed. The required energy is based on the resistance of the blade to flow in the downward motion ("Freeman Technology, Instruction documents: W7013 Stability and Variable Flow Rate," 2007). The basic flow energy (BFE) is defined by the required energy to move the blade downwards at test cycle 7. The specific energy (SE) represents the energy that is required during an upwards traverse at the same test cycle. The stability index (SI) is calculated by the ratio of the energy at test cycle 7 and test cycle 1. An SI value = 1 shows that the material is stable. If the SI is higher than 1, more energy is required over time due to possible agglomeration or segregation. If the value is <1 a probable cause can be de-agglomeration or over-blending. The flow rate index (FRI) reflects the results of the reducing blade tip speed, where the energy of the lowest rotational speed and the highest are set in ratio.

$$FRI = \frac{energy\ test\ 11\ \left(10\ \frac{mm}{s}\right)}{energy\ test\ 8\ \left(100\ \frac{mm}{s}\right)} \tag{5}$$

Basically, less energy is required at higher flow rates since the entrained air acts as a lubricant. At lower flow rates, the powder in front of the blades is more likely to be consolidated due to the absence of entrained air and therefore, interlocking of particles is more probable. Consequently, higher FRI values are expected for cohesive powders and FRI values <1 are typical for powders or blends containing lubricants. The conditioned bulk density (CBD) is measured after the initial conditioning cycle and the split of the powder, where agglomerates and air inclusions can be evened to ensure reproducible measurements (Escotet-Espinoza et al., 2018a; Freeman, 2007; "Freeman Technology, Instruction documents: W7012 Variable Flow Rate," 2007, "Freeman Technology, Instruction documents: W7030 Basic Flowability Energy," 2007; Madian et al., 2020). This method was used for raw materials and blends in chapters 5, 7, 8, 9 and 10.

4.4.2 **Powder Compressibility**

The compressibility method is used to investigate how the density of the measured powder changes with increasing normal stress. A split vessel (25 mm x 10 ml) was used in this work. After three conditioning cycles, the powder is split and the blade is changed for a vented piston. In total 8 compression steps were performed (1 kPa, 2 kPa, 4 kPa, 6 kPa, 8 kPa, 10 kPa, 12 kPa, 15 kPa) and were held for 60 seconds at each force. In this work, only compressibility (change in volume after compression [%]) is used. Low compressibility values occur at powders with a low amount of entrained air where particles are packed compactly. High compressibility values are seen if voids within the powder occur. This is likely with cohesive powders (Azad et al., 2019; "Freeman Technology, Instruction documents: W7008 Compressibility," 2007; Llusa et al., 2014; Madian et al., 2020). This method was used for raw materials and blends in all chapters.

4.4.3 **Shear Cell**

A shear cell test was performed using the FT4. For this method, a 25 mm x 10 ml split vessel was used. After 3 conditioning cycles, a vented piston was used to consolidate the powder sample. Then the vented piston was replaced by the shear cell and pre-shearing was performed to over-consolidate the powder until the shear stress τ reached steady-state. Subsequently, the normal stress σ was reduced to the setting according to the shear-cell method. The procedure of pre-shear and actual measurement was repeated for all normal stresses. As normal stress, 7 kPa, 6 kPa, 5 kPa, 4 kPa and 3 kPa were adjusted and the initial consolidation stress was 9 kPa. For this method, a $\tau - \sigma$-diagram can be obtained, where one pre-shear point and five yield points can be observed. Using a Mohr circle analysis, a linearized yield locus can be obtained, where the τ-axis intersection is interpreted as cohesion and presents the obtained shear stress during powder deformation when no normal stress is applied. The Angle of internal Friction (AIF) can be calculated with the slope of the linearized yield locus and shows how easily particles can slide past each another. The Unconfined Yield Stress (UYS) is the intercept of a Mohr circle passing through the origin and the tangent to the yield locus with the σ-axis. The Major Principal Stress (MPS) is the intercept with the σ-axis of another Mohr circle that is passing through the pre-shear point. The flow function coefficient (FFc) can be obtained by the ratio between MPS and UYS and can be interpreted according to Zegzulka et al., as shown in Table 2. (Freeman et al., 2009; Wang et al., 2016; Escotet-Espinoza et al., 2018a; "Freeman Technology, Instruction documents: W7018 Shear Cell," 2007, "Freeman Technology, Instruction documents: W7050 1ml Shear Cell," 2007; Zegzulka, 2020). This method was used for raw materials and blends in chapters 5, 7, 8, 9 and 10.

Table 2 shows the interpretation of the FFc regarding the flowability of the powder.

FFc	Interpretation
FFc < 1	non-flowing
1 < FFc < 2	very cohesive
2 < FFc < 4	cohesive
4 < FFc < 10	easy-flowing
10 < FFc	free-flowing

4.5 Particle Size Distribution

For particle size measurements for chapters 7, 9 and 10, a Sympatec QicPic (Sympatec GmbH, Clausthal-Zellerfeld, Germany) was used. It is a dynamic, high-speed image analysis system with a LED pulse light source and high resolution, high-speed camera. An M7 lens was used, which covers particles between 4.2 µm and 2888 µm. Dispersion pressure was set to 1 bar for all raw materials and blends to maintain comparability. As a dry dispersion line, RODOS/L with VIBRI attachment was in place and the sample size remained constant for each material (5 ml). To determine the particle size, the EQPC method was used, where d_{10}, d_{50} and d_{90} values were obtained. For chapter 8, a Sympatec Helos (Sympatec GmbH, Clausthal-Zellerfeld, Germany) was used. Through the laser diffraction method, the powder samples pass through a laser beam scattering the light. Detectors measured the intensity of the scattered light and calculated the particle sizes. As a dry dispersion line RODOS/L with VIBRI attachment was in place and the sample size remained constant for each material (400 mg $\pm$10 mg). The feed rate was set to 100 mm/s, dispersion pressure was set to 2 bar and an R5 lens was used, covering 4.5 to 875 µm. All samples were measured in triplicate and d_{10}, d_{50} and d_{90} values were obtained.

4.6 k-fold Cross-Validation

A k-fold cross-validation can be used to evaluate the quality of a predictive model. Therefore, the data set is split into k-folds of approximately equal size. To train the model, k-1 data sets are used to build the model and the remaining one is used as a testing set to validate it. This procedure is repeated until each data set is used as either a training or testing set (Berrar, 2019).

In chapter 10, a 5-fold cross-validation was used to evaluate the quality of the obtained models. Therefore, the data set was randomly partitioned into five equally sized subsets for each response.

Using MODDE Pro 12.1 (Sartorius Stedim Data Analytics AB, Umea, Sweden), a model was built with the four training sets for each fold. The obtained models were then applied to the

respective testing sets (Figure 6). To evaluate each model, R^2 and RMSE of the predicted and the observed values were used. R^2 was obtained by GraphPad Prism 9 (GraphPad Software, Inc., USA) and RMSE was calculated according to the following equation where P_i stands for the predicted values from the model, O_i for the observed values in the data set, n for the sample size of the data set and i for the fold (Wang and Lu, 2018):

$$RMSE = \sqrt{\frac{\sum_{i=1}^{n}(P_i - O_i)^2}{n}} \quad (6)$$

To evaluate the performance of the model, average values of R^2 and RMSE values of the training and testing sets were calculated.

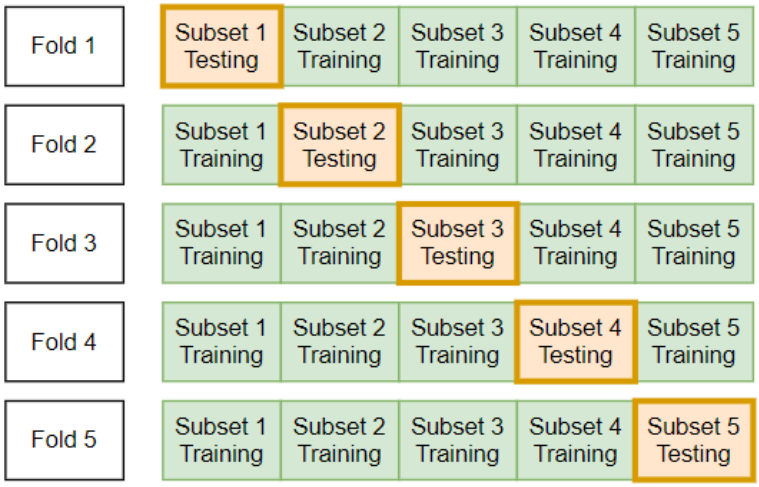

Figure 6 Demonstration of the 5-fold cross-validation. Four subsets of the data were used to build the model for each fold. The remaining subset, the testing set, was used to validate the training set. This was repeated until each subset was used as a testing set.

4.7 **Software**

4.7.1 **MODDE**

The DoEs in this work were designed using MODDE Pro 12.1 (Sartorius Stedim Data Analytics AB, Umea, Sweden). For each analysis, a Multiple Linear Regression (MLR) model was used to evaluate the significance of input factors on the responses, which were identifiable when error bars (= 95% confidence interval) did not cross the zero line. Otherwise, these model terms were non-significant. In this work, models with $Q^2 > 0.500$ (=estimate of prediction precision) and $R^2 \geq 0.800$ (=model fit) were considered suitable models, indicating a significant correlation between input variables and responses. The corresponding fit statistics are shown in the individual chapters.

For visualization, plots were built, where effects (chapter 10) and coefficients (chapters 5, 6, 7, 8 and 9) are displayed. Furthermore, MODDE was used to obtain model equations to predict the responses and the corresponding Q^2 and R^2 to evaluate the model performance.

4.7.2 **OSIsoft Pi**

A considerable benefit of the PCMM is the implementation of OsiPi (OSIsoft, San Leandro, California, USA), which enables access to all essential process values. All data generated by the PCMM are continuously monitored and stored using OsiPi. Pi Vision is a web-based tool where process data can be visualized in real-time. Since the process data are stored in the PI Server, PiVision also visualizes previous batches if process states need to be evaluated retrospectively. All process-related data were gathered using PiDataLink, an Add-in to Excel (Microsoft Corporation, USA) that enables importing data from the PI Server.

4.7.3 **GraphPad Prism**

GraphPad Prism 9 (GraphPad Software, Inc., USA) was used to generate the figures and to calculate the correlations (Pearson correlations) between the process parameters, including the p-values. Furthermore, the linear and non-linear regressions in chapter 6 were carried out by GraphPad Prism. For the cross-validation (chapter 10), R^2 values of the predicted and observed values were calculated by the linear regression using GraphPad Prism. To evaluate the size of the correlation, the following rule of thumb is used:

Table 3 Interpretation of Pearson correlation coefficients (Mukaka, 2012).

Correlation Coefficient	**Interpretation**
0.9 to 1.0 (- 0.9 to - 1.0)	very high correlation
0.7 to 0.9 (- 0.7 to - 0.9)	high correlation
0.5 to 0.7 (- 0.5 to - 0.7)	moderate correlation
0.3 to 0.5 (- 0.3 to - 0.5)	low correlation
0.0 to 0.3 (- 0.0 to - 0.3)	negligible correlation

5 A Screening to Evaluate the Impact of Screw Pitch, Refill Level, Top up Volume and Gearbox on the Feed Performance

5.1 Introduction

It is widely known that accurate feeding is substantial for the quality of a continuous process. So, deviations regarding the quality of blend and content uniformity of the tablets can be minimized (Engisch and Muzzio, 2015a; Hanson, 2018; Tahir et al., 2020; Toson et al., 2018). Since feeding is the first step within a continuous process, it is subsequently one of the first control elements which is crucial to focus on. Hence, numerous authors have already worked on the optimization of feeding processes. E.g. some papers focused on methods to evaluate the feed performance (Engisch and Muzzio, 2015b, 2012), on powder characterizations (Escotet-Espinoza et al., 2018b; Wang et al., 2017), on feed factors and screw speed (Nowak, 2016; Tahir et al., 2020) and the impact of hopper fill levels on the feed performance (Engisch and Muzzio, 2015a; Nowak, 2016; Tahir et al., 2020).

Hopkins addressed the potential risk that density deviations occur due to compression of powder at the lower parts of the hopper due to mass pressure (Hopkins, 2006). On the other hand, densities at the upper parts can be considered lower, resulting in a huge density gradient within the feeder hopper. Hence, at lower hopper fill levels, the feed factors decrease, which causes feed deviations due to the compensation with higher screw speeds. As Nowak (Nowak, 2016) mentioned, if screw speeds increase prior to the refill and the system switches into the volumetric mode, the screws may overfeed when switching back to gravimetric mode, resulting in feed rate peaks.

Since feeding during volumetric mode is considered one of the most challenging occasions regarding feeding (Hopkins, 2006), a potential improvement could be optimizing the refill level to bring screw speed and corresponding feed factors immediately before and after a refill more into line. Bostijn et al. suggested using the FF_{decay}, where the FF reaches 90% of the FF_{max},to consider the refill strategy (Bostijn et al., 2019).

For this trial, the modularity was used to focus on the feed performance only, where the CMT just acted like a funnel and the tablet press was not installed. So, basically, the powder was transferred from a Flecozip PE bag via a top up valve into an agitated Hopper, where co-rotating screws in the determined composition supplied the powder according to LiW-principle.

5.2 Aims and Scope

This screening aimed to gain a basic understanding of how the feed performance can be improved based on the feeder setting. Therefore, a DoE was designed, including screw pitch (ScP), refill level (RL), top up volume (TU), and gearbox type (GB) as the input factors.

5.3 **Materials**

For these trials, sodium starch glycolate (Roquette, Lestrem, France), dicalcium phosphate (A-Tab, Innophos, Chicago Heights, IL, USA) and microcrystalline cellulose (Avicel PH 102, FMC, Cork, Ireland) were used. For each raw material, a separate DoE was carried out. Corresponding material attributes are shown in Table 5.

5.4 **DoE Settings**

For this screening, a 2-level, full factorial interaction model was designed, fitted by MLR and is referred to as DoE 1. The same design was carried out for each raw material to compare the results. Based on experiences, for each raw material, the high and low values for the refill levels were adapted to a processable setting (SSG: 0.2 L and 0.5 L, DCP: 0,2 L and 0,35 L, MCC: 0.35 L and 0.5 L). The feeder throughput was set to 5 kg/h. Since feeding difficulties occurred at 10 mm/rev ScP during the MCC runs, the MCC feed rate was reduced from 5 kg/h to 3.5 kg/h.

Table 4 DoE Settings for SSG, DCP and MCC. The refill levels were adjusted individually.

Phase	**Screw Pitch [mm/rev]**	**Refill Level [L]**	**Top Up Volume [L]**	**Gearbox [Type]**
1	10	high	0.8	63
2	10	high	0.8	235
3	20	high	1.6	63
4	20	high	1.6	235
5	10	low	0.8	63
6	10	low	0.8	235
7	20	low	1.6	63
8	20	low	1.6	235
9	10	low	1.6	63
10	10	low	1.6	235
11	20	low	0.8	63
12	20	low	0.8	235
13	10	high	1.6	63
14	10	high	1.6	235
15	20	high	0.8	63
16	20	high	0.8	235

5.5 **Results and Discussion**

The DoEs reveal the impact of the feeder settings ScP, RL, TU and GB on the feed performance. Therefore, feed rate RSD, FF, FF RSD, screw speed and screw speed RSD were assessed. To estimate the performance during a refill, the deviations of feed rate, FF and screw speed values before and after a refill were analyzed. Furthermore, a normalization of the FF was examined, where FF values were divided by the corresponding ScP.

Table 5 Material attributes obtained by the FT4.

	CBD* **[g/ml]**	**FRI***	**Comp**** **[%]**	**Cohesion***** **[kP]**	**FFc*****
SSG	0.784±0.001	1.01±0.07	6.34±0.08	0.15±0.05	29.8±12.00
DCP	0.730±0.058	1.34±0.02	4.28±0.18	1.48±0.24	3.4±0.66
MCC	0.342±0.005	1.16±0.25	13.07±0.25	1.09±0.26	4.6±0.87

*Obtained by the stability and variable flow rate method.

**Obtained by the compressibility method.

***Obtained by the shear cell.

5.5.1 **Feed Rate RSD**

Since feeding is the first step within a continuous process, the uniformity of the feed rate is substantial for the subsequent process (Engisch and Muzzio, 2015a; Gao et al., 2011a; Hanson, 2018; Tahir et al., 2020; Toson et al., 2018). To evaluate which setting can improve the feed performance, Figure 7 shows the model terms.

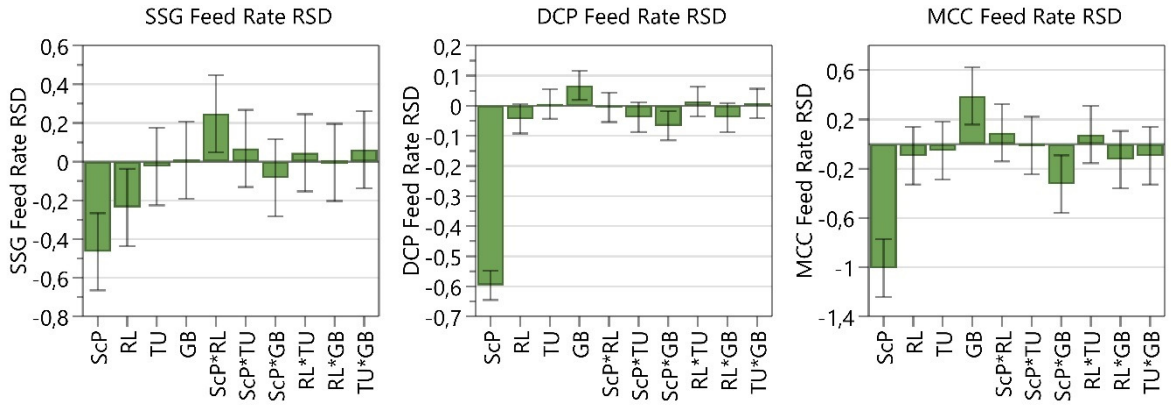

Figure 7 Coefficients plot of model terms regarding the feed rate RSD. The 95 % confidence interval is displayed as an error bar.

The mutual model term for all materials was the screw pitch, where the 20 mm screw pitches resulted in significantly lower feed rate RSD values. Furthermore, for SSG and DCP, RL can be considered significant, where higher RL resulted in lower feed rate RSDs. This could be explained by the higher density of SSG and DCP compared to MCC. At the same refill volume,

the weight of refilled material for SSG and DCP was higher, resulting in a more consolidated powder bed (Engisch and Muzzio, 2015a). For MCC, that means that even for higher RL, the mass pressure within the hopper was insufficient to provide a uniformly consolidated powder bed, which caused a slight deviation between feed factors before and after a refill (see also section 5.5.6). For DCP and MCC, the gearbox type 2 (1:235) led to higher RSD values.
After removing non-significant model terms, Table 6 shows the fit statistics:

Table 6 Fit statistics for SSG, DCP and MCC regarding the impact of the input parameters on the feed rate RSD.

Raw Material	Data transformation	Q^2	R^2	Adjusted R^2
SSG	-	0.775	0.873	0.842
DCP	-	0.978	0.994	0.989
MCC	-	0.873	0.950	0.926

5.5.2 **Feed Factor**

The FF is calculated as shown in equation (1) and reveals the amount of powder delivered per screw revolution (Tahir et al., 2020). To evaluate the impact of ScP, RL, TU and GB on the feed factor, Figure 8 shows the model terms.

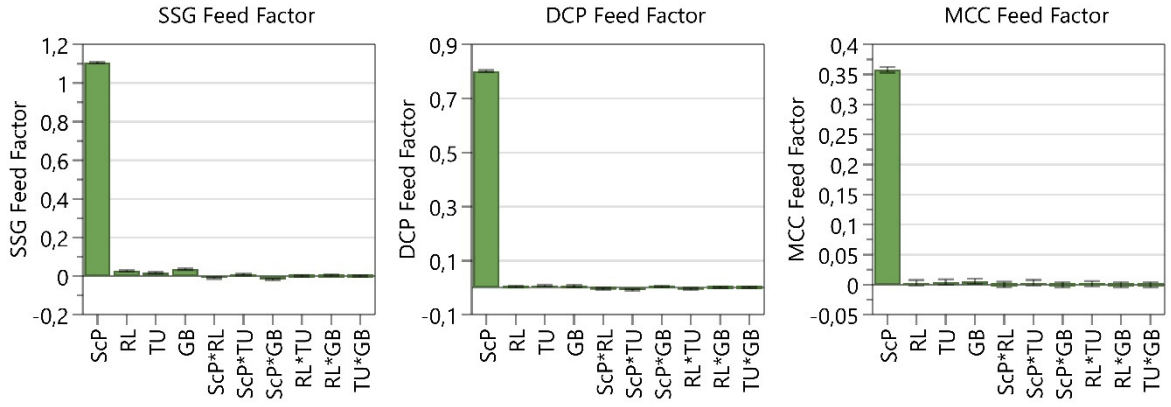

Figure 8 Coefficients plot of model terms regarding the FF. The 95 % confidence interval is displayed as an error bar.

Obviously, ScP showed the highest impact on the FF for all materials by far. A comparatively small impact could still be seen for RL, TU and GB, which could be considered negligible compared to ScP. Table 7 shows the fit statistics.

Table 7 Fit statistics for SSG, DCP and MCC regarding the impact of the input parameters on the feed factors.

Raw Material	Data transformation	Q^2	R^2	Adjusted R^2
SSG	-	1.000	1.000	1.000
DCP	-	1.000	1.000	1.000
MCC	-	1.000	1.000	1.000

5.5.3 **Feed Factor RSD**

Since the FF express the delivered amount of powder per screw revolution, variability in this value implies variability in the consolidation states within the powder in the feed hopper (Abdullah and Geldart, 1999; Engisch and Muzzio, 2015a). To minimize this variability Figure 9 displays the model terms.

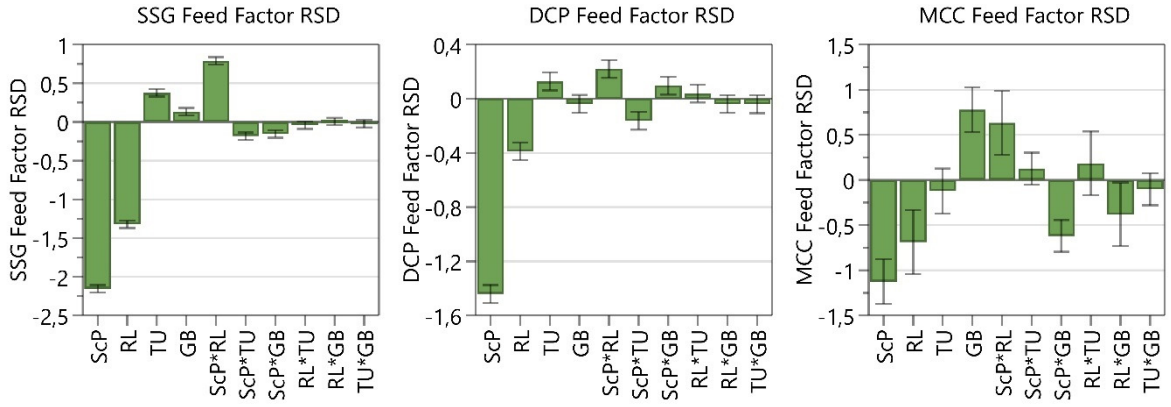

Figure 9 Coefficients plot of model terms regarding the FF RSD. The 95 % confidence interval is displayed as an error bar.

All materials' mutual significant model terms were ScP, RL, ScP*RL, ScP*TU and ScP*GB. Additionally, GB impacted the FF RSD significantly for SSG and MCC and TU influenced SSG and DCP. So, the variability of the FF can be minimized if the consolidation state of the powder within the feeder hopper is maintained relatively constant, which can be achieved with higher RLs and, with denser powders, at lower TUs. Furthermore, higher screw pitches provide more material that is delivered more uniformly per screw revolution.

After removing non-significant model terms, Table 8 shows the fit statistics:

Table 8 Fit statistics for SSG, DCP and MCC regarding the impact of the input parameters on the feed factor RSD.

Raw Material	Data transformation	Q^2	R^2	Adjusted R^2
SSG	-	0.998	1.000	0.999
DCP	-	0.986	0.997	0.994
MCC	-	0.869	0.975	0.946

5.5.4 **Screw Speed**

The screw speed is adjusted according to the PID control loop, which is based on the LiW principle to maintain the feed rate. The impact of ScP, RL, TU and GB on the screw speed is shown in Figure 10.

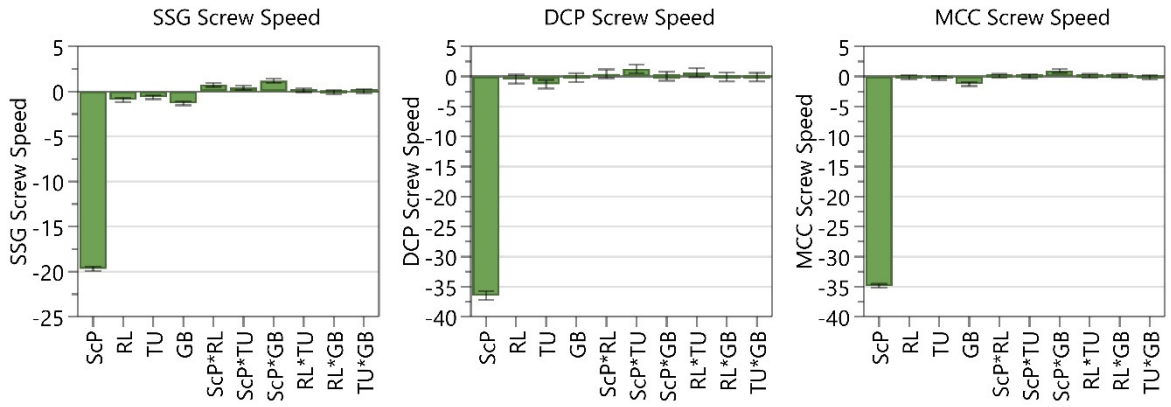

Figure 10 Coefficients plot of model terms regarding the screw speed. The 95 % confidence interval is displayed as an error bar.

Compared to the FF (section 5.5.2), ScP showed the highest impact on the screw speed for all materials, whereas the remaining input parameters can be considered negligible.
After removing non-significant model terms, Table 9 shows the fit statistics:

Table 9 Fit statistics for SSG, DCP and MCC regarding the impact of the input parameters on the screw speed.

Raw Material	Data transformation	Q^2	R^2	Adjusted R^2
SSG	-	0.999	1.000	1.000
DCP	-	0.999	1.000	0.999
MCC	-	1.000	1.000	1.000

5.5.5 **Screw Speed RSD**

To evaluate the impact of the feeder settings on the uniformity of the screw speed, Figure 11 displays the model terms.

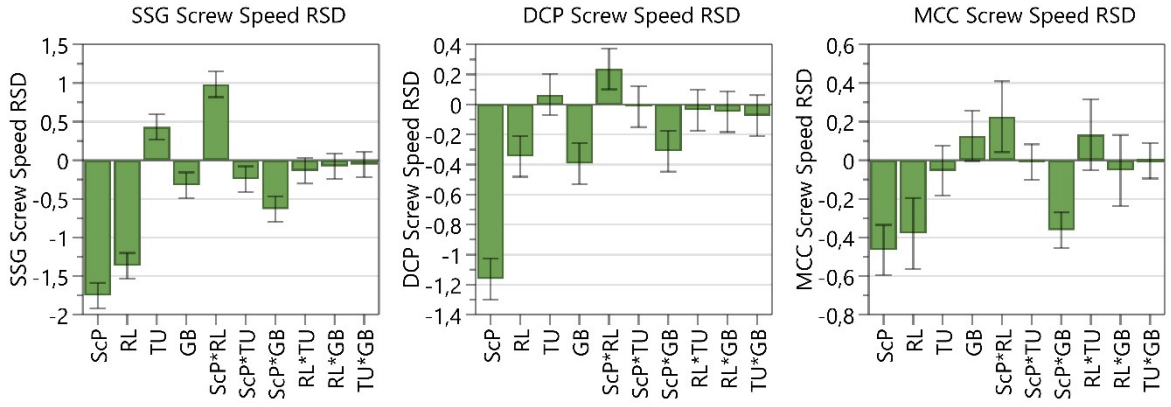

Figure 11 Coefficients plot of model terms regarding the screw speed RSD. The 95 % confidence interval is displayed as an error bar.

The mutual significant model terms for all materials were mainly ScP, RL, ScP*GB and ScP*RL, where 20 mm screw pitches and higher refill levels resulted in significantly lower

screw speed RSD values. As expected, these findings align with the results in section 5.5.3 Feed Factor RSD. After removing non-significant model terms, Table 10 shows the fit statistics:

Table 10 Fit statistics for SSG, DCP and MCC regarding the impact of the input parameters on the screw speed RSD.

Raw Material	Data transformation	Q^2	R^2	Adjusted R^2
SSG	-	0.977	0.996	0.990
DCP	-	0.960	0.990	0.981
MCC	-	0.912	0.978	0.959

5.5.6 Span of Feed Factor, Feed Rate and Screw Speed

The powder bed within the feeder hopper is divided into 10 mass zones. Each mass zone is subjected to the weight of the overlying mass zones and is consolidated accordingly. If the density gradient is too high, the deviation between the FF before and after a refill may be too high as well. I.e. adaptions of the screw speed to the current material consolidation state of the powder are not entirely correct during volumetric mode leading to an overshoot of the feed rate, as shown in Figure 12 (Nowak, 2016).

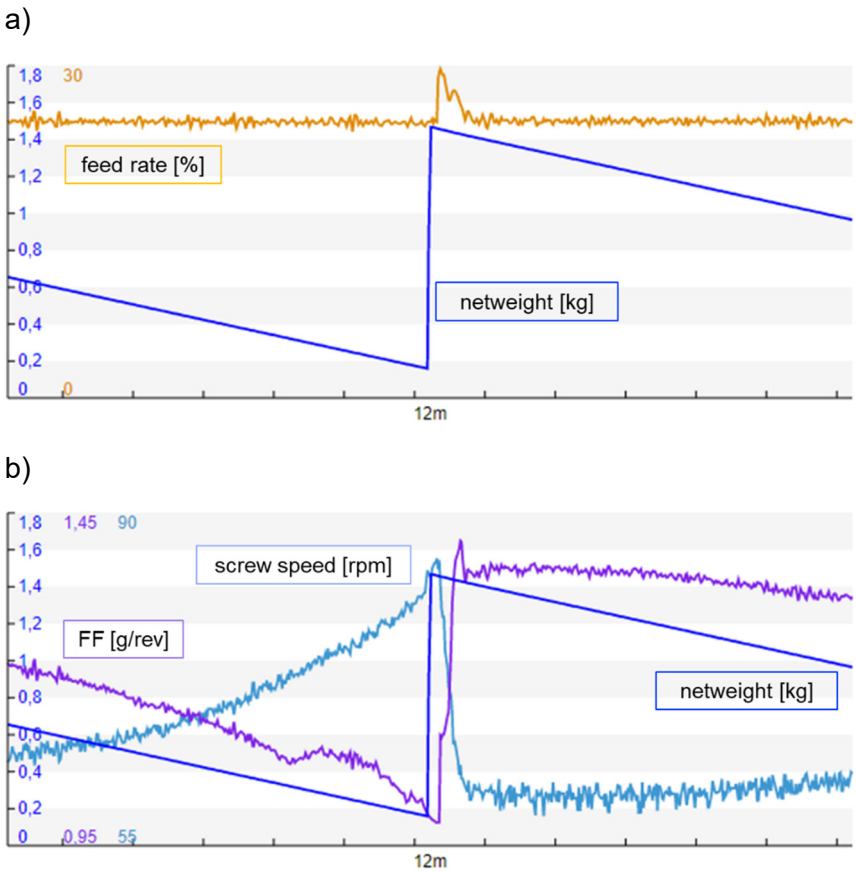

Figure 12 a) shows a PiVision screenshot of an SSG overshoot of the feed rate (orange). B) Prior to the refill the FF (purple) decrease, and the screw speed increases accordingly, resulting in a remarkable deviation between the values before and after the refill. This results in the feed rate overshoot since the screw speed adaption could not perform correctly.

5.5.6.1 **Span of Feed Rate**

As shown in Figure 12, the span of feed rate demonstrates the peak during a refill. To improve the feed performance accordingly, Figure 13 shows the impact of the feeder settings on the overshoot of the feed rate.

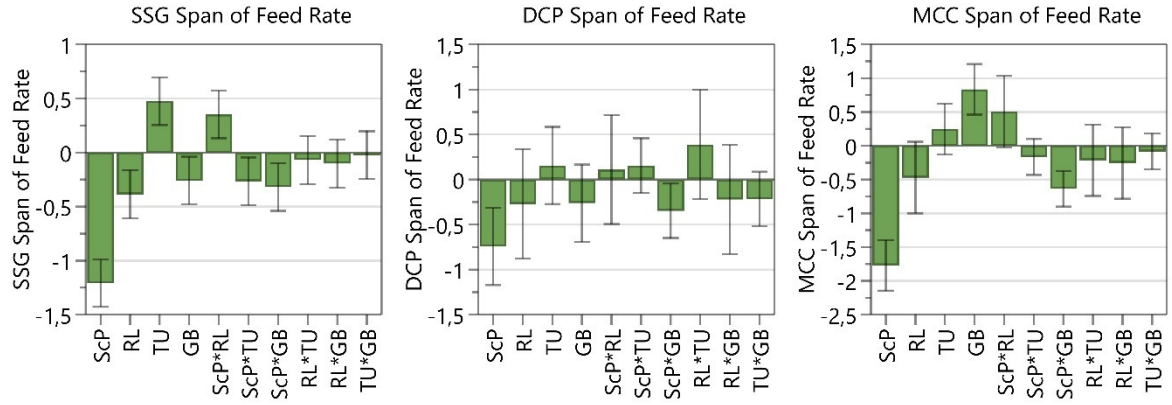

Figure 13 Coefficients plot of model terms regarding the span of feed rate. The 95 % confidence interval is displayed as an error bar.

For all materials, ScP and ScP*GB are mutual significant model terms. So, higher screw pitches reduced the risk of feed rate - overshooting after a refill. According to Engisch and Muzzio, it was expected that higher RL resulted in fewer deflections of the feed rate (Engisch and Muzzio, 2015a). Although a reciprocal connection between RL and the span of feed rate could be observed for all materials, only for SSG a significant impact could be seen.

Table 11 Fit statistics for SSG, DCP and MCC regarding the impact of the input parameters on the span of feed rate.

Raw Material	Data transformation	Q^2	R^2	Adjusted R^2
SSG	-	0.906	0.977	0.956
DCP	-	0.562	0.891	0.795
MCC	-	0.899	0.975	0.953

5.5.6.2 **Span of Feed Factors**

As described earlier, the deviations of FF before and after a refill may lead to an overshoot of the feed rate. To evaluate the possibility of minimizing the span of the feed factors, Figure 14 shows the model terms.

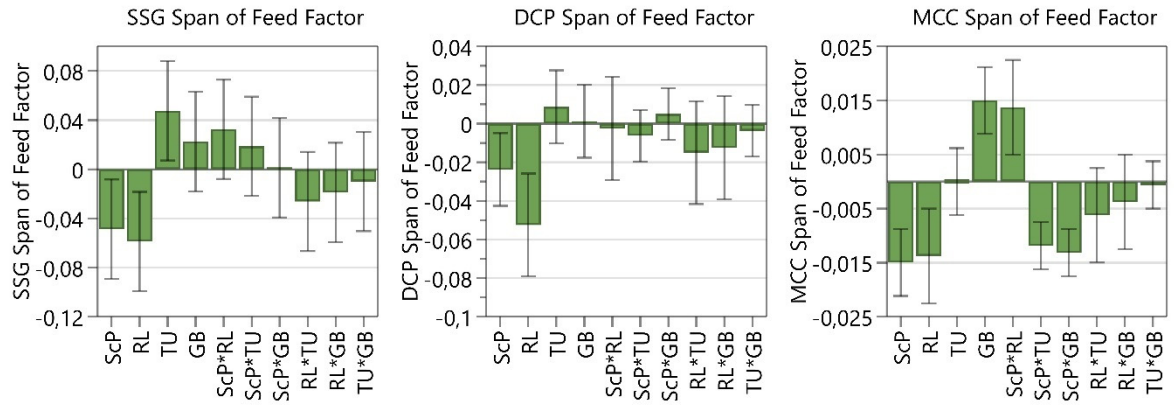

Figure 14 Coefficients plot of model terms regarding the span of feed factors before and after a refill. The 95 % confidence interval is displayed as an error bar.

Again, for all materials, a mutual significant model term was ScP, where higher ScP resulted in lower deviations of FF before and after a refill. As expected, for all materials, higher RL significantly reduced the span of FF, which aligns with the literature (Engisch and Muzzio, 2015a; Hopkins, 2006; Nowak, 2016; Tahir et al., 2020). Table 12 shows the corresponding fit statistics.

Table 12 Fit statistics for SSG, DCP and MCC regarding the impact of the input parameters on the span of feed factors.

Raw Material	Data transformation	Q^2	R^2	Adjusted R^2
SSG	-	0.479	0.835	0.725
DCP	-	0.645	0.861	0.792
MCC	-	0.860	0.973	0.942

5.5.6.3 **Span of Screw Speed**

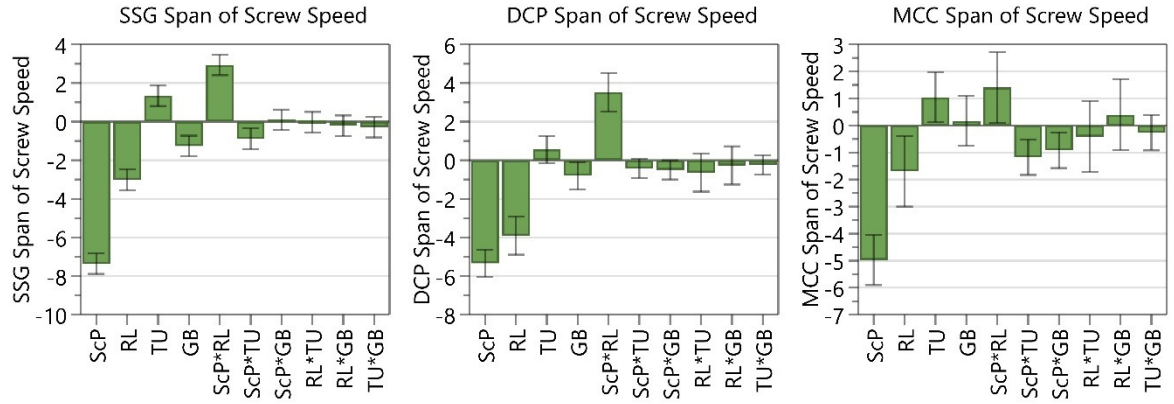

Figure 15 Coefficients plot of model terms regarding the span of screw speed before and after a refill. The 95 % confidence interval is displayed as an error bar.

As expected, ScP, RL and ScP*RL significantly impacted the span of screw speed, which is similar to the results regarding the span of FF. Although DCP did not show a significant impact, higher TU resulted in a higher span of screw speed. Table 13 shows the corresponding fit statistics.

Table 13 Fit statistics for SSG, DCP and MCC regarding the impact of the input parameters on the span of screw speed.

Raw Material	Data transformation	Q^2	R^2	Adjusted R^2
SSG	-	0.986	0.996	0.993
DCP	-	0.977	0.966	0.991
MCC	-	0.917	0.979	0.961

5.5.7 **Normalization of Feed Factor**

Since FF is mainly impacted by the screw pitch, it was tried to normalize the FF by dividing it by the screw pitch. The significant model terms are shown in Figure 16.

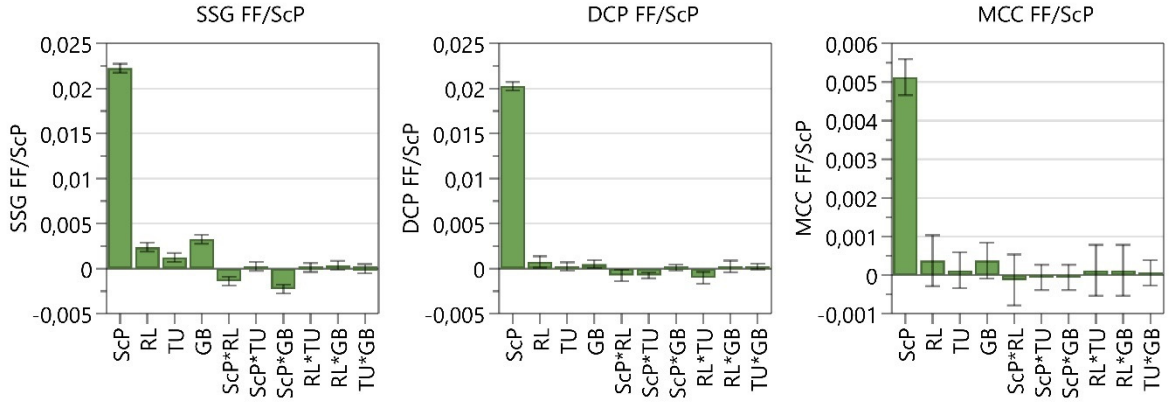

Figure 16 Coefficients plot of model terms regarding the normalized FF. The 95 % confidence interval is displayed as an error bar.

Obviously, the normalized FF are mainly impacted by ScP. That means higher ScP resulted in higher FF/ScP values, which shows that FF obtained at 20 mm/rev ScP are more than two times higher than FF at 10 mm/rev, which contradicts the initial assumption. That reveals that a simple conversion from FF obtained by one ScP into FF obtained by the other is not possible. Table 14 shows the corresponding fit statistics.

Table 14 Fit statistics for SSG, DCP and MCC regarding the impact of the input parameters on the normalized FF values.

Raw Material	Data transformation	Q^2	R^2	Adjusted R^2
SSG	-	0.996	1.000	0.999
DCP	-	0.998	1.000	0.999
MCC	-	0.968	0.997	0.991

5.6 **Conclusion**

The screening DoE revealed the impact of the feeder settings screw pitch (ScP), refill level (RL), top up volume (TU) and gearbox type (GB) on the feed rate, the feed factor (FF) and the screw speed. It could be shown that a reduction in feed rate RSD was achievable with higher ScP. Furthermore, for materials with higher density, an increase in RL could also reduce the feed rate RSDs.

As expected, FF and screw speed both showed similar results and were mainly impacted by the ScP. The influence of the remaining feeder settings can be considered negligible in this data set.

The FF RSD could be minimized by increasing the ScP. Furthermore, it is recommended to set up the feeder to provide a uniformly consolidated powder bed within the feeder hopper. Hence, it could be shown that higher RL and, for powders with higher density, lower TU were beneficial. Comparably to FF RSD, 20 mm/rev screw pitches and higher refill levels resulted in significantly lower screw speed RSD values.

To avoid feed rate peaks during a refill, it could be shown that higher ScP significantly reduced the feed rate deflections. To minimize the deviation between FF before and after a refill, higher ScP and higher RL reduced its value significantly. The span of screw speed could be reduced by increasing ScP, RL and decreasing TU.

To estimate the impact on the FF due to changes in ScP, a normalization of the FF was evaluated. Unfortunately, no linear behavior could be observed, so a simple conversion of the FF could not be calculated.

6 Developing a Method to Predict the Feed Factor Curve Based on Material Attributes, Screw Pitch and Feeder Throughput

6.1 Introduction

To maintain a consistent powder flow during continuous feeding, the feeder hopper needs to be refilled periodically. To minimize feed rate variability, the correct trigger for a refill depends on top up volume (TU), refill level (RL), throughput (THR) and material attributes of the raw material (Bostijn et al., 2019; Engisch and Muzzio, 2015a; Snick, 2017b). Bostijn et al. published the recommendation to trigger the refill when the feed factor (FF) of the powder falls below 90% of the maximum FF (FF_{decay}) (Bostijn et al., 2019). If lot-to-lot variabilities of one ingredient occur, a reconsideration of the correct refill level may be relevant since variations in density or compressibility of the powder can vary the FF_{decay} and result in a higher deviation between FF before and after a refill leading to feed rate variations (Bostijn et al., 2019; Nowak, 2016; Tahir et al., 2020). Since the FF are dependent on the density and the compressibility of the powder, higher powder density leads to higher FF and higher compressibility resulting in higher FF_{decay} values. On the other hand, low compressibility of the material results in a narrow FF distribution throughout the feeder hopper (Bostijn et al., 2019).
As described in chapter 5, the FF values do not increase linearly with increasing screw pitch (ScP). If the ScP needs to be changed to improve the feed performance, the initial FF_{decay} can no longer be used because the FF changes entirely. Since a simple FF conversion between 10 mm/rev and 20 mm/rev is not possible, the impact of ScP should be considered during model development. For this investigation, only the GEA Compact Feeder unit was used.

6.2 Aims and Scope

This trial aimed to develop a method to predict the FF curve over the entire dispensing of one hopper filling based on the material attributes conditioned bulk density and compressibility, the screw pitch and feeder throughput. The method should provide valuable information to optimize the refill strategy if lot-to-lot variations in a continuous production occur or if the screw pitch needs to be changed to improve the feed performance, as described in chapter 5.

6.3 Materials

To introduce different material attributes and therefore indicate lot-to-lot variabilities blends consisting of MCC and different amounts of SiO_2 (formulation 1 (F1)) were prepared using a 10 l laboratory blender LM40 (L.B. Bohle, Ennigerloh, Germany) and a 250 l container blender (Servolift GmbH, Offenburg, Germany) according to the following mixing conditions:

Table 15 Preparation of the MCC-SiO_2 blends used for the feed factor calibration.

Blend No.	Mixer type	SiO_2 concentration [%]	Blend time [min]	Revolutions [rpm]	Mass of the Blend [kg]
1	LM40	0.25	4	20	2.2
2		0.25	7	20	2.2
3		0.25	10	20	2.2
4		0.25	13	20	2.2
5	LM40	0.25	8.25	20	2.2
6		0.5	8.25	20	2.2
7		0.75	8.25	20	2.2
8		1	8.25	20	2.2
9	250 l container blender	0.125	4	12	55
10		0.25	4	12	55
11		0.5	4	12	55
12		0.75	4	12	55

To scale up the mixing condition used for the small blender following equation was used (Kushner and Moore, 2010):

$$r_2 = \frac{(V^{\frac{1}{3}} * F_{Headspace} * r)_1}{(V^{\frac{1}{3}} * F_{Headspace})_2} \quad (7)$$

Where r= number of revolutions of the mixer, V=Volume of the mixer, $F_{Headspace}$= empty volume within the mixer. The blends were characterized by the Freeman Powder Rheometer. For this evaluation, data obtained by the compressibility method were used, where the conditioned bulk density (CBD) and the compressibility at 15 kP compression force (Comp) were considered (see Table 21 and section A.1.1 Material Attributes of the Blends)

6.4 **Feed Factor Calibration**

For each blend mixed according to Table 15, the feed factor calibration was used for three different feeder settings (Table 16). Thus, for each feeder setting, 12 different runs were carried out.

Table 16 Settings used for the FF calibration. For each setting, approximately 700 g of powder was used.

Setting No.	Feeder Throughput [kg/h]	Screw Pitch [mm/rev]
1	5	10
2	5	20
3	10	20

6.5 **Results and Discussion**

6.5.1 **Non-linear regression carried out by GraphPad Prism**

Using PiDataLink, data regarding feed factors and corresponding net weight were exported. A non-linear regression (exponential plateau) was carried out using GraphPad Prism, where the following equation (eq. (8)) could be obtained to explain the FF curve. Y_0 is the FF at the end of the FF calibration, Y_M is the FF at the beginning of the FF calibration, k determines the rate constant in which the FF decrease at some point and x is the net weight of the powder within the feeder hopper.

$$Feed\ Factor = Y_M - (Y_M - Y_0) * e^{-k*X} \quad (8)$$

To evaluate the fit of the variables, R^2 and RMSE values of the non-linear regression obtained at 20 mm/rev ScP and 5 kg/h feeder throughput are shown in Table 17.

Table 17 shows the variables obtained by the non-linear regression using GraphPad Prism, where Y_M, Y_0 and k were obtained for FF at 20 mm screw pitch and 5 kg/h feeder throughput. Furthermore, corresponding R^2 (=Goodness of fit: non-linear regression: exponential plateau) and RMSE values are displayed.

Blend No.	Y_M	Y_0	k	R^2	RMSE
1	1.503	1.043	19.2	0.927	0.0146
2	1.457	0.9086	24.98	0.913	0.0276
3	1.464	0.7878	25.26	0.889	0.0335
4	1.493	0.8277	24.36	0.914	0.0375
5	1.399	0.8029	22.66	0.880	0.0344
6	1.306	0.7576	28.31	0.892	0.0248
7	1.259	0.6519	36.51	0.888	0.0235
8	1.206	0.4737	52.7	0.893	0.0219
9	1.474	0.8682	20.25	0.874	0.0330
10	1.404	0.7709	25.35	0.886	0.0352
11	1.303	0.5953	38.66	0.885	0.0261
12	1.251	0.5617	38.27	0.905	0.0232

R^2 and RMSE values of the non-linear regression obtained at 20 mm/rev ScP and 10 kg/h feeder throughput are shown in Table 18.

Table 18 shows the variables obtained by the non-linear regression using GraphPad Prism, where Y_M, Y_0 and k were obtained for FF at 20 mm screw pitch and 10 kg/h feeder throughput. Furthermore, corresponding R^2 (=Goodness of fit: non-linear regression: exponential plateau) and RMSE values are displayed.

Blend No.	Y_M	Y_0	k	R^2	RMSE
1	1.404	1.695E-08	70.89	0.789	0.0404
2	1.405	0.5419	69.11	0.960	0.0203
3	1.416	0.4266	70.17	0.958	0.0157
4	1.428	0.3804	73.68	0.956	0.0170
5	1.41	0.6538	47.9	0.939	0.0161
6	1.374	0.3956	62.35	0.954	0.0168
7	1.353	0.4091	63.28	0.954	0.0163
8	1.322	0.2066	74.95	0.951	0.0191
9	1.456	0.7374	41.45	0.899	0.0236
10	1.427	0.5654	55.9	0.959	0.0166
11	1.383	0.6213	51.46	0.933	0.0156
12	1.362	0.2448	68.96	0.968	0.0142

R^2 and RMSE values of the non-linear regression obtained at 10 mm/rev ScP and 5 kg/h feeder throughput are shown in Table 19.

Table 19 shows the variables obtained by the non-linear regression using GraphPad Prism, where Y_M, Y_0 and k were obtained for FF at 10 mm screw pitch and 5 kg/h feeder throughput. Furthermore, corresponding R^2 (=Goodness of fit: non-linear regression: exponential plateau) and RMSE values are displayed.

Blend No.	Y_M	Y_0	k	R^2	RMSE
1	0.6513	0.4589	16.69	0.891	0.0102
2	0.6317	0.4255	18.12	0.814	0.0158
3	0.6339	0.4388	16.5	0.841	0.0167
4	0.6411	0.442	14.49	0.890	0.0124
5	0.6119	0.4163	10.55	0.898	0.0137
6	0.5487	0.403	10.12	0.835	0.0140
7	0.5219	0.3782	13.49	0.806	0.0127
8	0.4958	0.3422	17.69	0.652	0.0170
9	0.6548	0.411	10.9	0.861	0.0195
10	0.5995	0.4149	10.6	0.871	0.0143
11	0.5387	0.3737	13.73	0.757	0.0172
12	0.5244	0.3167	17.88	0.888	0.0122

6.5.2 **Prediction of Y_M, Y_0 and k**

For each FF calibration run, the obtained Y_M, Y_0 and k were used as a response in MODDE, where the corresponding CBD, Comp, THR and ScP were set as input parameters. After removing non-significant model terms, Figure 17 visualizes the impact of the input parameters on the regression variables. Y_M was mainly impacted by CBD. Furthermore, Comp and ScP showed significant influence on Y_M, where an increase in all input parameters increased the FF at the beginning of the dispensing. For Y_0, CBD also showed a positive deflection regarding CBD and ScP, whereas higher THR decreased the FF at the end of the dispensing. In contrast to Y_M and Y_0, k showed a negative deflection of CBD. I.e. with lower density, the decrease rate of the FF increased. Moreover, higher THR and higher ScP resulted in higher rates.

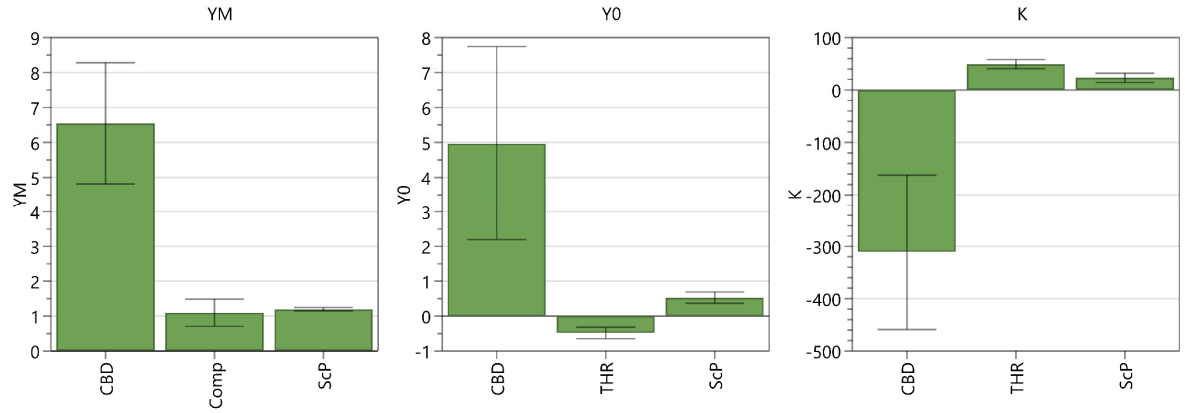

Figure 17 Coefficients plot of the significant model terms regarding k, Y_M and Y_0. The 95 % confidence interval is displayed as an error bar.

The predictions for the three variables in equation (8) could be obtained as shown below.

$$Y_M = -5.9963 + 13.0915 * CBD + 0.115507 * Comp + 0.0797983 * ScP \quad (9)$$

$$Y_0 = -3.42436 + 9.93714 * CBD - 0.06444 * THR + 0.0352342 * ScP \quad (10)$$

$$k = 203.265 - 621.239 * CBD + 6.55984 * THR + 1.54792 * ScP \quad (11)$$

The presented fit statistics in Table 20 implicate good models for the individual variables. Only Y_0, the FF at the end of dispensing, showed a lower R^2 which can be explained by the procedure of the FF calibration. During hopper dispensing, powder adhered to the hopper walls or remained on the impeller at the bottom of the hopper. So, the FFs at the end of the dispensing are unreliable because the endpoint of the dispensing is variable and not associated with a fixed net weight.

Further information regarding fit statistics is shown in section A.1.2 YM, Y0 and k Obtained by MODDE.

Table 20 Fit statistics of the predictions regarding Y_M, Y_0 and k obtained by MODDE.

	Q^2	R^2	Adjusted R^2
Y_M	0.986	0.988	0.987
Y_0	0.579	0.674	0.643
k	0.880	0.907	0.898

6.5.3 Evaluation of the Model Performance

Using Y_M, Y_0 and k obtained by GraphPad Prism (non-linear regression) and the MODDE-predictions (eq. (9) - (11)), the FFs were calculated according to eq. (8). For each calculated FF curve, the RMSE and R^2 (simple linear regression) were calculated to evaluate the performance of the models, as shown in Table 21. The calculated FF based on the variables obtained by MODDE showed only 4 predictions with R^2 <0.8. The RMSE were <0.01 for all predictions except for blend 12 at 20 mm/rev ScP and 5 kg/h (0.1098). Therefore, the model performance can be considered suitable for the used mixtures.

Table 21 shows the Blend No., the ScP, the feeder throughput and the corresponding material attributes of each blend (=input variables for the prediction of Y_M, Y_0 and k by MODDE). Additionally, the RMSE and R^2 values of each calculated FF curve are displayed. The FF curves were calculated by eq. (8), where the corresponding variables are predicted by MODDE and obtained by the non-linear regression by GraphPad Prism.

Blend No.	ScP [mm/rev]	THR [kg/h]	CBD [g/ml]	COMP [%]	RMSE MODDE	R^2 MODDE	RMSE GraphPad	R^2 GraphPad
1	20	5	0.372	8.33	0.0664	0.83	0.0146	0.93
2	20	5	0.384	6.70	0.0635	0.91	0.0276	0.91
3	20	5	0.386	6.89	0.0359	0.89	0.0335	0.88
4	20	5	0.385	6.62	0.0891	0.91	0.0375	0.91
5	20	5	0.394	5.95	0.0581	0.88	0.0344	0.88
6	20	5	0.382	6.31	0.0341	0.89	0.0248	0.89
7	20	5	0.374	6.94	0.0435	0.89	0.0235	0.89
8	20	5	0.367	7.66	0.0810	0.88	0.0219	0.90
9	20	5	0.391	6.50	0.0342	0.87	0.0330	0.87
10	20	5	0.392	5.74	0.0386	0.89	0.0352	0.89
11	20	5	0.381	6.67	0.0580	0.88	0.0261	0.88
12	20	5	0.376	7.26	0.1098	0.90	0.0232	0.90

Blend No.	ScP [mm/rev]	THR [kg/h]	CBD [g/ml]	COMP [%]	RMSE MODDE	R^2 MODDE	RMSE GraphPad	R^2 GraphPad
1	20	10	0.372	8.33	0.0541	0.78	0.0404	0.79
2	20	10	0.384	6.70	0.0250	0.95	0.0203	0.96
3	20	10	0.386	6.89	0.0346	0.95	0.0157	0.96
4	20	10	0.385	6.62	0.0319	0.95	0.0170	0.96
5	20	10	0.394	5.95	0.0395	0.93	0.0161	0.94
6	20	10	0.382	6.31	0.0465	0.95	0.0168	0.95
7	20	10	0.374	6.94	0.0563	0.95	0.0163	0.95
8	20	10	0.367	7.66	0.0373	0.95	0.0191	0.95
9	20	10	0.391	6.50	0.0295	0.89	0.0236	0.90
10	20	10	0.392	5.74	0.0362	0.96	0.0166	0.96
11	20	10	0.381	6.67	0.0290	0.93	0.0156	0.93
12	20	10	0.376	7.26	0.0156	0.97	0.0142	0.97
1	10	5	0.372	8.33	0.0286	0.87	0.0102	0.89
2	10	5	0.384	6.70	0.0369	0.80	0.0158	0.81
3	10	5	0.386	6.89	0.0214	0.82	0.0167	0.85
4	10	5	0.385	6.62	0.0377	0.87	0.0124	0.89
5	10	5	0.394	5.95	0.0394	0.84	0.0137	0.89
6	10	5	0.382	6.31	0.0189	0.81	0.0140	0.83
7	10	5	0.374	6.94	0.0243	0.78	0.0127	0.80
8	10	5	0.367	7.66	0.0197	0.64	0.0170	0.62
9	10	5	0.391	6.50	0.0286	0.85	0.0195	0.86
10	10	5	0.392	5.74	0.0221	0.82	0.0143	0.87
11	10	5	0.381	6.67	0.0282	0.75	0.0172	0.75
12	10	5	0.376	7.26	0.0395	0.89	0.0122	0.89

Figure 18 shows an example of the observed FF, the non-linear regression curve obtained by GraphPad Prism and the calculated FF based on the predicted Y_M, Y_0 and k by MODDE and eq. (8). The remaining graphs are shown in sections A.1.3 and A.1.4.

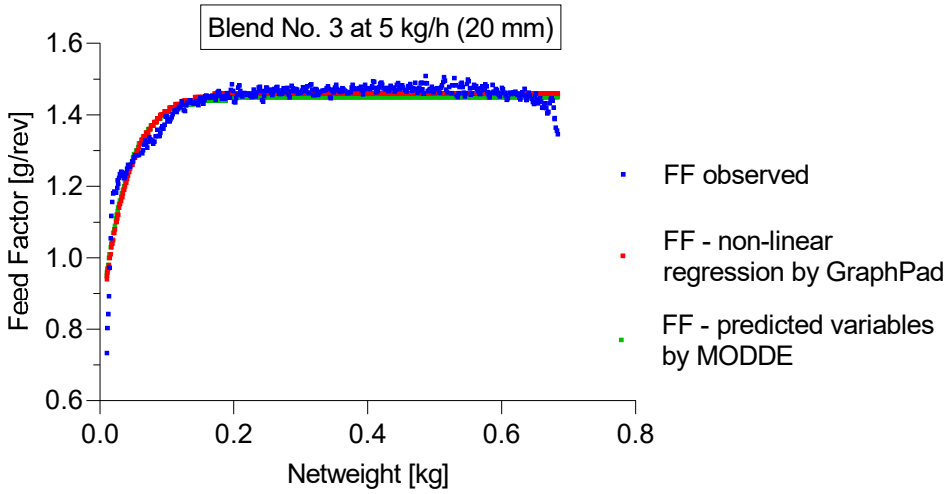

Figure 18 shows an example of the observed and calculated FF values of blend no. 3 at 5 kg/h feeder throughput and 20 mm/rev screw pitches. The observed FF obtained by the FF calibration are shown as blue squares, the red squares show the non-linear regression curve obtained by GraphPad Prism and the green squares are the calculated FF based on the predicted Y_M, Y_0 and k by MODDE and eq. (8).

6.6 **Conclusion**

For the mixtures consisting of MCC and SiO_2, a method could be developed to predict the FF curve using a GEA Compact Feeder. For that, the following steps were carried out.

1. Mixing MCC and SiO_2 in several compositions and different blenders and blending conditions to induce lot-to-lot variability as shown in Table 15.
2. Obtaining CBD and Comp using the FT4.
3. Carrying out FF calibrations for all mixtures using a GEA Compact Feeder.
4. Performing a non-linear regression with the FF and corresponding net weight data and obtaining the model equation (eq. (8)) as well as Y_0, Y_M and k for each FF calibration using GraphPad Prism.
5. Predicting Y_0, Y_M and k based on ScP, THR, CBD and Comp using MODDE.
6. Insert the predicted Y_0, Y_M and k in equation (8) to calculate the FF curve for the corresponding feeder settings and material attributes.

High R^2 and low RMSE values for the predicted FF curves imply good applicability of this procedure for this set of materials. However, the applicability for different powders was not investigated and needs to be confirmed prior to use in the future for ingredients of a commercial product. The next step could be expanding the model to other powders with different material attributes. In the future, an elaboration of this procedure for commercial products could be scheduled and the feasibility of carrying out FF calibration during the development phase of a product should be checked.

7 Impact of Vertical Blender Unit Parameters on Subsequent Process Parameters and Tablet Properties in a Continuous Direct Compression Line

7.1 Introduction

The continuous manufacturing process consists of several connected process units with individual functionalities combined into one single equipment train. Thus, the individual units and the corresponding parameters and process states are inevitably linked. For example, several authors investigated the impact of the feeder set-up and the refill strategy on the feed performance. Consequently, the link between feed rate variability and content uniformity was described (Engisch and Muzzio, 2015a; Hanson, 2018; Tahir et al., 2020; Toson et al., 2018). Other works focused on the impact of impeller speed (IMP), hold up mass (HUM) and throughput (THR) on the residence time distribution (RTD), describing the impact of the mixer parameters on the API distribution within the blend, which impacts the content uniformity of the tablets (Gao et al., 2011b; Lee et al., 2021). Järvinen et al. published their findings regarding the impact of API content, IMP and THR on tablet properties and content uniformity of the tablets using a horizontal mixer (Järvinen et al., 2013).
The continuous direct compression (DC) line includes only one mixing step for all components, including the lubricant. An impact especially on lubricant-sensitive mixtures, as well as on material attributes of the blend, uniformity of the mixture and, subsequently, content uniformity of the tablets, can be expected (Lee et al., 2021; Mehrotra et al., 2007; Swaminathan and Kildsig, 2002).

7.2 Aims and Scope

This investigation assessed to what extent HUM, IMP and THR impact the downstream process of a direct compression mixture. It focused on correlations and coherence and evaluated the predictability of process parameters based on the CMT settings, especially since lubricant and all other formulation constituents are mixed simultaneously in one single mixing step.

7.3 **Materials**

For this DoE (DoE 2), formulation 2 (F2) was used and is shown in Table 22. As a model formulation, saccharin monohydrate was used as an API surrogate. Furthermore, the following feeder set-up was assembled to provide a consistent powder supply.

Table 22 Composition and feeder settings for each raw material of F2.

	MCC	**Saccharin**	**DCP**	**SSG**	**MgSt**
Composition [%]	49.104	21.844	24.552	3.000	1.500
Top up Volume [L]	1.6	1.2	1.6	1.2	0.8
Gearbox Type	1 (63:1)	2 (235:1)	2 (235:1)	3 (455:1)	3 (455:1)
Screw Pitch [mm/rev]	20	10	20	10	20
Refill Level [L]	0.50	0.74	0.30	0.25	1.50

Corresponding material attributes are shown in Table 27.

7.4 **DoE Settings**

A central composite face design with star points at the face of each side defined by a 2-level factorial design was conducted using MODDE. A quadratic model was used, where the following parameters were considered, as shown in Table 23.

Table 23 Overview of considered responses, where HUM, IMP and THR were adjusted as input variables.

Responses	
Mixing parameters	$T_{L,}$
	EV
	HUM
	Blend potency as predicted by the NIR model
Material attributes of the blend	FRI
	Particle size (d_{10})
	CBD
Tableting parameters	FD
	BCH
	EF
Tablet properties	TS
	TT
	TW

Compounds and composition remained constant over the entire experiment. In general, 17 runs, including 3 replicates of a center point, were performed (Table 24). After adjusting the new CMT parameters, a transition phase (3 x MRT) was initiated to wash out the powder mixed at the former setting. A compression pressure/tensile strength profile was conducted using 118, 157, 169, 236 and 275 MPa compression pressure and 21 MPa pre-compression pressure for each phase. Subsequently, the process was run for at least 10 minutes in a steady-state phase.

During the transition phase and the compression pressure/tensile strength profile, the tablet press was operated in manual mode without using the combitester to analyze tablet properties. In manual mode, samples were taken and weighed manually to select the correct fill depth. During each steady-state phase, manual mode was switched to automatic mode, in which the NIR probe was active. For each steady state phase, 275 MPa compression pressure was set, a tablet sample was taken in the middle of the steady state phase using the combitester and a powder sample was withdrawn at the end of each steady state phase by opening the sampling port underneath the feed frame and collecting approximately 300 g of powder.

Table 24 DoE settings, where phase 7, 9 and 11 are the replicates of the center point. MRT and TBP are calculated based on the CMT parameters (eq. (2) and (3)).

phase	Experiment No.	THR [kg/h]	HUM [g]	IMP [rpm]	MRT [min]	TBP [rev]
1	2	10	400	200	2.4	480
2	1	10	400	650	2.4	1560
3	11	10	600	425	3.6	1530
4	13	10	800	200	4.8	960
5	17	10	800	650	4.8	3120
6	10	20	400	425	1.2	510
7	12	20	600	425	1.8	765
8	15	20	600	200	1.8	360
9	16	20	600	425	1.8	765
10	9	20	800	425	2.4	1020
11	6	20	600	425	1.8	765
12	5	20	600	650	1.8	1170
13	4	30	400	200	0.8	160
14	3	30	400	650	0.8	520
15	14	30	600	425	1.2	510
16	7	30	800	650	1.6	1040
17	8	30	800	200	1.6	320

7.5 Results and Discussion

The DoE reveals to what extent the input variables throughput (THR), hold up mass (HUM) and impeller speed (IMP) affect the response parameters regarding the mixing step, like exit valve opening width and SD, torque of the lower impeller and corresponding SD, HUM SD and blend potency uniformity as measured by NIR. Furthermore, the impact on material attributes of the blend (FRI, CBD and d_{10} values), tablet press parameters (FD, BCH and EF) and tablet properties (TS, TW, TT and corresponding standard deviation) are presented. Visualization of where responses are expected is shown in Figure 19. For models with $Q^2 > 0.500$ reliable, predictive equations could be obtained.

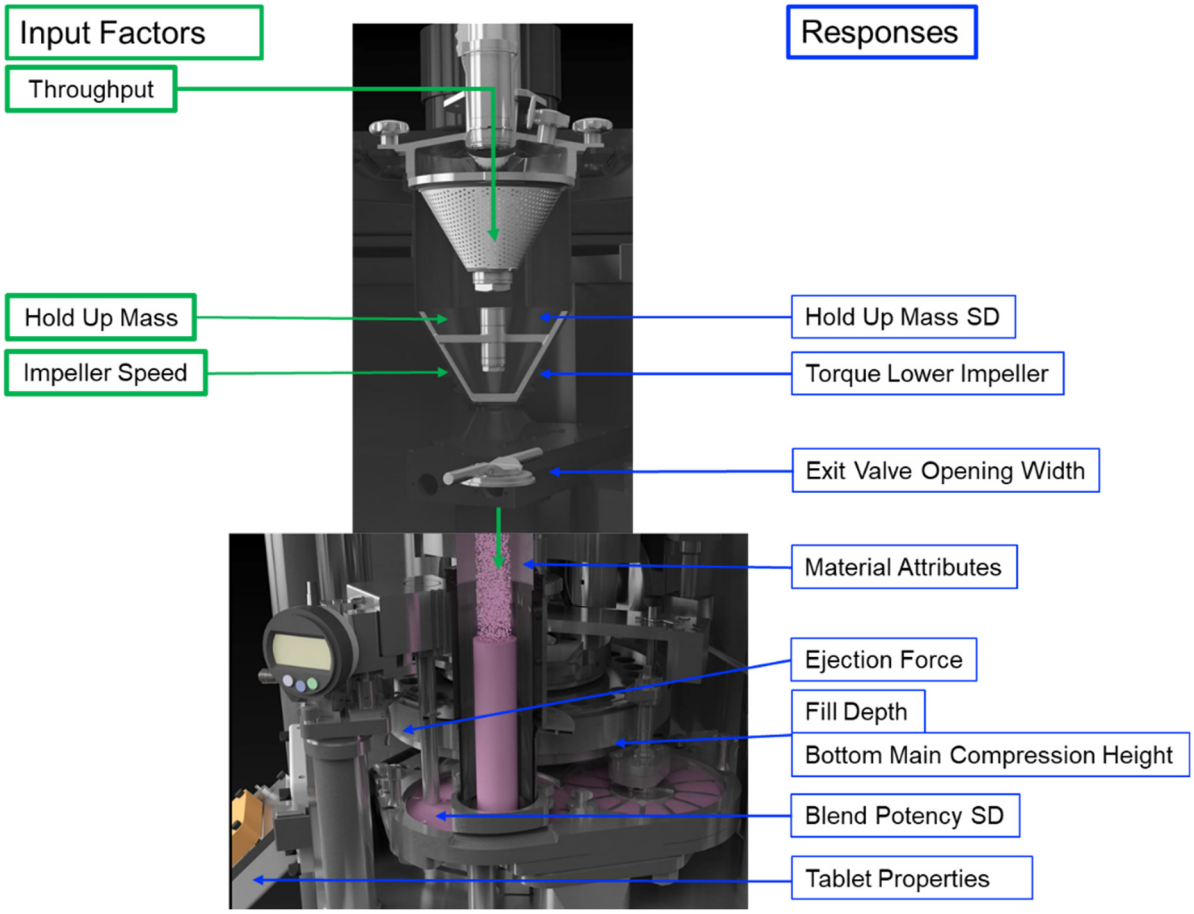

Figure 19. Process overview of input factors (green, left side) and observed responses (blue, right side).

For recapitulation, Figure 20 demonstrates relationships between all parameters obtained and evaluated within this DoE. Starting from the CMT settings, the flowchart depicts the downstream process parameters where correlations are expected to be found. A correlation matrix of all parameters is shown in the appendix, Figure A 48.

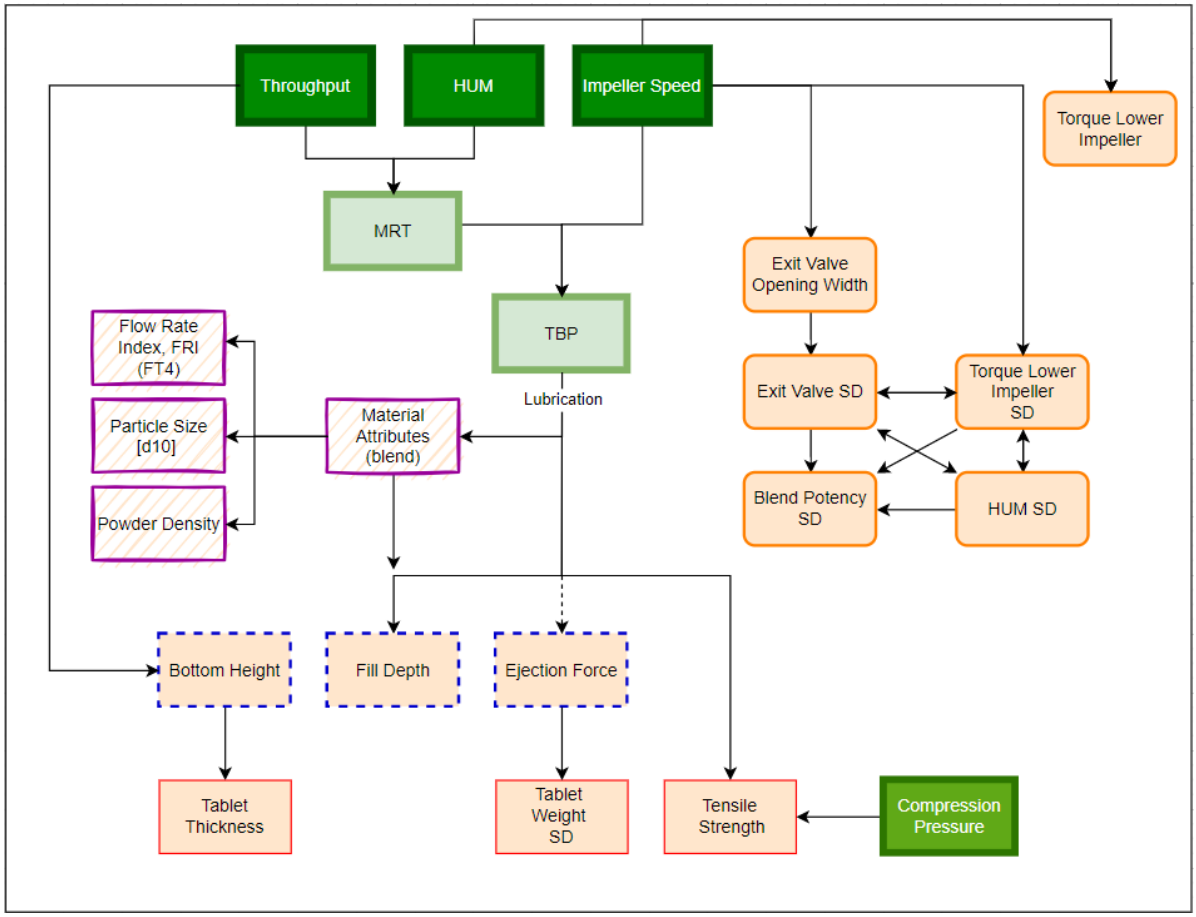

Figure 20 Qualitative overview of process parameter connections and correlations. Input factors are marked in dark green (thick borders), confounding input parameters are marked in light green and the considered response parameters are shown in light orange. The color/shape of the borders classifies the responses into mixing parameters (orange line, rounded corners), material attributes of the blend (purple, striped background), tableting parameters (blue, dotted borders) and tablet properties (red, thin borders). Compression pressure (green) is considered an independent input factor of the tablet press.

7.5.1 Mixing Parameters

Impeller speed was a significant model term for each presented response regarding mixing quality (Figure 21). The DoE revealed that the influence on the exit valve opening width is driven by THR and IMP, resulting in higher opening widths if throughput and impeller speed are high as well. Regarding variability in EV, torque and blend potency, the impeller speed is the only significant model term. For torque values, HUM and IMP seem to share the same extent of deflection. Concerning HUM SD, all three input factors and HUM*IMP were significant.

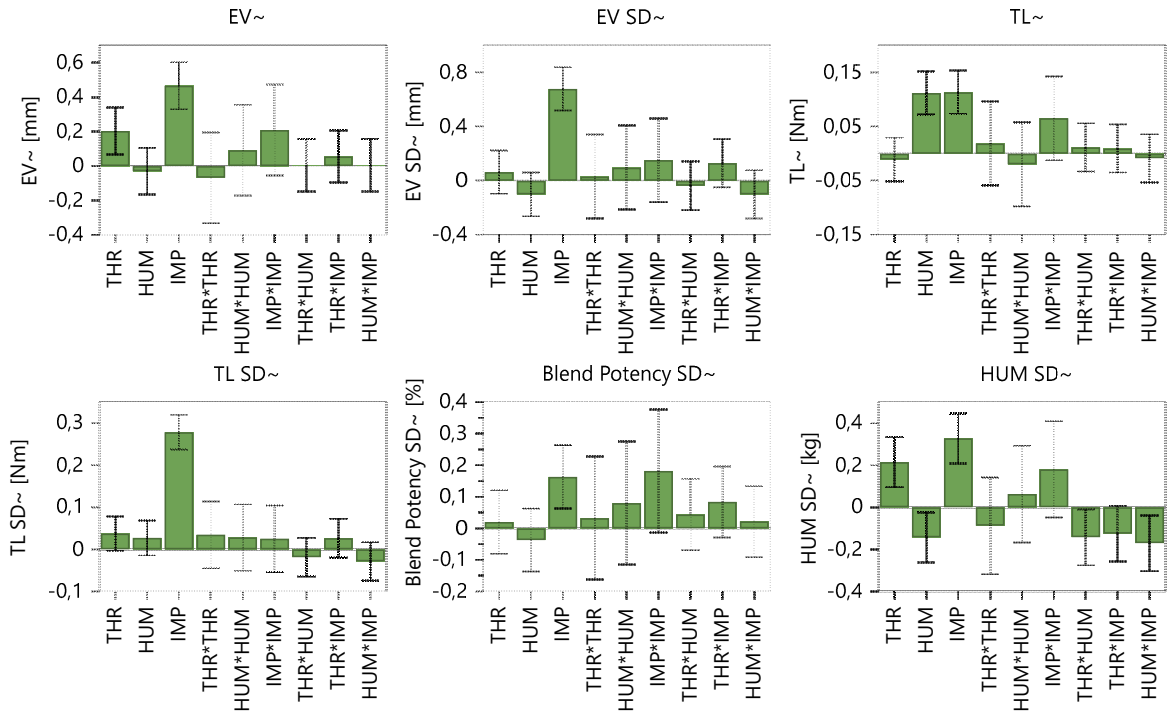

Figure 21 Coefficients plot of the impact of input variables on responses regarding the blending unit and blend uniformity. The 95 % confidence interval is displayed as an error bar.

As shown in Table 25, Q^2 and R^2 imply that exit valve opening width (+SD) and torque (+SD) can be considered good models. As the variabilities of the responses were not linearly distributed, a logarithmic data transformation was conducted.

Table 25 Overview of fit statistics regarding mixing parameters.

Response Factor	Data Transformation	Q^2	R^2	Adjusted R^2
Exit Valve Opening Width	Logarithmic	0.860	0.905	0.883
Exit Valve Opening Width SD	Logarithmic	0.822	0.933	0.893
Torque Lower Impeller	Logarithmic	0.851	0.916	0.896
Torque Lower Impeller SD	Logarithmic	0.882	0.949	0.933
Blend Potency SD	Logarithmic	0.491	0.669	0.622
HUM SD	Logarithmic	0.428	0.727	0.664

For the mixing parameters, the following model equations could be obtained:

$$Log_{10}(EV) = 0.125741 + 0.020304 * THR - 0.00164767 * IMP + 4.37955 * 10^{-6} * IMP^2 \quad (12)$$

$$Log_{10}(EV\ SD) = -0.895478 - 0.0180823 * THR + 0.000444799 * HUM - 0.000454596 * IMP + 4.30254 * 10^{-6} * IMP^2 + 5.75986 * 10^{-5} * THR * IMP - 2.22512 * 10^{-6}\ HUM * IMP \quad (13)$$

$$Log_{10}(T_L) = -1.11007 + 0.000560652 * HUM - 0.000591002 * IMP + 1.28941 * 10^{-6} * IMP^2 \quad (14)$$

$$Log_{10}(T_L\ SD) = -2.15687 + 0.00377409 * THR - 0.00165284 * HUM + 0.00123844 * IMP + 1.4924 * 10^{-6} * HUM^2 \quad (15)$$

$$Log_{10}(HUM\ SD) = -4.62943 + 0.0875789 * THR + 0.00230934 * HUM + 0.00202194 * IMP + 3.31232 * 10^{-6} * IMP^2 - 7.08257 * 10^{-5}\ THR * HUM - 5.55935 * 10^{-5}\ THR * IMP - 3.78083 * 10^{-6}\ HUM * IMP \quad (16)$$

$$Log_{10}(Blend\ Potency\ SD) = 0.655084 - 0.00330149 * IMP + 4.73778 * 10^{-6} * IMP^2 \quad (17)$$

The following figures show further information regarding the model fit.

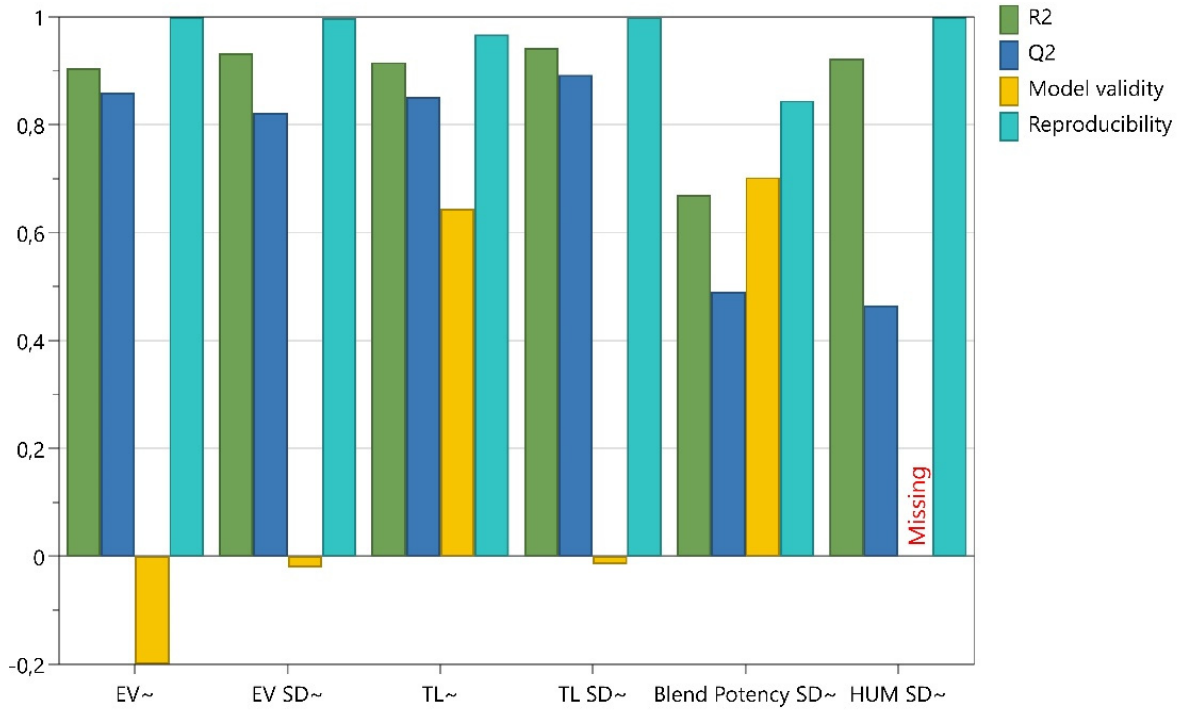

Figure 22 Summary of fit including R^2, Q^2, Model validity and Reproducibility for all mixing parameters.

The model validity for EV, EV SD, TL SD and HUM SD are low or missing, which can be explained by the minimal variability of the data points at the three replicates (EV: 3.706 – 3.786 mm; EV SD: 0.215 – 0.245 mm; Torque SD: 0.0096 – 0.01 Nm; HUM SD: 0.00426 – 0.00439 kg).

Figure 23 shows the residuals of the corresponding response vs. the normal probability of the distribution. An ideal result would be if all data points were on a straight line on a diagonal. If the pattern happens to be curved, non-modeled quadratic relations or false transformations of the responses are indicated. Points outside the red lines (4 SD) are considered outliers and should be checked. The data points for all responses in Figure 23 can be considered a straight line, whereas outliers can be observed. For EV point 11, for T_L point 12 and for HUM Point 1. Considering Figure 24, only for EV, the outlier seems to differ from the predicted value.

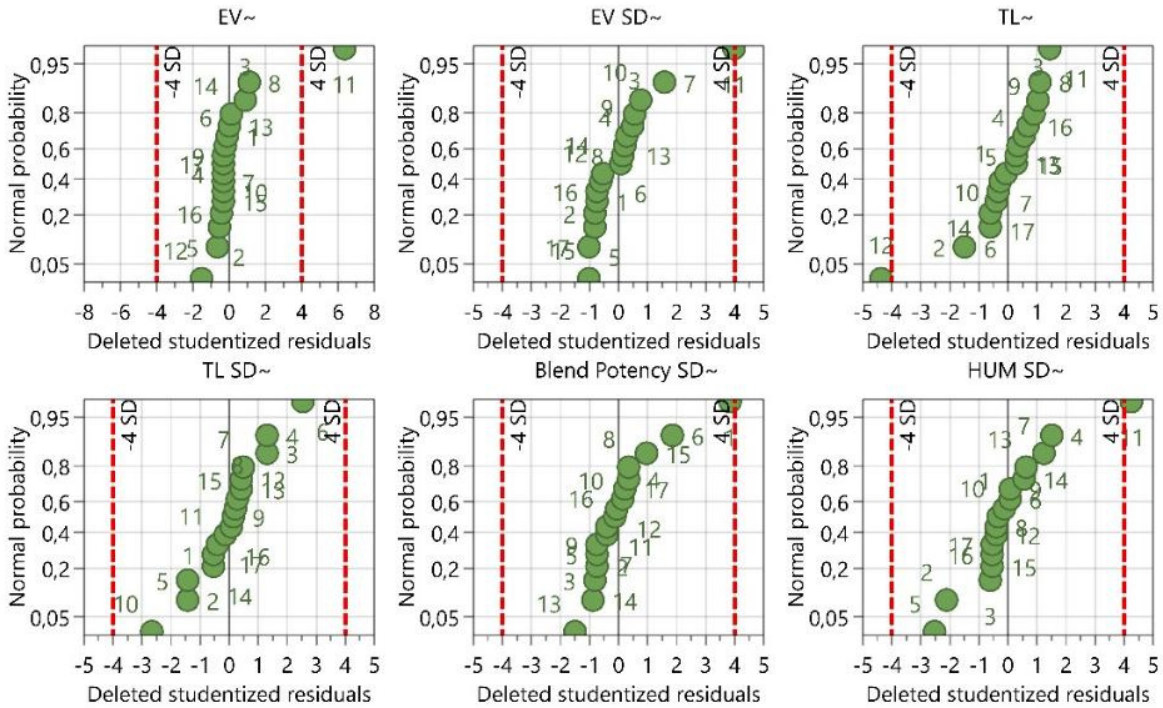

Figure 23 Overview of the residuals normal probability plots for all mixing parameters. The numbers of the data points are referred to the experiment no., as shown in Table 24.

Figure 24 shows the observed vs. predicted values. The dotted line indicates a theoretical perfect fit. Only for blend potency SD, the predicted values differ noticeably from the observed values.

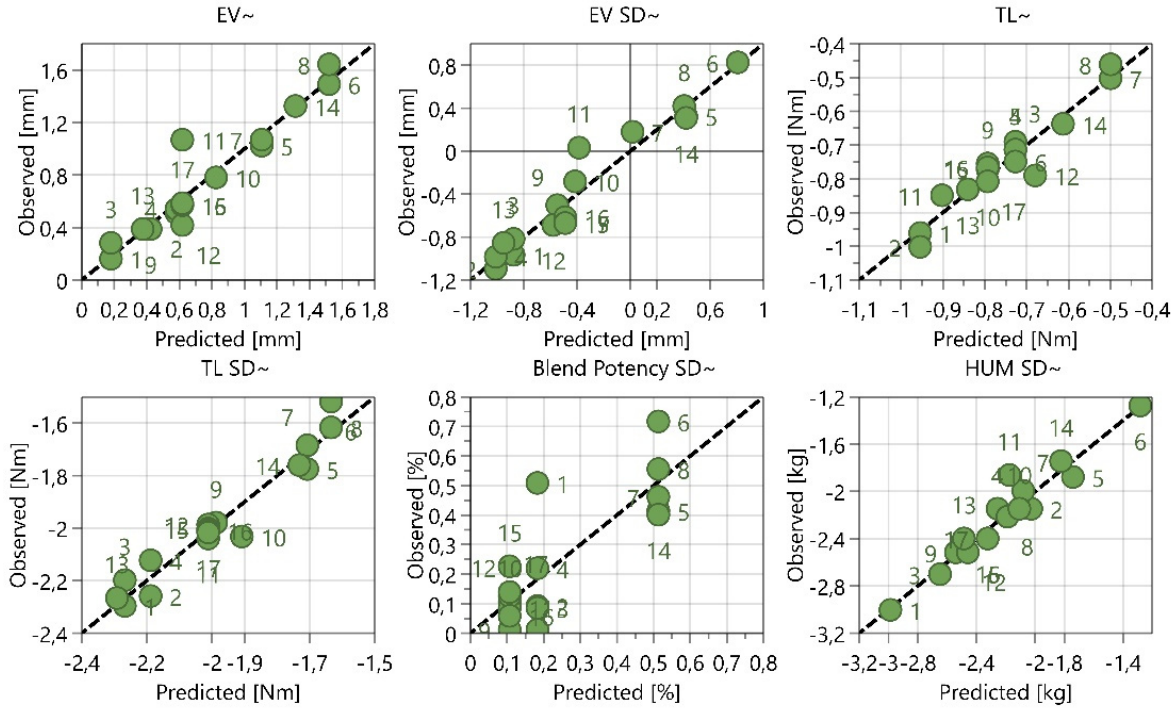

Figure 24 Overview of the comparison between observed and predicted values. The numbers of the data points are referred to the experiment no., as shown in Table 24.

7.5.1.1 **Exit Valve Opening Width**

As presented in Figure 21, throughput and impeller speed were the significant model terms for the exit valve opening width (Q^2=0.860 & R^2=0.905). The low model validity observed was due to the extremely low variability seen in the replicated center points and hence, not a reason for concern.

In this regard, Figure 26 a) shows the exit valve opening width dependent on overall mass throughput, where increasing throughput led to an increasing opening width. Furthermore, all EV opening widths at 650 rpm were higher than 10 mm. Figure 26 b) shows the exit valve in dependence on impeller speed. It confirms that high impeller speed was an important reason for an increasing EV, while variations in HUM seemingly did not impact the exit valve (0.042 p=0.874). Furthermore, a contour plot demonstrates the significance of both model terms throughput and impeller speed (Figure 25). To determine suitable CMT settings based on this plot, small exit valve opening widths are preferable, which is in line with the findings of Toson (Toson et al., 2018). Additionally, using data regarding blend potency SD, a maximum of 5 mm opening value of the exit valve was theoretically set for this DoE (further details below).

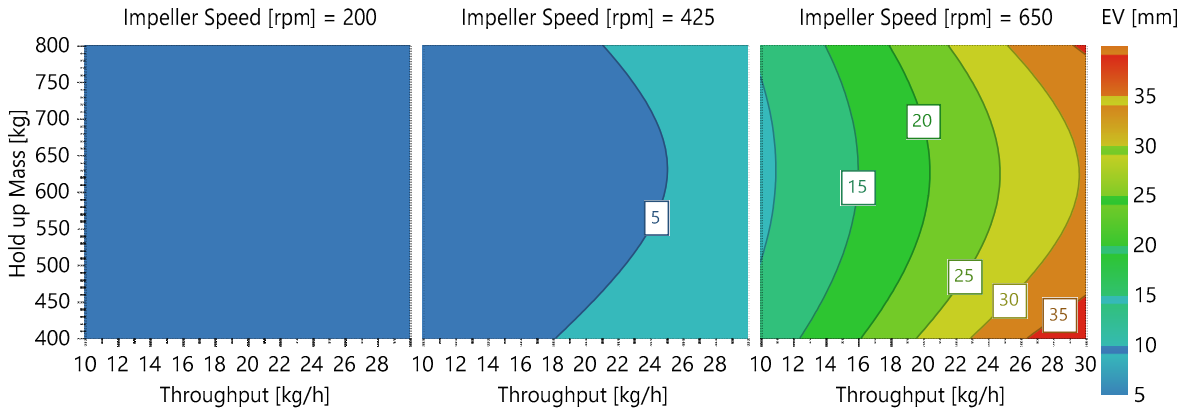

Figure 25 Contour plot of exit valve opening width depending on throughput, HUM and impeller speed.

Regarding EV SD, Figure 21 reveals that impeller speed was the only significant model term (Q^2=0.822 and R^2=0.933). Furthermore, Figure 26 c) shows the EV standard deviation as a function of the EV opening width (0.785 p=0.0002). This correlation leads to the conclusion that higher EV values increased the risk of a fluctuating opening width, impacting the variability of the blend potency values (0.952 p<0.0001) and subsequently affecting the content uniformity of the tablets. A correlation matrix with downstream parameters concerning the EV is shown in Figure 27.

Figure 26 d) shows a correlation of the EV opening width with the ratio of $\frac{HUM\ [g]}{IMP\ [rpm]^2 * THR\ \left[\frac{kg}{h}\right]}$.

This empirically found normalization revealed good processing for values exceeding $2x10^{-4}$.

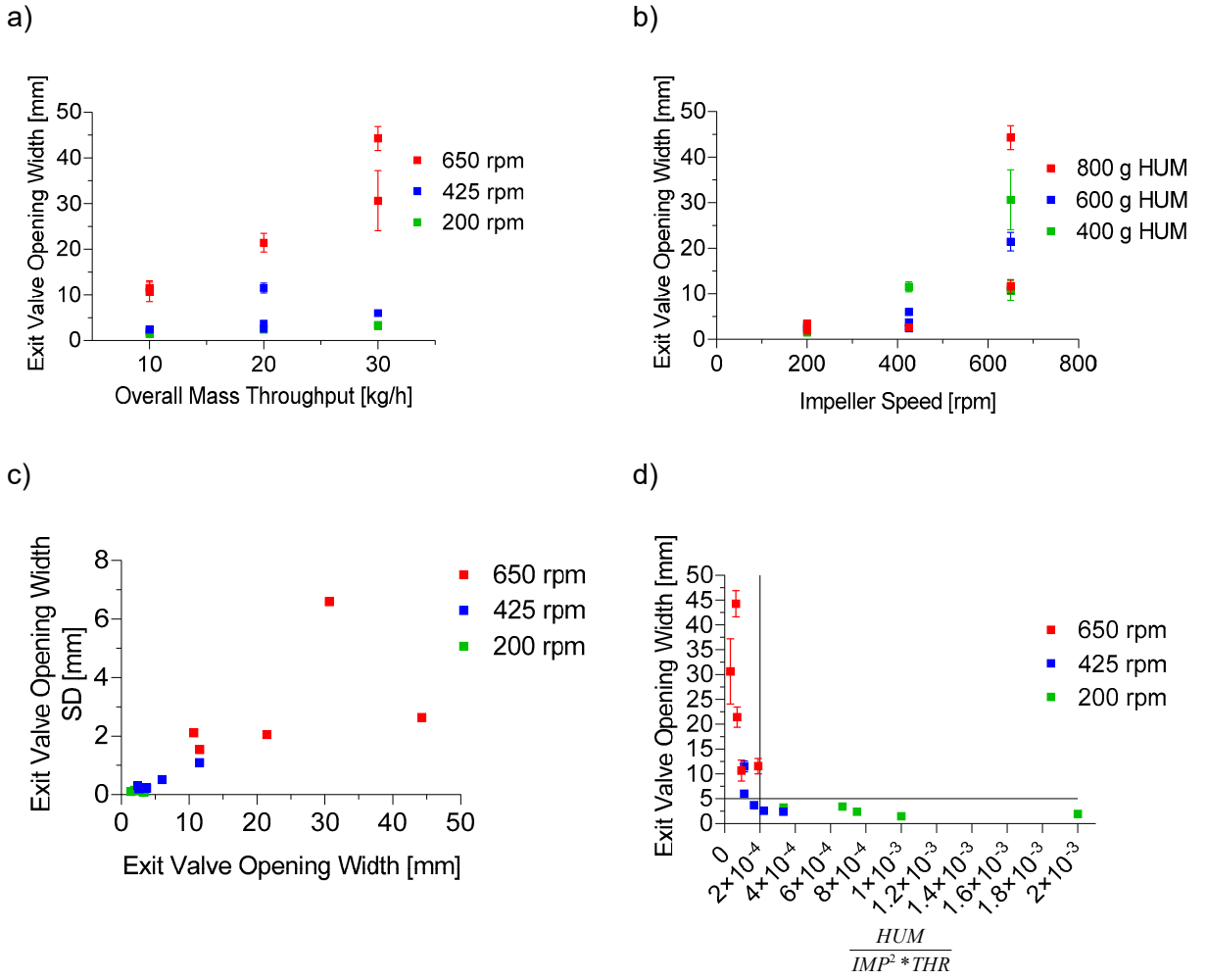

Figure 26 a) Exit valve opening width vs throughput [kg/h] in relation to varying impeller speeds. b) EV in dependence on impeller speed. c) EV SD vs EV opening width d) EV opening width as a function of $\frac{\text{HUM [g]}}{\text{IMP [rpm]}^2 * \text{THR}\left[\frac{\text{kg}}{\text{h}}\right]}$ where x-values higher than $2x10^{-4}$ result in EV opening widths below 5 mm.

As decreased impeller speed proved to have the highest impact on reducing exit valve opening width, it is certainly the primary parameter for reducing the EV. However, one needs to consider the impact on the powder attributes of the blend because a decrease in impeller speed decreases the TBP and, therefore, the extent of lubrication as further discussed below, where the following sections state that TBP impacted CBD, FRI, d_{10} values, FD and TS.

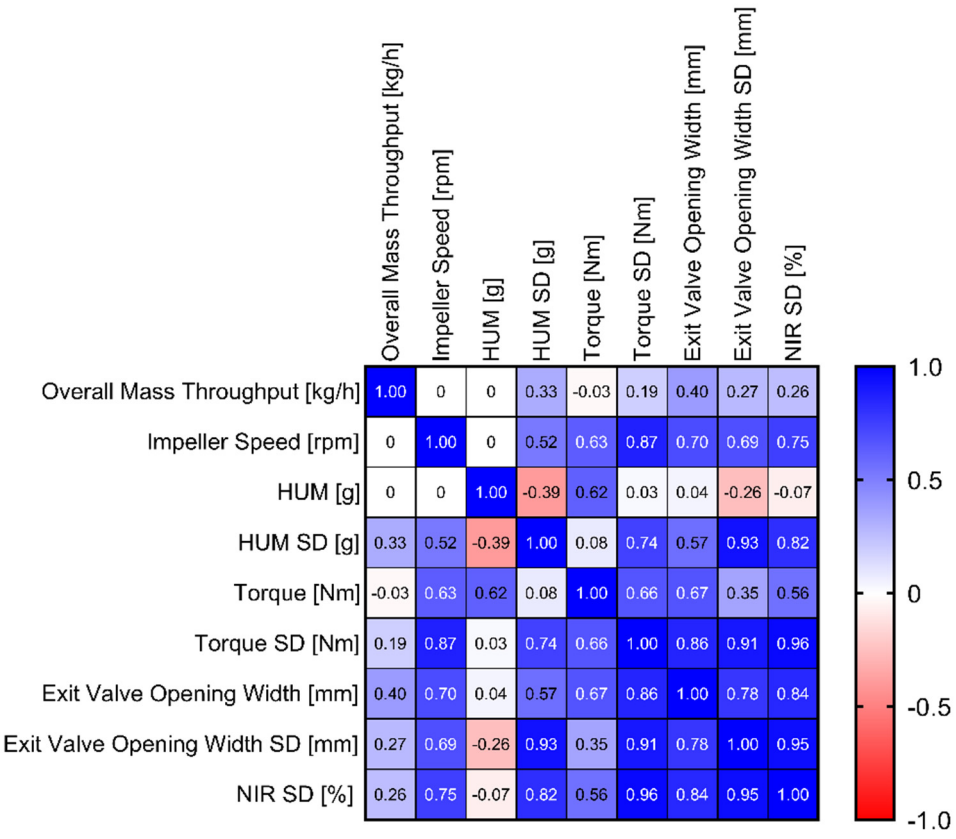

Figure 27 Correlation matrix of input variables and mixing parameters.

7.5.1.2 **HUM SD**

HUM is an essential variable in MRT and TBP (eq. (2) and (3)), so it is crucial to choose suitable blender parameters to maintain a consistent process. Accordingly, fluctuation in HUM led to variabilities in the mean residence time and TBP.

Figure 28 a) shows the HUM SD as a function of impeller speed (0.514 p=0.035). It reveals that HUM standard deviations were not directly impacted by throughput. However, throughput is a significant model term since comparatively low HUM SD were obtained at low throughputs. On the other hand, higher impeller speeds tended to result in a larger span of HUM SD, which could be caused by an unfavorable powder bed shape due to higher centrifugal forces as described by Toson et al (Toson et al., 2018).

Figure 28 b) shows that the previously mentioned EV SD correlated with HUM SD (0.929 p<0.001). That could be traced back to the PID control loop between HUM and EV, where EV is a function of HUM process values in order to maintain $mass_{in}$ = $mass_{out}$. Therefore, if variability could be observed in the HUM, it also occurred in EV. To avoid those fluctuations, it can also be relied on the previous section, where impeller speed is the recommended parameter to control the corresponding process parameters.

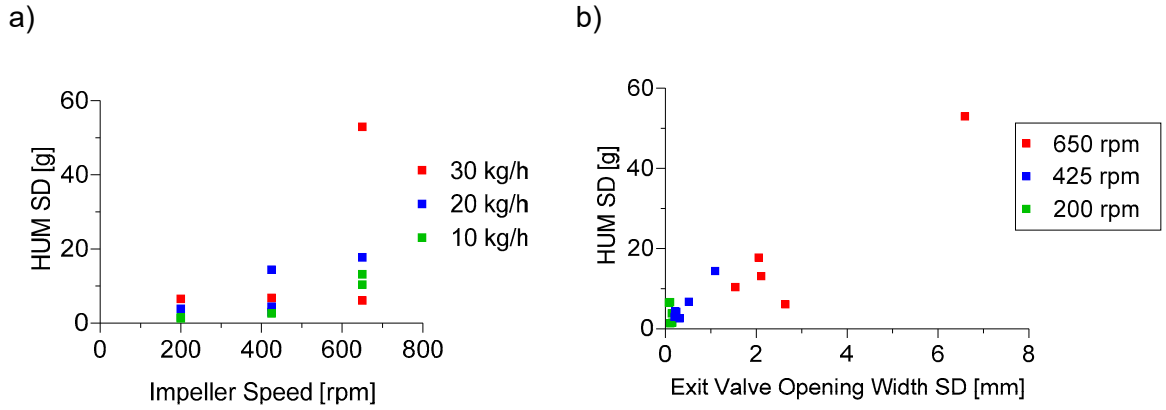

Figure 28 a) HUM standard deviation as a function of impeller speed. b) Dependencies between SD in EV and HUM.

To demonstrate the impact of impeller speed, Figure 29 shows two PiVision screenshots of phases 13 and 14 of the DoE. In both runs, HUM and THR were 400 g and 30 kg/h, respectively. IMP was adjusted at 200 rpm in Figure 29 a) and 650 rpm in Figure 29 b). The y-axis of both figures shares the same values for HUM process value (PV) and setpoint (SP), whereas the numbers regarding EV differ due to the phases' vast discrepancies. In Figure 29 a), consistent HUM and EV trajectories are shown.

In Figure 29 b), it can be observed that the HUM increased the most at the beginning of the process (after a process stop). In general, high impeller speeds push the powder at the walls and in the upper region of the mixer. The amount of powder in the area close to the exit valve decreases, which is why the exit valve has to increase the opening width to ensure a consistent outflow out of the mixer (Toson et al., 2018).

Since the impeller speed was too high at these settings, the powder could leave the CMT hardly and built up. Simultaneously, the exit valve opening width increased to extreme values (up to 41 mm) to compensate for the accumulation until it overshoots. To balance this overshoot, the EV opening width decreased, undershot and HUM rose again. This procedure went on until an equilibrium was reached. By this, it only adjusted slowly to the HUM SP, causing fluctuations.

It is essential to avoid such process states to enable steady-state conditions quickly. Since HUM is used to determine the TBP, highly fluctuating blend conditions resulted in deviations regarding the blend's powder attributes and affected the tablet properties. Hence, fill depth could not be adjusted, among others, since the powder density frequently changed due to fluctuations causing variability in tablet weight.

a) phase 13

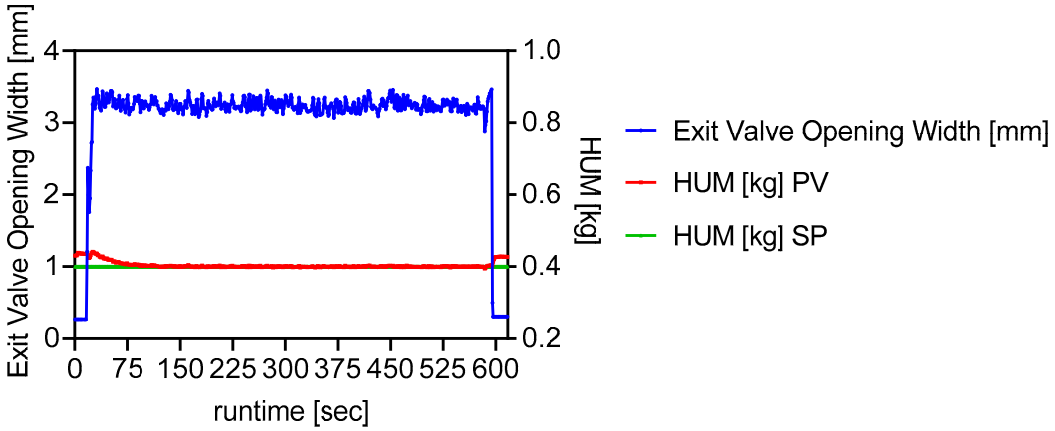

b) phase 14

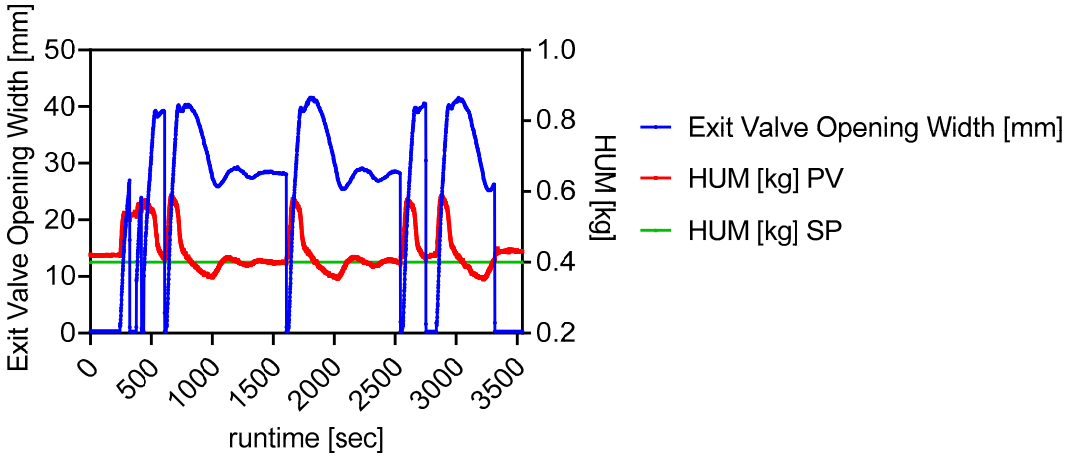

Figure 29 HUM set point = 0.4 kg (green), HUM process value (blue) and corresponding EV (red) at 200 rpm impeller speed during steady state – approx. 10 min. b) HUM set point = 0.4 kg (green), HUM process value (blue) and corresponding EV (red) at 650 rpm impeller speed for approx. 1 h.

7.5.1.3 **Torque of Lower Impeller**

Regarding Table 25, the models for T_L (Q^2=0.851 & R^2=0.916) and T_L SD (Q^2=0.882 & R^2=0.949) could be considered good models. The low model validity for torque SD is again caused by low variability in the replicated center points and, therefore, not a reason for concern. Basically, torque represents the required energy to turn the impeller within the CMT and can be used to monitor the mixing process (Knight et al., 2001).

Since the model terms in Figure 21 showed similar coefficients of HUM and IMP, T_L could be seen as a function of the sum of both factors (0.888 $p<0.0001$) (Figure 30 a).

Figure 30 b) demonstrates the linearity between T_L SD and EV SD (0.906 $p<0.0001$). The correlation between these standard deviations is based on the impact of impeller speed (IMP – T_L SD: 0.874 $p<0.0001$), where higher impeller rotation resulted in higher variabilities in both parameters (Figure 21 and Figure 30 c).

Since standard deviations in both torque and exit valve were strongly correlated, it is recommended to only focus on the EV values if further monitoring is required.

a)

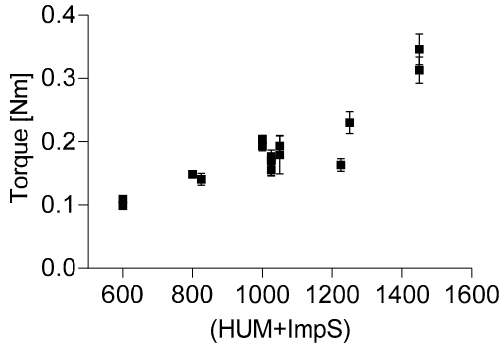

b)

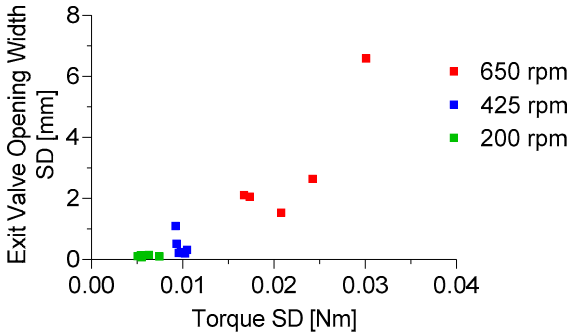

c)

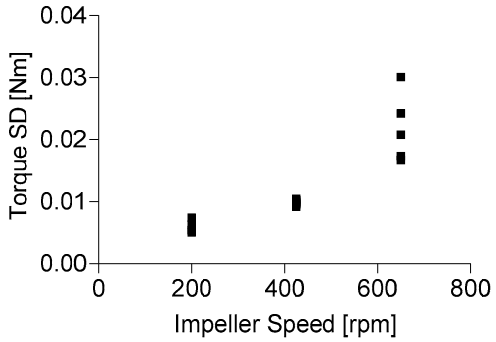

Figure 30 a) Shows torque of the lower impeller as a function of the sum of HUM and IMP. b) Shows the correlation between variability in torque and exit valve opening width. c) Reflects the impact of impeller speed on the torque values.

7.5.1.4 **Blend Potency SD**

Reflecting previously described process parameters, correlations between blend potency SD and EV (0.843 $p<0.0001$), EV SD (0.952 $p<0.0001$), HUM SD (0.817 $p<0.0001$), T_L SD (0.965 $p<0.0001$) and IMP (0.753 $p=0.0005$) could be observed (Figure 27).

Higher exit valve opening widths implicate that the bottom of the CMT was not entirely covered with powder and particles newly entering the CMT could exit unmixed (Toson et al., 2018). Consequently, blend potency SDs and therefore blend inhomogeneities could be explained by insufficient mixing based on the structure of the powder bed within the blend. Figure 31 a) shows the blend potency standard deviation as a function of impeller speed, where all values at 650 rpm exceeded 2.5 %. This observation could also be confirmed using Figure 21, where IMP was the significant model term. So, reducing the impeller speed is proposed again to reduce blend potency SDs and improve blend homogeneity and content uniformity of the tablets.

Figure 31 b) shows that all blend potency values obtained at exit valve opening widths below 10 mm were smaller than 2.5%. To minimize the risk of higher blend potency SD, the presented results confirm maximum EV values below 5 mm, although low blend potency SD could also be obtained at EV>10mm.

Furthermore, independent of the blender variables, a potential risk for blend potency inhomogeneity could be the adhesion of API at the walls due to the electrostatic charging of particles (Moghtadernejad et al., 2018).

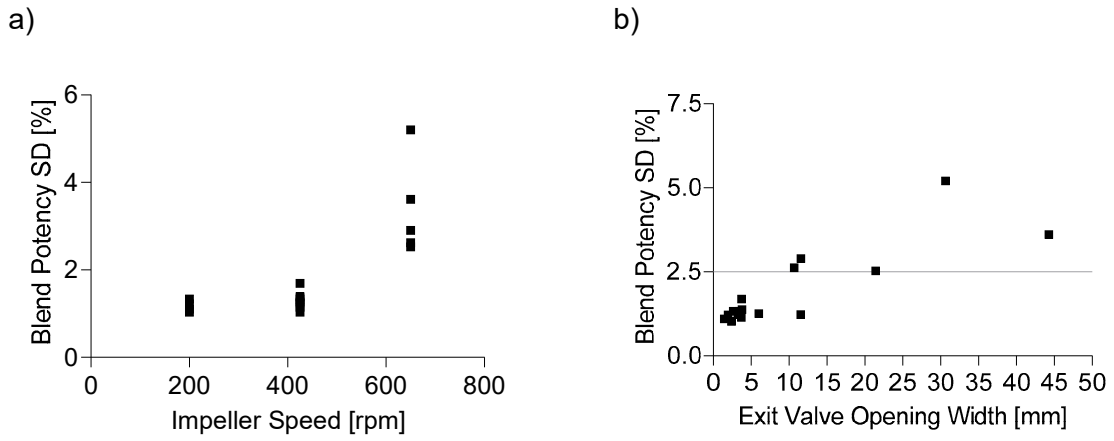

Figure 31 Blend Potency SD as a function of a) impeller speed and b) exit valve opening width.

7.5.2 **Material Attributes of the Blend**

The conditioned bulk density (CBD), flow rate index (FRI) and d_{10} values of the blend were evaluated in Figure 32. THR, HUM and IMP show a similar impact on CBD and d_{10} values of the powder. In contrast, the coefficients regarding FRI show a positive impact of THR and a negative influence by IMP and THR*THR

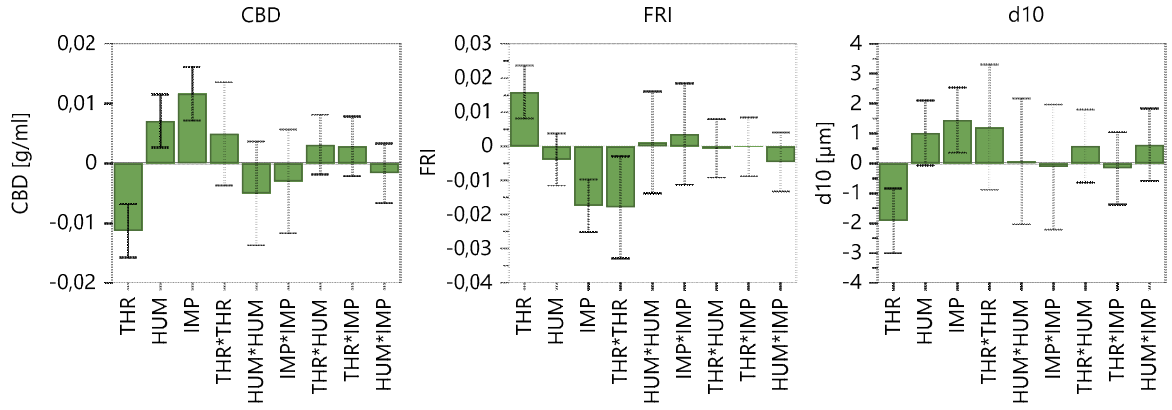

Figure 32 Coefficients plot of model terms regarding material attributes of the blends. The 95 % confidence interval is displayed as an error bar.

Table 26 shows the fit statistics after removing non-significant model terms, where models regarding CBD, FRI and d_{10} can be considered good models.

Table 26 Overview of fit statistics regarding material attributes of the blend.

Response Factor	Data Transformation	Q^2	R^2	Adjusted R^2
Conditioned Bulk Density	-	0.735	0.850	0.816
Flow Rate Index	-	0.800	0.896	0.848
Particle Size (d_{10})	-	0.587	0.842	0.747

For the material attributes, the following model equations could be obtained:

$$CBD = 0.558553 - 0.00113 * THR + 3.54999 * 10^{-5} * HUM + 5.2 * 10^{-5} * IMP \quad (18)$$

$$FRI = 0.803244 + 0.0077786 * THR + 2.41807 * 10^{-5} * HUM - 1.56664 * 10^{-5} * IMP - 0.000154715 * THR^2 - 1.02778 * 10^{-7} * HUM * IMP \quad (19)$$

$$d_{10} = 41.7377 - 0.839812 * THR - 0.00661847 * HUM - 0.00185889 * IMP + 0.0118172 * IMP^2 + 0.000291875 * THR * HUM + 1.38611 * 10^{-5} * HUM * IMP \quad (20)$$

The following figures show further information regarding the model fit and demonstrate a good model performance.

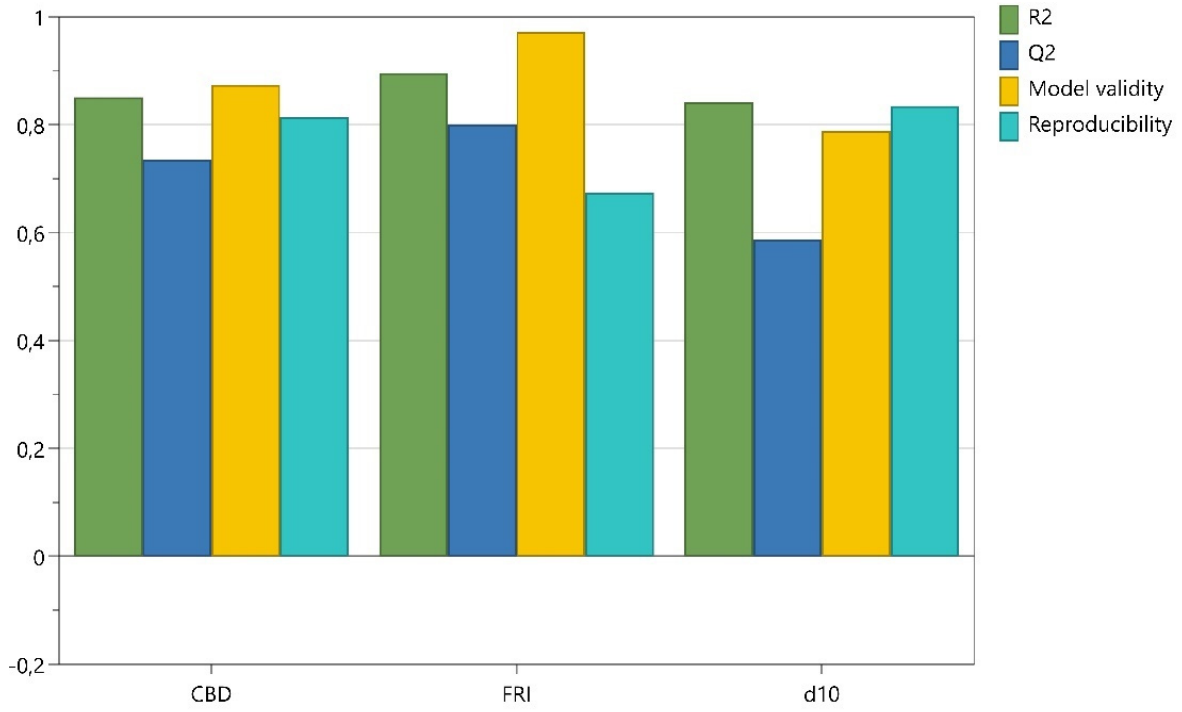

Figure 33 Summary of fit including R^2, Q^2, Model validity and Reproducibility for all material attributes.

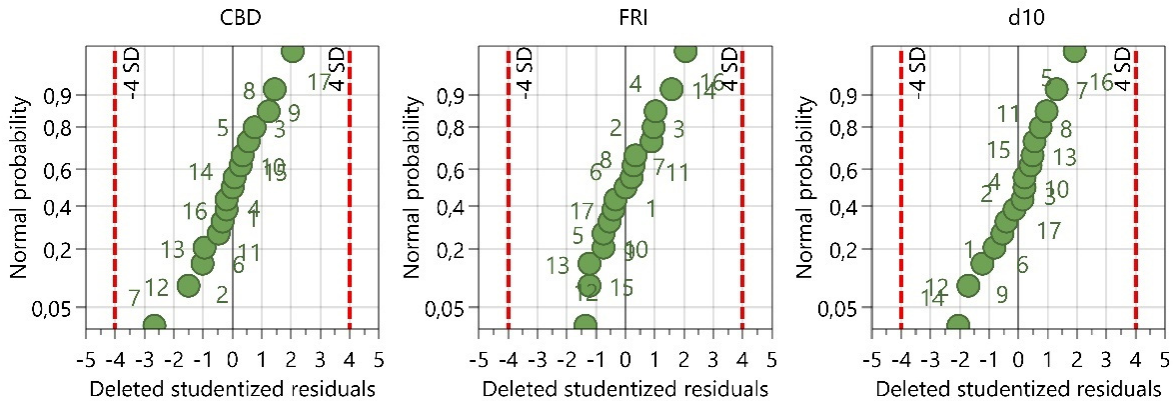

Figure 34 Overview of the residuals normal probability plots for all material attributes. The numbers of the data points are referred to the experiment no., as shown in Table 24.

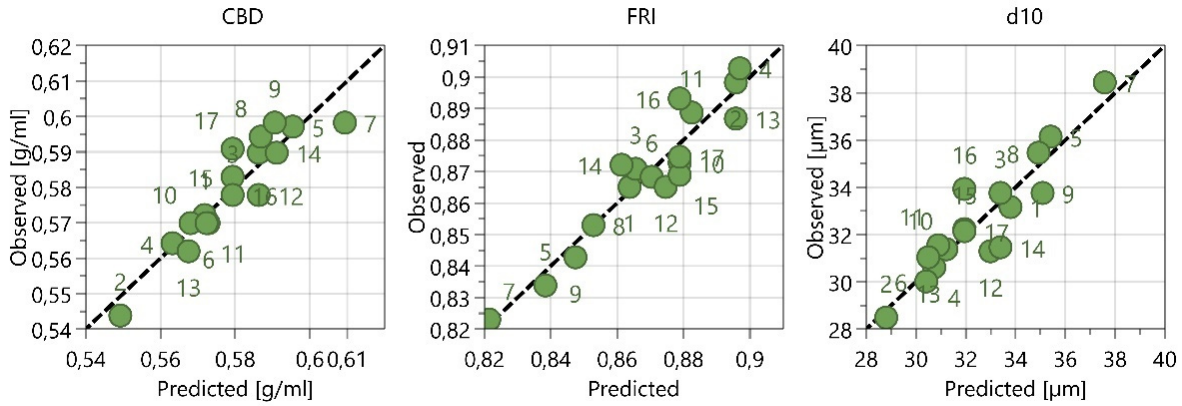

Figure 35 Overview of the comparison between observed and predicted values. The numbers of the data points are referred to the experiment no., as shown in Table 24.

Table 27 shows the material attributes of the raw materials.

Table 27 FT4 data and particle size distribution (QicPic) of the individual raw materials.

	CBD* [g/ml]	**FRI***	**Comp**** [%]	**Cohesion***** [kPa]	**FFc*****	**d_{10}****** [µm]	**d_{50}** [µm]	**d_{90}** [µm]
MCC	0.351±0.001	1.38±0.04	13.13±0.01	0.60±0.45	10.4±5.7	40.53	113.35	222.04
Saccharin	0.756±0.021	0.94±0.03	19.27±0.00	0.99±0.64	5.8±2.7	27.46	208.94	374.48
DCP	0.789±0.005	1.40±0.08	3.06±0.03	0.92±0.11	5.0±0.6	38.58	109.11	213.9
SSG	0.758±0.002	1.18±0.20	10.06±0.06	0.26±0.07	16.9±5.1	26.07	50.03	74.18
MgSt	0.176±0.004	2.68±0.28	46.50±0.01	0.83±0.17	5.8±1.1	12.12	39.05	289.52

*Obtained by the stability and variable flow rate method.

**Obtained by the compressibility method.

***Obtained by the shear cell.

****Obtained by Sympatec QicPic.

7.5.2.1 **Total Blade Passes**

TBP is the decisive factor in describing the impact on material attributes during continuous mixing with a vertical blender since magnesium stearate is mixed simultaneously throughout the entire mixing process. The TBP combines the blend time (MRT) and IMP (eq. (3)), governing shear and mixing intensity of the lubricant into the blend. For improvements regarding EV position and HUM uniformity following changes in material attributes must be considered:

Higher TBP represents more contact between impeller and powder particles; hence, it is implied that lubricant can be distributed more homogeneously into the blend with the potential risk of film formation. This would impact the tablet's tensile strength and is further discussed in section 7.5.4.2 Tensile Strength.

7.5.2.2 **Powder Density**

With increasing impeller revolutions, mixing intensity is increasing, too. That likely reduces particle-particle frictions due to magnesium stearate film formation. Particles can now arrange more compactly, increasing the powder density (Morin and Briens, 2013; Razavi et al., 2018). Figure 36 a) demonstrates an exponential relationship between TBP and CBD, asymptotically reaching 0.598 g/ml at 1560 TBP. At extreme values, like 3120 revolutions, powder density did not increase any further and a maximum was reached, which led to the conclusion that increasing TBP only affected the material up to a specific limit.

Considering Figure 32 and the equation for TBP (eq. (3)), the significant model terms of the DoE revealed the same information, where higher values in HUM and impeller speed increased CBD and higher throughputs decreased the powder density (Q^2=0.735 & R^2=0.850).

7.5.2.3 **Flow Rate Index**

Figure 36 b) shows the flow rate index (FRI) as a function of TBP (-0.846 $p<0.0001$). Unlike CBD, FRI decreased with rising TBP. Due to an increasing lubrication effect at higher TBP, less energy was needed to move the blade through the powder bed since the required energy is based on the resistance at the downward motion. Again, a plateau could be observed, where increasing TBP did not necessarily impact the FRI any further. The MLR analysis showed a model fit of Q^2=0.800 & R^2=0.896.

7.5.2.4 **Particle Size**

The description of density changes based on TBP also applies to the particle size (d_{10}), as shown in Figure 36 c). At high TBP, more magnesium stearate adhered to the particles, leading to a lower amount of remaining free MgSt particles within the blend, increasing the d_{10} values

(0.836 p<0.0001). As a reference, a blend without magnesium stearate was mixed using a Turbula blender (Willy A. Bachofen AG, Muttenz, Switzerland), where a d_{10} value of 38.4 µm was obtained (Figure 36 c).

So, the appearance of smaller particle sizes in the blend could be traced back to MgSt. As seen at 3120 revolutions, the d_{10} value was similar to the blend without MgSt, implicating that the fine fraction of MgSt was almost entirely attached to the remaining raw materials at higher TBP. Moreover, particle size changes due to the destruction of particles could be ruled out. In this case, the d_{10} values would have decreased with higher shear.

Regarding the DoE results in Figure 32, a good model for d_{10} values could be obtained (R^2=0.842 & Q^2=0.587). Particle sizes of raw materials and blends are shown in Table 27.

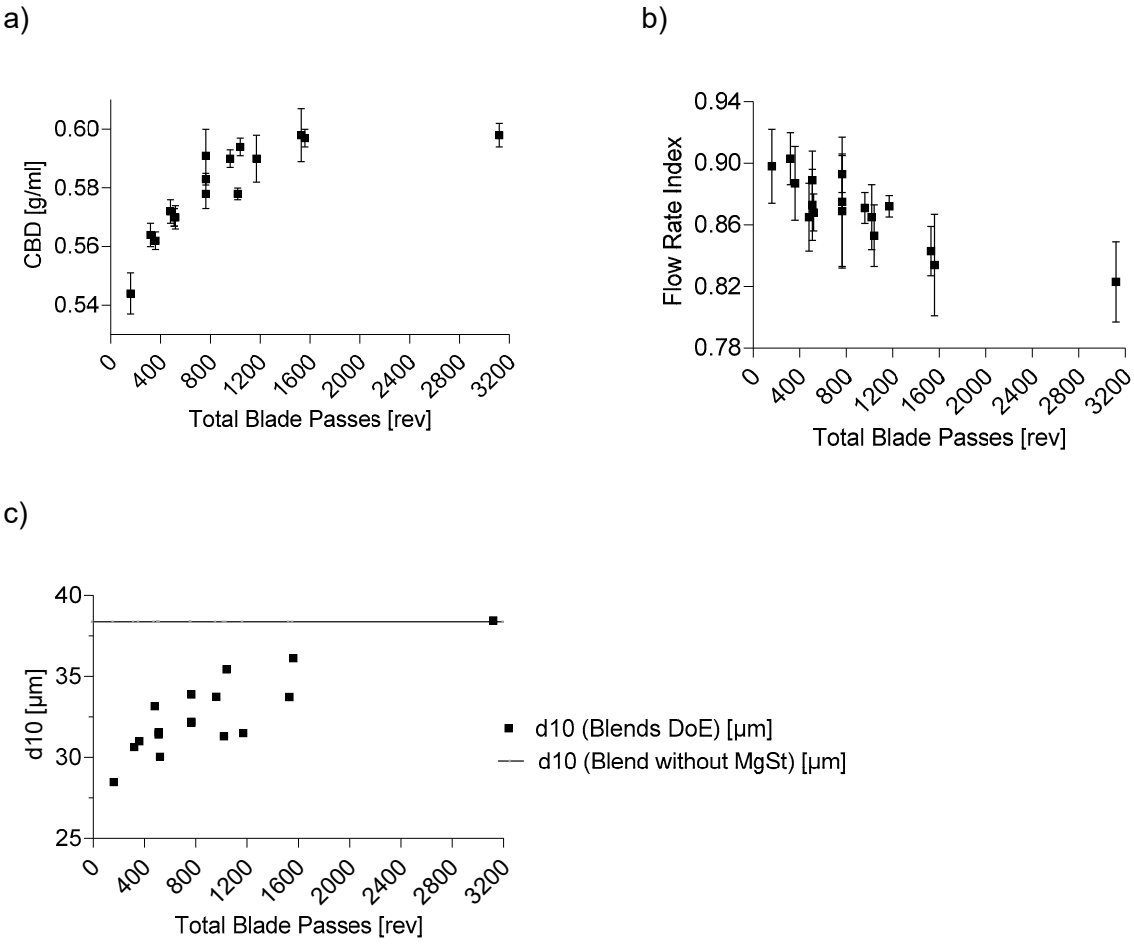

Figure 36 a) Conditioned bulk density (CBD) [g/ml], b) flow rate index (FRI) and c) particle size (d_{10}) [µm] as a function of total blade passes.

7.5.3 **Tableting Parameters**

Regarding tableting parameters, the fill depth, bottom main compression height and ejection force were evaluated, wherein throughput and impeller speed are significant model terms for all three parameters (Figure 37). I.e., these input factors have a statistically significant impact on all three tableting parameters. For example, higher throughput and lower impeller speed

resulted in lower TBP and, therefore, lower lubrication, leading to lower powder densities, higher required fill depths and higher ejection forces.

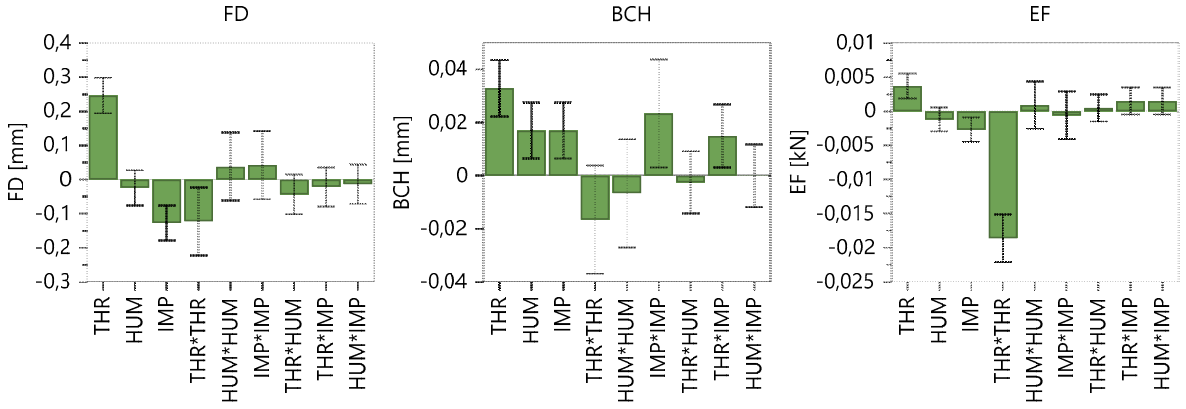

Figure 37 Coefficients plot of model terms regarding tablet press parameters. The 95 % confidence interval is displayed as an error bar.

Furthermore, the fill depth and ejection force share the same deflection of the three significant model terms, namely THR, IMP and THR*THR.

Table 28 shows the fit statistics after removing non-significant model terms. All three parameters show high values regarding Q^2 and R^2.

Table 28 Overview of fit statistics regarding tablet press parameters.

Response Factor	Data Transformation	Q^2	R^2	Adjusted R^2
Fill Depth	-	0.873	0.941	0.914
Bottom Main Compression Height	-	0.774	0.928	0.885
Ejection Force	-	0.892	0.944	0.931

For the tableting parameters, the following model equations could be obtained:

$$FD = 9.63996 + 0.0701824 * THR + 0.000317503 * HUM - 0.000564445 * IMP - 0.000811434 * THR^2 - 2.18752 * 10^{-5} * THR * HUM \quad (21)$$

$$BCH = 5.11499 + 0.00797587 * THR + 8.49982 * 10^{-5} * HUM - 0.000414171 * IMP - 0.000187731 * THR^2 + 4.19285 * 10^{-7} * IMP^2 + 6.6667 * 10^{-6} * THR * IMP \quad (22)$$

$$EF = 0.0260715 + 0.00774714 * THR - 1.2 * 10^{-5} * IMP - 0.000184428 * THR^2 \quad (23)$$

The following figures show further information regarding the model fit, where the model validity of all parameters shown in Figure 38 was acceptable.

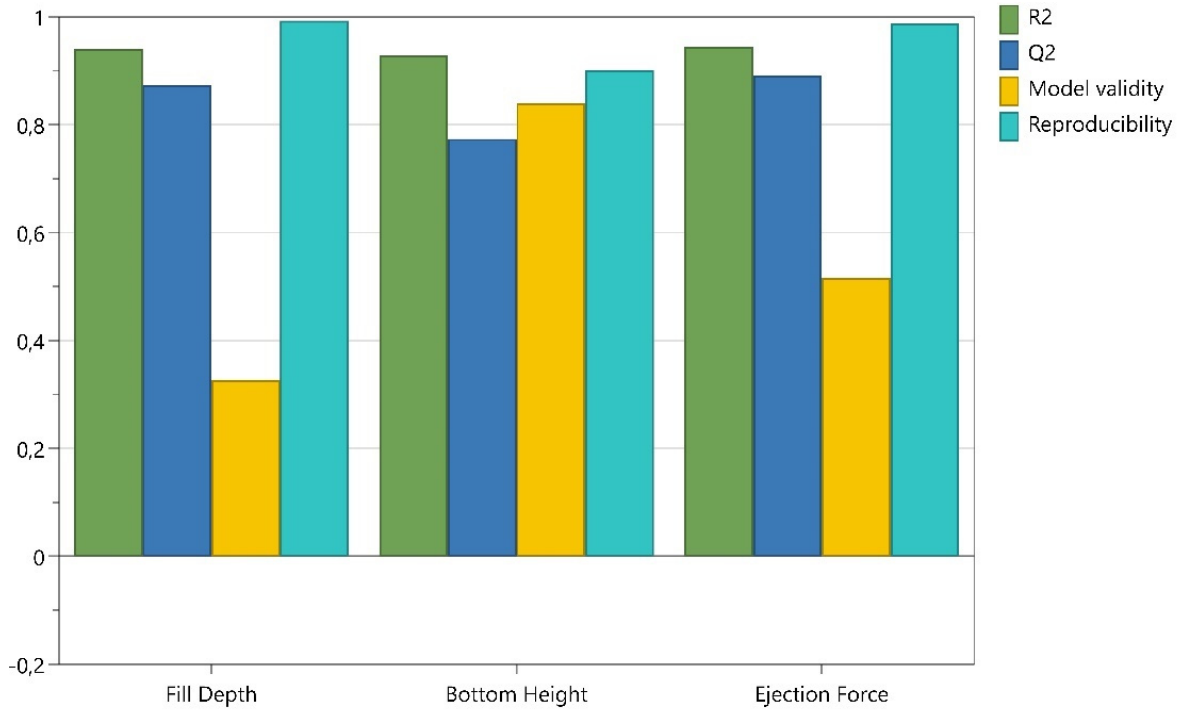

Figure 38 Summary of fit including R^2, Q^2, Model validity and Reproducibility for all tableting parameters.

The data points showed a straight line on a diagonal and only data point 1 of EF was outside the red lines. Considering Figure 40, point 1 did not differ noticeably from the observed value. Moreover, the predictions were similar to the observed values indicating a good model performance.

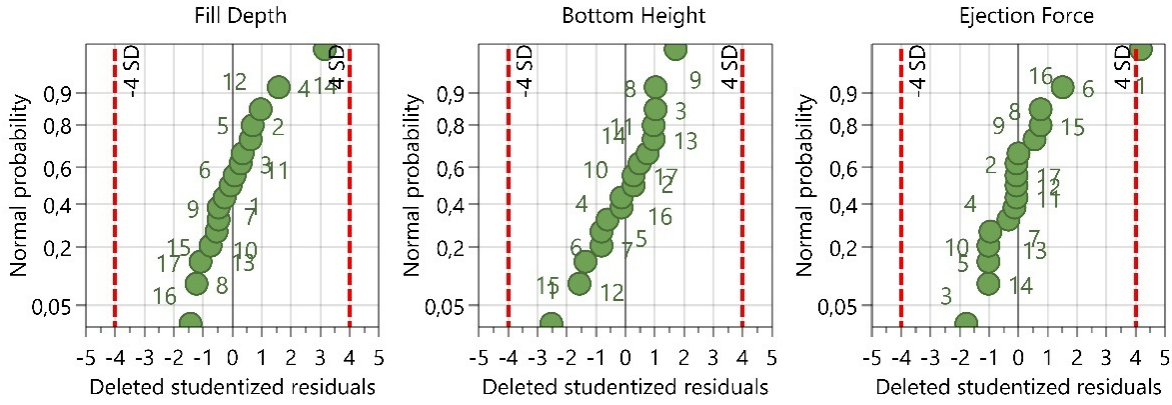

Figure 39 Overview of the residuals normal probability plots for all tableting parameters. The numbers of the data points are referred to the experiment no., as shown in Table 24.

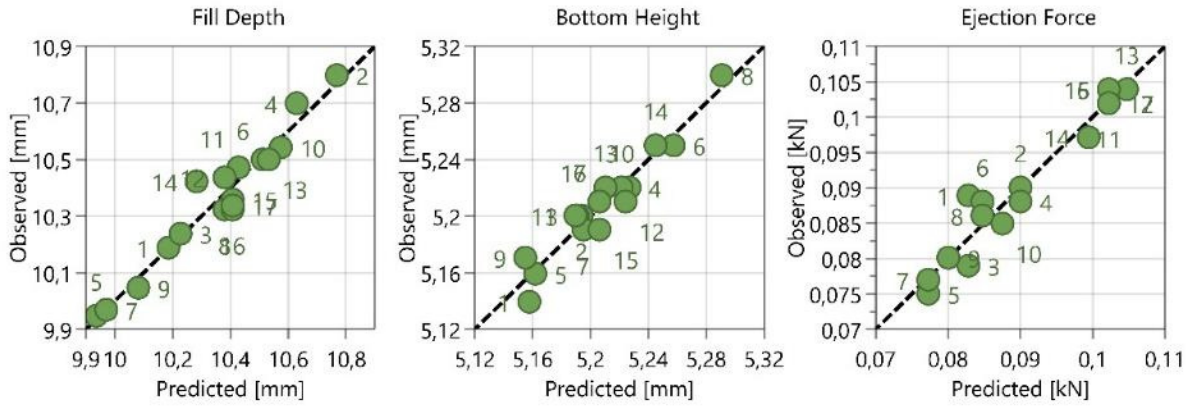

Figure 40 Overview of the comparison between observed and predicted values. The numbers of the data points are referred to the experiment no., as shown in Table 24.

7.5.3.1 **Fill Depth**

Higher powder density (CBD) resulted in lower fill depths to fulfill the weight requirements, which could be confirmed in this paper (-0.844 p<0.0001). As described above, the density of the blend was a function of TBP. That was why fill depth was also adjusted according to changes in TBP (-0.775 p<0.0001). Figure 41 a) shows the comparison between CBD and fill depth in dependence of TBP, where increasing TBP resulted in higher density values and, therefore, lower required fill depths. According to the TBP (eq. (3)) and DoE results in Figure 37, this observation could be confirmed since impeller speed was shown as negative and throughput as a positive model term on fill depth values.

As already described, after a specific number of revolutions, neither CBD nor FD values showed further changes with increasing TBP.

Figure 41 b) shows the fill depth as a function of particle size (d_{10}). In general, smaller particle sizes are considered to decrease essential flowability, impacting a complete fill of the dies (Goh et al., 2018).

Regarding the die filling process described by Xie and Puri (Xie and Puri, 2006), for powders with smaller particles, it is more challenging to lose entrained air due to cohesion during filling. Therefore, it needs more volume and higher fill depths, respectively. In this work, the correlation could be traced back again to lubrication as described before and not to cohesion (-0.224 p=0.387).

Osorio and Muzzio showed that higher powder compressibility values increase weight variability during capsule filling. Additionally, capsule weight decreased as powder compressibility increased (Osorio and Muzzio, 2013). The same principle applies for die filling in this study, where higher powder compressibility led to higher fill depth values (0.703 p<0.002), as shown in Figure 41 c). This observation may also be helpful if a capsule machine would be used instead of a tablet press in continuous downstream processing.

a)

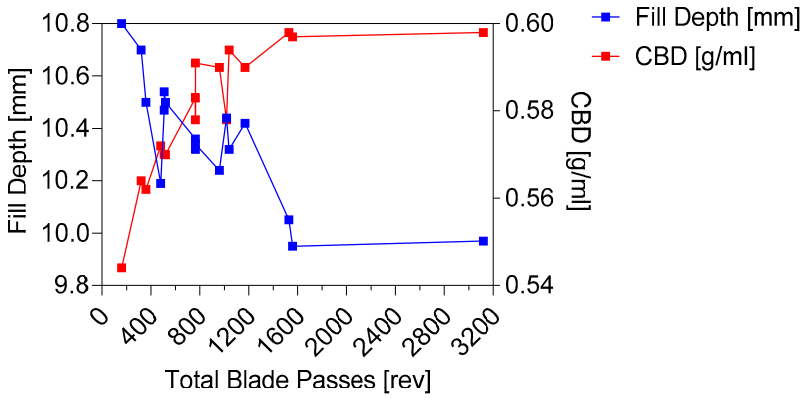

b)

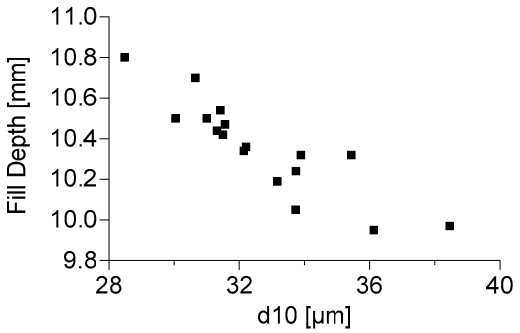

c)

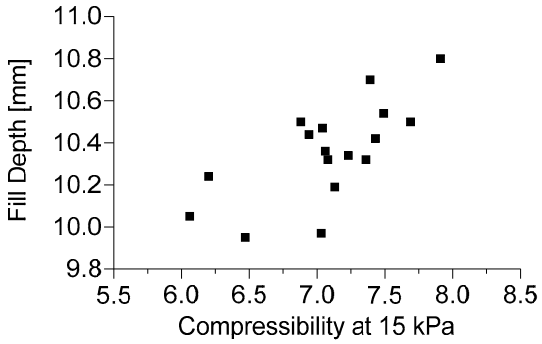

Figure 41 Shows fill depth as a function of total blade passes compared to bulk density (a). b) Shows the linearity between fill depth and d_{10} values and c) reflects the impact of compressibility on fill depth.

7.5.3.2 **Ejection Force**

The ejection force is required to eject the tablet from the die and depends on the friction between the tablet and the die walls. Consequently, the reduction in ejection force is mainly influenced by the lubrication of the powder (Uzondu et al., 2018). Usually, high ejection forces are accompanied by tableting problems and may cause damage to the tooling (Anuar and Briscoe, 2009; Dun et al., 2020).

Regarding this data set, the model terms throughput and impeller speed shared the same deflections as for fill depth (Figure 37). I.e. it is indicated that higher TBP result in higher lubrication and lower ejection forces. However, although a strong correlation between ejection force and TBP was expected, only a correlation between ejection force and tablet weight variability could be found (0.787 p=0.0002). Nevertheless, a robust model regarding ejection force could be obtained by an MLR analysis (Q^2=0.892 & R^2=0.944). For further explanation regarding TBP and ejection force, see section A.2.1 Ejection Force.

7.5.4 **Tablet Properties**

To investigate the impact of CMT parameters on the tablet properties, the tensile strength (TS), tablet weight (TW) and tablet thickness (TT) obtained during steady-state at 275 MPa compression pressure were evaluated.

In Figure 42, it can be observed that, besides the three input factors, THR, HUM and IMP, THR*THR, THR*IMP and HUM*IMP are significant model terms for tensile strength. That means higher THR, lower HUM and lower IMP resulted in lower TBP and, therefore, lower lubrication, which increased the tensile strength of the tablets. Further explanations regarding TBP and tablet properties can be seen in paragraph 7.5.4.2 Tensile Strength.

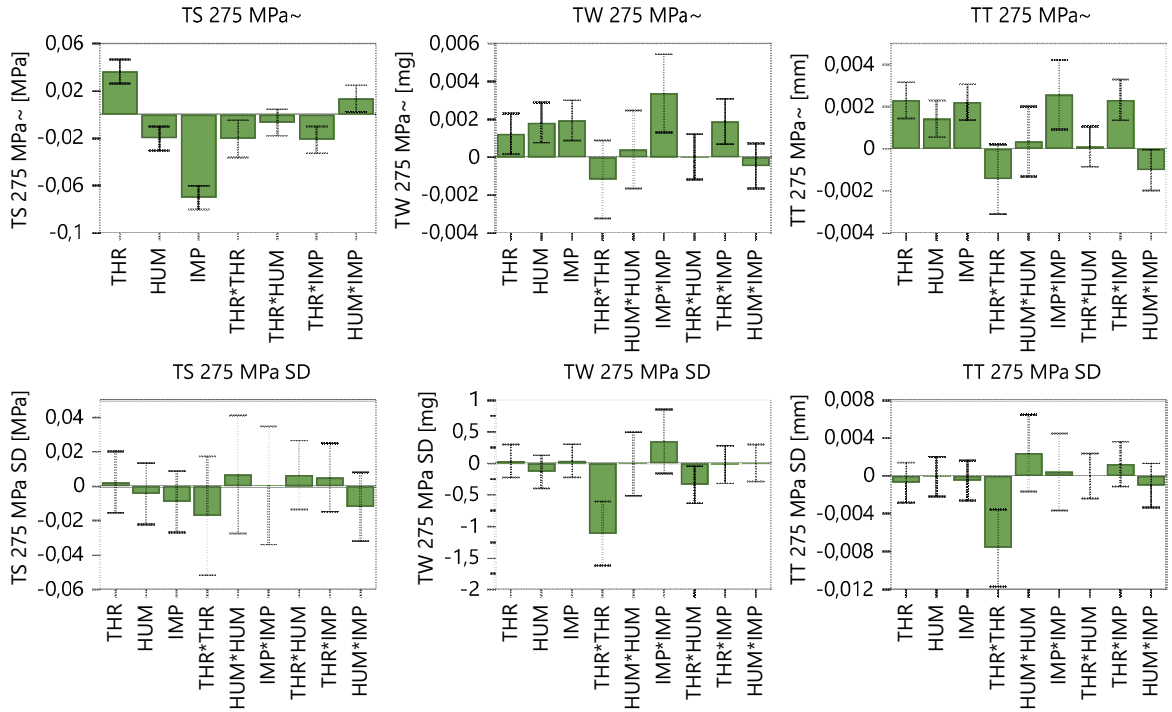

Figure 42 Model terms regarding tensile strength (TS), tablet weight (TW), tablet thickness (TT) and corresponding standard deviation. The 95 % confidence interval is displayed as an error bar.

On the other hand, the tablet weight and thickness are both influenced by similar input variables. As the tablet-weight variance was always within control limits, an automatic weight adjustment did not occur. Consequently, TW was impacted by the density of the blends and

FD. Considering the MLR, the high IMP, high IMP^2 and high THR*IMP resulted in higher TBP and densities. Since the FD adjustments only occasionally occurred when the pre-compression displacement exceeded internal limits at which the calculated weights were too high/low, higher powder density resulted in higher TW. Regarding variability in tablet properties, throughput has the highest impact on tablet weight and thickness standard deviations, whereas no significant model term regarding TS SD could be found.

According to Table 29, tensile strength, tablet weight and tablet thickness can be considered good models. Again, as the variabilities of the responses were not linearly distributed, a logarithmic data transformation was conducted.

Table 29 Overview of fit statistics regarding tablet properties.

Response Factor	Data Transformation	Q^2	R^2	Adjusted R^2
Tensile Strength	Logarithmic	0.907	0.976	0.958
Tensile Strength SD	-	-0.090	0.283	0.117
Tablet Weight	Logarithmic	0.641	0.904	0.847
Tablet Weight SD	-	0.472	0.856	0.770
Tablet Thickness	Logarithmic	0.718	0.953	0.917
Tablet Thickness SD	-	0.395	0.694	0.592

For the tableting properties, the following model equations could be obtained:

$$Log_{10}(TS) = 0.364822 + 0.017798 * THR - 0.000162112 * HUM - 0.00030635 * IMP - 0.000204041 * THR^2 - 3.32993 * 10^{-6} * THR * HUM - 9.37246 * 10^{-6} * THR * IMP + 3.0309 * 10^{-7} * HUM * IMP \quad (24)$$

$$Log_{10}(TW) = 604.751 + 0.245558 * THR + 0.0126548 * HUM - 0.0934296 * IMP - 0.0142736 * THR^2 + 9.65444 * 10^{-5} * IMP^2 + 0.00117056 * THR * IMP \quad (25)$$

$$Log_{10}(TT) = 0.680735 + 0.000321726 * THR + 1.6724 * 10^{-5} * HUM - 4.24101 * 10^{-5} * IMP - 1.32394 * 10^{-5} * THR^2 + 5.31267 * 10^{-8} * IMP^2 + 1.0325 * 10^{-6} * THR * IMP - 2.25652 * 10^{-8} * HUM * IMP \quad (26)$$

The following figures show further information regarding the model fit.

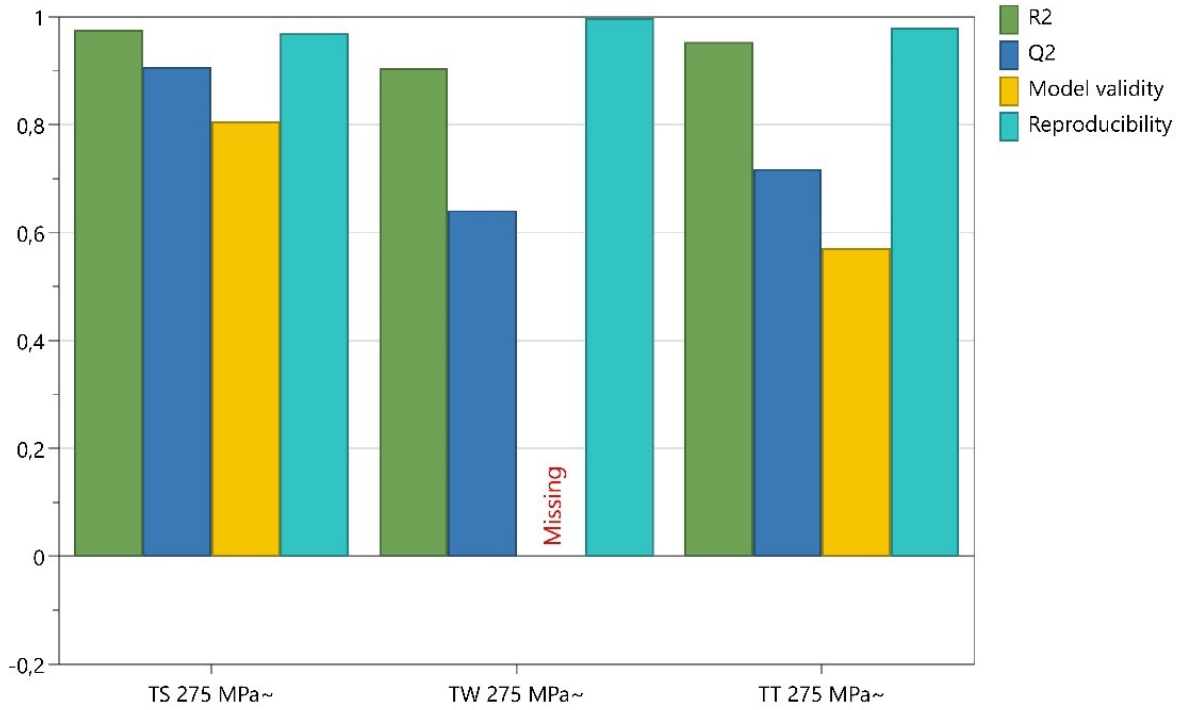

Figure 43 Summary of fit including R^2, Q^2, Model validity and Reproducibility for all tablet properties.

A minimal variability can explain the missing model validity in tablet weight at the three replicates, where two values are identical (597.97 mg / 597.97 mg/ 598.34 mg). The model validity of TS and TT was acceptable. Straight data lines on a diagonal in the residual normal probability plot and good data coverage of observed vs. predicted values indicate a good model performance.

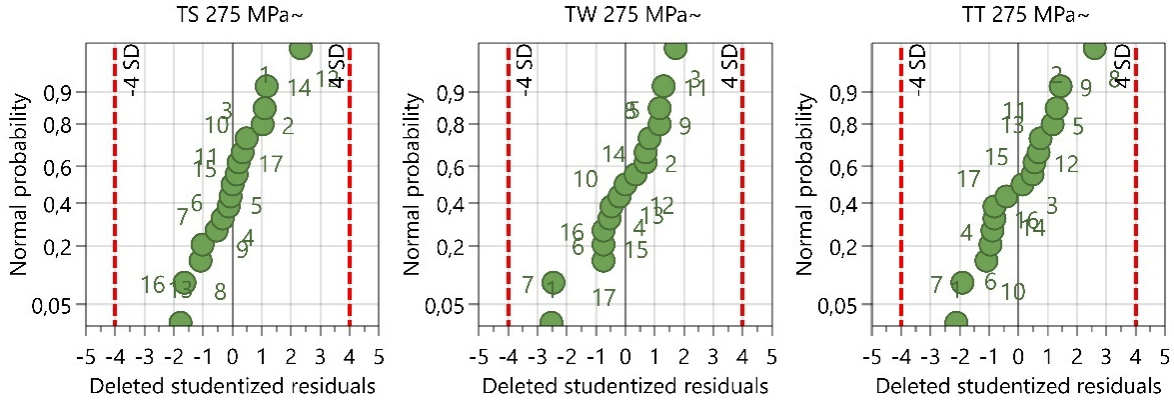

Figure 44 Overview of the residuals normal probability plots for all tablet properties. The numbers of the data points are referred to the experiment no., as shown in Table 24.

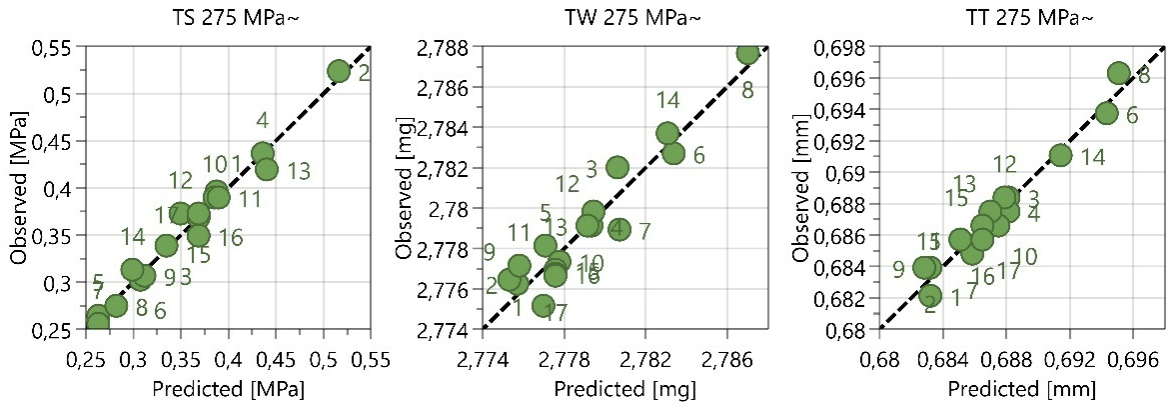

Figure 45 Overview of the comparison between observed and predicted values. The numbers of the data points are referred to the experiment no., as shown in Table 24.

7.5.4.1 **Tablet Weight and Tablet Thickness**

Even if good models for TS, TW and TT could be found, only a few correlations regarding TW and TT could be obtained (see paragraph 7.5.3.2 Ejection Force).

7.5.4.2 **Tensile Strength**

Figure 46 demonstrates the TS as a function of TBP (-0.704 p=0.002) where higher TBP resulted in lower TS at the same compression pressure (275 MPa) due to increased lubrication efficiency. According to the DoE results in Figure 42, the significant model terms corresponded to the TBP equation (3), where higher throughput, lower HUM, and lower impeller speed result in lower TBP and, therefore, higher tensile strengths of the tablets. If previous process states need to be optimized by adapting CMT parameters, similar TBP should be maintained to ensure the correct TS.

Again, exceeding 1560 revolutions, a plateau was reached and no further reduction in tensile strength could be noticed at increasing TBP.

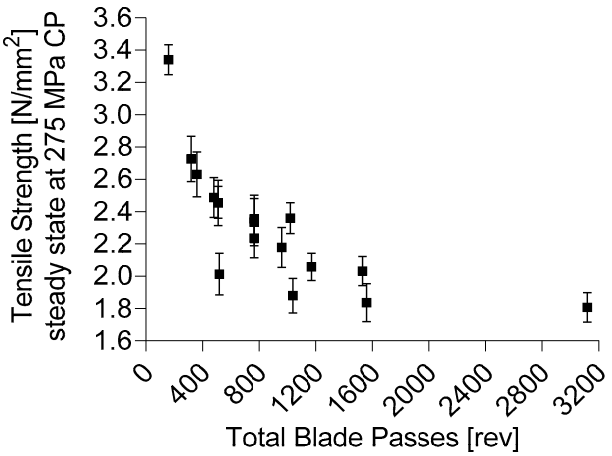

Figure 46 TS as a function of TBP at 275 MPa compression pressure.

7.5.4.3 **Compression Pressure/Tensile Strength Profile**

Compression pressure/tensile strength profiles were conducted using 118, 157, 169, 236 and 275 MPa compression pressure. During phase 16 (=experiment 16), no compression pressure/tensile strength profile could be performed because HUM increased from 0.8 kg to ~1.1 kg and the exit valve opened up to 45 mm without any chance to decrease. So, a consistent process flow could not be reached and the correct FD and compression pressure setting was not possible. Figure 47 includes the TS as a function of the corresponding compression pressure and TBP. Figure 47 a) demonstrates the profiles of each phase as a function of compression pressure, where the lowest TBP showed the highest values. Figure 47 b) reflects the TS as a function of TBP, where higher compression pressure led to profiles with higher values.

a)

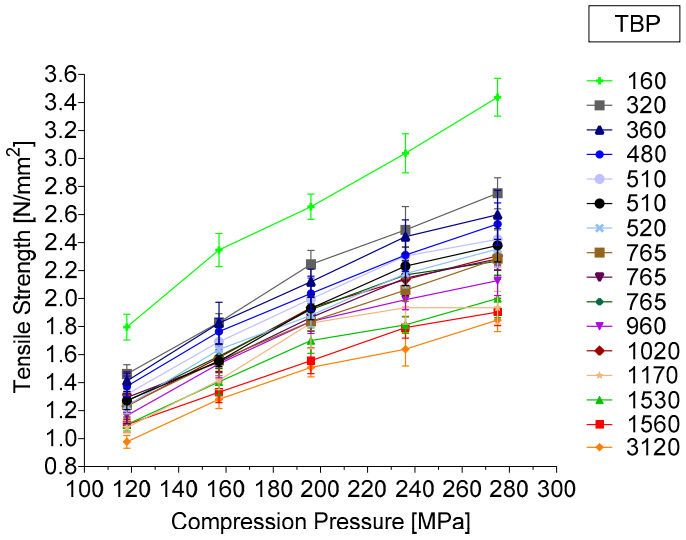

b)

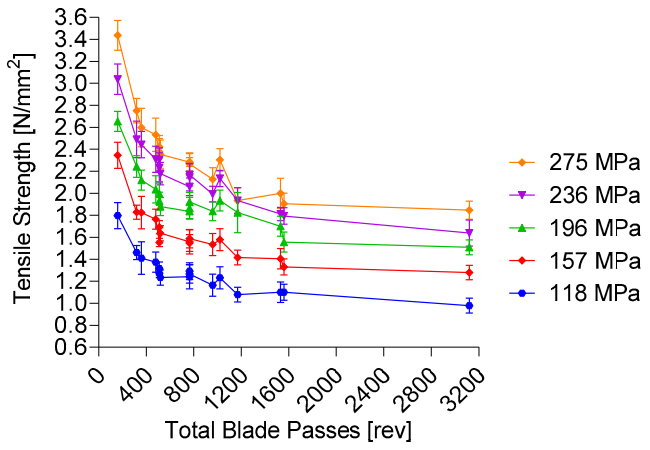

Figure 47 a) Shows an overview of all phases (TBP) regarding compression pressure and tensile strength. b) Shows an overview of all compression pressures and the corresponding tensile strength based on the lubrication (TBP).

Table 30 shows the fit statistics regarding the TS obtained dependent on the applied compression pressure.

Table 30 Overview of fit statistics regarding tensile strengths obtained dependent on the applied compression pressure.

Response Factor	Data Transformation	Q^2	R^2	Adjusted R^2
Tensile Strength at 118 MPa	Logarithmic	0.905	0.958	0.942
Tensile Strength at 157 MPa	Logarithmic	0.877	0.963	0.944
Tensile Strength at 169 MPa	Logarithmic	0.870	0.940	0.918
Tensile Strength at 236 MPa	Logarithmic	0.923	0.978	0.964
Tensile Strength at 275 MPa	Logarithmic	0.927	0.975	0.963

7.6 **Sweet Spot**

Using MODDE, it is possible to detect a sweet spot where several criteria are met. For this chapter, exit valve opening width (1 – 5 mm), blend potency SD (0 – 3 %), tensile strength (2 – 3 MPa) and tablet weight variability (0 – 2.5 mg) are considered critical parameters. In parentheses, the range of favorable process values are given. Figure 48 shows a visualization at which combination of input variables (throughput, hold up mass and impeller speed) all criteria are met (light green). No sweet spot could be achieved at an impeller speed of 650 rpm. With reducing impeller speeds, sweet spots at low throughputs are possible at 425 and 200 rpm. At 200 rpm, sweet spots could be achieved at low throughputs independent of HUM. Since running the process with higher throughputs is preferred, an optimal setting for this formulation can be observed at a combination of high throughputs and high HUM values at 200 rpm impeller speed.

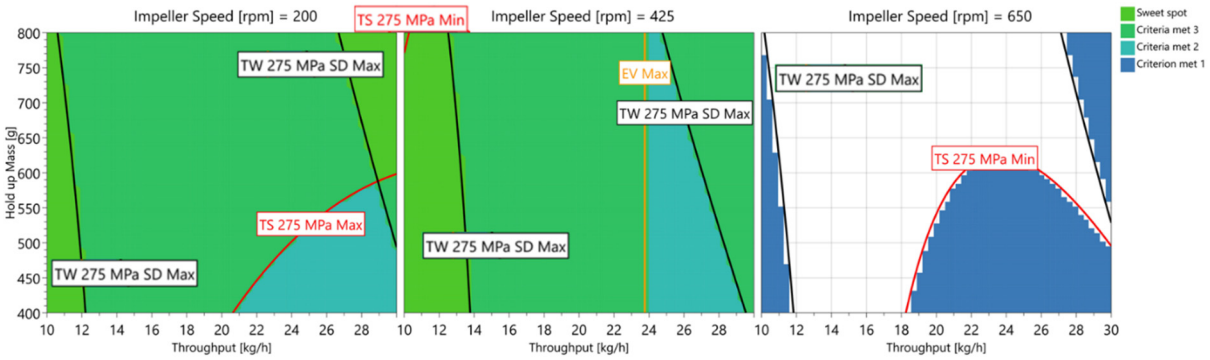

Figure 48 The sweet spot (light green) reveals the combination of the DoE input variables in which the criteria are met. The color of the borders indicates which criterion is not met anymore. Black borders = TW SD, red borders = TS and orange boarders = EV.

7.7 **Conclusion**

This chapter evaluated the downstream process states based on throughput, hold up mass and impeller speed in a continuous direct compression line, including a single blending step in a vertical blender (CMT). For all settings in the performed DoE, the same composition and compounds were used to maintain the initial material attributes and lubrication sensitivity.
In this study, the model terms of process states based on the CMT parameters were evaluated by means of an MLR analysis. Corresponding fit statistics are shown in Table 31.

Table 31 Overview of the models obtained in this study.

Responses	**Q^2**	**R^2**	**Adjusted R^2**
Exit Valve Opening Width	0.860	0.905	0.883
Exit Valve Opening Width SD	0.822	0.933	0.893
Torque of Lower Impeller	0.851	0.916	0.896
Torque of Lower Impeller SD	0.882	0.949	0.933
Conditioned Bulk Density	0.735	0.850	0.816
Flow Rate Index	0.800	0.896	0.848
Fill Depth	0.873	0.941	0.914
Bottom Main Compression Height	0.774	0.928	0.885
Ejection Force	0.892	0.944	0.931
Tablet Thickness	0.718	0.953	0.917
Tablet Weight	0.642	0.904	0.847
Tensile Strength	0.907	0.976	0.958

Furthermore, the connections between the parameters were evaluated. Regarding mixing parameters, it has been shown that exit valve opening width and variability in exit valve, hold up mass, torque and blend potency correlate significantly, which can all be controlled mainly by impeller speed. If improvement of these parameters is required, it needs to be considered that changes in impeller speed also led to changes in TBP.
With higher TBP, more shear is transmitted to the powder and more magnesium stearate is adhered to the remaining particles, leading to more lubrication and higher variation in material attributes. Hence, TBP significantly correlated with the blend's material attributes (CBD, d_{10} values and flow rate index), fill depth and tensile strength of the tablets.
Target criteria (exit valve opening width (1 – 5 mm), blend potency SD (0 – 3 %), tensile strength (2 – 3 MPa) and tablet weight variability (0 – 2.5 mg)) could generally be found at impeller speeds between 200 rpm and 425 rpm and at throughputs between 10 and 12 kg/h independent of HUM. To run the process as fast as possible, high THR, high HUM, and 200 rpm IMP are required to fulfil the target criteria and represent the optimal setting for this formulation.

8 Verification of the Derived Process Model Using Alternative Raw Materials

8.1 Introduction

In ICH Q8 “Pharmaceutical Development”, it is described that material attributes of the ingredients in a pharmaceutical process need to be defined to provide a consistent quality of the excipients to ensure a stable process performance and operate within a specific design space (ICH, 2009). If a change regarding the formulation or powder composition needs to be made, the impact of material attributes within the new formulation should therefore be evaluated and the design space and corresponding quality attributes (see section 2.1.4) investigated again. Therefore, a holistic understanding of the process is beneficial for estimating the potentially affected process parameters. For that, comprehension of the fundamental process dependencies is required. Many studies focused on that matter to investigate the impact of material attributes on individual process steps. To name a few, Van Snick et al. described that the impact on critical process parameters could differ from one material to another (Snick, 2017a). Furukawa et al. described the MRT in the feed frame and the dependence on the material attributes (Furukawa, 2020).

Moreover, several studies confirmed the impact of material grades on tablets. Landin et al. showed that different grades of MCC changed the properties of the tablets and Haware et al. published that smaller particle sizes resulted in higher tensile strengths of the tablets, which confirms the studies of Almaya et al. who described the dependence of particle size on the TS as well (Almaya and Aburub, 2008; Haware et al., 2010; Landín et al., 1993). Furthermore, they showed the impact of raw material grades on the individual lubricant sensitivity, where smaller particles were less affected by MgSt. Van Snick et al. found that ingredients with better flowability properties resulted in lower tablet weight variability (Snick, 2017a). These findings implicate a strong influence on tablet properties by varying excipients and attributes of the ingredients, respectively. So, altering raw materials within a formulation impacts the pharmaceutical manufacturing process and needs further investigation. As described in ICH Q8, changes in formulations should be seen as additional gain in information to establish a design space (ICH, 2009). Therefore, using an alternative formulation, this chapter evaluates the process dependencies in a continuous process intending to confirm universal process connections.

8.2 Aims and Scope

In chapter 7, a comprehensive study was carried out to investigate the impact of CMT parameters on the downstream continuous process using F2. Predictive models, correlations and parameter connections could be found. To evaluate the applicability of the models, an alternative formulation was determined and applied in this chapter. For better comparability, the same design was used with slight changes in impeller speed. This study aimed to confirm the qualitative parameter relationships with a different set of materials.

8.3 Materials

To confirm the findings of chapter 7, an alternative formulation was evaluated. To identify suitable ingredient combinations, pretests were conducted to develop the formulation.

8.3.1 Mixtures for the Pretest

To determine a practical alternative formulation and to evaluate the differences in the potential raw materials, nine tests were carried out, where THR, HUM and IMP remained constant and a compression pressure/tensile strength profile was conducted using 100, 150, 200, 250 MPa compression pressure for each combination. Table 32 shows the material combination, the corresponding composition and the CMT settings. The results of the compression pressure/tensile strength profile are shown in section 8.5.1 Pre-test Results and Determination of the Formulation.

Table 32 Settings used for the pre-tests to evaluate the impact of the different raw materials on the tensile strength of the tablets. The CMT parameters remained constant at 10 kg/h, 800 g and 575 rpm impeller speed.

Blend No.	CMT Settings	Composition	
		Material Combination	[%]
R1		TCC/SSF	98:2
R2		MCC/SSF	98:2
R3		Lactose/SSF	98:2
R4	THR: 10 kg/h	Mannitol/SSF	98:2
M1	HUM: 800 g	TCC/Mannitol/SSF	49:49:2
M1a	IMP: 575 rpm	TCC/Mannitol/SSF	48.5:48.5:3
M2		TCC/MCC/SSF	49:49:2
M3		TCC/Lactose/SSF	49:49:2
M4		TCC/Saccharin/SSF	68.6:29.4:2

To ensure a consistent powder supply following feeder settings were adjusted

Table 33 Composition and feeder settings used for the pretests to determine a suitable formulation.

Blend No.	Raw Material	Composition [%]	Top Up Volume [L]	Screw Pitch [mm/rev]	Gearbox Type	Refill Level [L]
R1	TCC TB	98	1.6	20	1	0.5
	SSF	2	0.8	10	3	1.0
R2	MCC	98	1.6	20	1	0.5
	SSF	2	0.8	10	3	1.0
R3	Lactose	98	1.6	20	1	0.5
	SSF	2	0.8	10	3	1.0
R4	Mannitol	98	1.6	20	1	0.5
	SSF	2	0.8	10	3	1.0
M1	TCC	49	1.6	20	1	0.5
	Mannitol	49	1.6	20	1	0.5
	SSF	2	0.8	10	3	1.0
M1a	TCC	48.5	1.6	20	1	0.5
	Mannitol	48.5	1.6	20	1	0.5
	SSF	3	0.8	10	3	1.0
M2	TCC	49	1.6	20	1	0.5
	MCC	49	1.6	20	1	0.5
	SSF	2	0.8	10	3	1.0
M3	TCC	49	1.6	20	1	0.5
	Lactose	49	1.6	20	1	0.5
	SSF	2	0.8	10	3	1.0
M4	TCC	68.6	1.6	20	1	0.5
	Saccharin	29.4	1.6	20	1	0.5
	SSF	2	0.8	10	3	1.0

8.4 **DoE Settings**

For this DoE, referred to as DoE 3, the same design used in chapter 7 was utilized. Therefore, the central composite face design with star points at the face of each side defined by a 2-level factorial design was repeated where a quadratic model was used. The impeller speed in this design was reduced to 500 rpm to prevent an extensive opening of the exit valve, as shown in Table 34.

Compounds and composition remained constant over the entire experiment. In general, 17 runs, including 3 replicates of a center point, were performed. After adjusting the new CMT parameters, a transition phase (3 x MRT) was initiated to wash out the powder mixed at the

former setting. After the transition phase, the process was run for at least 10 minutes in a steady-state phase. By means of the combitester, a compression pressure/tensile strength profile was conducted using 100, 150, 200 and 250 MPa compression pressure and 21 MPa pre-compression pressure for each phase. The tablet press was operated in manual mode the entire time and FD was adjusted manually. After each compression pressure/tensile strength profile, a powder sample was withdrawn at the end of each steady-state phase by opening the sampling port underneath the feed frame and collecting approximately 300 g of powder.

Table 34 DoE settings, where phase 7, 9 and 11 are the replicates of the center point. MRT and TBP are calculated based on the CMT parameters (eq. (2) and (3)).

phase	Experiment No.	THR [kg/h]	HUM [g]	IMP [rpm]	MRT [min]	TBP [rev]
1	1	10	400	200	2.4	480
2	5	10	400	500	2.4	1200
3	9	10	600	350	3.6	1260
4	3	10	800	200	4.8	960
5	7	10	800	500	4.8	2400
6	11	20	400	350	1.2	420
7	15	20	600	350	1.8	630
8	13	20	600	200	1.8	360
9	16	20	600	350	1.8	630
10	12	20	800	350	2.4	840
11	17	20	600	350	1.8	630
12	14	20	600	500	1.8	900
13	2	30	400	200	0.8	160
14	6	30	400	500	0.8	400
15	10	30	600	350	1.2	420
16	8	30	800	500	1.6	800
17	4	30	800	200	1.6	320

8.5 **Results and Discussion**

8.5.1 **Pre-test Results and Determination of the Formulation**

To determine an alternative formulation, pretests were conducted with TCC, MCC, lactose, mannitol, saccharin and SSF.

Figure 49 shows the TS at different CPs. In a) the TS of the individual raw materials TCC, MCC, lactose and mannitol mixed only with the lubricant (SSF) at 98% and 2% are shown. It is noticeable that lactose and SSF resulted in the lowest tensile strength, whereas TCC/SSF, MCC/SSF and mannitol/SSF resulted in considerably higher TS. In b) the used formulations are based on TCC and SSF. So, five runs were carried out to evaluate the impact of the raw material combinations on the TS. As already shown in a), the run with lactose resulted again in low TS. Also, the test run with saccharin revealed low TS values. Since saccharin is used as an API surrogate, an ingredient combination that resulted in higher TS values was required. Therefore, it was decided to use mannitol as the second filling material in the formulation since the exit valve behavior with this composition was better than at the settings with TCC and MCC. Hence, to determine F3, the API surrogate saccharin and the disintegrant SSG were added to M3, as shown in Table 35.

a)

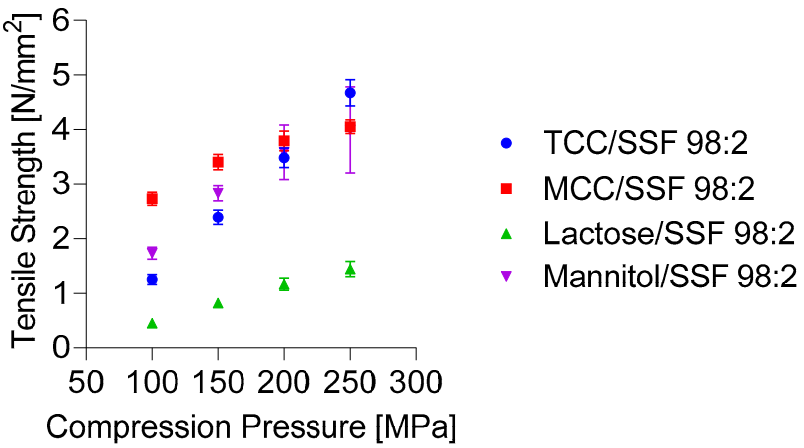

b)

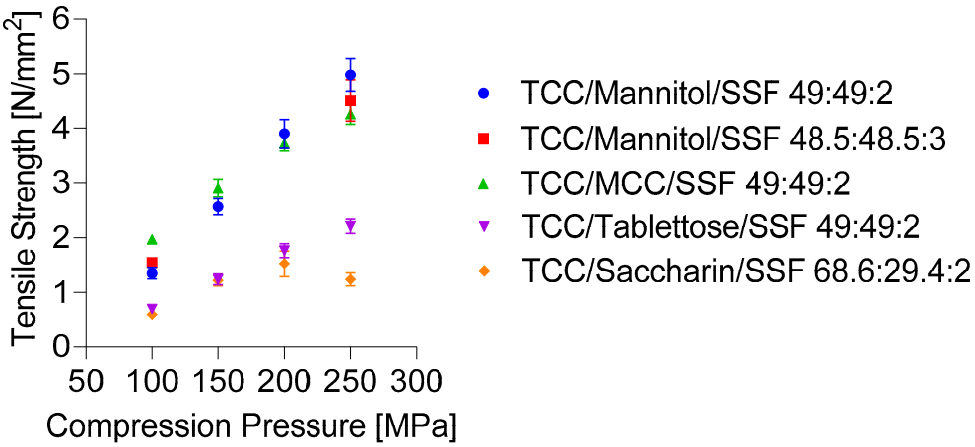

Figure 49 a) shows the TS at different CP of the four potential raw materials used in the formulation only mixed with SSF. b) shows the TS obtained by different combinations of TCC, SSF and mannitol, MCC, lactose or saccharin.

Based on experience, saccharin was set to 22 %, SSG to 3 % and SSF to 2 %. TCC and mannitol were set in a 2:1 ratio.

Table 35 Composition and feeder settings for each raw material of F3.

	TCC	**Saccharin**	**Mannitol**	**SSG**	**SSF**
Composition [%]	48.67	22.00	24.33	3.00	2.00
Top up Volume [L]	1.6	1.2	1.6	0.8	0.8
Gearbox Type	1 (63:1)	2 (235:1)	2 (235:1)	3 (455:1)	3 (455:1)
Screw Pitch [mm/rev]	20	10	20	10	10
Refill Level [L]	0.55	0.74	0.5	0.85	1.0

The corresponding raw material attributes are shown in Table 36.

Table 36 FT4 data and particle size distribution (Helos) of the individual raw materials.

	CBD* **[g/ml]**	**FRI***	**Comp**** **[%]**	**Cohesion***** **[kPa]**	**FFc*****
Mannitol	0.491±0.002	1.06±0.03	7.30±0.34	0.49±0.004	35.4±19.93
TCC	0.610±0.004	1.04±0.05	5.37±0.15	0.63±0.013	42.6±n/a
Saccharin	0.583±0.014	1.05±0.08	34.80±0.56	0.56±0.018	2.1±0.14
SSG	0.757±0.007	1.03±0.05	6.11±0.52	0.75±0.006	29.7±1.89
SSF	0.300±0.010	3.58±0.37	38.37±1.99	0.31±0.010	3.5±0.32
Lactose	0.632±0.002	1.20±0.06	10.67±0.06	0.62±0.003	2.9±0.47
MCC	0.340±0.001	1.50±0.05	15.80±0.14	0.33±0.004	3.3±0.19

	d_{10}** **[µm]**	**d_{50}** **[µm]**	**d_{90}** **[µm]**
Mannitol	18.16±0.08	103.47±0.68	178.71±0.90
TCC	94.57±1.07	165.55±0.78	245.51±1.58
Saccharin	4.27±0.01	40.29±0.13	178.09±0.55
SSG	23.18±0.08	43.19±0.09	69.36±0.09
SSF	2.12±0.02	11.14±0.26	453.95±22.81
Lactose	29.24±0.64	154.35±5.33	421.14±37.37
MCC	30.03±1.1	118.09±3.37	242.95±13.95

*Obtained by the stability and variable flow rate method.

**Obtained by the compressibility method.

***Obtained by the shear cell.

****Obtained by Sympatec Helos.

8.5.2 DoE Results and Discussion

The same process steps, as shown in chapter 7, were evaluated in this chapter. The data set revealed the impact of THR, HUM and IMP on the response parameters regarding the mixing step (EV, EV SD, HUM SD, T_L and T_L SD), the material attributes of the blend (FRI, CBD and d_{10}), the tableting parameters (FD, BCH and EF) and the tablet properties (TS and TS SD). A visualization of where responses are expected is shown in Figure 50. For models with Q^2 > 0.500 reliable, predictive equations could be obtained.

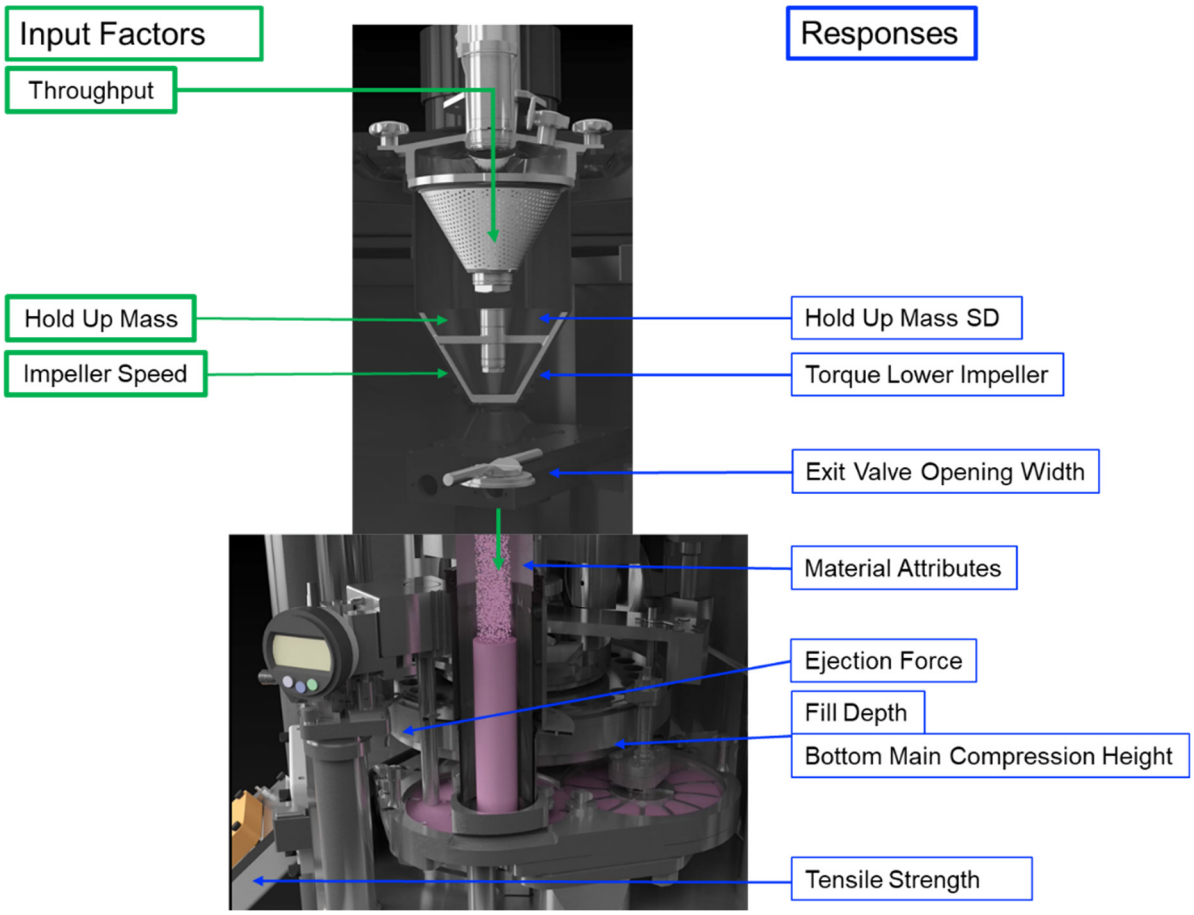

Figure 50 Process overview of input factors (green, left side) and observed responses (blue, right side).

Figure 51 demonstrates relationships between all parameters obtained and evaluated within this DoE. Starting from the CMT settings, the flowchart depicts the downstream process parameters where correlations are expected to be found. An equivalent flowchart for F2/DoE 2 in chapter 7 is shown in Figure 20, where similar parameter associations could be found.

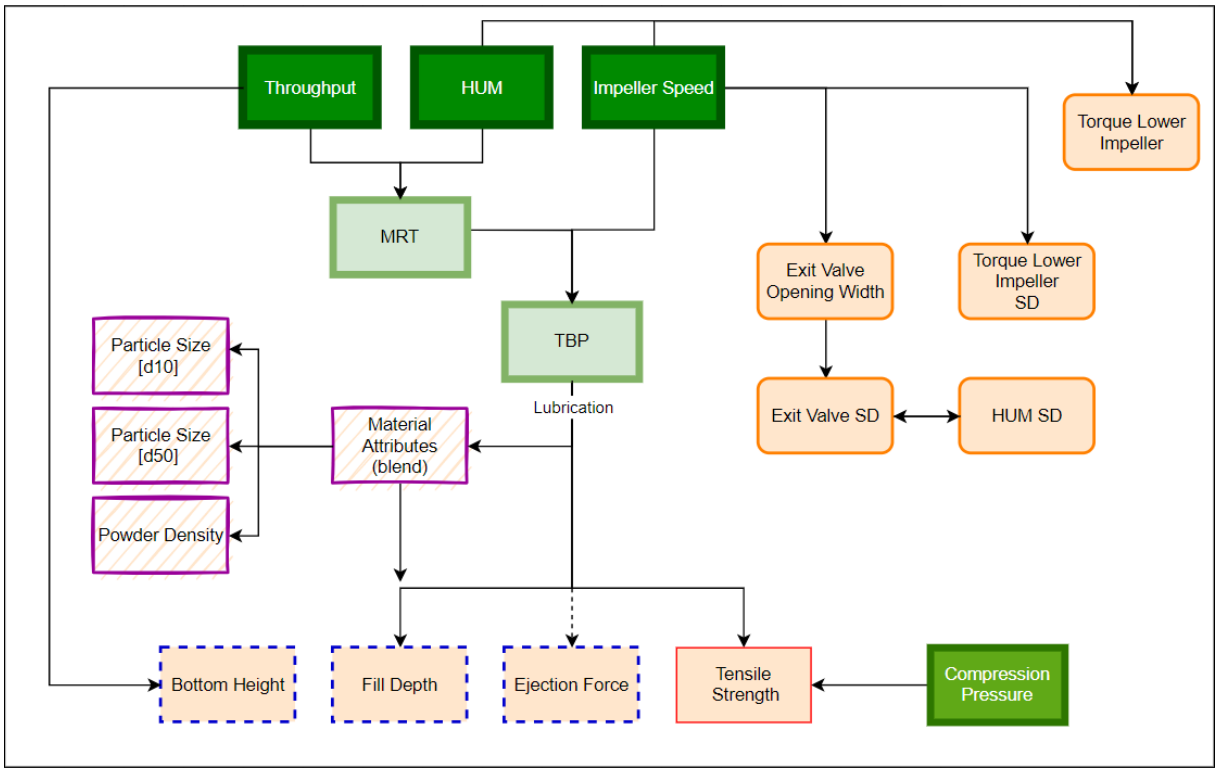

Figure 51 Qualitative overview of process parameter connections and correlations. Input factors are marked in dark green (thick borders), confounding input parameters are marked in light green and the considered response parameters are shown in light orange. The color/shape of the borders classifies the responses into mixing parameters (orange line, rounded corners), material attributes of the blend (purple, striped background), tableting parameters (blue, dotted borders) and tensile strength (red, thin borders). Compression pressure (green) is considered an independent input factor of the tablet press.

8.5.2.1 **Mixing Parameters**

Figure 52 shows the model terms of the mixing parameters EV, EV SD, HUM SD, T_L and T_L SD. Blend Potency SD was not included since no NIR probe was installed during the DoE.

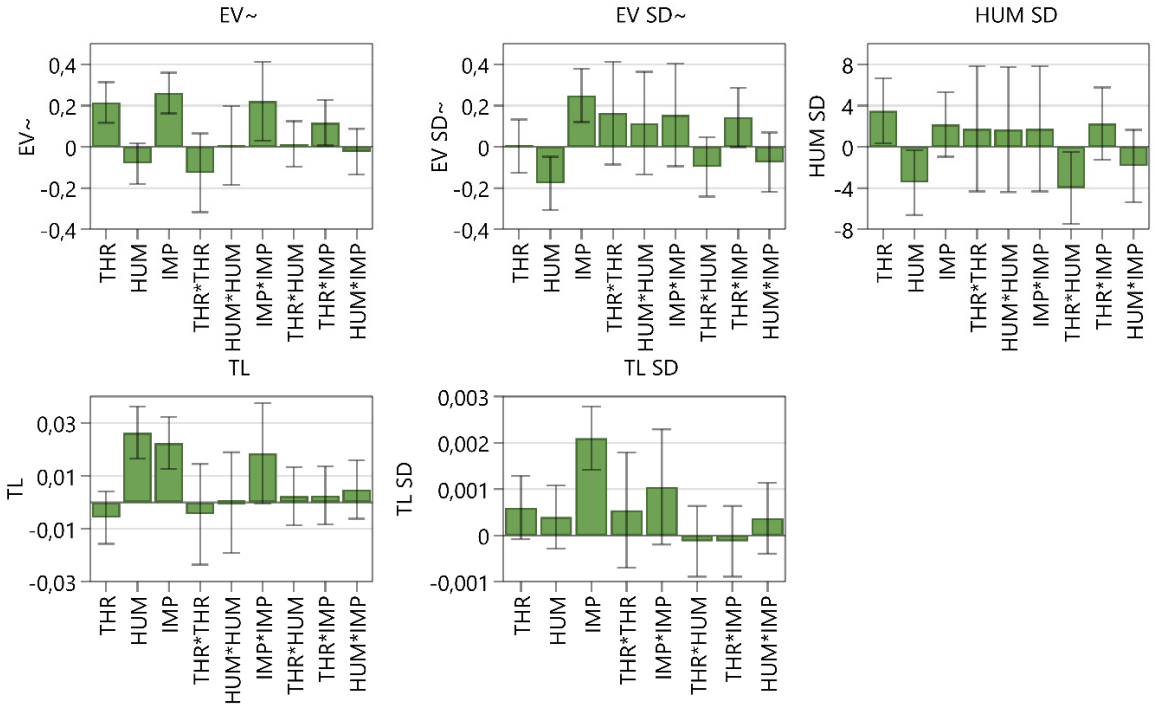

Figure 52 Coefficients plot of the impact of input variables on responses regarding the blending unit. The 95 % confidence interval is displayed as an error bar.

This DoE revealed that THR, IMP, IMP*IMP and THR*IMP significantly impacted the EV proving the importance of both CMT parameters for the powder bed shape for this formulation. Furthermore, lower EV SD could be obtained at high HUM and low IMP. The significant model term THR*IMP again proves the impact of these parameters on the powder bed. Lower HUM SD could be obtained at higher HUM, lower THR and higher THR*HUM.

As expected, the T_L was significantly impacted by HUM and IMP with a similar extent of deflection. The model term IMP*IMP shows a positive impact on T_L.

Regarding T_L variability, only IMP could be identified as a significant model term.

As shown in Table 37, Q^2 and R^2 imply that exit valve opening width and torque (+SD) can be considered good models.

Table 37 Overview of fit statistics regarding mixing parameters.

Response Factor	Data Transformation	Q^2	R^2	Adjusted R^2
Exit Valve Opening Width	Logarithmic	0.758	0.891	0.841
Exit Valve Opening Width SD	Logarithmic	0.293	0.814	0.702
HUM SD	Logarithmic	0.331	0.664	0.511
Torque Lower Impeller	-	0.780	0.895	0.860
Torque Lower Impeller SD	-	0.802	0.902	0.858

For the mixing parameters, the following model equations could be obtained:

$$Log_{10}(EV) = 1.10662 - 0.00577374 * THR - 0.00040323 * HUM - 0.00481688 * IMP + 7.13869 * 10^{-6} * IMP^2 + 7.79959 * 10^{-5} * THR * IMP \quad (27)$$

$$Log_{10}(EV\ SD) = 1.57806 - 0.11405 * THR - 0.000886621 * HUM - 0.00626313 * IMP + 0.00202846 * THR^2 + 8.60821 * 10^{-6} * IMP^2 + 9.51048 * 10^{-5} * THR * IMP \quad (28)$$

$$Log_{10}(HUM\ SD) = 0.0707124 - 0.0245042 * \mathrm{THR} + 0.000716434 * \mathrm{HUM} + 0.000923286 * \mathrm{IMP} + 0.00241599 * THR^2 - 8.86096 * 10^{-5} * THR * HUM \quad (29)$$

$$T_L = 1.10662 - 0.00058 * THR - 0.0001315 * HUM - 0.000353778 * IMP + 7.1873 * 10^{-7} * IMP^2 \quad (30)$$

$$T_L\ \mathrm{SD} = 0.0102209 - 5.7 * 10^{-5} * THR - 2.57501 * 10^{-6} * \mathrm{HUM} + 2.86111 * 10^{-5} * \mathrm{IMP} + 5.01587 * 10^{-8} * IMP^2 + 1.25 * 10^{-8} * HUM * IMP \quad (31)$$

Fit statistics of the obtained models were comparable to chapter 7 (Figure 33 - Figure 35), as shown in the following figures.

The model validity for EV, T_L and T_L SD is low or missing, which can be explained by the minimal variability of the data points at the three replicates (EV: 2.925 – 2.997 mm; T_L: 0.118 – 0.122 mm; T_L SD: 0.0080 – 0.0082 Nm).

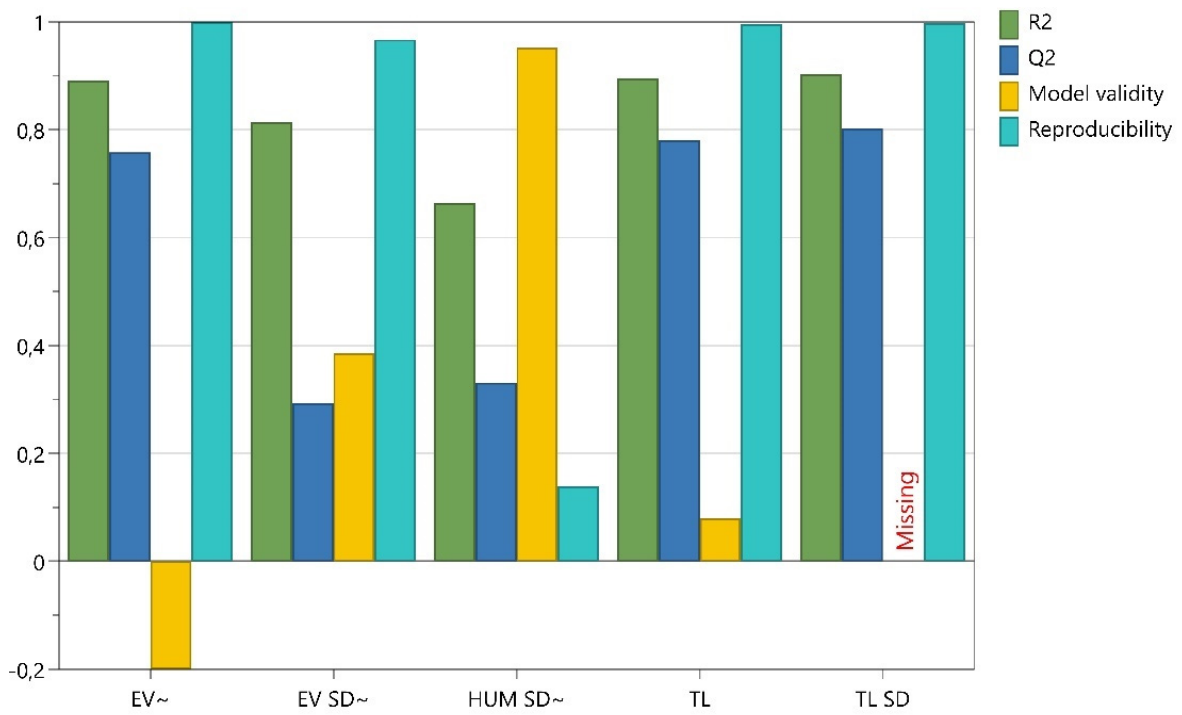

Figure 53 Summary of fit including R^2, Q^2, Model validity and Reproducibility for all mixing parameters.

The data points in Figure 54 can be considered a straight line on a diagonal, whereas for EV and T_L SD, a slightly curved pattern can be observed. Furthermore, an outlier can be observed for EV SD (point 6), which also differs from the remaining ones in Figure 55. Basically, the predictions were similar to the observed values indicating a good model performance. Only HUM SD showed noticeable differences between observed and predicted values (points 10 and 17), which the low Q^2 can explain.

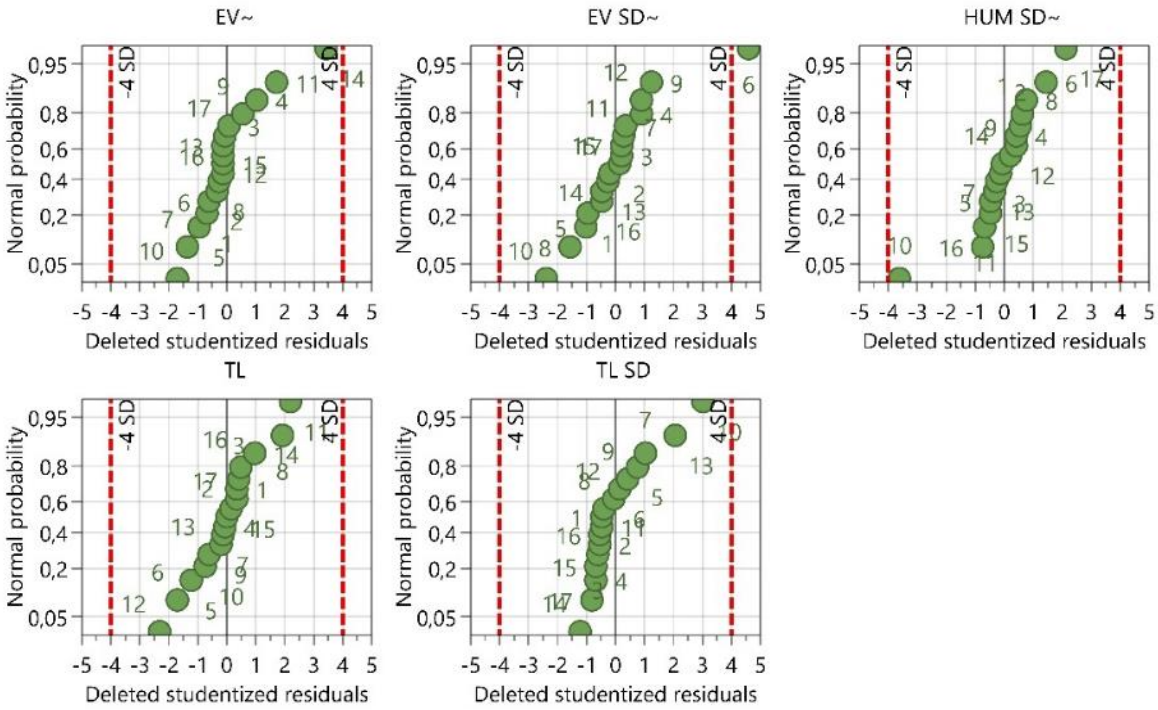

Figure 54 Overview of the residuals normal probability plots for all mixing parameters. The numbers of the data points are referred to the experiment no., as shown in Table 34.

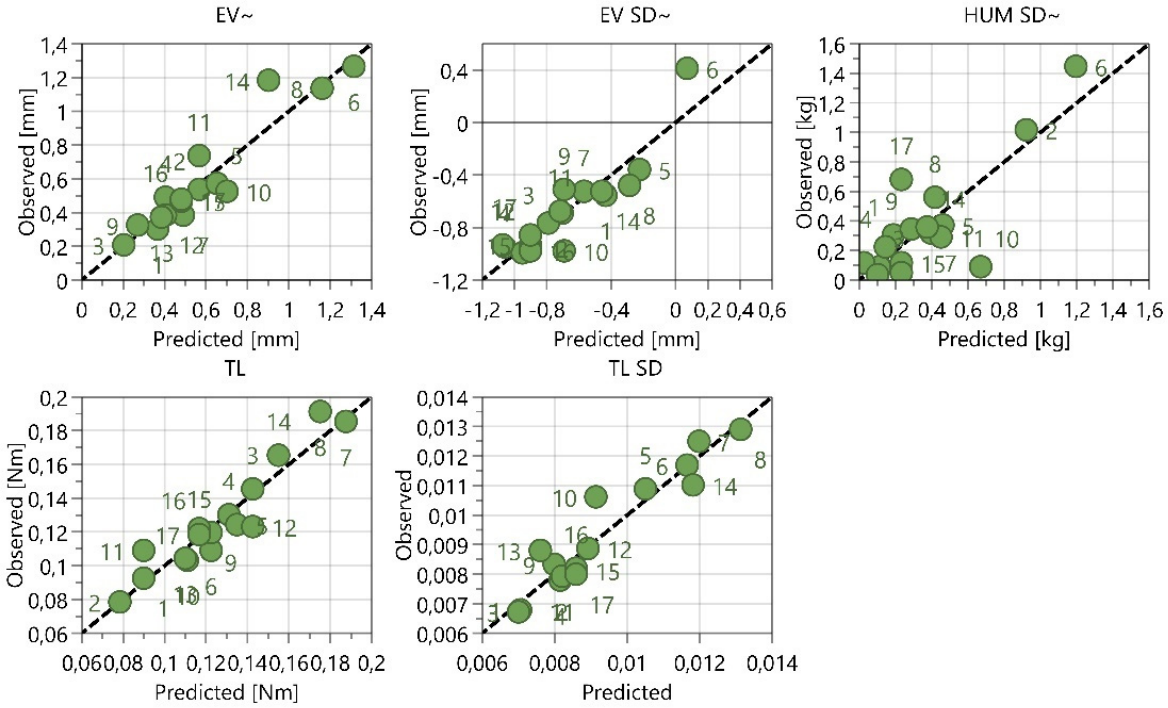

Figure 55 Overview of the comparison between observed and predicted values. The numbers of the data points are referred to the experiment no., as shown in Table 34.

Compared to Figure 21, which displays the model terms of the mixing parameter results obtained in chapter 7, similar findings could be obtained as compared in Table 38.

Table 38 Comparison of the significant model terms between F3 and F2. The mutual model terms are highlighted in bold.

	Formulation 3 (chapter 8)	**Formulation 2 (chapter 7)**
EV	**THR, IMP**, IMP*IMP, THR*IMP	**THR, IMP**
EV SD	HUM, **IMP**, THR*IMP	**IMP**
HUM SD	**THR**, **HUM**, THR*HUM	**THR, HUM,** IMP
T_L	**HUM, IMP**, IMP*IMP	**HUM, IMP**
T_L SD	**IMP**	**IMP**
Blend Potency SD	-	IMP

Therefore, the fundamental dependencies between CMT input and mixing parameters are independent of the formulation and mainly driven by THR and IMP. For example, figures regarding EV and TL were rebuilt to demonstrate the comparable behavior during the process, where higher Impeller speed and higher THR resulted in higher EV and higher HUM+IMP showed higher torque values of the lower impeller. Furthermore, HUM was not a significant model term regarding EV behavior for either F2 or this DoE and can be considered negligible for this.

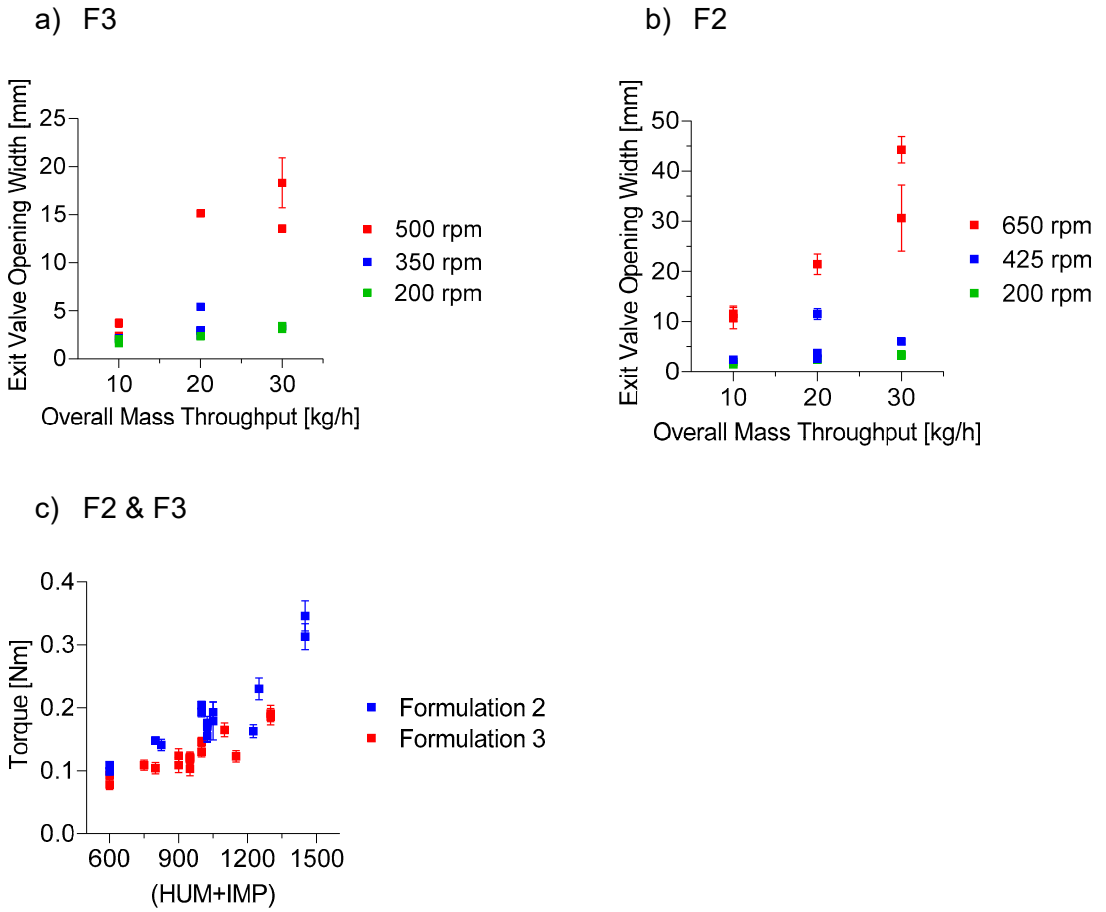

Figure 56 a+b show the comparison of the data of chapters 7 (F2) and 8 (F3) regarding EV as a function of THR and IMP. The same data sets were compared regarding TL as a function of HUM+IMP in c.

8.5.2.2 **Material Attributes of the Blend**

Figure 57 shows the model terms of the material attributes of the blend (CBD, FRI and d_{10} values), which were also discussed in chapter 7.

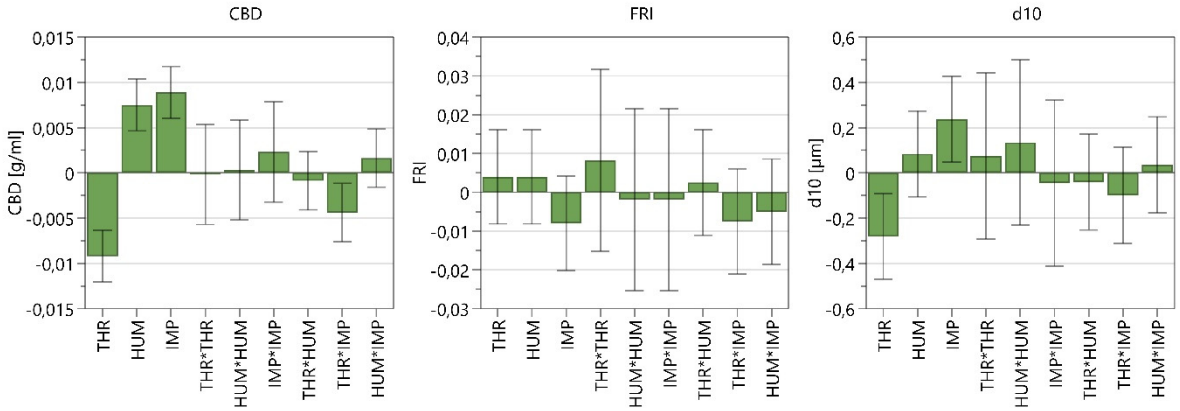

Figure 57 Coefficients plot of the impact of input variables on responses regarding the material attributes of the blend. The 95 % confidence interval is displayed as an error bar.

As expected, the significant model terms for CBD were THR, HUM and IMP, where higher THR, lower HUM and lower IMP resulted in lower TBP (eq. (3)), less lubrication and lower densities. This process behavior could already be seen in chapter 7.5.2 and was discussed in chapter 7.5.2.1 Total Blade Passes.

Figure 58 a) compares the CBD with varying TBP for both formulations. The curves looked similar, but higher values were obtained by F3, although the CBD values of the excipients in F2 were higher, as shown in Table 27 and Table 36.

For FRI, no significant model terms could be obtained as opposed to the previous chapter, where the FRI values were interpreted as a function of TBP and therefore impacted by the lubrication of the blend (-0.846 $p<0.0001$). Furthermore, no correlation between FRI and TBP for F3 could be found (-0.215 $p=0.4083$). Generally, FRI values <1 are expected for blends containing a lubricant. Surprisingly, the values obtained in this study were >1 and varied between 1.10 and 1.50, which implies less lubrication than seen for F2 (“Freeman Technology, Instruction documents: W7013 Stability and Variable Flow Rate,” 2007).

The d_{10} values were significantly impacted by THR and IMP. According to the deflection, higher TBP resulted in higher d_{10} values, which aligns with chapter 7. Figure 58 c) shows the d_{10} values of F2 and F3 as a function of TBP. Both curves show equivalent courses, whereas the values for F3 are much lower. This can be explained by the particle sizes of the excipients where SSF and saccharin showed d_{10} values <5 µm (Table 36). Again, it can be assumed that the dependence on TBP can be explained by increased magnesium stearate film formation due to higher mixing intensity, i.e. increased extent of impeller rotation, as discussed in chapter 7.5.2.4 Particle Size. This behavior resulted in a more compact powder arrangement, which can be proved by the correlation between CBD and d_{10} (0.816 $p<0.0001$). Since saccharin showed similar small values, it is expected that SSF and saccharin adhered to the particles due to the shear.

Due to the FRI results and the comparison of d_{10} values, it can be concluded, that the lubrication sensitivity and the impact of the CMT parameters on the lubrication of F3 is less pronounced than for F2, which is also further discussed in section 8.5.2.4 Tensile Strength. This can be traced back to the presence of TCC, which is, according to Hagelstein et al., not sensitive to lubricants since the binding of brittle materials is not affected by the lubricant (Hagelstein et al., 2018).

Table 39 displays the significant model terms for both formulations to reveal the mutual CMT parameters, which impact the material attributes.

Table 39 Comparison of the significant model terms between F3 and F2. The mutual model terms are highlighted in bold.

	Formulation 3 (chapter 8)	**Formulation 2 (chapter 7)**
CBD	**THR, HUM, IMP**, THR*IMP	**THR, HUM, IMP**
FRI	-	THR, IMP, THR*THR
d_{10}	**THR, IMP**	**THR**, HUM, **IMP**

It could be confirmed that the CMT parameters comparably impact the material attributes across the formulations. THR, HUM and IMP affected the CBD confirming the fundamental connection between TBP and the density of the blend. Furthermore, THR and IMP were identified as model terms for the d_{10} values implicating a dependence on TBP, whereas THR and IMP seemed to be more important than HUM. For FRI, no independent process connection by the CMT parameters could be observed.

a)

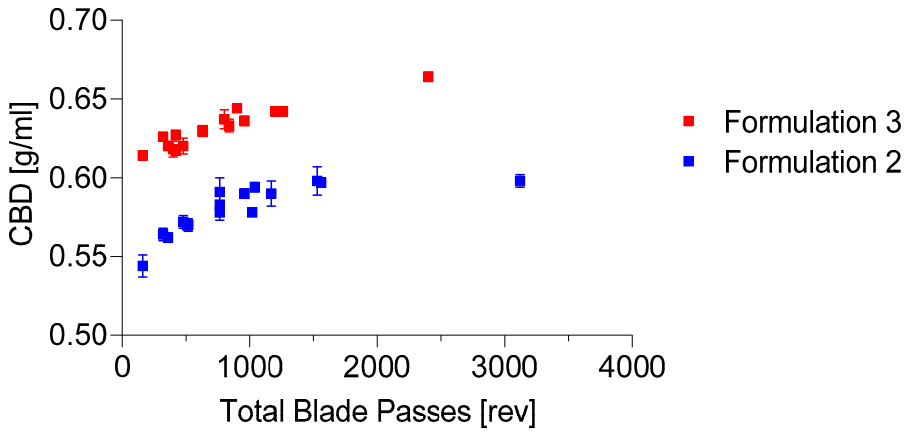

b)

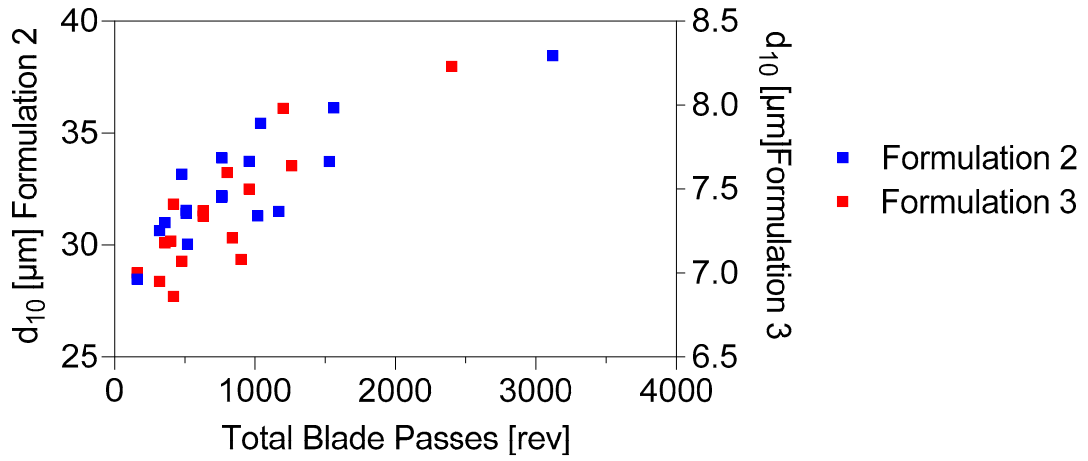

Figure 58 a) Shows a similar process behavior regarding CBD of the blend with varying TBP. Furthermore, the comparison between the d_{10} values as a function of the TBP of both formulations is shown in b).

After removing non-significant model terms, the following fit statistics could be obtained for this DoE (DoE 3).

Table 40 Overview of fit statistics regarding material attributes of the blend.

Response Factor	Data Transformation	Q^2	R^2	Adjusted R^2
Conditioned Bulk Density	-	0.862	0.939	0.918
Flow Rate Index	-	0.077	0.338	0.186
d_{10}	-	0.429	0.728	0.638

To predict the material attributes following model equations could be obtained:

$$CBD = 0.585835 + 0.000100826 * THR + 3.74999 * 10^{-5} * HUM + 0.000117666 * IMP - 2.91665 * 10^{-6} * THR * IMP \quad (32)$$

$$FRI = 1.09508 + 0.00214999 * THR + 4.66666 * 10^{-5} * IMP - 4.99999 * 10^{-6} * THR * IMP \quad (33)$$

$$d_{10} = 8.36839 - 0.0282 * THR - 0.00407145 * HUM + 0.00158667 * IMP + 3.74287 * 10^{-6} * HUM^2 \quad (34)$$

The model validity for CBD and d_{10} showed low and negative values. This can be explained by the minimal variability of the data points at the three replicates (CBD: 0.629 – 0.630 mm; d_{10}: 7.34 – 7.38 µm).

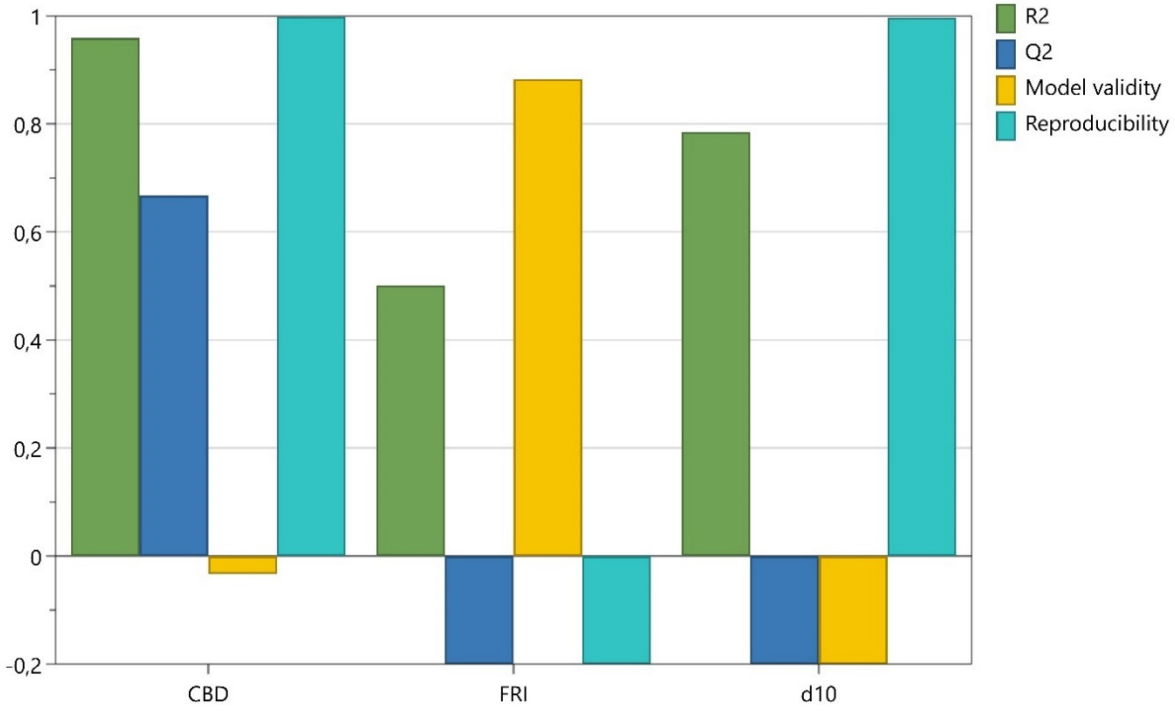

Figure 59 Summary of fit including R^2, Q^2, Model validity and Reproducibility for all material attributes.

The data points shown in Figure 60 seem to be diagonal straight lines for CBD and FRI. For d_{10} and d_{50}, a curved pattern is visible, indicating non-modeled quadratic relations.

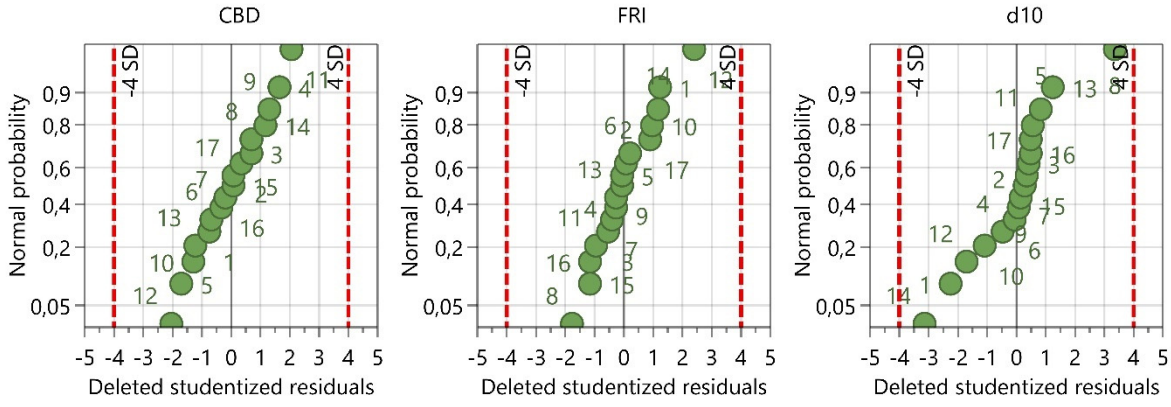

Figure 60 Overview of the residuals normal probability plots for all material attributes. The numbers of the data points are referred to the experiment no., as shown in Table 34.

The comparison between observed and predicted values shows a good fit for CBD, whereas for d_{10} and $d_{50,}$ only a few predicted values differed from the observed values. According to R^2 and Q^2, the predicted and observed values for FRI did not fit well.

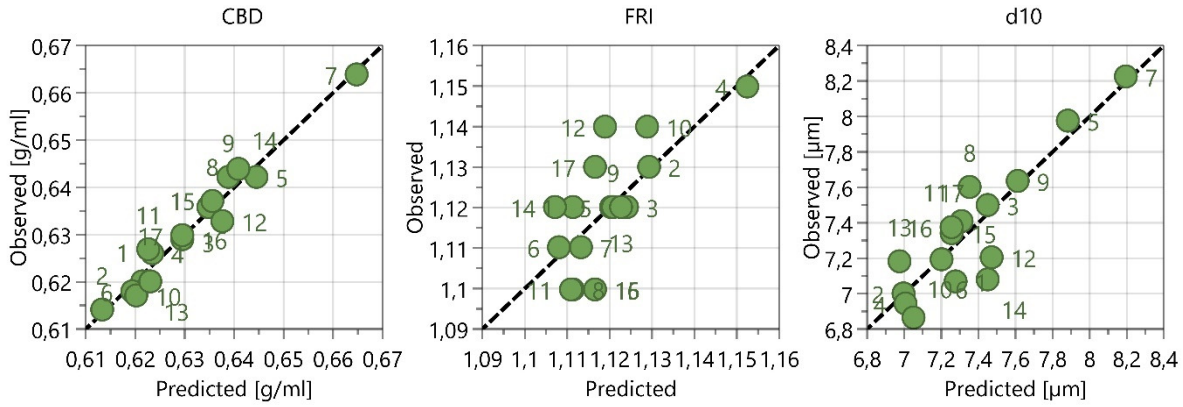

Figure 61 Overview of the comparison between observed and predicted values. The numbers of the data points are referred to the experiment no., as shown in Table 34.

8.5.2.3 **Tableting Parameters**

Figure 62 shows the model terms for FD, BCH and EF. For better comparability to F2, the BCH values at 250 MPa were used. The FD remained constant during the compression pressure/tensile strength profile.

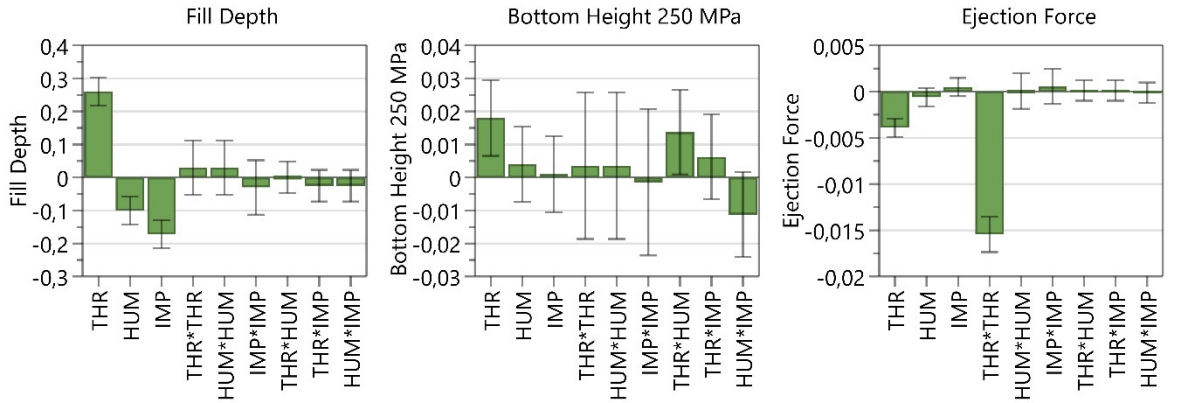

Figure 62 Coefficients plot of the impact of input variables on responses regarding the tableting parameters. The 95 % confidence interval is displayed as an error bar.

THR, HUM and IMP significantly impacted the FD. According to the TBP equation (eq.(3)), high THR, low HUM and low IMP result in low TBP, low lubrication, low powder densities and high FDs. This observation can also be seen in F2 (Figure 37 and Table 41), where high THR and low IMP have significantly resulted in high FD values.

For BCH, the significant model terms are THR and THR*HUM, indicating that higher BCHs are needed to maintain the compression pressure at higher THR. Compared to F2, where THR, HUM, IMP, IMP*IMP and THR*IMP (all positive deflected) are the significant model terms, the

number of significant input parameters is reduced. Nevertheless, the data confirmed the dependencies regarding THR.

The model terms regarding EF showed the significant impact of THR and THR*THR, which can partly be explained by the TBP equation, where lower THR results in higher TBP and higher lubrication, reducing the ejection force. However, no correlation between TBP and EF could be found, which is in line with chapter 7.

Table 41 Comparison of the significant model terms between F3 and F2. The mutual model terms are highlighted in bold.

	Formulation 3 (chapter 8)	**Formulation 2 (chapter 7)**
FD	**THR**, HUM, **IMP**	**THR, IMP,** THR*THR
BCH	**THR**, THR*HUM	**THR**, HUM, IMP, IMP*IMP, THR*IMP
EF	**THR, THR*THR**	**THR**, IMP, **THR*THR**

To show the comparability of the regularities in the process behavior, Figure 63 displays the FD as a function of TBP. For both formulations, higher TBP resulted in lower FD. The only difference is the FDs themselves, which depend on the blend's density (pearson correlation: -0.890 p<0.0001) and the raw materials.

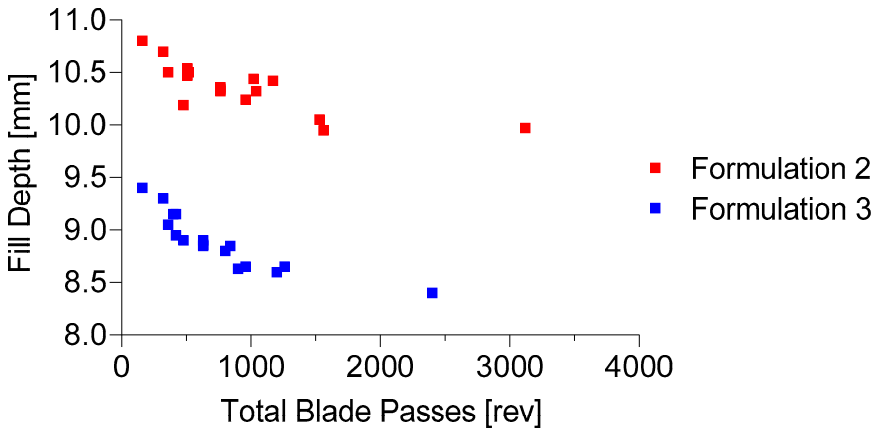

Figure 63 FD as a function of TBP for both formulations.

After removing non-significant model terms, the following fit statistics could be obtained for this DoE.

Table 42 After removing non-significant model terms the following fit statistics could be obtained.

Response Factor	**Data Transformation**	**Q^2**	**R^2**	**Adjusted R^2**
Fill Depth	-	0.927	0.964	0.956
Bottom Main Compression Height	-	-0.282	0.741	0.623
Ejection Force	-	0.975	0.988	0.984

The following model equations could be obtained:

$$FD = 9.06898 + 0.026 * THR - 0.0005 * HUM - 0.00114667 * IMP \quad (35)$$

$$BCH = 5.47754 - 0.00232502 * THR + 1.37479 * 10^{-5} * HUM + 0.000231662 * IMP + 6.87502 * 10^{-6} * THR * HUM - 3.74993 * 10^{-7} * HUM * IMP \quad (36)$$

$$EF = 0.0843476 + 0.00566143 * \mathrm{THR} - 2.99999 * 10^{-6} * HUM + 3.33333 * 10^{-6} * IMP - 0.000151286 * THR^2 \quad (37)$$

The following figures show further information regarding the model fit, where the model validity of all parameters shown in Figure 64 was acceptable. Only for BCH the estimate of the future prediction precision (Q^2) is low and therefore not considered a good model.

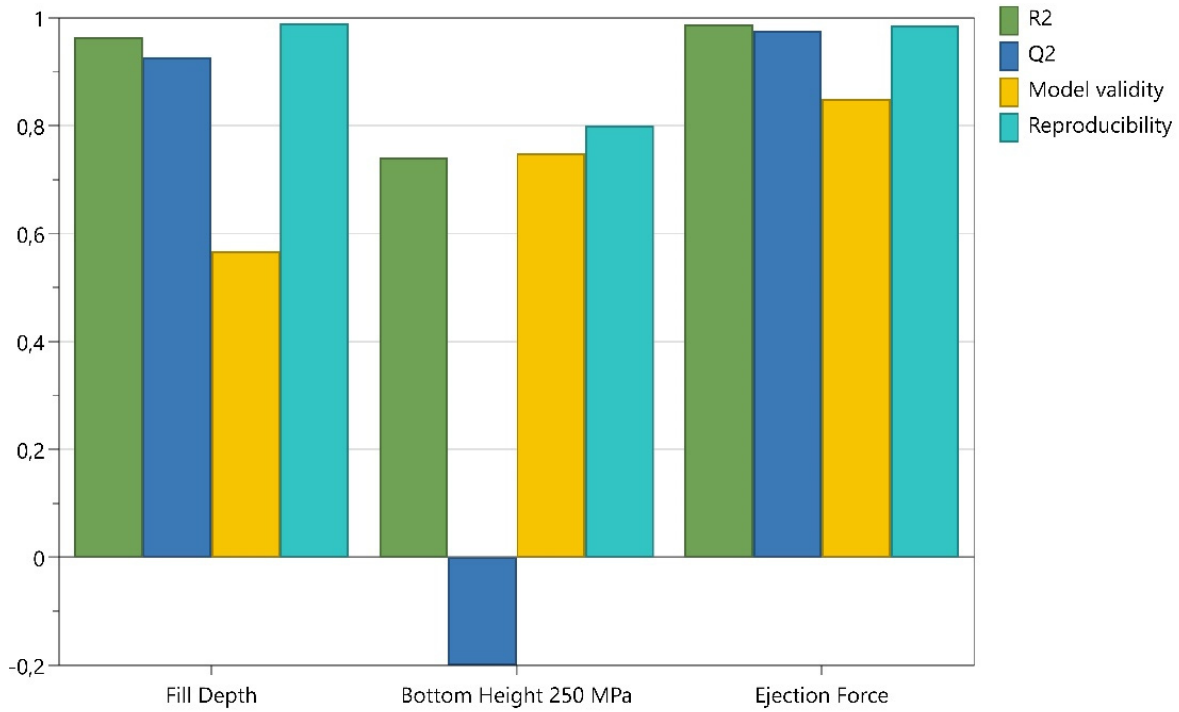

Figure 64 Summary of fit including R^2, Q^2, Model validity and Reproducibility for all tableting parameters.

Regarding the residuals normal probability plot, only point 4 (BCH) was outside of 4 SD. Considering Figure 66, the predicted value differed from the observed value and can be seen as an outlier. Nevertheless, the data points show a straight line in a diagonal, indicating a normally distributed noise.

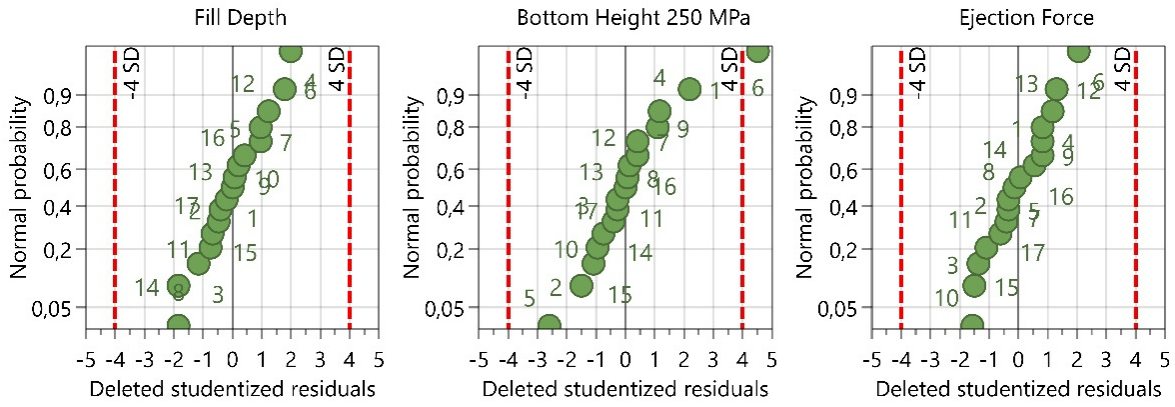

Figure 65 Overview of the residuals normal probability plots for all tableting parameters. The numbers of the data points are referred to the experiment no., as shown in Table 34.

The data are displayed close to a straight line, indicating a good model fit for FD and EF. Only for BCH, differences between observed and predicted values are shown, which can be seen in the low Q^2 value.

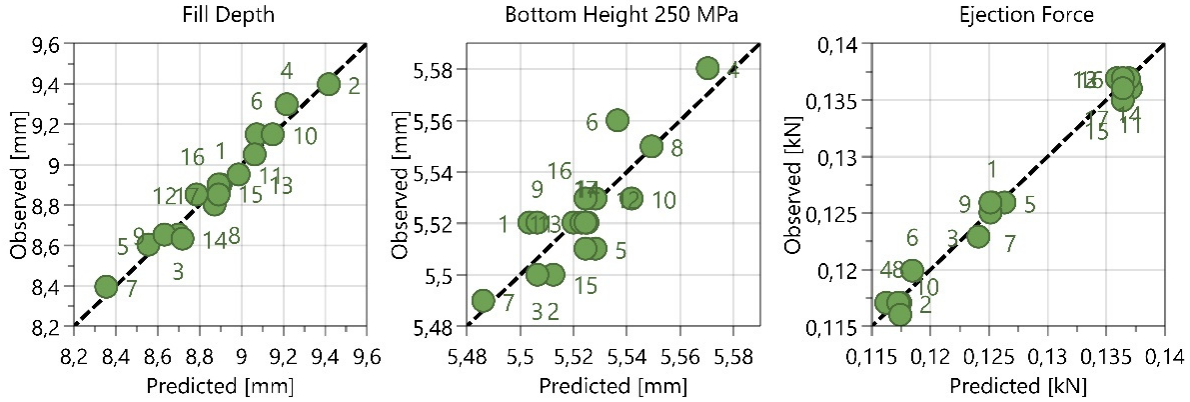

Figure 66 Overview of the comparison between observed and predicted values. The numbers of the data points are referred to the experiment no., as shown in Table 34.

8.5.2.4 **Tensile Strength**

Figure 67 shows the model terms regarding TS and TS SD.

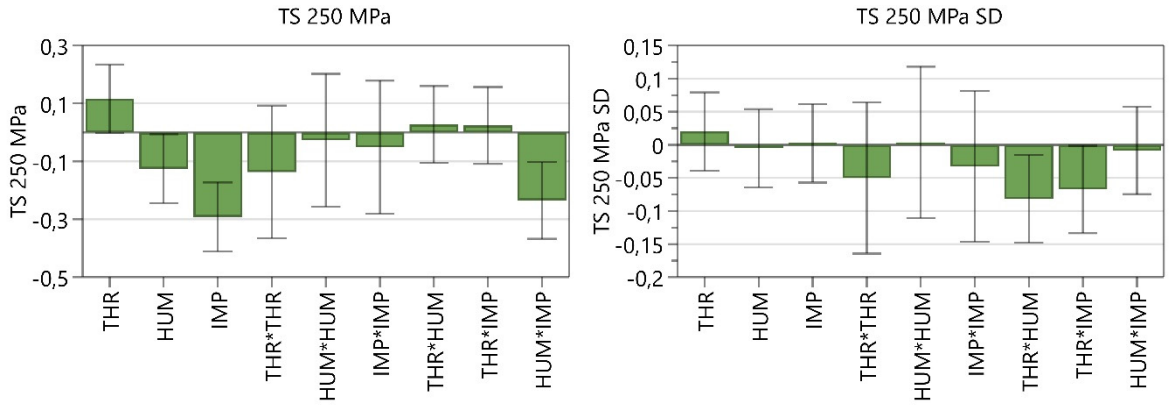

Figure 67 Coefficients plot of the impact of input variables on responses regarding TS. The 95 % confidence interval is displayed as an error bar.

As already discussed in chapter 7.5.4.2 Tensile Strength the TBP significantly impacted the TS. As expected, this finding can be confirmed with the alternative formulation used in this DoE, where the model terms reveal that high THR, low HUM and low IMP resulted in low lubrication and high TS values, again. Furthermore, low HUM*IMP resulted in high TS, highlighting the importance of HUM and IMP in the TBP equation with regards to TS.
Furthermore, the significant model terms of TS SD were THR*HUM and THR*IMP.
After removing non-significant model terms, the following fit statistics could be obtained.

Table 43 Overview of fit statistics regarding TS.

Response Factor	Data Transformation	Q^2	R^2	Adjusted R^2
TS	-	0.763	0.895	0.848
TS SD	-	0.202	0.702	0.523

To predict TS and TS SD the following model equations were obtained.

$$TS = 1.6503 + 0.0823372 * \mathrm{THR} + 0.00211079 * HUM + 0.0027485 * IMP - 0.00176743 * THR * THR - 7{,}82083 * 10^{-6} \quad (38)$$

$$TS\ SD = -0.757329 + 0.0681972 * THR + 0.000789 * HUM + 0.000914 * IMP - 0.000649429 * THR^2 - 4.075 * 10^{-5} * THR * HUM - 4.5 * 10^{-5} * THR * IMP \quad (39)$$

The model validity for TS is low, which can be explained by the minimal variability of the data points at the three replicates (3.076 – 3.113 N/mm²). Furthermore, the reproducibility of TS SD

is very low. A log transformation could have improved that, but the transformation decreased Q^2 to 0.075.

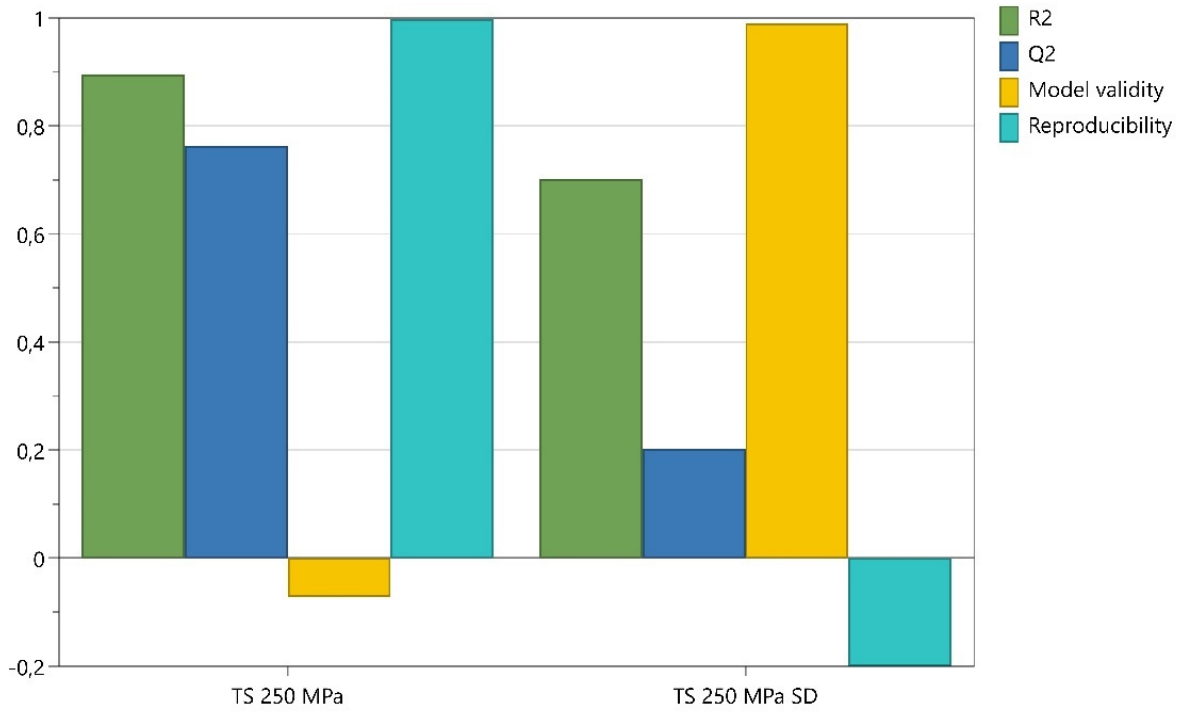

Figure 68 Summary of fit including R^2, Q^2, Model validity and Reproducibility for TS and TS SD.

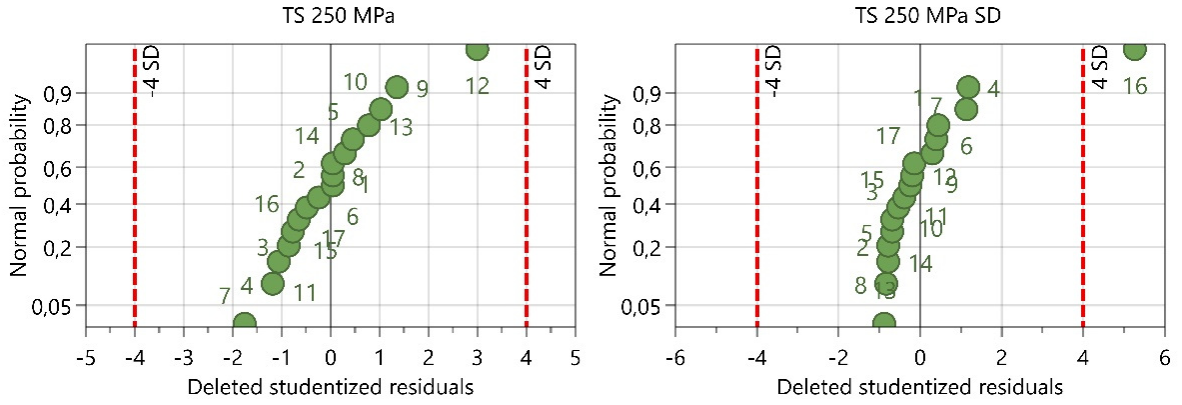

Figure 69 Overview of the residuals normal probability plots for TS and TS SD. The numbers of the data points are referred to the experiment no., as shown in Table 34.

In Figure 69, the data points are in a straight, diagonal line indicating that the residuals are normally distributed noise. For TS SD, a slightly curved pattern can be seen and point 16 is outside of the red lines. This can be considered an outlier since the predicted value differs from the observed one (Figure 70). Regarding the Q^2 value, the precision of the prediction is low, indicating a low model performance for TS SD. For TS, the majority of the predicted values were close to the observed values.

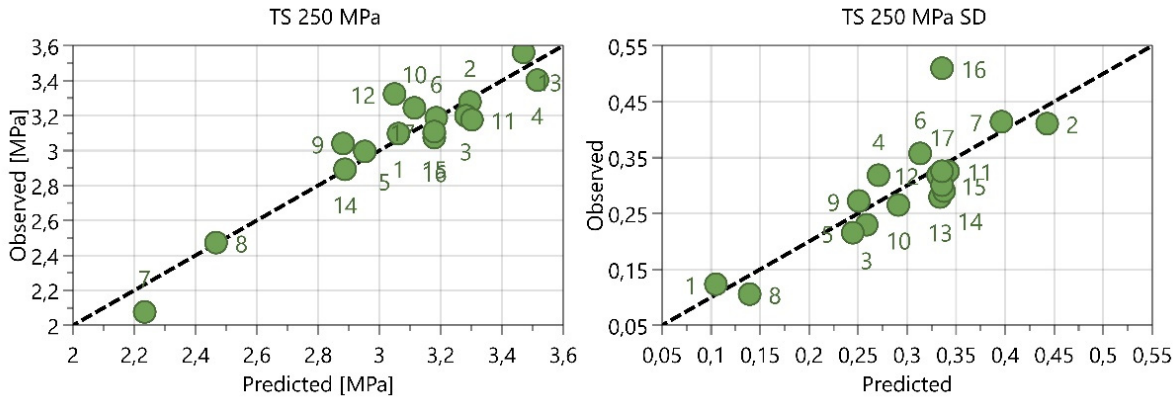

Figure 70 Overview of the comparison between observed and predicted values. The numbers of the data points are referred to the experiment no., as shown in Table 34.

A compression pressure/tensile strength profile was carried out in these test runs where 100, 150, 200 and 250 MPa compression pressure was set. In Figure 71, the obtained TS of both DoEs is displayed as a function of TBP and CP. In a), the decrease of TS at rising TBP is only visible at high CP, whereas only minimal variation in TS is recognizable at 100 MPa. In general, the decrease of TS is slightly linear and less exponential than the TS values obtained with F2. In b) the impact of the CMT parameters on the TS is clearer where lower TBP are visibly accompanied by higher TS. While in a) the TS values decrease only slightly, the values in b) drop quickly at first and then approach a plateau. A possible reason could be the difference in type and concentration of the lubricant in each formulation. F2 consisted of MgSt (1.5%) and F3 consisted of SSF (2%), where the use of SSF resulted in comparably less TS reduction, which is in line with the literature (Louw, 2003; Shah et al., 1986). Therefore, the blends in this DoE seemed comparably less lubricated. Considering the data for both DoEs at 1200 rev, for a) higher TS values can be observed at CP > 200 MPa indicating generally harder tablets, which can also be traced back to the lubrication insensitivity of the powder, which is caused by the brittle deformation behavior of TCC (Abdel-Hamid et al., 2012; Hagelstein et al., 2018).
Table 44 confirms the dependence of TS on TBP as THR, HUM and IMP were significant model terms for both formulations. Furthermore, the importance of HUM and IMP was emphasized by the model term HUM*IMP. Whereas no significant model terms could be found for TS SD in F2, THR*HUM and THR*IMP impacted the TS SD in F3 highlighting the influence of THR.

Table 44 Comparison of the significant model terms between F3 and F2. The mutual model terms are highlighted in bold.

	Formulation 3 (chapter 8)	**Formulation 2 (chapter 7)**
TS	**THR, HUM, IMP, HUM*IMP**	**THR, HUM, IMP**, THR*THR, THR*IMP, **HUM*IMP**
TS SD	THR*HUM, THR*IMP	-

So, the same process behavior in both test runs can be confirmed, but it needs to be considered that the extent to which the TS is dependent on TBP varies between different formulations and the corresponding lubrication sensitivity of the excipients.

a) F3

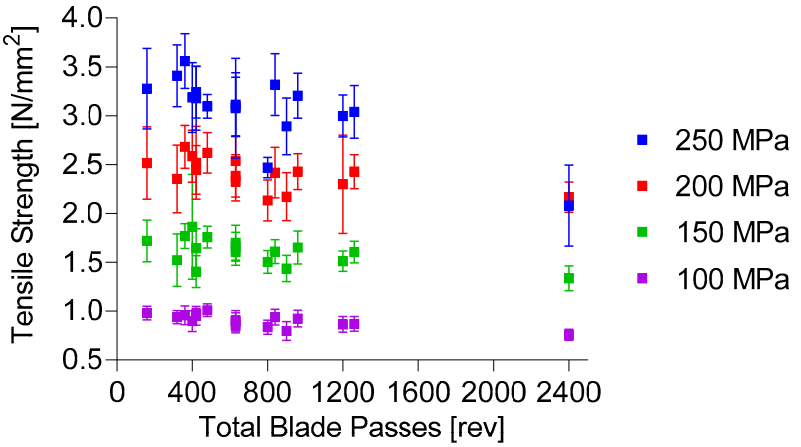

b) F2

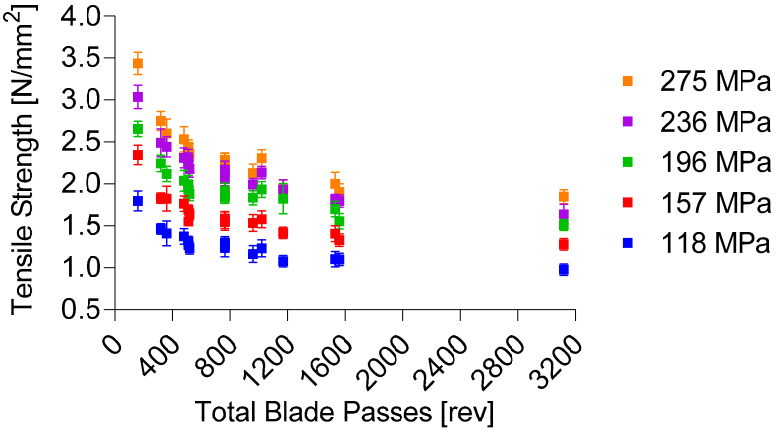

Figure 71 Comparison of compression pressure/tensile strength profiles as function of TBP for both formulations.

8.6 **Conclusion**

In this investigation, the same test settings as for F2 were carried out where only impeller speed was adapted to ensure processability. This repeated DoE aimed to confirm the process models developed in chapter 7 to establish an understanding of fundamental process behaviors. Table 45 shows an overview of the compared model terms to demonstrate mutual CMT parameters which impact the respective process parameter. The mutuality strongly suggests a formulation-independent parameter connection between the CMT and the downstream continuous process. Therefore, a qualitative reaction of the continuous process can be estimated based on changes in CMT parameters. Nevertheless, the extent to which the respective process responses may be impacted depends on the used material.

For example, Figure 58 showed increasing CBD and d_{10} values with increasing TBP until a plateau is reached. Still, the absolute values differed based on the composition and the attributes, respectively.

Table 45 Overview of the significant model terms obtained by F3 and F2. The mutual model terms are highlighted in bold.

	Formulation 3 (chapter 8)	**Formulation 2 (chapter 7)**
EV	**THR, IMP**, IMP*IMP, THR*IMP	**THR, IMP**
EV SD	HUM, **IMP**, THR*IMP	**IMP**
HUM SD	**THR**, **HUM**, THR*HUM	**THR, HUM,** IMP
T_L	**HUM, IMP**, IMP*IMP	**HUM, IMP**
T_L SD	**IMP**	**IMP**
Blend Potency SD	-	IMP
CBD	**THR, HUM, IMP**, THR*IMP	**THR, HUM, IMP**
FRI	-	THR, IMP, THR*THR
d_{10}	**THR, IMP**	**THR**, HUM, **IMP**
FD	**THR**, HUM, **IMP**	**THR, IMP,** THR*THR
BCH	**THR**, THR*HUM	**THR**, HUM, IMP, IMP*IMP, THR*IMP
EF	**THR, THR*THR**	**THR**, IMP, **THR*THR**
TS	**THR, HUM, IMP, HUM*IMP**	**THR, HUM, IMP**, THR*THR, THR*IMP, **HUM*IMP**
TS SD	THR*HUM, THR*IMP	-

9 Impact of Impeller Speed, Throughput and Drug Load on Continuous Process Parameters, Material Attributes of the Blend and Blend Uniformity

9.1 Introduction

For specific treatments like cancer or hormone therapies, high potent APIs with doses smaller than 1 mg per tablet are typical (Michalson, 2007). The processing of such a small drug load (DL) is described as a high-risk formulation in the literature (Lee et al., 2015).

Processing low DLs on the continuous manufacturing line affect the entire process. Beginning with the first process unit, low proportions of API in the formulation consequently require low feed rates, which result more likely in higher dosing variability (Bekaert, 2021; Ervasti, 2015). Since APIs are not selected based on their material attributes but on their pharmacological effect the flowability of the material is generally poorer. According to Megarry et al., who analyzed 3606 APIs via shear cell measurements, the APIs showed the poorest flowability (FFc < 2) compared to usual tableting excipients (Megarry, 2019). Therefore, the uniform distribution throughout the blend with low DLs may be challenging (Bi et al., 2011). Additionally, Van Snick et al. could confirm that lower DL may be associated with higher variability of API content within the blend (Snick, 2017a).

To evaluate which DL is still processable by the PCMM, a DoE with varying DLs between 2 and 18 % was carried out. For additional reference runs, the CMT settings of the replicates were repeated with 5, 20 and 30 % DL. So, for each DL, the composition of the formulation was changed. As discussed in chapter 8, the process and parameter dependencies from chapter 7 could be largely confirmed, whereas the individual parameter values depended on the alternative formulation and the material attributes, respectively. So, this DoE not only investigated the impact of DL solely on the process but moreover evaluated the impact of DL in combination with THR and IMP on material attributes of the blend (conditioned bulk density (CBD), compressibility (Comp), basic flow energy (BFE)), process parameters (exit valve opening width (EV), fill depth (FD), tablet tensile strength (TS)) and blend uniformity (mass balance model (MBM) and blend potency measured by NIR).

9.2 Aims and Scope

The aim of this study was the evaluation of the continuous process with changing DL and blender variables. Using a DoE, where throughput (THR), impeller speed (IMP) and DL were set as input parameters, the impact on the MBM and the potency measured by NIR were investigated to assess the blend uniformity. Furthermore, this DoE evaluated the impact on several continuous process parameters based on the composition and CMT parameter changes.

9.3 **Materials**

To investigate the continuous process regarding the impact of different compositions of the same set of materials, formulation 4 (F4) was used, as shown in Table 46. To compensate for changes in the DL, MCC and DCP were adapted accordingly in a 2:1 ratio.

Table 46 Composition for each raw material of F4.

	Saccharin	**MCC**	**DCP**	**SSG**	**MgSt**
Composition [%]	2.00	62.33	31.17	3.00	1.50
	5.00	60.33	30.17	3.00	1.50
	10.00	57.00	28.50	3.00	1.50
	18.00	51.67	25.83	3.00	1.50
	25.00	47.00	23.50	3.00	1.50
	30.00	43.67	21.83	3.00	1.50

Corresponding feeder settings are shown in Table 47.

Table 47 Feeder setting for each raw material of F4.

	Saccharin	**MCC**	**DCP**	**SSG**	**MgSt**
Top up Volume [L]	0.8	1.6	1.6	1.2	0.8
Gearbox Type	3 (455:1) 2 (235:1)*	1 (63:1)	2 (235:1)	3 (455:1)	3 (455:1)
Screw Pitch [mm/rev]	10	20	20	20	20
Refill Level [L]	1.0	0.5	0.3	0.25	1.5

*GB of saccharin was changed due to increasing feeder throughput. For 2, 5 and 10 % GB type 3 was used and for 18, 25 and 30 % DL, GB type 2 was in place. A higher screw speed is required to maintain the feed rate with increasing throughput. Limited by a maximum servo motor speed of 9000 rpm, GB type 3 only could provide sufficient screw rotations for lower feeder throughputs.

Corresponding material attributes are shown in Table 50.

9.4 **DoE Settings**

A full factorial DoE (DoE 4) was carried out using MODDE, where saccharin concentration, referred to as DL, THR and IMP, were used as input factors. In this trial, HUM, CP and precompression pressure were kept constant at 800 g, 275 MPa and 21 MPa and the used compounds remained constant over the entire experiment. In general, 18 experiments were performed, including 3 replicates of a center point and 3 additional runs (Table 48). After adjusting the new CMT parameters, a transition phase (3 x MRT) was initiated to wash out the

powder mixed at the former setting. During the transition phase, the tablet press was operated in manual mode without using the combitester to analyze tablet properties. In manual mode, samples of the tablets were taken and weighed manually to select the correct fill depth. During each steady-state phase, manual mode was switched to automatic mode, in which the NIR probe was active. For each steady-state phase, 275 MPa compression pressure was set, a tablet sample was taken in the middle of the steady-state phase using the combitester and a powder sample was withdrawn at the end of each steady-state phase by opening the sampling port underneath the feed frame and collecting approximately 300 g of powder.

Table 48 DoE settings, where phase 8, 10 and 12 are the replicates of the center point. Furthermore, phase 15, 17 and 18 were additional sets with 5 %, 25 % and 30 % DL. MRT and TBP are calculated based on the CMT parameters (eq. (2) and (3)).

phase	Experiment No.	THR [kg/h]	IMP [rpm]	DL [%]	MRT [min]	TBP [rev]
1	4	30	550	2	1.6	880
2	12	30	550	18	1.6	880
3	1	10	200	2	4.8	960
4	3	10	550	2	4.8	2640
5	2	30	200	2	1.6	320
6	5	10	200	10	4.8	960
7	7	10	550	10	4.8	2640
8	13	20	375	10	2.4	900
9	6	30	200	10	1.6	320
10	14	20	375	10	2.4	900
11	8	30	550	10	1.6	880
12	15	20	375	10	2.4	900
13	9	10	200	18	4.8	960
14	11	10	550	18	4.8	2640
15	10	30	200	18	1.6	320
16	16	20	375	5	2.4	900
17	17	20	375	25	2.4	900
18	18	20	375	30	2.4	900

9.5 Results and Discussion

The DoE reveals the impact of DL in combination with THR and IMP on the continuous manufacturing process. As shown in Figure 72, the 4 categories feeder performance (feed rate RSD, feed factor RSD, screw speed RSD), material attributes of the blend (CBD, Comp and BFE), process parameters (EV, FD, TS) and blend uniformity (MBM and blend potency as measured by NIR) were assessed. Since IMP has no possible impact on the feed performance, the feeder data were not analyzed by MODDE.

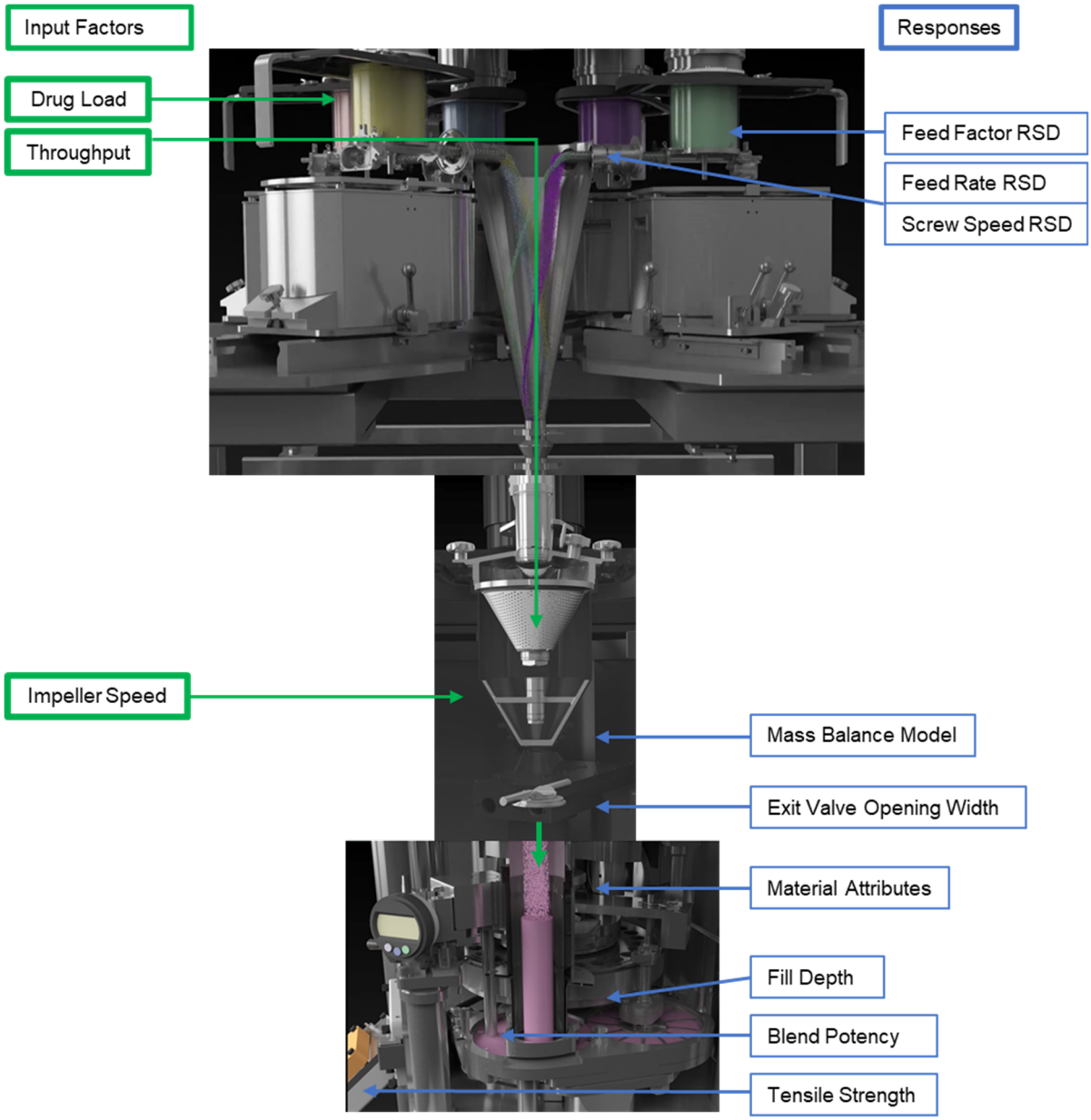

Figure 72 Process overview of input factors (green, left side) and observed responses (blue, right side).

Figure 73 demonstrates relationships between the parameters obtained and evaluated within this DoE. Starting from the CMT settings, the flowchart depicts the downstream process parameters where correlations and process dependencies are expected to be found.

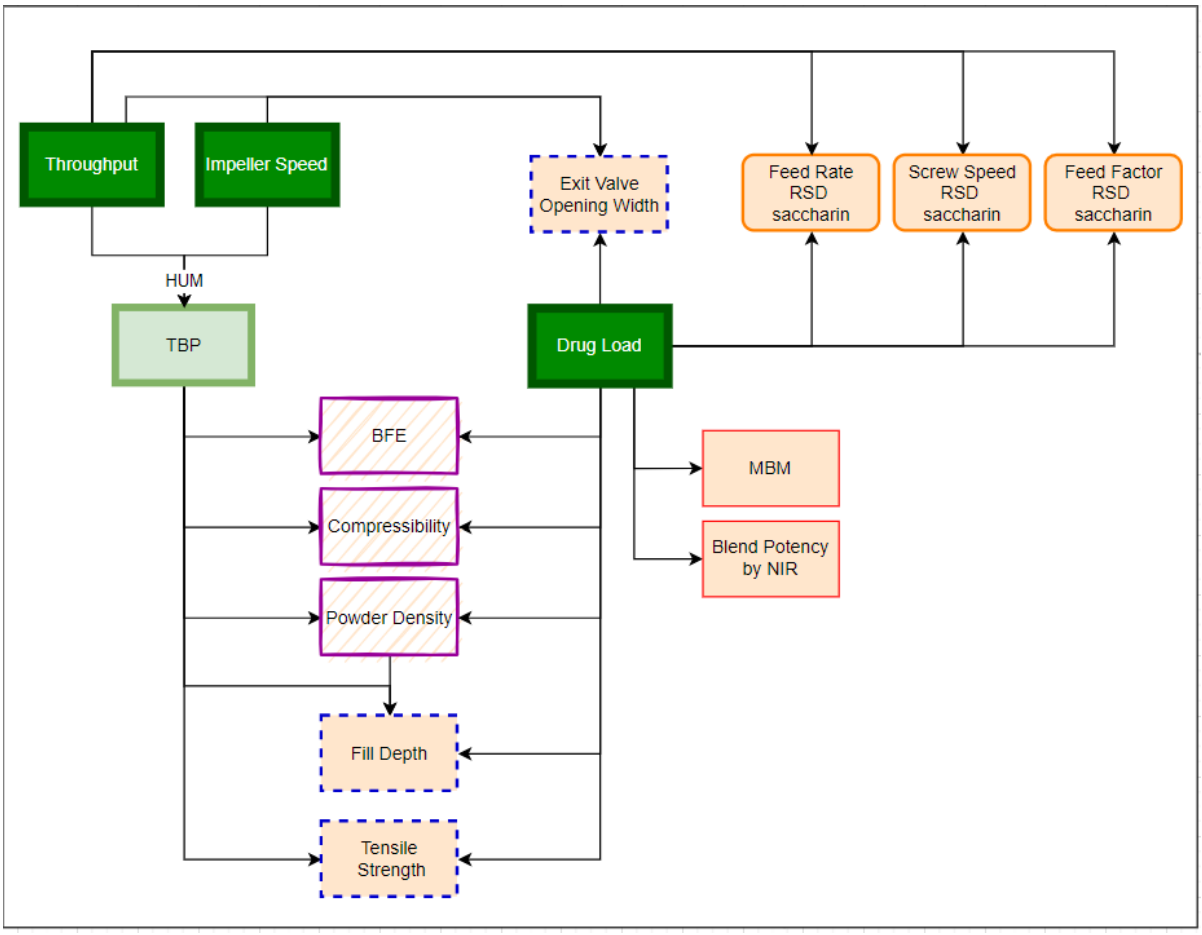

Figure 73 Qualitative overview of process parameter links and correlations. Input factors are marked in dark green (thick borders), confounding input parameters are marked in light green and the considered response parameters are shown in light orange. The color/shape of the borders classifies the responses into feed performance (orange line, rounded corners), material attributes of the blend (purple, striped background), process parameters (blue, dotted borders) and blend uniformity (red, thin borders).

9.5.1 Feed Performance

As shown in Table 46 and Table 48, the concentration of saccharin varied between 2 and 30 % and the throughput of the continuous manufacturing line was set at 10, 20 and 30 kg/h. To provide the correct proportion within the blend, the feed rates of MCC and DCP were adjusted accordingly.

To evaluate the impact of the feeder throughput on the feed performance, data of the corresponding settings were used. Figure 74 a) shows the feed rate uniformity displayed as RSD as a function of the feed rate. For saccharin, it demonstrates that higher feed rates improved the feed accuracy and reduced the feed rate RSD values. In other words, low feeder throughputs increased the risk of high feed rate variability, which aligns with the findings from Gao et al. (Gao et al., 2011b). For MCC and DCP, the range of feeder throughputs in this study did not impact the feed rate variability since only low RSDs were obtained except for 3 data points, which were not related to the throughput.

To maintain the feed rate, the screws rotate to convey the correct proportion of the individual raw material, which is controlled by a PID control loop. This controller adjusts the screw speed according to the loss-in-weight information obtained by the weighing cells. As expected, Figure 74 b) demonstrates a decrease in screw speed uniformity at lower feed rates for saccharin as well. As expected, MCC and DCP are not impacted by throughput again.

The feed factor is the calculated mass that is conveyed per screw revolution (eq.(1)). Figure 74 c) illustrates the feed factor variability as a function of feed rate. According to the screw speed RSD, the FF RSD of MCC and DCP were again not impacted by the feed rate.

On the other hand, for saccharin, lower feed rates resulted in higher feed factor RSDs again. In general, it could be shown that all feed rate RSD values < 2.8 % are obtained at feed rates ≥ 1 kg/h, providing good processing at higher feeder throughputs

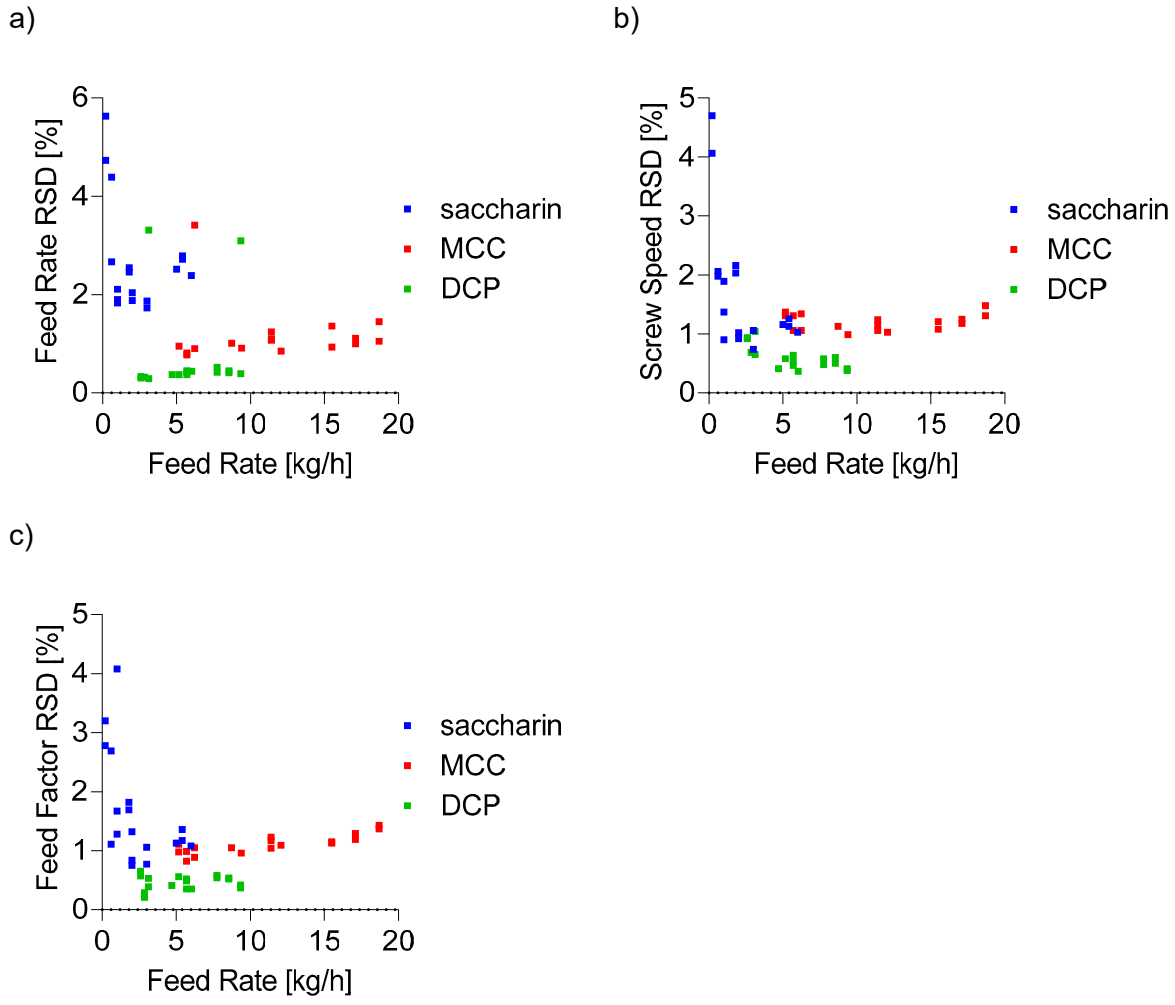

Figure 74 a) Feed rate RSD as a function of feed rate. b) Screw speed RSD as a function of feed rate. c) Feed factor RSD as a function of feed rate.

Moreover, since only saccharin was affected by the feeder throughputs in these runs, a correlation matrix was built to evaluate the link between feed rate, feed factor and screw speed for the API feeder (Figure 75). High feed rates are accompanied by low feed rate RSDs, high screw speeds, low screw speed RSDs and low feed factor RSDs.

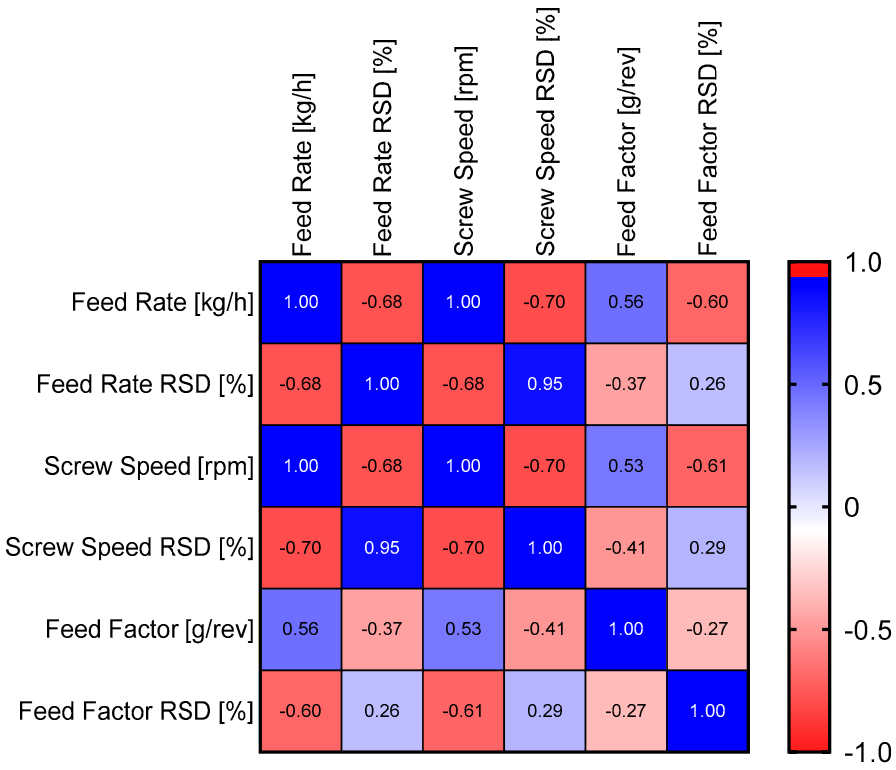

Figure 75 Pearson correlation matrix of the GEA Compact Feeder parameters for saccharin. Blue represents a positive and red a negative correlation.

9.5.2 **Material Attributes of the blend**

Figure 76 shows the model terms of CBD, Comp and BFE, which are explained and discussed in separate chapters below.

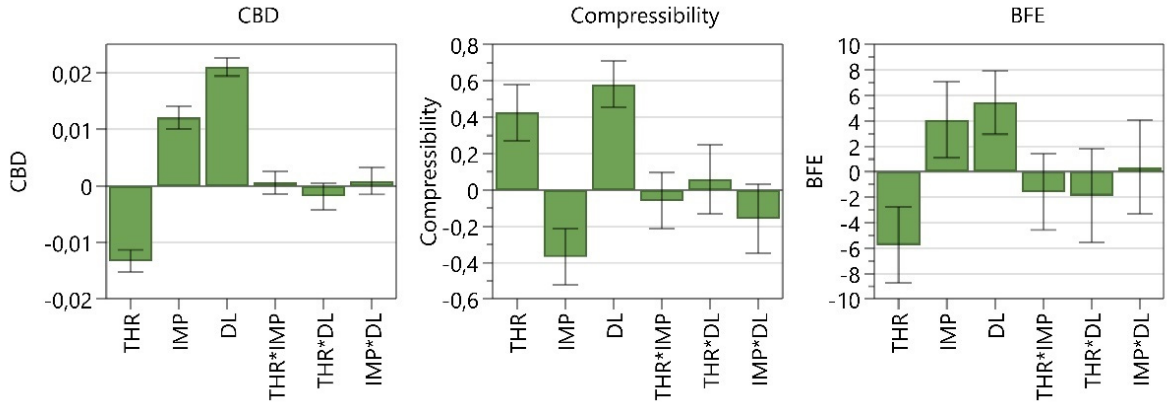

Figure 76 shows the coefficients of CBD [g/ml], Compressibility [%] and BFE [mJ].

After removing non-significant model terms, the following fit statistics could be obtained.

Table 49 Overview of fit statistics regarding material attributes of the blend.

Response Factor	Data Transformation	Q^2	R^2	Adjusted R^2
Conditioned Bulk Density	-	0.984	0.990	0.987
Compressibility	-	0.829	0.939	0.906
Basic Flow Energy	-	0.658	0.785	0.739

The following figures show further information regarding the model fit and demonstrate a good model performance.

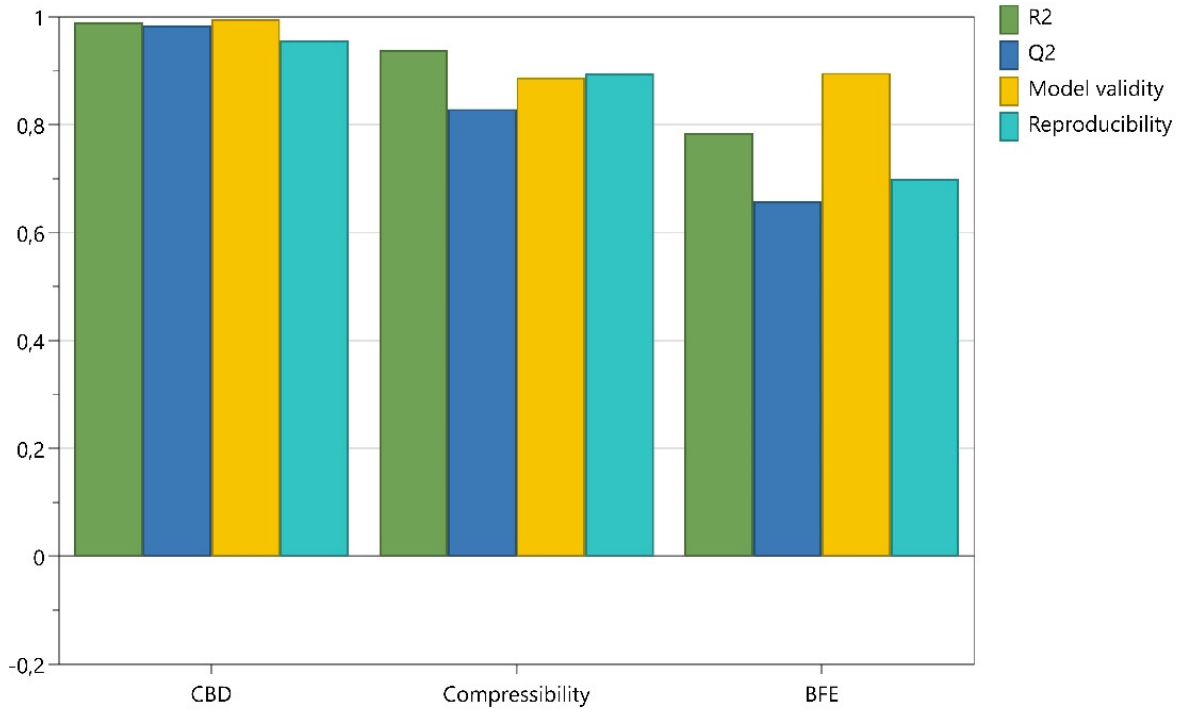

Figure 77 Summary of fit including R^2, Q^2, Model validity and Reproducibility for the material attributes of the blend.

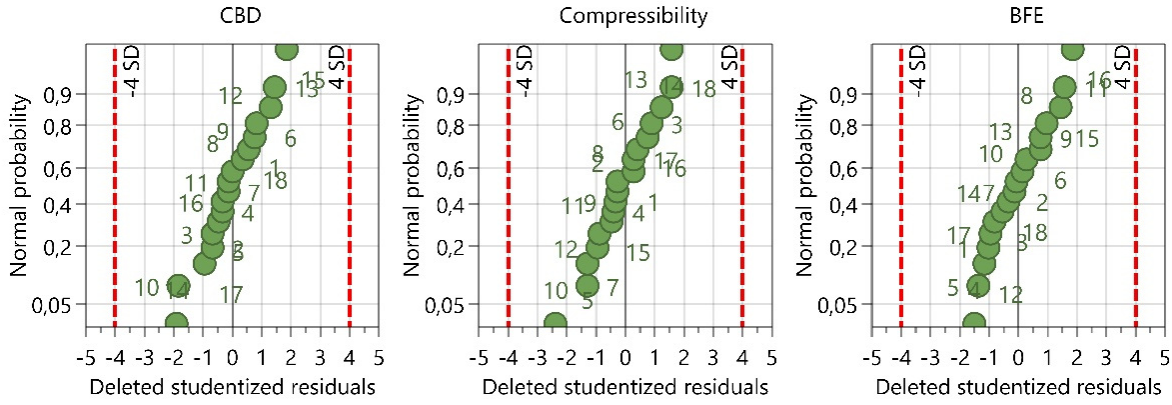

Figure 78 Overview of the residuals normal probability plots for the material attributes of the blend. The numbers of the data points are referred to the experiment no., as shown in Table 48.

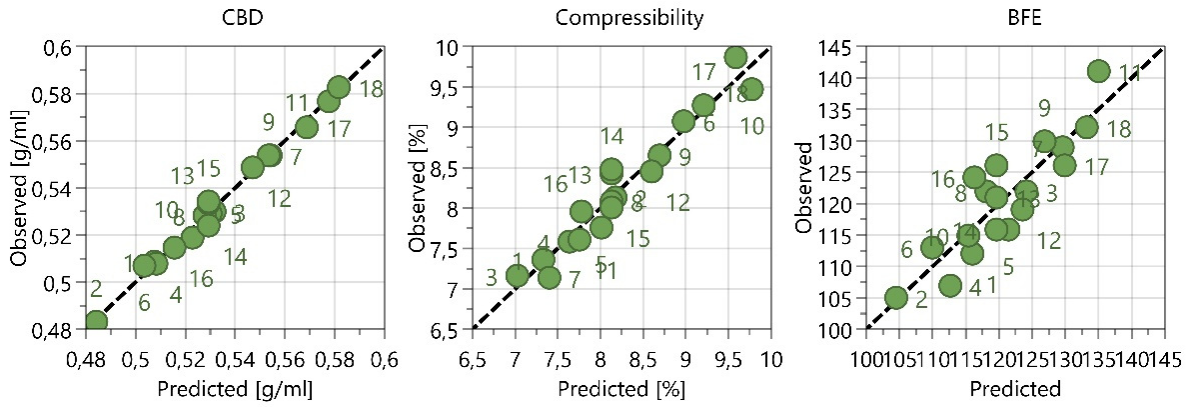

Figure 79 Overview of the comparison between observed and predicted values. The numbers of the data points are referred to the experiment no., as shown in Table 48.

Table 50 shows the material attributes of the used excipients.

Table 50 FT4 data and particle size distribution (QicPic) of the individual raw materials.

	CBD* [g/ml]	**FRI***	**Comp**** [%]	**Cohesion***** [kPa]	**FFc*****	**d_{10}**** [µm]	**d_{50}** [µm]	**d_{90}** [µm]
MCC	0.356±0.007	1.49±0.05	14.27±0.12	0.89±0.04	5.2±0.11	32.36	99.79	199.4
Saccharin	0.639±0.009	1.20±0.13	30.53±0.65	1.53±0.09	3.0±0.16	15.66	57.59	176.71
DCP	0.677±0.002	1.36±0.05	4.87±0.4	1.61±0.11	3.2±0.16	36.92	158.14	286.84
SSG	0.769±0.003	1.18±0.06	6.30±0.29	0.17±0.05	26.0±7.78	23.98	41.78	67.66
MgSt	0.199±0.011	3.24±0.35	38.70±0.75	0.74±0.09	6.4±0.66	8.41	17.01	26.22

*Obtained by the stability and variable flow rate method.

**Obtained by the compressibility method.

***Obtained by the shear cell.

****Obtained by Sympatec QicPic.

9.5.2.1 **Conditioned Bulk Density**

According to the TBP equation (eq.(3)), Figure 76 shows that low THR and high IMP resulted in high TBP and, therefore, high densities of the blend.

To compensate for changes in saccharin concentrations, MCC and DCP were adapted accordingly, as shown in Table 46.The respective CBD values are shown in Table 50, where saccharin = 0.639 g/ml, MCC = 0.356 g/ml and DCP = 0.677 g/ml. Thus, the DL-model term can be explained by the higher amount of saccharin in the blend, whereas the proportion of DCP decreased comparably less and SSG and MgSt remained constant (Sierra-Vega et al., 2019).

Figure 80 illustrates the CBD of the blend as a function of DL and TBP, where a linear relationship between DL and CBD can be observed dependent on TBP. Performing a simple linear regression, the slopes of each data row could be obtained (2640 rev: 0.002938; 920 rev:

0.002627 and 320 rev:0.002250). The similarity of the slopes indicates that the powder is evenly affected by the TBP and only showed a difference in absolute values based on the proportion of ingredients in the formulation.

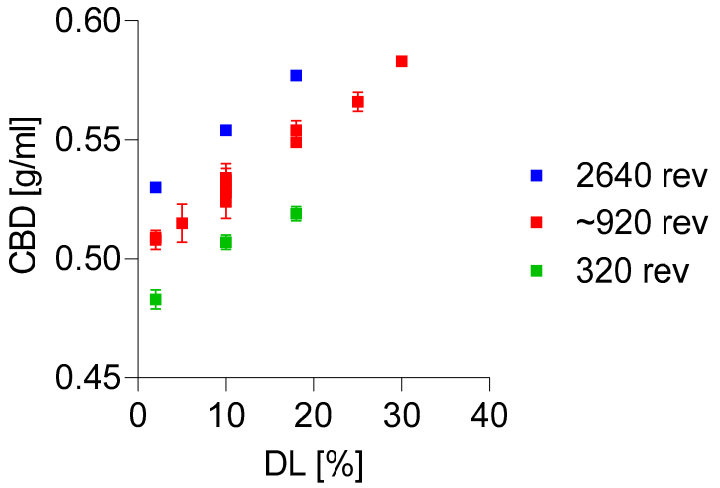

Figure 80 shows CBD as a function of DL. The data points were classified according to the extent of lubrication exerted on the blend, where low (320 rev, green), medium (880 – 960 rev, red) and high TBP (2640 rev, blue) are displayed differentiated.

An equation to predict the CBD of a blend mixed with the CMT could be obtained:

$$CBD = 0.49869 - 0.00109062 * THR + 6.90476 * 10^{-5} * IMP + 0.00309795 * DL - 2.34376 * 10^{-5} * THR * DL \quad (40)$$

9.5.2.2 **Compressibility of the powder**

The FT4 - compressibility method is used to investigate how the density of the measured powder changes with increasing normal stress. The data displayed in Figure 76 and Figure 81 refer to the percentage compression of the powder at 15 kPa.

The significant model terms in Figure 76 show that low THR and high IMP resulted in lower compressibility of the blend samples. With higher TBP, MgSt could be distributed more homogeneously, causing a higher density and a more compact powder bed. Due to the compact arrangement of the particles, the exerted pressure could only compress the powder slightly, resulting in low compressibility values. As seen at low TPB, a less compact arrangement is associated with more voids within the powder that are more easily compressed by pressure, leading to higher compressibility values (Freeman, 2007).

Furthermore, higher DL resulted in higher compressibility of the blend. This impact could be caused by the higher proportion of saccharin which initially showed comparably high compressibility (30.53 %) compared to the other raw materials (see also Table 50).

Figure 81 demonstrates the compressibility as a function of TBP. As already mentioned, higher TBP resulted in lower compressibility due to a more compact powder bed, which consequently requires lower FDs to meet the tablet weight. Highlighted in color, the impact of the DL is displayed, where high saccharin concentrations led to higher compressibility of the blend.

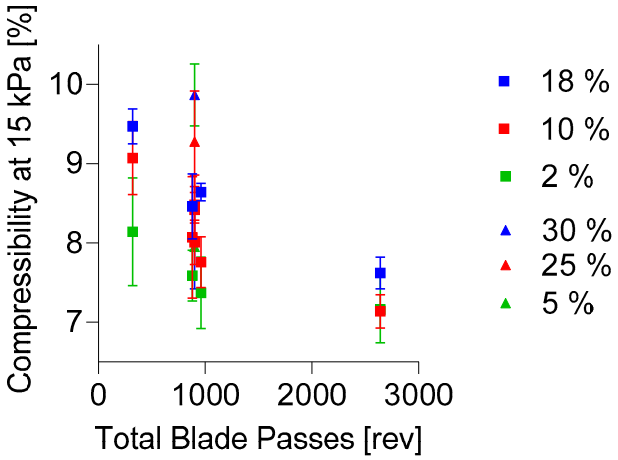

Figure 81 Compressibility values measured by the FT4 as a function of TBP, where blue squared data points are obtained at 18 % DL, red squared data points are obtained at 10 % DL and green squared data points are obtained at 2 % DL. Additionally, the blue, triangled data point is obtained at 30 % DL, the red, triangled data point at 25 % and the green, triangled one at 5 % DL.

An equation to predict the compressibility of a blend mixed by the CMT could be obtained:

$$\begin{aligned} Comp = {} & 6.8063 + 0.0479182 * THR - 0.000289879 * IMP + 0.100488 * DL \\ & - 3.38096 * 10^{-5} * THR * IMP + 0.000734373 * THR * DL \\ & - 0.000113393 * IMP * DL \end{aligned} \quad (41)$$

9.5.2.3 **Basic Flow Energy**

The BFE is measured by the FT4 and defined by the required energy to move the blade downwards at a test cycle with 100 mm/s blade tip speed. The resistance to flow is calculated during the downwards motion and is expressed as BFE (Freeman et al., 2009). Thus, the lower the flow energy, the less the resistance of the blade to the powder (Santana et al., 2011). It is generally assumed that lower BFE of uncompressed blends are accompanied by better flowability due to the reduction of cohesion of the individual ingredients (Mangal et al., 2016). To explain the significant model terms in Figure 76, the TBP equation can be used. Low THR and high IMP resulted in higher TBP, CBD, and BFE values. A possible reason could be that higher density resulted in a more compact powder arrangement. The consolidated powder apparently increased the resistance of the blend to the blade since more particles needed to be moved at once since they were located closer to each other without air pockets within (Freeman, 2007) (see also section 9.5.2.2 Compressibility of the powder). This is also shown

in Figure 82, where higher CBD values are accompanied by higher BFE values (Pearson correlation, r=0.882 p<0.0001).

Furthermore, higher DL led to higher BFE values. Since saccharin showed comparably high density values, it can be derived that the raw material attributes are transferred to the blend with a higher weighting through higher proportions of saccharin.

Although the model showed a high R^2 (=0.827), the Q^2 (=0.490) was relatively low. This should be considered if the following equation for this formulation is used for this set of materials.

$$BFE = 115.714 - 0.575 * THR + 0.02333334 * IMP + 0.679256 * DL \quad (42)$$

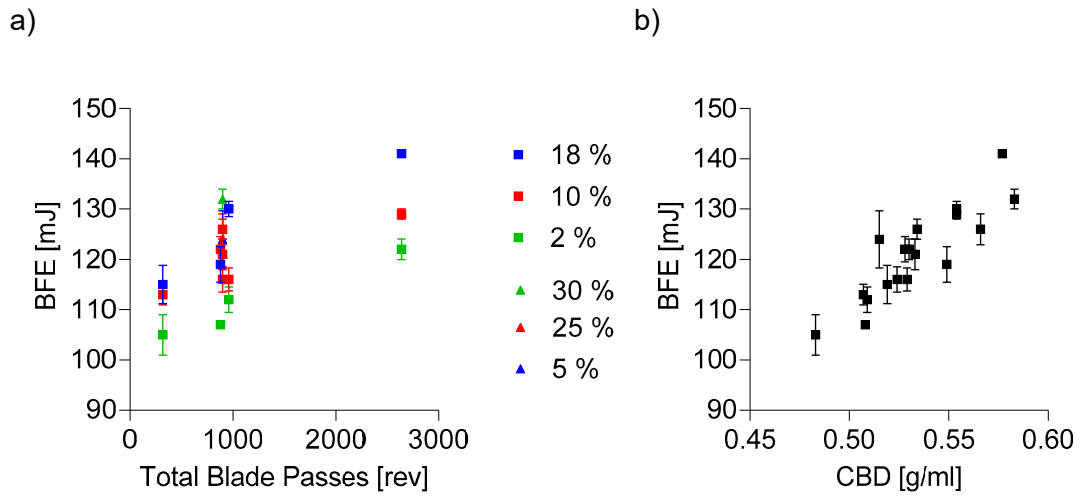

Figure 82 a) shows the BFE as a function of TBP and the corresponding DL. To emphasize the impact of TBP on CBD b) shows BFE as a function of CBD.

9.5.3 **Process Parameters**

To evaluate the impact of THR, IMP and DL on the continuous process, only one parameter of each category was assessed, where EV represents the mixing parameters, FD the tableting parameters and TS the tablet properties. Figure 83 shows the model terms regarding these three parameters based on THR, IMP and DL. Each process parameter is discussed in a separate chapter below.

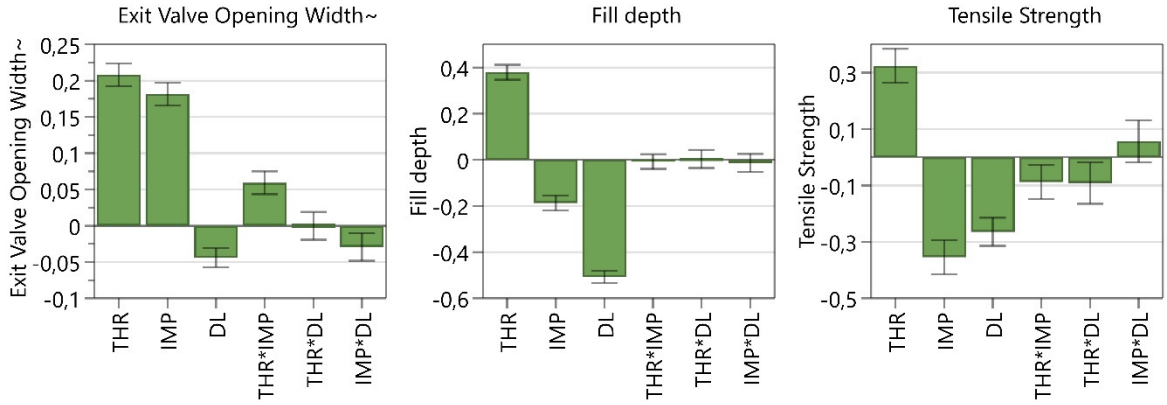

Figure 83 Coefficients plot of the impact of THR, IMP and DL on EV [mm], FD [mm] and TS [N/mm^2]**.** The 95 % confidence interval is displayed as an error bar.

After removing non-significant model terms, the following fit statistics could be obtained.

Table 51 Overview of fit statistics regarding the continuous process parameters.

Response Factor	Data Transformation	Q^2	R^2	Adjusted R^2
Exit Valve Opening Width	Logarithmic	0.984	0.993	0.991
Fill Depth	-	0.992	0.995	0.994
Tensile Strength	-	0.935	0.977	0.964

The following figures show further information regarding the model fit and demonstrate a good model performance.

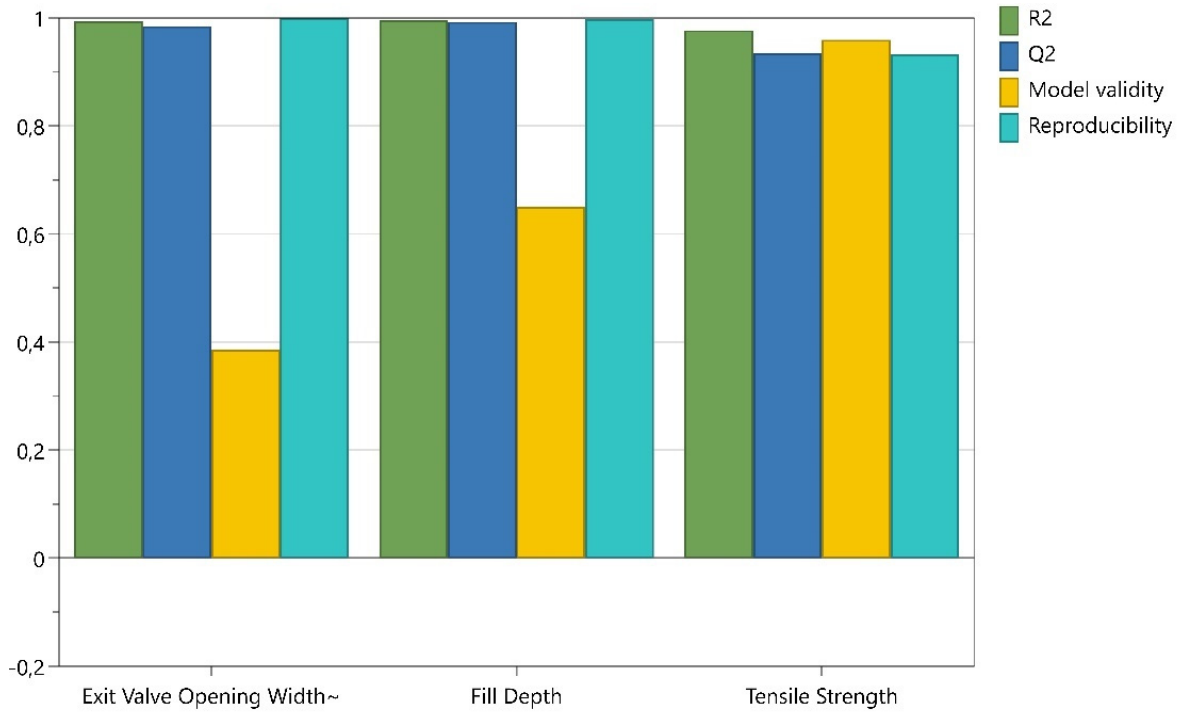

Figure 84 Summary of fit including R^2, Q^2, Model validity and Reproducibility for the considered process parameters.

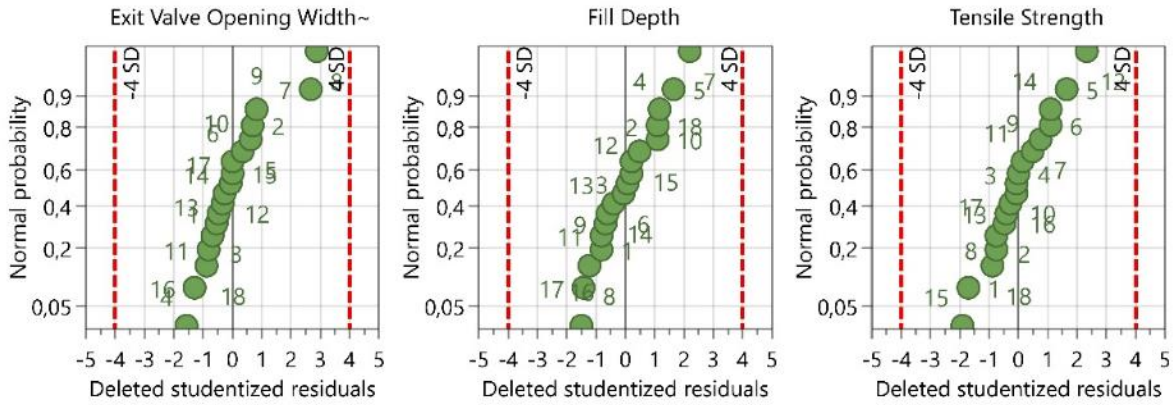

Figure 85 Overview of the residuals normal probability plots for the considered process parameters. The numbers of the data points are referred to the experiment no., as shown in Table 48.

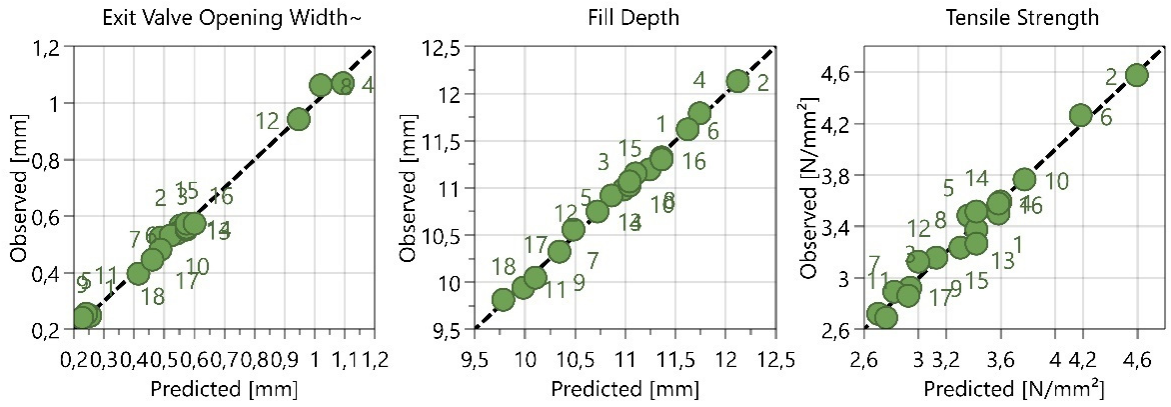

Figure 86 Overview of the comparison between observed and predicted values. The numbers of the data points are referred to the experiment no., as shown in Table 48.

9.5.3.1 Exit Valve Opening Width

Figure 83 shows the impact of the input parameters on the exit valve opening width. Higher IMP and THR resulted in higher EV values, which aligns with the previous findings in chapters 7 and 8. Moreover, lower DL resulted in higher EV values. Considering Figure 76 and Figure 82, where lower DL implied lower BFE values, it can be derived that better flowability of the powder influenced the blend to be more prone to centrifugal forces causing an 'open' powder bed and higher exit valve openings. Figure 87 demonstrates the connection between EV, DL and IMP, where higher opening widths of the exit valve could be observed at higher IMP (550 rpm).

According to the DoE Settings (Table 48), all phases with 375 rpm were run at 20 kg/h. Hence, an evaluation regarding DL and EV without the impact of IMP and THR could be carried out. Considering these data points, a slight but significant decrease in EV could be noticed with increasing DL (Pearson correlation, r=-0.985 p=0.0003).

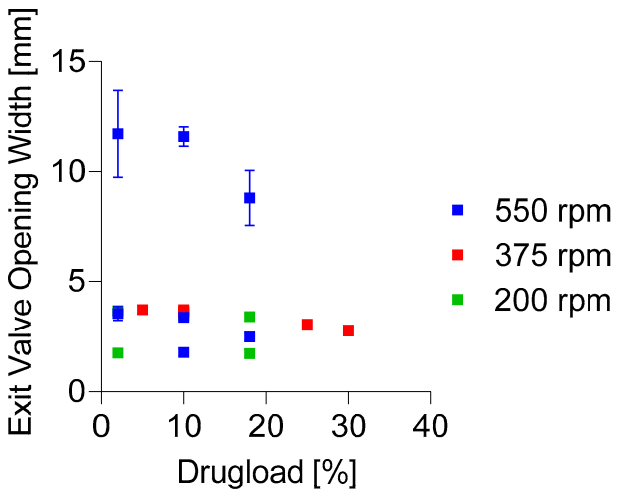

Figure 87 EV as a function of DL. The data points display the EV at 550 rpm (blue), 375 rpm (red) and 200 rpm (green).

An equation to predict the EV could be obtained:

$$Log_{10}(EV) = -0.00288867 + 0.00810256 * THR + 0.000567753 * IMP + 0.023019 * DL + 3.38677 * 10^{-5} * THR * IMP - 2.08147 * 10^{-5} * IMP * DL \quad (43)$$

9.5.3.2 **Fill Depth**

Figure 83 shows the model terms of FD. Comparable to section 9.5.2.1 Conditioned Bulk Density, high THR and low IMP resulted in low TBP, low CBD, and thus high FD to fulfil the weight requirements. Moreover, high DL led to lower FD values. Since FD depends on the blend's density, the explanation discussed for CBD applies to FD as well (Figure 88). Saccharin has a comparably high density and as the proportion of saccharin increased, the density of the blend increased, likewise resulting in lower required FDs.

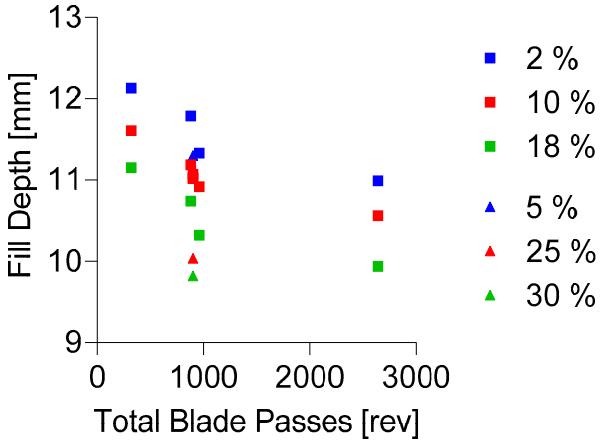

Figure 88 shows FD as a function of TBP, where blue squared data points are obtained at 2 % DL, red squared data points are obtained at 10 % DL and green squared data points are obtained at 18 % DL. Additionally, the blue, triangled data point is obtained at 5 % DL, the red, triangled data point at 25 % and the green, triangled one at 30 % DL.

An equation to predict the FD could be obtained:

$$FD = 11.3245 + 0.0379166 * THR - 0.00107143 * IMP - 0.0633723 * DL \quad (44)$$

9.5.3.3 **Tensile Strength**

The significant model terms of TS are shown in Figure 83. As discussed earlier, high THR and low IMP resulted in low TBP and, thus, low lubrication. Consequently, higher tensile strength of the tablets were obtained, as seen in the previous chapters and the literature (Kushner and Moore, 2010). Furthermore, tablets produced at lower DL showed higher TS at similar TBP, as shown in Figure 89. This illustrates the influence of alternating proportions of ingredients within the formulation on the tablet properties even if the raw materials remained unchanged. Thus, a change in material attributes based on the proportion of the ingredients in the

formulation is indicated. It can be assumed that the lubrication sensitivity of the blend increased linearly with higher DL, which can be confirmed by the findings of Bos et al., who published the linear relationship between bulk density and lubrication sensitivity (Bos et al., 1991). Considering Figure 80, where higher DL resulted in higher CBD, it can be derived that high DL also resulted in increased lubrication sensitivity.

Furthermore, THR*IMP and THR*DL significantly impacted the TS, indicating that the negative deflection of IMP and DL is dominating.

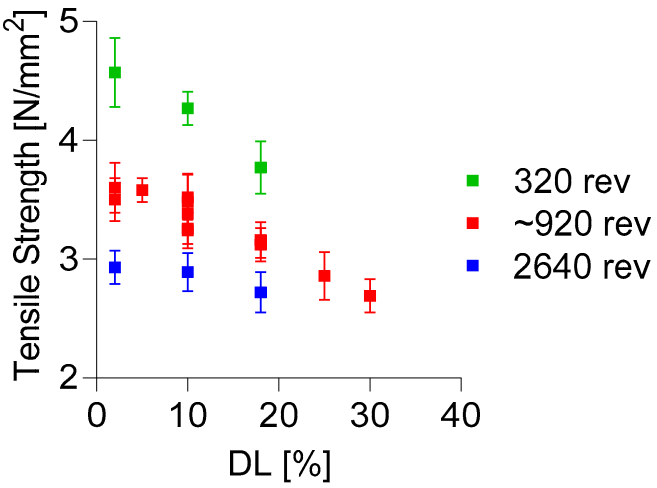

Figure 89 shows TS as a function of DL. The data points were classified according to the amount of lubrication exerted on the blend, where low (320 rev, green), medium (880 – 960 rev, red) and high TBP (2640 rev, blue) are displayed differentiated.

An equation to predict the TS could be obtained:

$$TS = 3.40964 + 0.0625729 * THR - 0.00142559 * IMP - 0.0252941 * DL - 5.00001 * 10^{-5} * THR * IMP - 0.00114062 * THR * DL + 4.01786 * 10^{-5} * \mathrm{IMP} * \mathrm{DL} \quad (45)$$

9.5.4 **Blend Uniformity**

To evaluate the impact of THR, IMP and the DL on the uniformity of API concentration in the blend, Figure 90 shows the model terms regarding MBM RSD and blend potency RSD. In this evaluation, only the API was considered, so MBM is referred to as the concentration of API within the CMT in this chapter. The blend potency was measured by the NIR probe in the feed frame as described earlier and used to calculate the API content within a tablet.

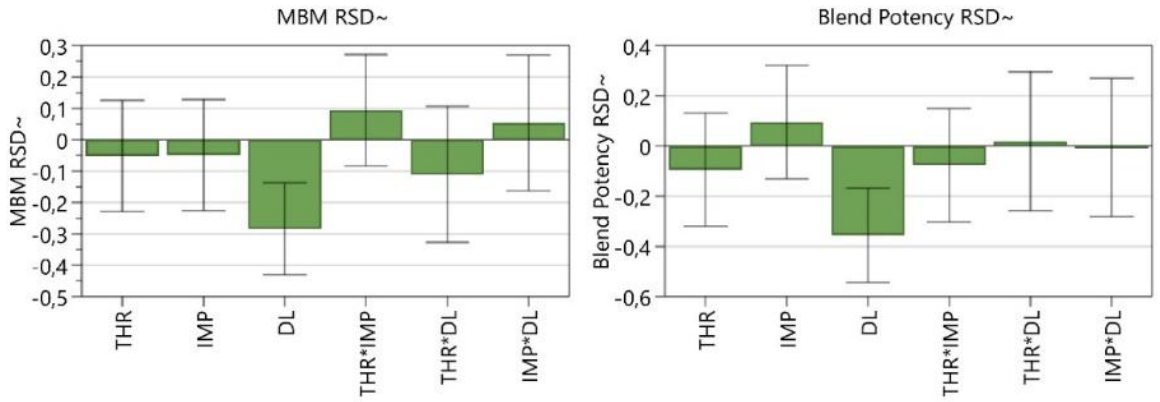

Figure 90 Coefficients plot of the impact of THR, IMP and DL on the MBM RSD [%] and Blend Potency RSD [%] measured by NIR. The 95 % confidence interval is displayed as an error bar.

After removing non-significant model terms, the following fit statistics could be obtained.

Table 52 Overview of fit statistics regarding the blend uniformity.

Response Factor	Data Transformation	Q^2	R^2	Adjusted R^2
MBM RSD	Logarithmic	0.431	0.550	0.522
Blend Potency RSD	Logarithmic	0.426	0.567	0.540

The model validity for blend potency RSD is low, which can be explained by the low variability of the data points at the three replicates (1.44 – 1.56 %).

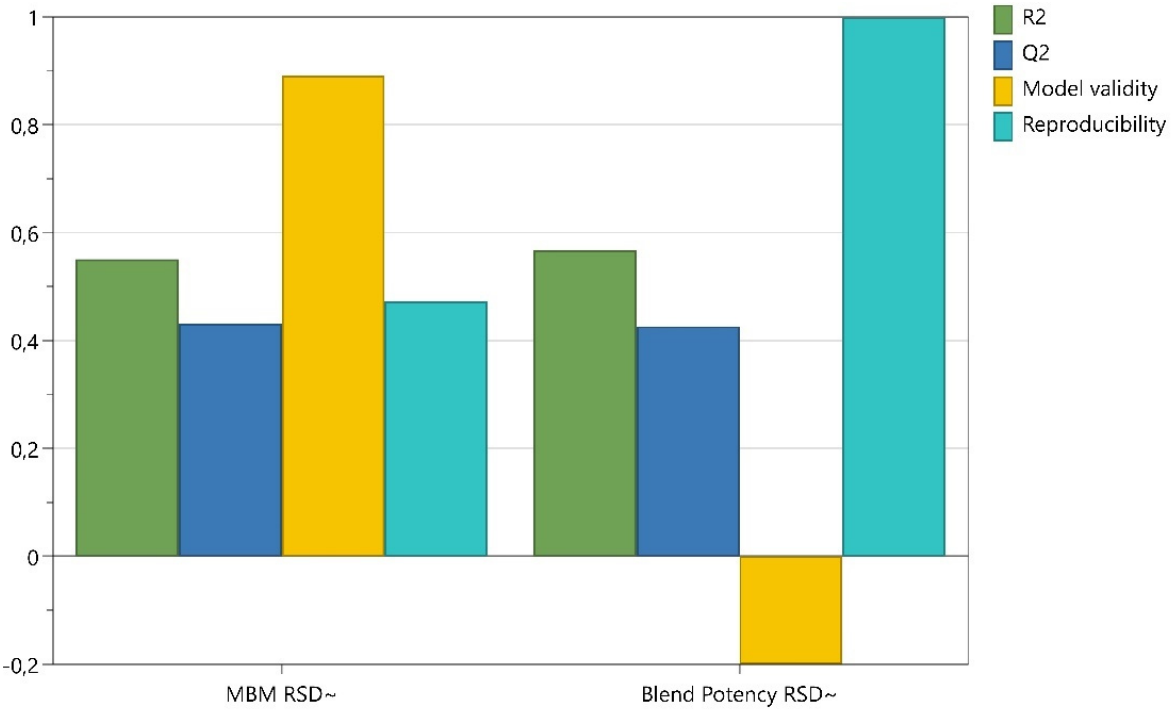

Figure 91 Summary of fit including R^2, Q^2, Model validity and Reproducibility regarding blend uniformity parameters.

The curved pattern in Figure 92 indicates non-modeled quadratic relations and, therefore, model issues for both parameters.

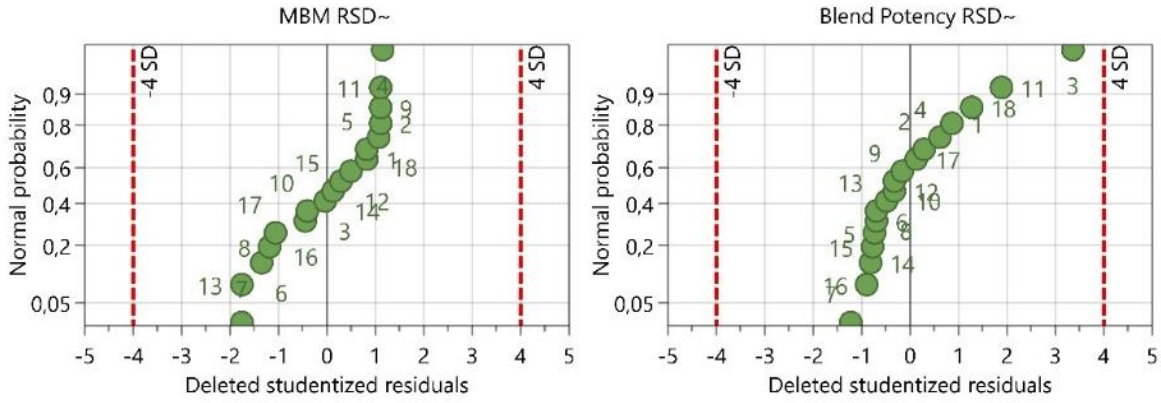

Figure 92 Overview of the residuals normal probability plots for the blend uniformity parameters. The numbers of the data points are referred to the experiment no., as shown in Table 48.

The predicted values of both parameters differed noticeably from the observed values, indicating a low model performance.

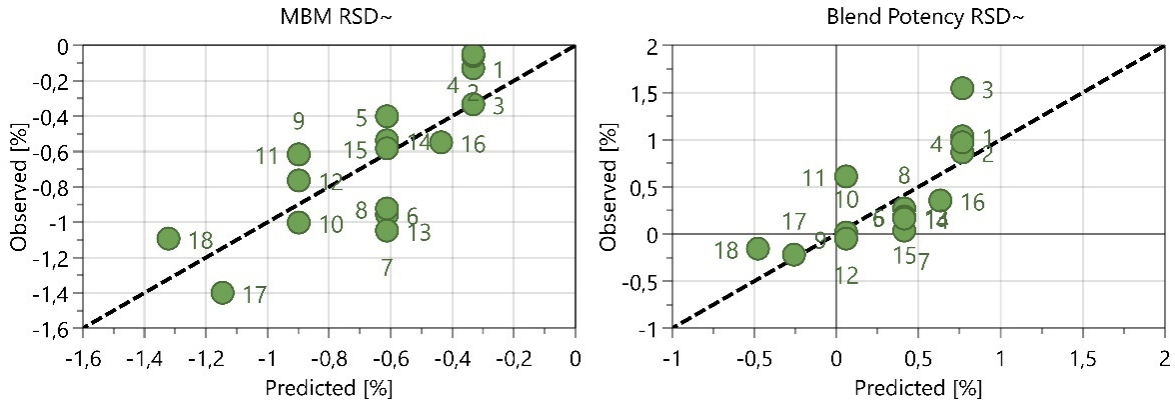

Figure 93 Overview of the comparison between observed and predicted values. The numbers of the data points are referred to the experiment no., as shown in Table 48.

9.5.4.1 **Mass Balance Model**

The MBM calculates the concentration of each raw material within the blend in real-time. Thus, it is one of the control elements of the PCMM since inhomogeneities can be detected before actual tablets are produced (see also section 2.1.4Process Control of the). Since low DLs are more prone to insufficient mixing and inhomogeneities (Bi et al., 2011; Gao et al., 2011b; Snick, 2017a), particular attention should be paid to them. Figure 90 shows the significant model terms, where only DL showed a negative deflection. So, Figure 94 shows the RSD of the saccharin concentration within the mixer as a function of DL. As expected, lower DLs resulted in higher RSDs, with the highest value being 0.89 %. This increase in RSD at lower DLs was

also seen at the feed rate RSD. However, the general low API RSD values of the MBM prove a highly sufficient mixing of this vertical, continuous mixer even for the 2 % DL runs.

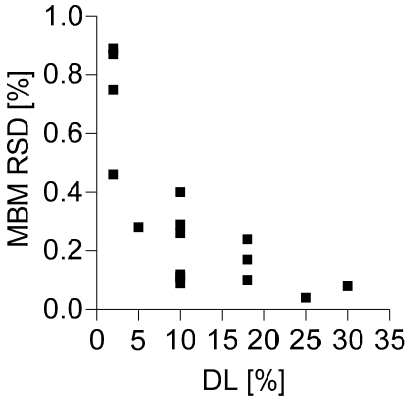

Figure 94 RSD of the saccharin concentration within the CMT as a function of the DL.

Although low R^2=0.550 and Q^2=0.431 indicate low prediction precision, the following equation could be obtained:

$$Log_{10}(MBM\ RSD) = -0.259767 - 0.0354562 * \mathrm{DL} \quad (46)$$

9.5.4.2 **Blend Potency by NIR**

As expected, in Figure 90, the same significant model term for MBM RSD was obtained, where higher DLs resulted in lower blend potency RSDs. A visualization is shown in Figure 95, where the RSD values were below 2.25 % for all runs between 5 and 30 % DL, except for one run at 18 % (3.99%). However, for 2 % DL, all four runs resulted in RSD values higher than 5 %, indicating an unfavorable process behavior compared to the other DLs.

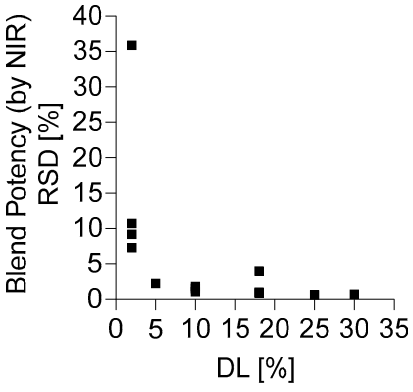

Figure 95 shows the variability of the NIR measurements in the feed frame dependent on the DL.

Comparably to MBM RSD, the low R^2=0.567 and Q^2=0.426 indicate low prediction precision as well. However, the following equation could be obtained:

$$Log_{10}(Blend\ Potency\ RSD) = 0.857509 - 0.0444184 * \mathrm{DL} \quad (47)$$

9.6 **Conclusion**

The study aimed to investigate the limits regarding the processability of continuous manufacturing if low DL were used. Therefore, a DoE was carried out where API concentrations between 2 and 18 % DL were adjusted. The design space was expanded to 30 % DL using three additional runs. Furthermore, it was evaluated to what extent specific continuous process parameters were affected by the change of the composition due to the adaption of the DL. Considering the feed performance of the adjusted ingredients, low feeder throughputs resulted in an unfavourable process condition where variability regarding the feed rate and the corresponding screw speed and FF started to increase. A minimum feeder throughput of 1 kg/h was required for this data set to provide low dosing variability. Furthermore, the impact of THR, IMP and DL on the material attributes was assessed. A linear relationship between DL and CBD could be identified indicating a relationship between the proportion of the ingredients and the respective density with the CBD of the blend.

Moreover, CBD, Comp and BFE were all functions of TBP, where the DL impacted all discussed attributes. It seemed that the attributes of saccharin were transferred to the blend according to the proportion in the formulation. This and the linear relationship between DL and the CBD of the blend are further investigated in chapter 10.

To evaluate the impact on the continuous process, three parameters were selected based on which the processability was assessed with varying THR, IMP and DL. First, the impact of TBP on FD (tableting parameter) and TS (tablet properties) could be confirmed again and the impact of THR and IMP on EV (mixing parameter) showed similar results as in chapters 7 and 8. Higher DL resulted in lower process values regarding all three parameters, which is assumed to be based on the transferred powder attributes of saccharin on the blend.

Regarding the uniformity of the blend, the MBM and blend potency measured by a NIR probe in the feed frame were analyzed. The only significant model term for both parameters was DL. In comparison, it could be seen that MBM RSD values were lower than the blend potency RSD measured by the NIR probe. However, it could be identified that both MBM RSD and blend potency RSD increased with lower API concentration. Therefore, a recommendation for F4 is a minimum DL of 5 %, maintaining a feeder throughput for saccharin > 1 kg/h.

10 Development of a Simplified Model Based on Raw Material Densities, Drug Load and Mixing Parameters

10.1 Introduction

If commercial products are manufactured by continuous manufacturing (CM), a basic process understanding is required. From time to time, it is possible that expected parameter values like required fill depth (FD) or tablet tensile strength (TS) can differ from one batch to another, even if the setting parameters remain constant. As shown in chapter 9, changes in the formulation were associated with an impact on the continuous process. So, differences between parameter levels could be caused exemplarily by density variabilities. That is why it is crucial to understand the impact of the raw materials and to consider lot-to-lot variability already during the development stages to define a robust design space of the process because moisture uptake or an adaption of the syntheses route may cause density variabilities (Almaya et al., 2017; Dave et al., 2015; Fonteyne et al., 2015; ICH, 2009; Stauffer et al., 2018).

The impact of lot-to-lot variability was already investigated in chapter 6, where the conditioned bulk density (CBD) showed significant influence on the feed factors (FF). That is why this consideration was expanded from the impact on the FF curves to the influence on the entire continuous process. So, the CBD of the raw materials were considered as another input factor to examine the fundamental impact of the raw material densities. To combine all raw material CBDs, a theoretical input density was calculated, which is explained in section 10.5.1 Conditioned Bulk Density.

In this context, the exit valve opening width (EV) could be identified as the first response to be monitored to evaluate if the combination of CMT parameters and raw material attributes are compatible during the process. So far, it could be examined that lower exit valve opening widths could result in lower EV variability and, therefore, in more uniform blend potency values measured by a NIR probe in the feed frame. In this regard, higher impeller speed (IMP) and throughput (THR) more likely resulted in higher EVs, as shown in the previous chapters.

Since the combination of CMT settings impacts the extent of lubrication, it could be seen that higher lubrication was associated with a higher density of the blend, lower fill depths, and lower tensile strengths, as shown, for example, in chapter 7 and in the literature (Kushner and Moore, 2010). Thus, regarding lot-to-lot variabilities, the complexity of the connections and dependencies within the entire continuous process needs to be considered, where each input factor influences the subsequent continuous process parameters qualitatively and quantitatively.

10.2 **Aims and Scope**

The aim of the study was to examine the impact of varying CMT settings, alternating proportion of the raw materials in the formulation and differences in densities of the excipients on continuous process parameters (EV, FD) and resulting attributes like CBD of the blend and TS. Thus, this study investigated the influence of CMT parameters in a vertical blender in combination with the theoretical ingoing density on downstream process parameters.

10.3 **Materials**

For this investigation, data of both F2 (chapter 7) and F4 (chapter 9) were combined into a new model, as shown below.

10.4 **DoE Settings and Model Building**

10.4.1 **Database**

For this chapter, the data of the DoEs carried out with F2 (DoE 2) and F4 (DoE 4) were combined to develop a new model, as shown below by means of MODDE.

10.4.2 **Combined Model**

To normalize the different proportions of mixture components in the formulation and evaluate the influence of variations in bulk density of the raw materials, a theoretical value, the input conditioned bulk density (CBDi) was calculated as shown in equation (48). This value represents the theoretical density of the blend based on the mass fraction of the composition and bulk density of each raw material. Further explanations are shown in section 10.5.1 Conditioned Bulk Density.

$$CBD_i = \frac{\sum Composition_n * CBD_n}{100} \tag{48}$$

In this equation, i stands for input and n represents each raw material. Furthermore, the input factors and responses considered in this work are shown in Table 53 and Figure 96.

Table 53 Input factors and responses considered in the model of this study.

Input Factors	**Responses**
THR [kg/h]	EV [mm]
IMP [rpm]	CBD [g/ml]
HUM [g]	FD [mm]
CBD_i [g/ml]	TS [N/mm^2]
CP [MPa]	

A linear model was used to evaluate the significant terms and included 115 TS values and 35 values for each CBD, EV and FD as shown in the appendix section A.3.1 and A.3.2. To assess the quality of the models, Q^2 (estimate of the future prediction precision) and R^2 (model fit) obtained by MODDE were considered. In addition, a k-fold cross-validation was carried out where R^2 and RMSE were calculated.

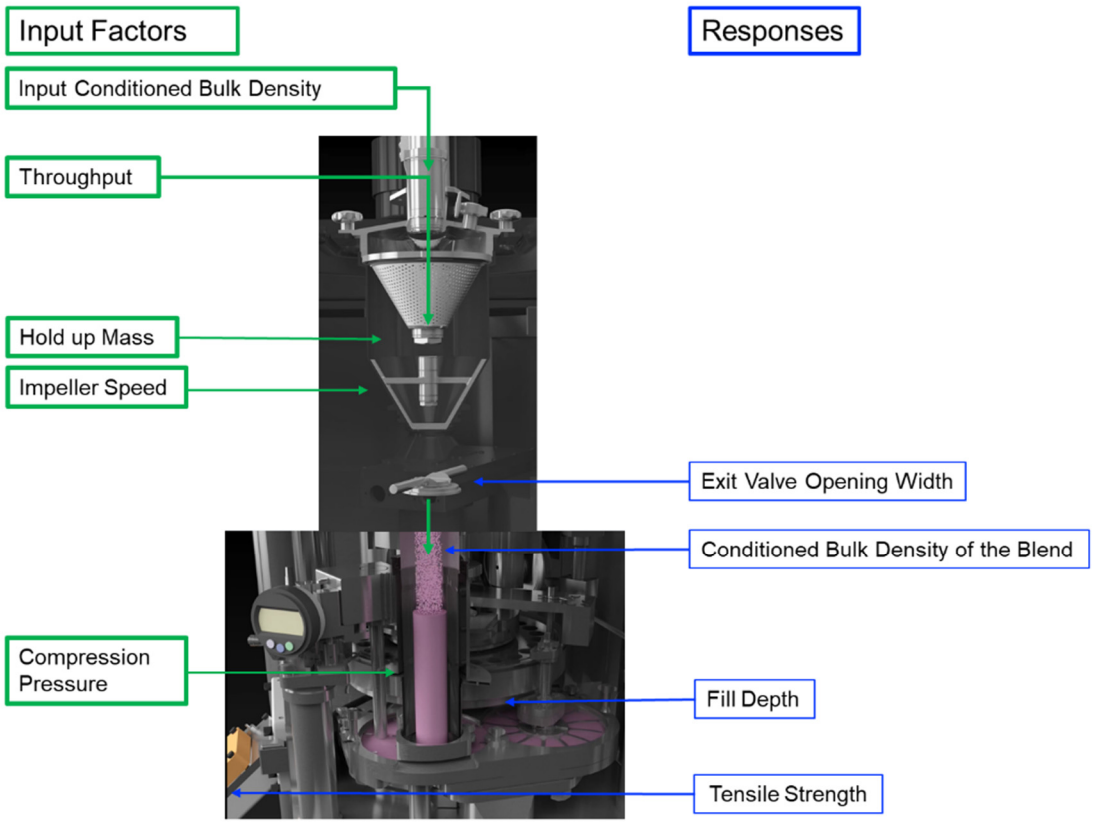

Figure 96 Visualization of the input factors (leift, green) and responses (rigth, blue) considered in the model of this study.

10.5 **Results and Discussion**

Using MODDE, the impact on the process stability (EV and FD) as well as the resulting material attributes (CBD of the blends, and TS) were evaluated against a change in input process parameters (THR, IMP, and HUM) in combination with varying composition of the formulations (incorporated as material attribute CBD_i). To examine the impact on the tensile strength the compression pressure was included, additionally. Furthermore, a k-fold cross-validation was carried out to provide additional information on the applicability of the models.

10.5.1 **Conditioned Bulk Density**

To evaluate to what extent lot-to-lot variations regarding density of the used raw materials or changes in the composition of the formulation impact the downstream process in a routine production, this study used the CBD_i as a calculated input factor to show the fundamental

influence of density on the process. As shown in equation (48), each raw material and the corresponding density, as well as the weight fraction within the formulation, were included. I.e., for each used DL, a different CBD_i could be calculated (Table 54).

10.5.1.1 **CBD Input**

Table 54 shows the CBD_i values according to the DL.

Table 54 Theoretical density of the blends (CBDi) depending on the drug load settings and CBD of each raw material calculated according to equation (48).

Formulation	DL [%]	CBDi [g/ml]
F2	21.844	0.557
F4	2	0.472
F4	5	0.477
F4	10	0.486
F4	18	0.500
F4	25	0.512
F4	30	0.521

As observed in Figure 97 and Table 55, there is a linear relationship between the measured CBD of the blends and the calculated CBD_i of the blends. For demonstration, blends mixed at high (2650 rev), medium (~900 rev) and low TBP (320 rev) were depicted in this figure. The data set of ~900 TBP includes blends mixed at 880 – 960 rev. It confirmed the linear relationship between the additively calculated CBD_i and the CBD of the blends even if the weight fraction of raw materials with varying particle sizes are included and hence, volume fractions of the constituents of the mixture are likely to deviate from their respective weight fraction. So, the use of CBD_i is a suitable approach to estimate the tableting mixture's CBD. Based on this linearity, a simplified model could be built that explains the fundamental impact of raw material densities on continuous process parameters, as further explained in the following chapter.

Table 55 fit statistics of the linear regression of the data sets shown Figure 97.

TBP [rev]	**R^2**	**p - value**	**Equation**
2650	1.000	0.0078	$CBD = 1.679 * CBD_i - 0.2621$
920	0.985	<0.0001	$CBD = 1.503 * CBD_i - 0.2009$
320	0.981	<0.0001	$CBD = 0.9181 * CBD_i + 0.05613$

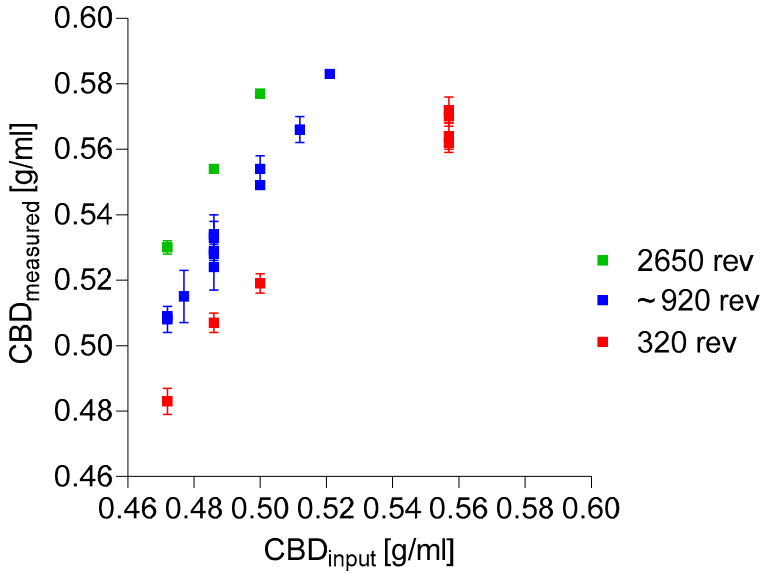

Figure 97. CBD samples taken from the feed frame and analyzed by the FT4 powder rheometer in dependence of the calculated input CBD. Green data points show the CBD of the blends mixed at 2650 rev. The blue data points show the data of blends mixed between 880 and 960 rev and the red data points represent the CBD obtained by 320 rev.

10.5.1.2 **CBD of the Blend**

As expected, the CBD_i revealed the highest impact on the CBD of the blend (Figure 98). I.e. with higher initial densities of the raw materials, the density of the blend was higher at the same CMT parameter settings. This should be considered if a different grade of raw material is used, lot-to-lot variabilities are to be expected, or if the drug load or composition changes in early development stages (Almaya et al., 2017; Dave et al., 2015; Stauffer et al., 2018). Furthermore, the knowledge about the impact of CBD_i is increasingly important if sequential addition of API is considered, where two different API lots are used in the same production run.

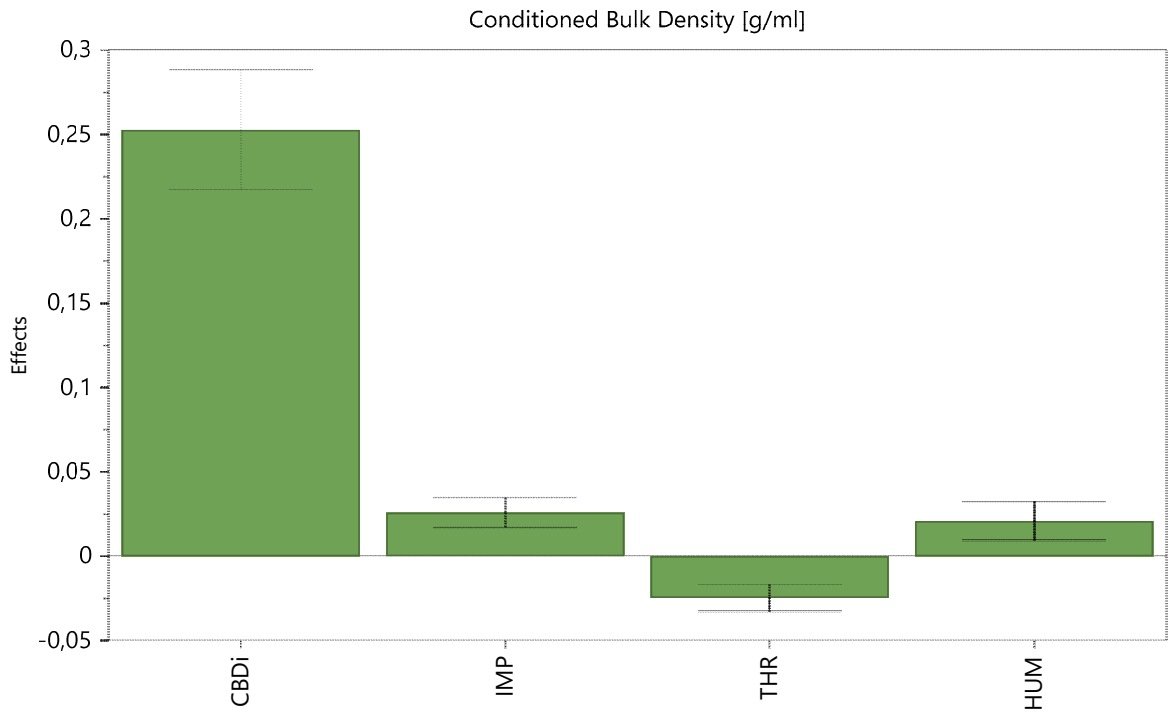

Figure 98. Impact of the input density (CBD_i) and the blender variables on the CBD of the blend measured by the FT4. The 95 % confidence interval is displayed as an error bar.

According to the TBP equation (eq. (3)), Figure 98 shows that high IMP, low THR and high HUM resulted in high TBP and, therefore, in high densities of the blend.

An equation to predict the CBD of a blend mixed by the CMT and the corresponding fit statistics are shown below.

$$CBD = 0.0814866 - 0.00123636 * THR + 5.72787 * 10^{-5} * IMP + 5.20273 * 10^{-5} * HUM + 0.842333 * CBD_i \quad (49)$$

Table 56 Overview of fit statistics regarding the conditioned bulk density of the blend.

Fit Statistics	
Q^2	0.903
R^2	0.926
Adjusted R^2	0.917

The following figures show further information regarding the model fit and demonstrate a good model performance.

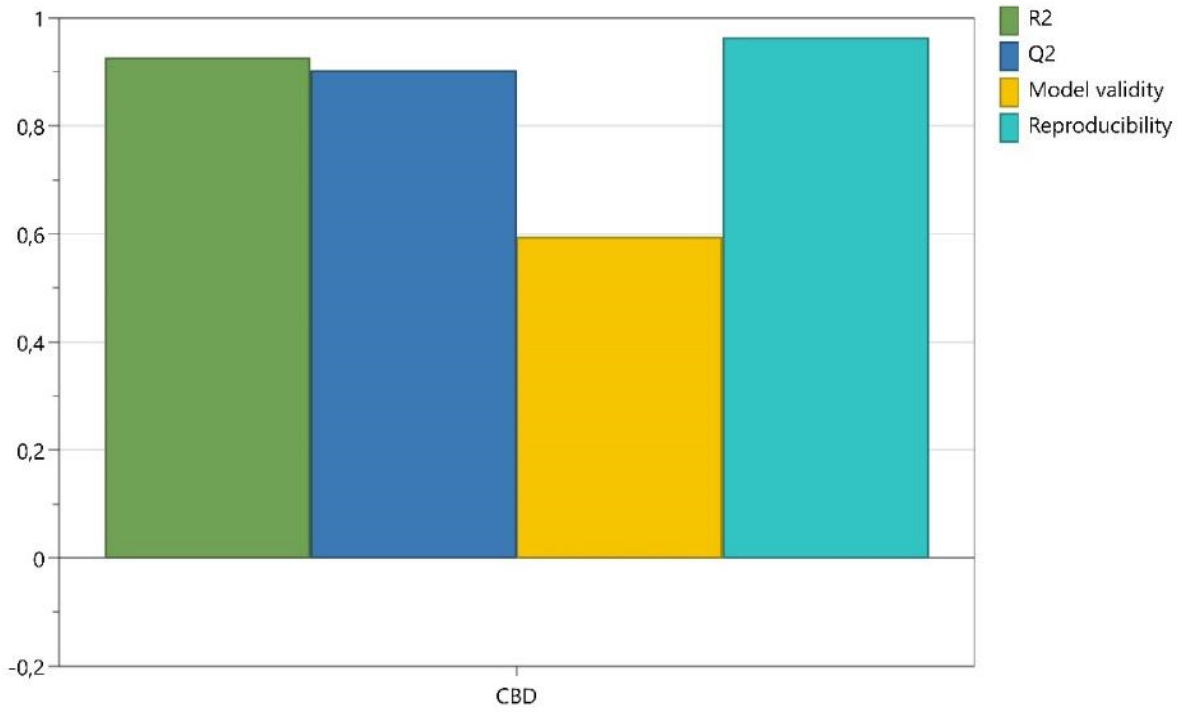

Figure 99 Summary of fit including R^2, Q^2, Model validity and Reproducibility for the CBD of the blend.

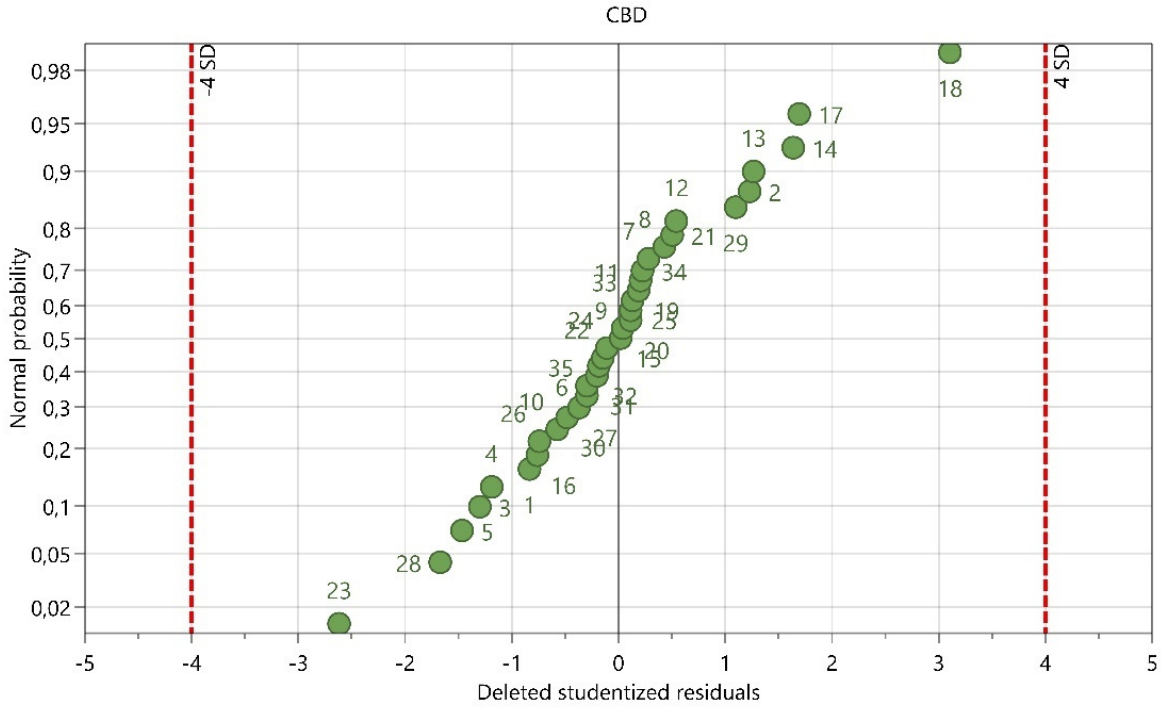

Figure 100 Overview of the residuals normal probability plots for CBD of the blend. The numbers of the data points are referred to the experiment no., as shown in Table A 2.

To additionally evaluate the predictive model, a cross validation was carried out, where the 35 settings of the DoE were partitioned into 5 data sets à 7 settings. As described earlier, 4 data

sets were used as training sets and the remaining one was used to validate the model. Therefore, for each fold, R^2 and RMSE were calculated. The averaged R^2 and RMSE of the 5 folds are shown in Table 57 and present a good model to predict the CBD of the blend based on the CMT parameters and the input density of the raw materials.

Table 57 Average values of R^2 and RMSE obtained by the k-fold cross-validation (k=5).

	Training Set	**Testing Set**
R^2	0.929	0.924
RMSE	0.008	0.010

Figure 101 compares the predicted and observed values of the CBD of the blends based on the obtained model where all 35 settings were included. The dotted line theoretically represents R^2=1.

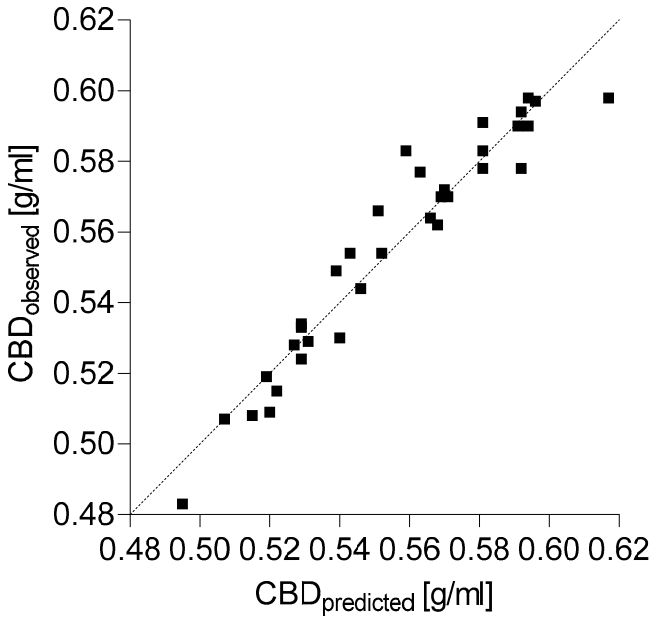

Figure 101 shows the predicted CBD values of the blend compared to the observed values of the data set, where R^2= 0.926 and RMSE=0.008 could be calculated. A reference line (dotted line) was inserted to demonstrate a theoretical perfect fit.

10.5.2 **Tensile Strength**

Figure 102 reveals the impact on TS by the combination of process parameters (THR, IMP, HUM) and material attributes (CBD_i). By far, the highest effect was obtained by the CBD_i, where higher densities resulted in lower TS. For example, in a routine production in CM, the necessity to combine two different API lots through a sequential API addition may occur. If these API lots differ in density, it impacts the TS as described in this section. To quantify this

impact, a predictive equation based on the CBD_i, the CMT parameters and the CP could be obtained.

$$TS = 9.8545 + 0.0217693 * THR - 0.00128739 * IMP - 0.000568179 * HUM - 15.6873 * CBD_i + 0.00613741 * CP \quad (50)$$

The relationship between CBD_i and TS, observed for the used materials, could be traced back to the findings of Bos et al., where an increase in lubrication sensitivity was accompanied by rising bulk densities (Bos et al., 1991).

As expected, the second input parameter is the CP, where higher pressure values resulted in higher tensile strengths of the tablet, which aligns with the literature (Shotton and Ganderton, 2011; Snick, 2017a; Sun and Grant, 2001).

Furthermore, an increase in IMP and a reduction in THR led to higher TBP, which indicates more lubrication within the blend and lower TS values, as already well documented in the literature and shown in previous chapters (Johansson, 1984; Ketterhagen et al., 2018; Mehrotra et al., 2007).

Depending on the used formulation, an increase in impeller speed may also result in higher exit valve opening widths and higher variations regarding blend potency values, as shown in chapter 7. The HUM showed only little impact, where higher values resulted in lower TS values.

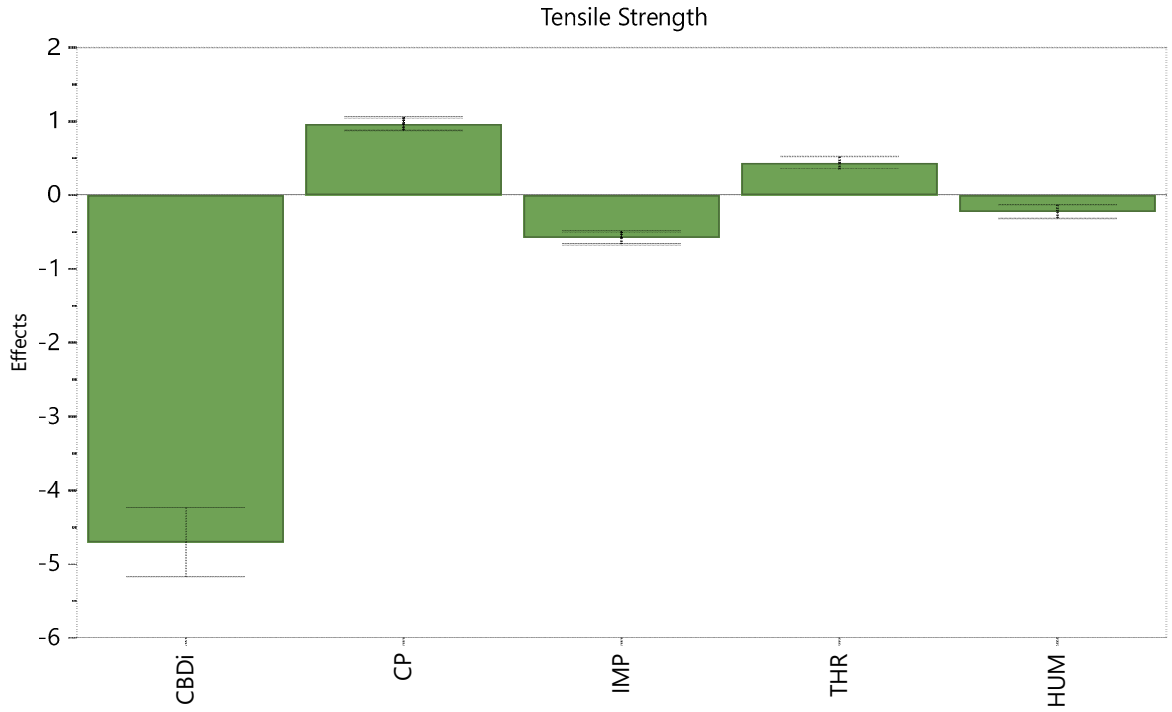

Figure 102 Impact of the input density (CBD_i), the blender variables and the compression pressure on the tensile strength of the tablets [N/mm^2]. The 95 % confidence interval is displayed as an error bar.

Corresponding fit statistics are shown in Table 58.

Table 58 Fit statistics regarding Q^2, R^2 and Adjusted R^2 obtained by the predictive model for TS.

Fit Statistics	
Q^2	0.934
R^2	0.942
Adjusted R^2	0.940

The following figures show further information regarding the model fit and demonstrate a good model performance.

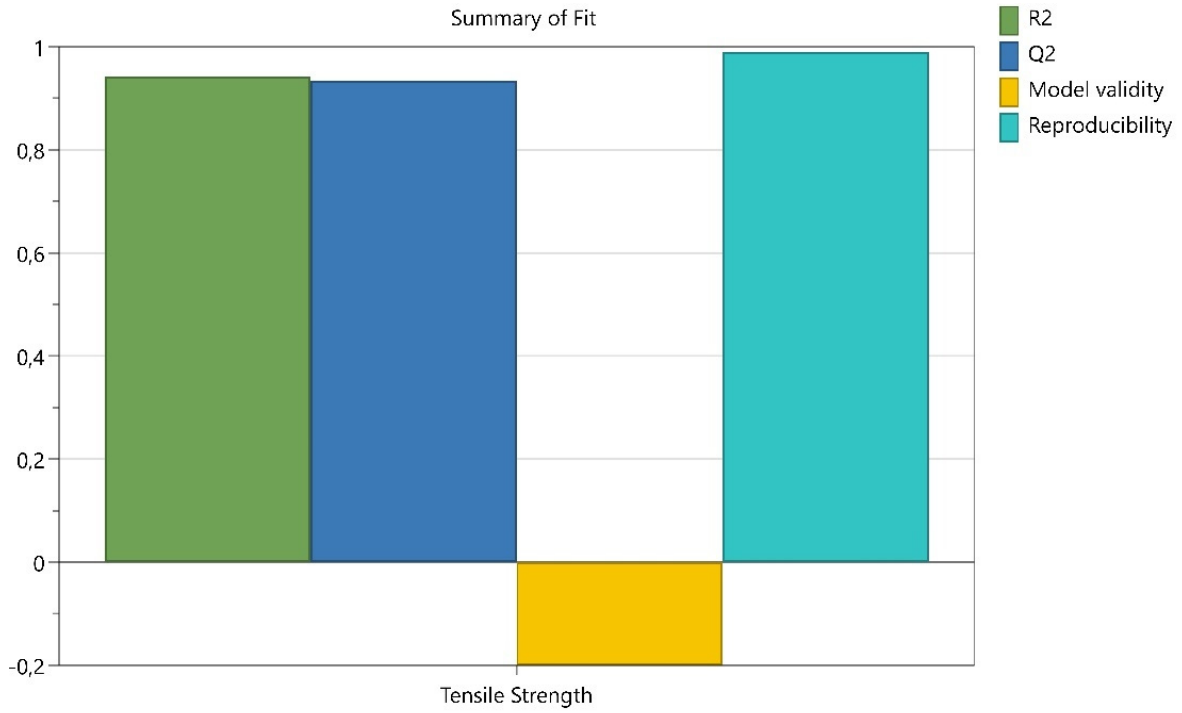

Figure 103 Summary of fit including R^2, Q^2, Model validity and Reproducibility for TS.

Low model validity can occur in very good models (Q^2>0.9) due to high sensitivity in the test. The residuals normal probability plot shows a straight line in a diagonal, indicating that the residuals are normally distributed noise.

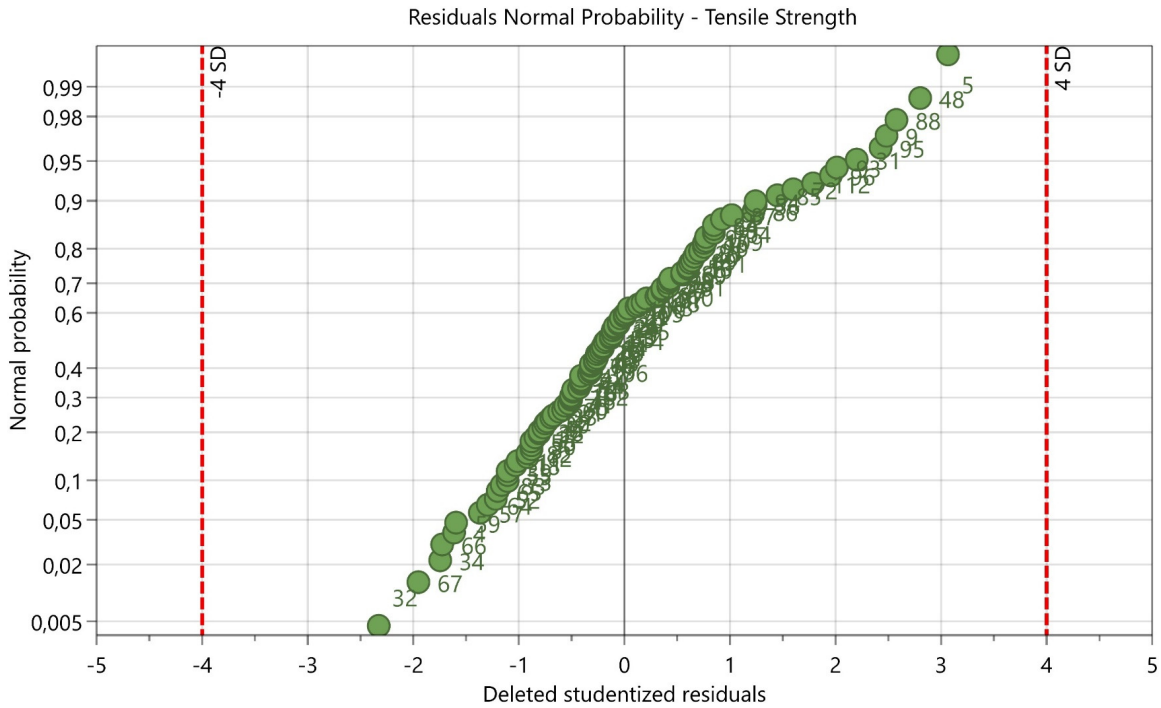

Figure 104 Overview of the residuals normal probability plot for TS. The numbers of the data points are referred to the experiment no., as shown in Table A 3.

For TS, a k-fold cross-validation was conducted, where 115 DoE settings were partitioned into 5 folds à 23 settings. Average values of R^2 and RMSE were used to evaluate the model (Table 59).

Table 59 Average values of R^2 and RMSE obtained by the k-fold cross-validation (k=5).

	Training Set	Testing Set
R^2	0.943	0.937
RMSE	0.170	0.182

Figure 105 shows the predicted and the observed values of the TS based on the obtained model where all 115 settings were included. The dotted line theoretically represents R^2=1.

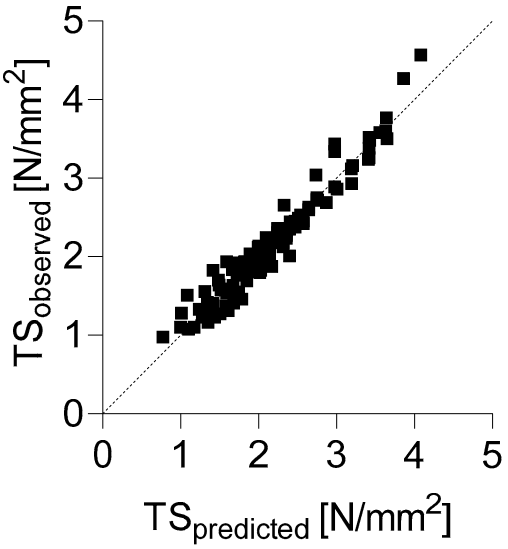

Figure 105 shows the predicted TS values compared to the observed values of the data set, where R^2=0.942 and RMSE=0.171 could be calculated. A reference line (dotted line) was inserted to demonstrate a theoretical perfect fit.

10.5.3 **Exit Valve Opening Width**

Figure 106 shows the impact of the input parameters on the exit valve opening width. It can be noticed that higher IMP and THR both resulted in higher EV values, which aligns with the findings of this work.

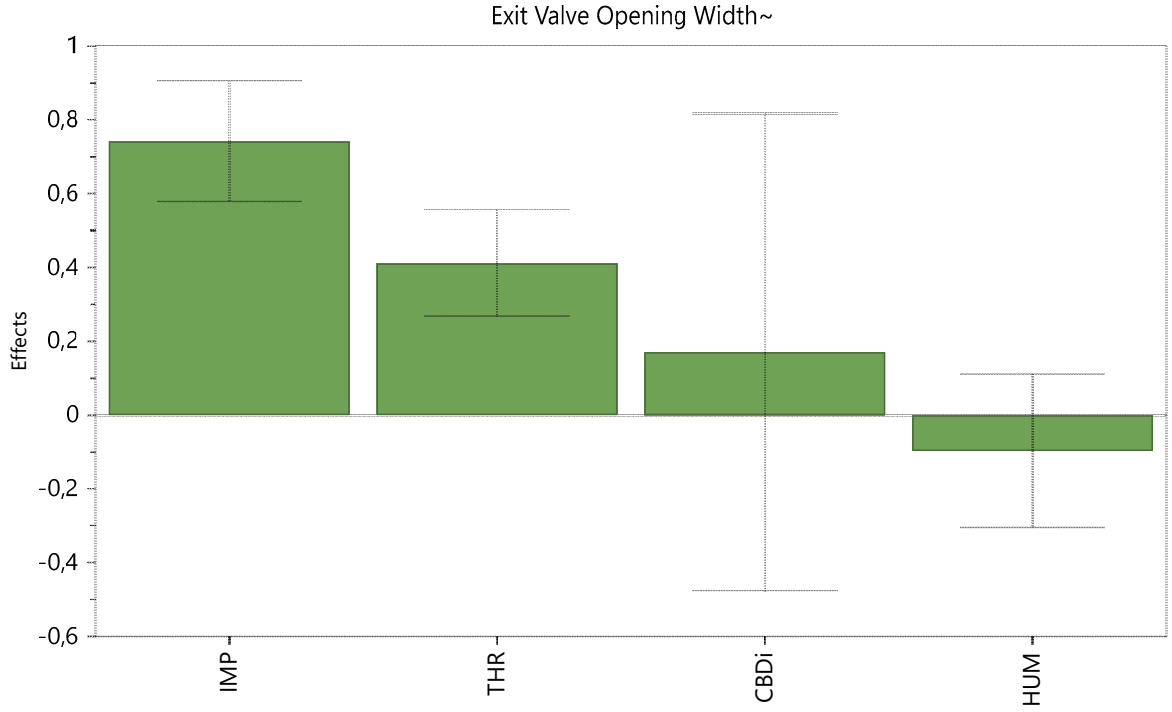

Figure 106 Impact of the input density (CBD_i) and the blender variables on the exit valve opening width [mm]. The 95 % confidence interval is displayed as an error bar.

Although the significance of the model term was not given, an increase in CBD_i indicated an increase in EV as well. A possible reason could be that higher initial densities led to increased densities of the blend (see section 10.5.1.2 CBD of the Blend). In this case, the particles were arranged more compactly and could therefore be pushed upwards by the impeller at the conical mixing area of the CMT due to the high centrifugal forces. The upwards movement of the powder at the mixer walls might cause a funnel-shaped recess in the middle of the powder bed, which requires higher exit valve opening widths to maintain a constant throughput, as shown in Figure 107 (Toson et al., 2018).

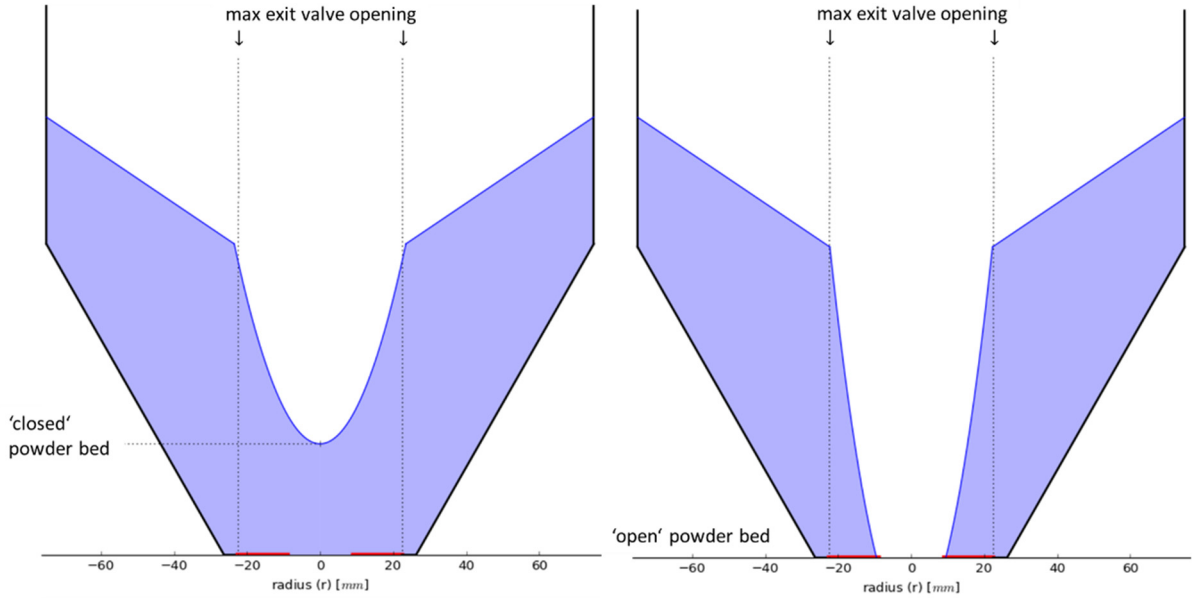

Figure 107 A theoretical, cross-sectional view of the CMT, where the left image pictures a 'closed' powder bed and the right one demonstrates a higher exit valve opening width, where the powder is pushed upwards at the wall due to high centrifugal forces.

Furthermore, a non-significant, low effect is shown by HUM.

For more clarity, a contour plot is shown in Figure 108. At low impeller speed, only low exit valve opening widths could be observed. Despite different THR, HUM and CBD_i,the process conditions within the blender were constantly favorable. At 425 rpm, the impact of throughput becomes clearer. With increasing THR, the CBD_i values are seemingly getting more important. Whereas at 10 kg/h, no impact was identifiable, at 20 kg/h EV started to rise with increasing CBD_i and HUM. With 30 kg/h, this phenomenon could be seen again, where even higher EV values resulted from the same process parameters.

In general, the figure shows that the higher the IMP (650 rpm) paired with high THR (20-30 kg/h) and CBD_i can result in wider EV openings. Additionally, it is seen that a low HUM paired with a high RPM is the worst-case scenario, resulting in the highest EV openings.

Seemingly, the impact of HUM remains constant at settings with IMP >425 rpm.

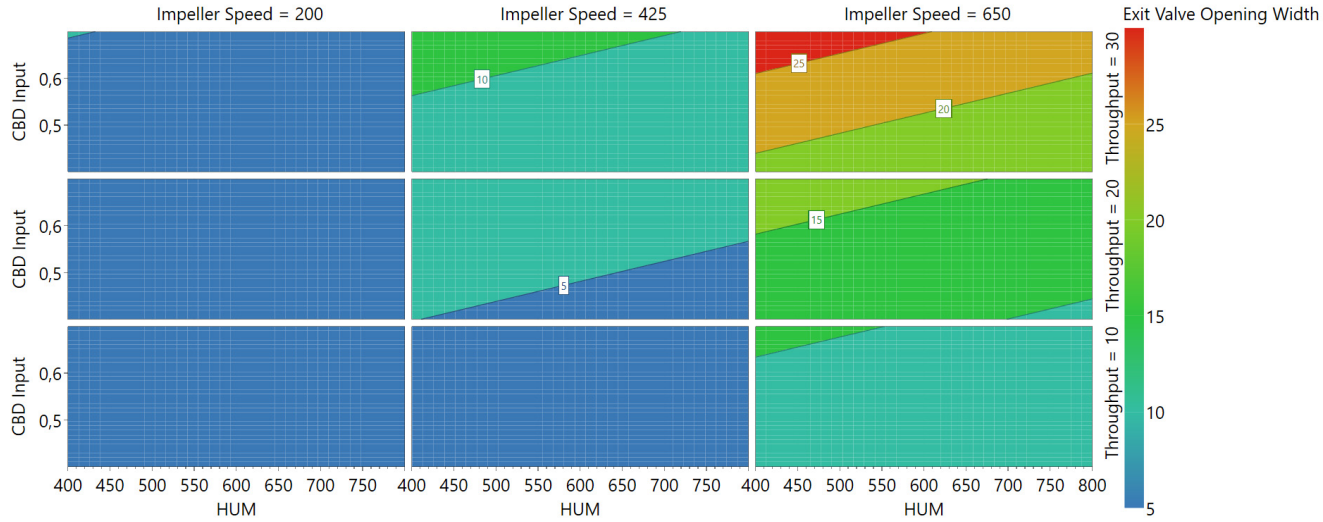

Figure 108 Contour Plot of EV [mm], where impact of CBDi [g/ml], HUM [g], IMP [rpm] and throughput [kg/h] is visualized.

By MODDE, a predictive equation could be obtained to calculate the exit valve opening widths. The equation and corresponding fit statistics are shown below. As the variability of the responses was not linearly distributed, a logarithmic data transformation was conducted.

$$log_{10}(EV) = -0.540602 + 0.0205761 * THR + 0.00164906 * IMP - 0.000243649 * HUM + 0.568407 * CBD_i \quad (51)$$

Table 60 Fit statistics regarding Q^2, R^2 and Adjusted R^2 obtained by the predictive model for EV

Fit Statistics	
Q^2	0.731
R^2	0.813
Adjusted R^2	0.788

The model validity for EV is low, which can be explained by the minimal variability of the data points at the replicates.

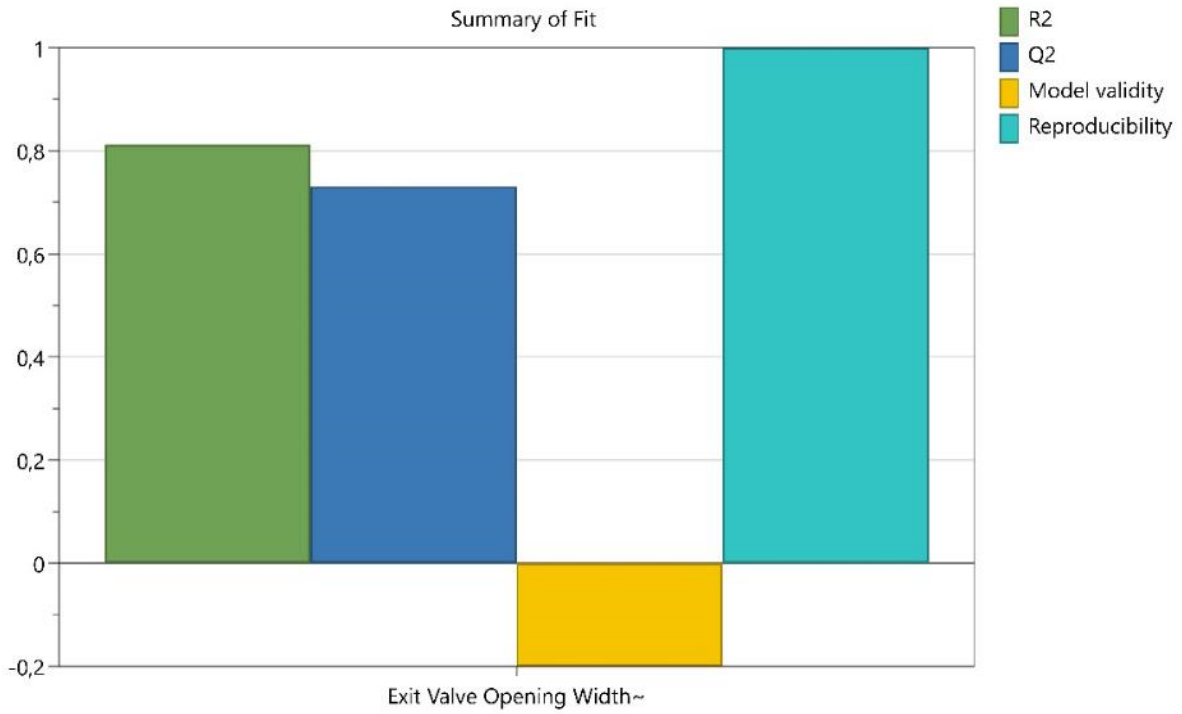

Figure 109 Summary of fit including R^2, Q^2, Model validity and Reproducibility for EV.

The normal probability plot of the residuals does not show a perfectly straight line in a diagonal but implies that the residuals are normally distributed noise.

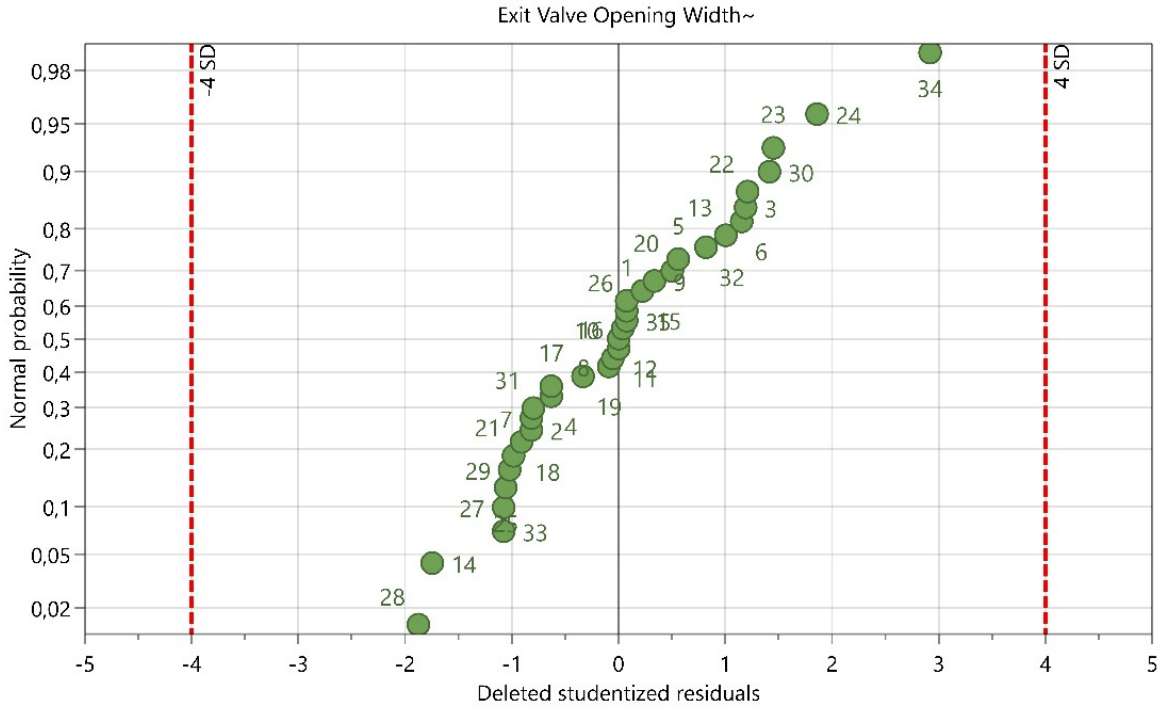

Figure 110 Overview of the residuals normal probability plot for EV. The numbers of the data points are referred to the experiment no., as shown in Table A 2.

A cross-validation was conducted to evaluate the predictive model for the exit valve opening width, where the same folds as for the CBD validation were used. The 35 settings were split into 5 sets à 7 data settings. Table 61 shows the averaged values of R^2 and RMSE of the 5 folds.

Table 61 Average values of R^2 and RMSE obtained by the k-fold cross-validation (k=5).

	Training Set	Testing Set
R^2	0.812	0.860
RMSE	4.870	4.239

The high RMSE values can be explained by the large span of exit valve opening widths obtained throughout the DoEs (1.47 – 44.28 mm), where the model did not show accurate results at higher values (Figure 111).

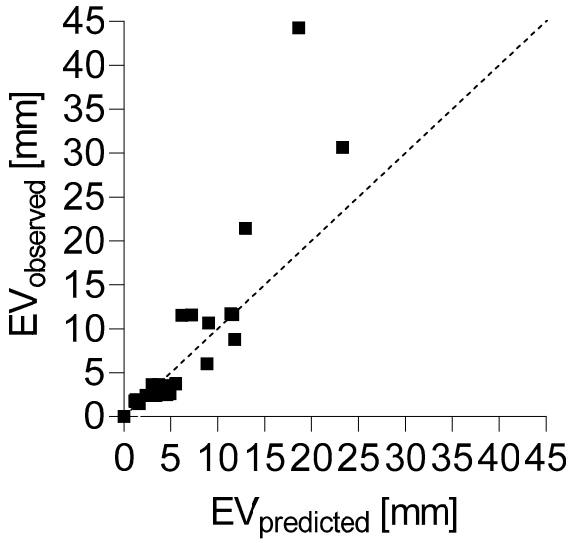

Figure 111 shows the predicted EV values compared to the observed values of the data set, where R^2=0.800 and RMSE=5.011 could be calculated. A reference line (dotted line) was inserted to demonstrate a theoretical perfect fit.

Another approach is the normalization of the CMT parameters HUM, IMP and THR to the term $\frac{HUM}{IMP^2 * THR}$, with which visualizations can help to assess the impact of the CMT process parameters on the EV. Figure 112 shows the EV as a function of this term for 10, 20 and 30 kg/h. The EV data are the calculated results of the predictive equation for EV (eq. (51)), where CBD_i was randomly set to 0.536 g/ml, IMP varied between 200 and 700 rpm, as highlighted in the legend of the graphs and HUM was used between 400 and 800 g. For example, the black data points in Figure 112 a) are the calculated EV values at 200 rpm. The data point on the right side is obtained at 400 g and the one on the left at 800 g. With increasing IMP, the values shift further to the left and therefore to smaller values of $\frac{HUM}{IMP^2 * THR}$. Simultaneously, the EV

values increase at a certain point. In this case the displayed data points for each IMP are a straight line, dependent on HUM. The slopes of these lines increase with higher IMP and THR. Furthermore, the normalization of the input parameters can help to define the ranges in which IMP and THR can be adapted to the continuous manufacturing process.

a)

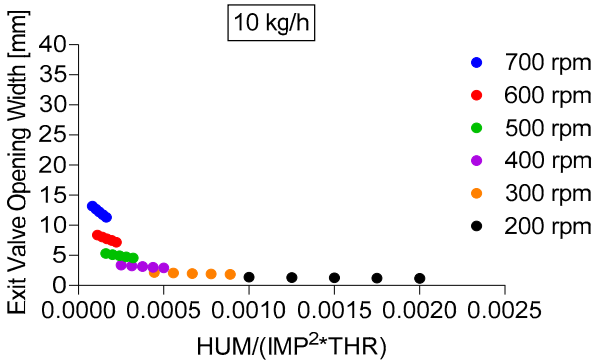

b)

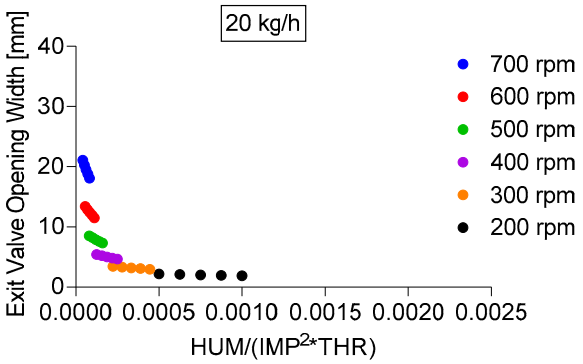

c)

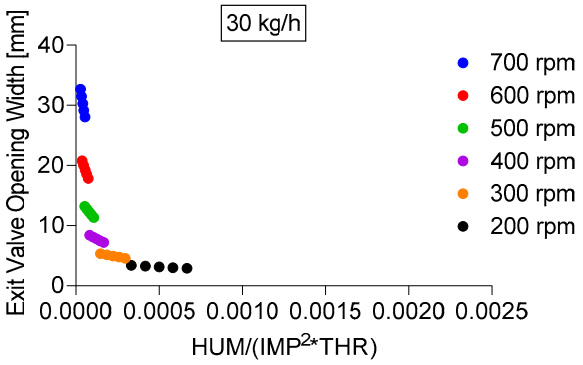

Figure 112 Exit valve opening width predictions at a) 10 kg/h, b) 20 kg/h and c) 30 kg/h. For better comparability, the x- and y-axis remained equal for the three throughputs. Exit valve opening widths shown left of the black line within the graph are higher than 5 mm.

10.5.4 **Fill Depth**

To decrease the amount of time and material needed to tune the tablet press to the required tablet weight specifications, a model equation can be used to predict the fill depth value to fulfil the requirements. Since FD and CBD of the blend strongly correlate (-0.913 p<0.0001), the impact of CBD_i must clearly be considered. As shown in Figure 113, the input density represents the highest impact on FD. Furthermore, as explained in section 10.5.1 Conditioned Bulk Density, higher TBP resulted in higher powder densities of the blend and, therefore, lower required FD settings. The deflection of the displayed effects of THR, IMP and HUM is equivalent to the TBP equation, where higher THR, lower IMP and lower HUM resulted in low TBP, low CBD and higher FDs.

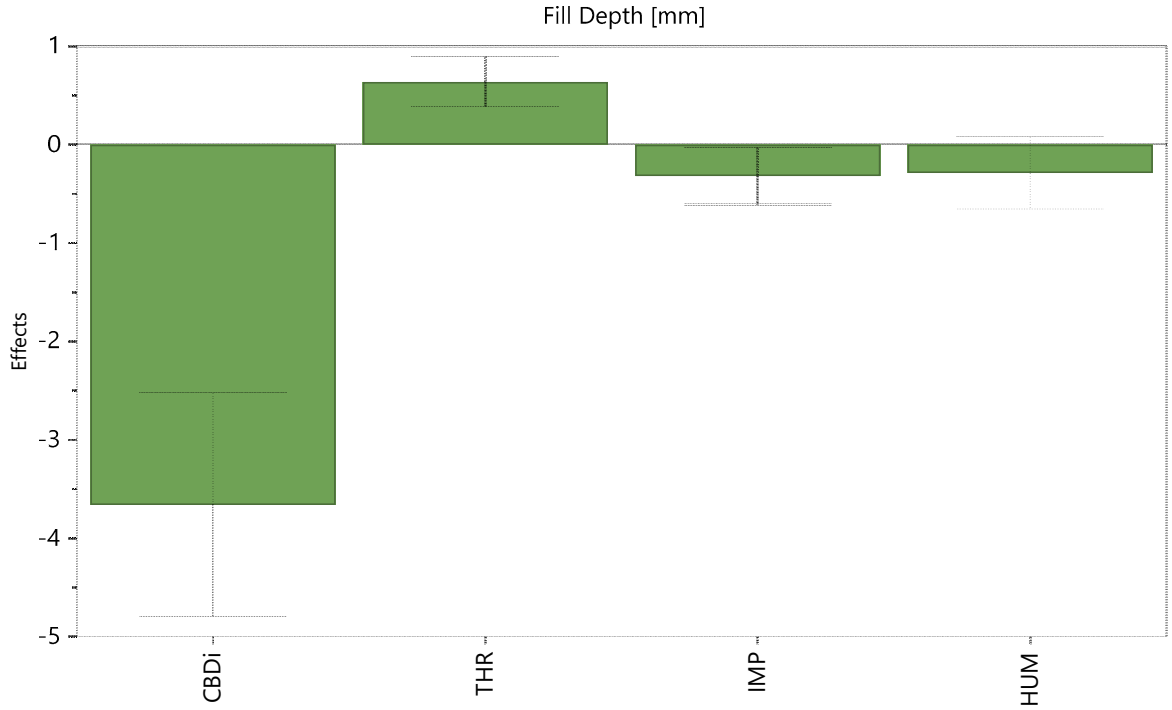

Figure 113 Impact of the input density (CBD_i) and the CMT parameters on fill depth values [mm]. The 95 % confidence interval is displayed as an error bar.

To predict the FD following equation can be used. Furthermore, corresponding fit statistics are shown below.

$$FD = 17.1808 + 0.0318637 * THR - 0.000708715 * IMP - 0.000722612 * HUM - 12{,}2042 * CBD_i \quad (52)$$

Table 62 Fit statistics regarding Q^2, R^2 and Adjusted R^2 obtained by the predictive model for FD.

Fit Statistics	
Q^2	0.689
R^2	0.757
Adjusted R^2	0.724

The model validity for FD is low, which can be explained by the minimal variability of the data points at the replicates.

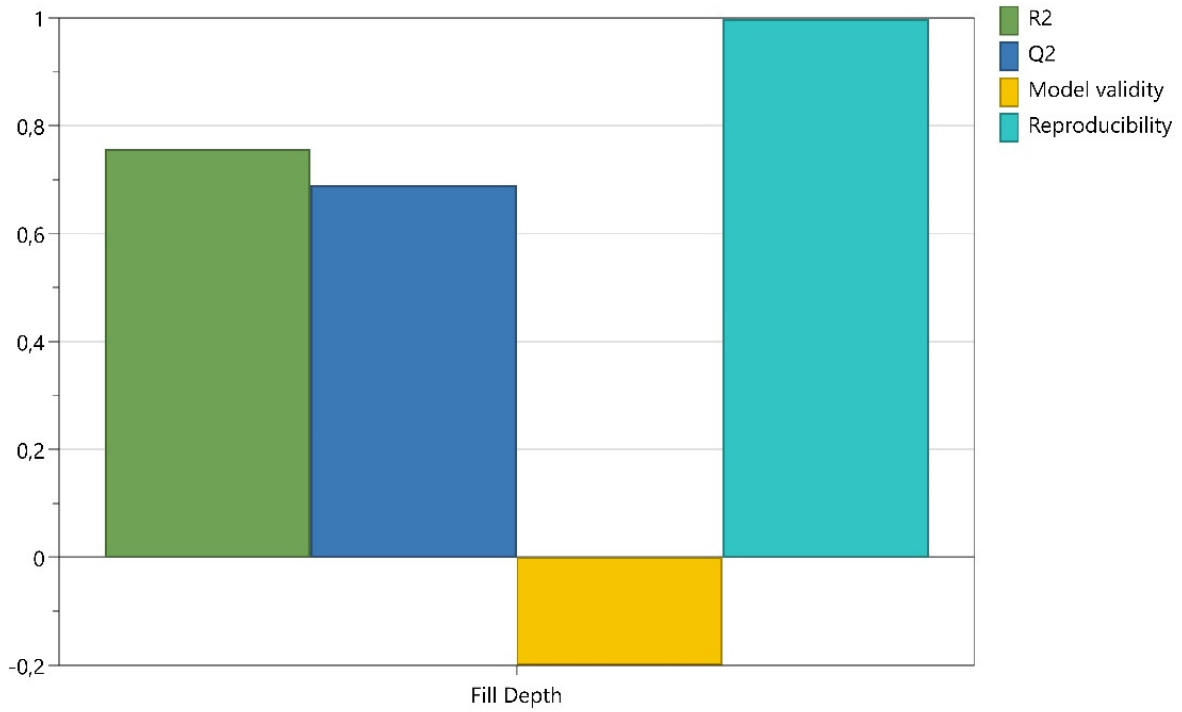

Figure 114 Summary of fit including R^2, Q^2, Model validity and Reproducibility for FD.

The curved pattern of the data points indicates model issues for FD, which is why predictions must be treated with caution.

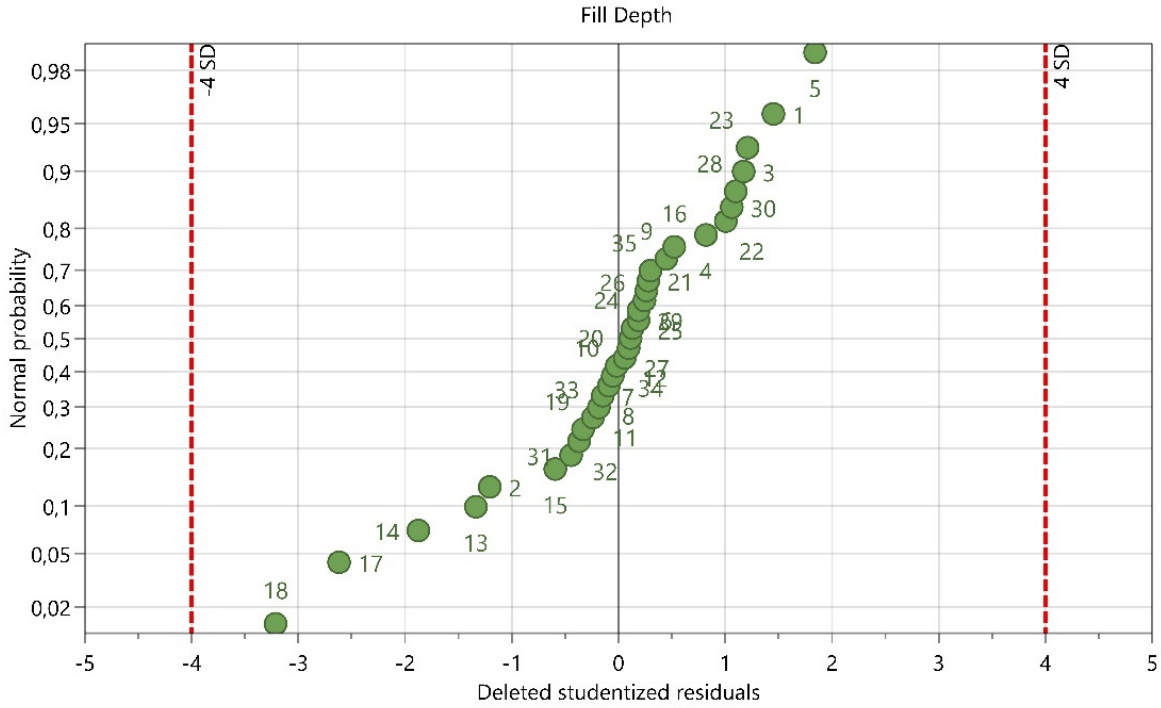

Figure 115 Overview of the residuals normal probability plot for FD. The numbers of the data points are referred to the experiment no., as shown in Table A 2.

Again, the 5-fold cross-validation was conducted for FD, where the same folds as for CBD and EV were used.

Table 63 Average values of R^2 and RMSE obtained by the k-fold cross-validation (k=5).

	Training Set	Testing Set
R^2	0.766	0.745
RMSE	0.2631	0.3246

Figure 116 shows the predicted and the observed values of the FD based on the obtained model where all 35 settings were included, where only a few data points differed between the predicted and the observed values. The dotted line theoretically represents R^2=1.

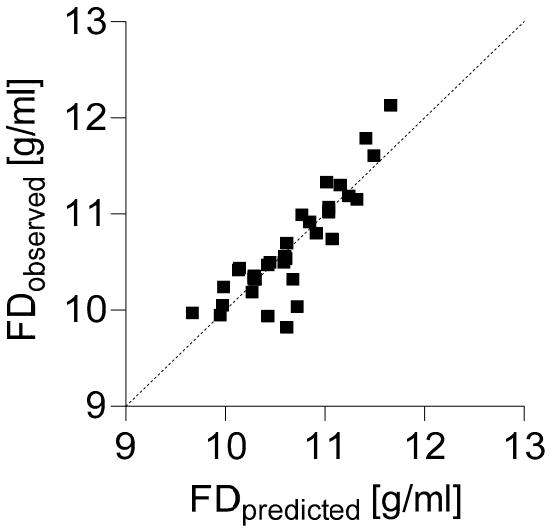

Figure 116 shows the predicted FD values compared to the observed values of the data set, where R^2=0.756 and RMSE=0.270 could be calculated. A reference line (dotted line) was inserted to demonstrate a theoretical perfect fit.

10.6 **Conclusion**

This chapter showed the evaluation of the process stability (EV and FD) and the resulting material attributes (CBD of the blends, and TS) based on THR, HUM, IMP and CBD_i in a continuous direct compression line using a vertical blender (CMT). It focused on the impact of theoretical input CBD values, which depend on the raw material densities and the proportion in the formulation. It could be examined that the ingoing CBD_i significantly impacted the CBD of the blend, the FD and the TS in a continuous process. With the implementation of the simplified model based on the calculated CBD_i and the CMT variables, the adjustment of the considered process parameters can be facilitated when different grades of ingredients need to be taken into account.

Furthermore, CBD, FD and TS were impacted by the TBP, where more revolutions resulted in higher CBD, lower FD and lower TS.

For TS, CP was added as an additional input factor to the model and presented a significant impact, where higher CP resulted in higher TS values.

Regarding EV, high THR and high IMP significantly increased the opening width of this valve. For further information, a normalization of the CMT parameters was shown to evaluate the process window of acceptable exit valve opening widths based on THR, HUM and IMP, proving the importance of THR and IMP.

Additionally, a k-fold cross-validation (k=5) was carried out to evaluate the model performance. For that, the average values of R^2 and RMSE of the training and the testing sets were calculated. The obtained R^2 and RMSE of the training and the testing sets indicated a good

model fit for TS and CBD. Slight model weakness for FD and EV could be observed, whereas the relatively high RMSE values for the EV could be caused by the high span of process data (1.47 – 44.28 mm).

In general, if changes in the input variables are to be expected, predictive equations could be obtained by MODDE, with which the impact on the continuous process can be assessed.

11 Summary and Outlook

The modularity of the continuous manufacturing line PCMM is accompanied by a complexity of parameter connections and process dependencies. To develop a holistic understanding of the continuous process, this work examined the interaction of material attributes, setting parameters and the influence on the subsequent parameters and tablet properties.

The first process unit of the PCMM is the feeder. To investigate the impact of screw pitch (ScP), refill level (RL), gearbox type (GB) and top up volume (TU) on the feed performance, a DoE was carried out using three different raw materials (chapter 5). To evaluate the process response to the varying settings, feed rate, feed factor (FF), screw speed and the corresponding RSD values of each parameter were considered. By means of this screening, potential adjustments to improve the feed performance could be found. So, increasing ScP could reduce the variability of feed rate, FF and screw speed and lower the risk of feed rate peaks during a refill, accompanied by a reduced span of FF and screw speed. Raising the RL could optimize the feed rate for powders with higher density.
Furthermore, variability, as well as the range before and after a refill of FF and screw speed, could be minimized. Lower TU could reduce the span of screw speed and, at higher densities, the FF RSD. In this DoE, the material attributes were not included in the design but were involved due to the repetition of this trial with three different raw materials. Further investigations are recommended to assess the interaction of material attributes, feeder settings, feeder throughput, and feed performance.

A method to predict the FF was developed in chapter 6. For that, FF calibrations with mixtures consisting of MCC and SiO_2 were conducted. Using a non-linear regression, the FF curves could be replicated and the variables Y_0, Y_M and k were obtained. Y_0 is the FF at the end of the FF calibration, Y_M is the FF at the beginning of the FF calibration and k determines the rate constant in which the FF decrease at some point. Using MODDE, the three variables could be predicted based on screw pitch (ScP), throughput (THR), conditioned bulk density (CBD) and compressibility (Comp). Suitable applicability was implied due to high R^2 and low RMSE values.
Nevertheless, only one set of materials was investigated, with which the basic feasibility of this method could be shown. The applicability for different powders was not investigated and needs to be done if this method will be used in the future for ingredients of a commercial product. The next step could be expanding the model to other powders with different material attributes. In the future, an elaboration of this procedure for commercial products could be scheduled and the feasibility of carrying out FF calibration during the development phase of a product should be checked.

The PCMM is equipped with a vertical continuous blender, where THR, HUM and IMP are considered the setting parameters. Different combinations of the three parameters result in different MRTs and TBP, influence the lubrication of the blend and impact the downstream process parameters. To comprehend the impact of the CMT parameters, two DoEs using two different formulations were carried out to investigate correlations and connections between the CMT settings and the downstream process and, moreover, between the individual process states along the continuous process. In chapter 7, it could be shown that exit valve opening width and variability in exit valve, hold up mass, torque and blend potency correlate significantly, which can all be controlled mainly by impeller speed. If improvement of these parameters is required, it could be observed that changes in impeller speed also led to changes in TBP, which significantly correlated with the blend's material attributes, fill depth and tensile strength of the tablets. For F2, a sweet spot could be obtained by MODDE, where the optimal setting for this formulation was high throughput, high HUM and 200 rpm IMP to maintain setpoints regarding EV, blend potency, TW SD and TS. In chapter 8, an alternative formulation was used to confirm the process connections and parameter dependencies found in chapter 7 to establish a fundamental understanding of the process behavior based on the CMT settings. Therefore, Table 64 highlights the mutual, significant model terms in bold and can be considered formulation independent. So, according to the results of both DoEs, the process dependencies shown in Table 64 will most likely occur in future formulations. To expand these studies, a closer look at the lubrication sensitivity can be taken, where particle shapes and different lubricant grades may be considered.

Table 64 Overview of the significant model terms obtained by F3 (chapter 8) and F2 (chapter 7). The mutual model terms are highlighted in bold.

	Formulation 3 (chapter 8)	**Formulation 2 (chapter 7)**
EV	**THR, IMP**, IMP*IMP, THR*IMP	**THR, IMP**
EV SD	HUM, **IMP**, THR*IMP	**IMP**
HUM SD	**THR**, **HUM**, THR*HUM	**THR, HUM,** IMP
T_L	**HUM, IMP**, IMP*IMP	**HUM, IMP**
T_L SD	**IMP**	**IMP**
Blend Potency SD	-	IMP
CBD	**THR, HUM, IMP**, THR*IMP	**THR, HUM, IMP**
FRI	-	THR, IMP, THR*THR
d_{10}	**THR, IMP**	**THR**, HUM, **IMP**
FD	**THR**, HUM, **IMP**	**THR, IMP,** THR*THR
BCH	**THR**, THR*HUM	**THR**, HUM, IMP, IMP*IMP, THR*IMP
EF	**THR, THR*THR**	**THR**, IMP, **THR*THR**
TS	**THR, HUM, IMP, HUM*IMP**	**THR, HUM, IMP**, THR*THR, THR*IMP, **HUM*IMP**
TS SD	THR*HUM, THR*IMP	-

To evaluate a suitable process window in which different DLs are still processable, a DoE with varying DL between 2% and 30 % saccharin concentration was carried out (chapter 9). It could be shown that lower DL resulted in higher variability of MBM and blend potency measured by NIR. Nevertheless, the highest MBM RSD was 0.89 %, demonstrating a highly efficient mixing, whereas, for the blend potency, all values obtained at 2 % DL were higher than 5 % blend potency RSD. Therefore, a minimum DL of 5 % is recommended for this formulation. Using this DoE, it was evaluated to what extent specific continuous process parameters were affected by the change of the composition due to the adaption of the DL. Considering the feed performance of the adjusted ingredients, low feeder throughputs resulted in an unfavorable process condition where variability regarding the feed rate and the corresponding screw speed and FF started to increase. A minimum feeder throughput of 1 kg/h was required for this data set to provide low dosing variability.

Furthermore, CBD, Comp and BFE were all functions of TBP, where the DL impacted all material attributes. It seemed that the attributes of saccharin were transferred to the blend according to the proportion in the formulation resulting in high CBD, Comp and BFE with higher

DLs. Regarding fill depth (FD) and tensile strength (TS), the impact of TBP could be confirmed again. Furthermore, THR and IMP impacted the EV, as shown in chapters 7 and 8.
Regarding DL, it could be seen that the higher saccharin concentrations resulted in lower process values regarding all three process parameters. To expand these findings, future work could repeat the study with alternative materials and API, respectively, to obtain more experience regarding the processability of low DLs and analyze possible influencing factors for the process behavior.

As the impact of lot-to-lot variability was already investigated in chapter 6, this consideration was expanded from the impact on the FF to the influence on the entire continuous process. Therefore, the data from chapters 7 and 9 were combined and a new model was built (chapter 10). Since the basic formulation was the same and only composition changes were made, a theoretical “input density“ (CBD_i) could be calculated.
It could be shown that CBD_i and TBP significantly impacted the apparent CBD of the blend, the FD and the TS. For TS, the compression pressure (CP) was added as an additional input factor to the model and presented a significant impact, where higher CP resulted in higher TS values.
Regarding EV, high THR and high IMP significantly increased the opening width of this valve, as already shown in the previous chapters. For further information, a normalization of the CMT parameters was introduced to evaluate the process window of acceptable exit valve opening widths based on THR, HUM and IMP, proving the importance of THR and IMP.
A k-fold cross-validation (k=5) was carried out to evaluate the model performance. The obtained R^2 and RMSE of the training and the testing sets indicated a good model fit for TS and CBD. Slight model weakness for FD and EV could be observed, whereas the high RMSE values for the EV could be caused by the high span of process data (1.47 – 44.28 mm).
Future work should assess if the theoretical calculation of material attributes, like CBD_i, is applicable for further attributes and materials. So, the risks regarding implementing, e.g., different API grades or sequential API addition, can be assessed upfront more thoroughly.

12 Publication

Excerpts from the work were previously published at the following location:

Kreiser, Marius J., Christoph Wabel, and Karl G. Wagner. 2022. "Impact of Vertical Blender Unit Parameters on Subsequent Process Parameters and Tablet Properties in a Continuous Direct Compression Line" *Pharmaceutics* 14, no. 2: 278. https://doi.org/10.3390/pharmaceutics14020278

13 References

Abdel-Hamid, S., Koziolek, M., Betz, G., 2012. Study of radial die-wall pressure during high speed tableting: effect of formulation variables. Drug Development and Industrial Pharmacy 13.

Abdullah, E.C., Geldart, D., 1999. The use of bulk density measurements as flowability indicators 15.

Almaya, A., Aburub, A., 2008. Effect of Particle Size on Compaction of Materials with Different Deformation Mechanisms with and without Lubricants 5.

Almaya, A., De Belder, L., Meyer, R., Nagapudi, K., Lin, H.-R.H., Leavesley, I., Jayanth, J., Bajwa, G., DiNunzio, J., Tantuccio, A., Blackwood, D., Abebe, A., 2017. Control Strategies for Drug Product Continuous Direct Compression—State of Control, Product Collection Strategies, and Startup/Shutdown Operations for the Production of Clinical Trial Materials and Commercial Products. Journal of Pharmaceutical Sciences 106, 930–943. https://doi.org/10.1016/j.xphs.2016.12.014

Anuar, M.S., Briscoe, B.J., 2009. The elastic relaxation of starch tablets during ejection. Powder Technology 195, 96–104. https://doi.org/10.1016/j.powtec.2009.05.019

Azad, M.A., Osorio, J.G., Wang, A., Klee, D.M., Eccles, M.E., Grela, E., Sloan, R., Hammersmith, G., Rapp, K., Brancazio, D., Myerson, A.S., 2019. On-Demand Manufacturing of Direct Compressible Tablets: Can Formulation Be Simplified? Pharmaceutical Research 36. https://doi.org/10.1007/s11095-019-2716-2

Badman, C., Trout, B.L., 2014. Achieving Continuous Manufacturing 2.

Bekaert, B., 2021. Determination of a quantitative relationship between material properties, process settings and screw feeding behavior via multivariate data-analysis. International Journal of Pharmaceutics 18.

Berrar, D., 2019. Cross-Validation, in: Encyclopedia of Bioinformatics and Computational Biology. Elsevier, pp. 542–545. https://doi.org/10.1016/B978-0-12-809633-8.20349-X

Bi, M., Sun, C.C., Alvarez, F., Alvarez-Nunez, F., 2011. The Manufacture of Low-Dose Oral Solid Dosage Form to Support Early Clinical Studies Using an Automated Micro-Filing System 8.

Blackwood, D.O., Bonnassieux, A., Cogoni, G., 2019. CONTINUOUS DIRECT COMPRESSION USING PORTABLE CONTINUOUS MINIATURE MODULAR & MANUFACTURING (PCM&M), in: Chemical Engineering in the Pharmaceutical Industry. John Wiley & Sons, Ltd, pp. 547–560. https://doi.org/10.1002/9781119600800.ch72

Bos, C.E., Vromans, H., Lerk, C.F., 1991. Lubricant sensitivity in relation to bulk density for granulations based on starch or cellulose 11.

Bostijn, N., Dhondt, J., Ryckaert, A., Szabó, E., Dhondt, W., Van Snick, B., Vanhoorne, V., Vervaet, C., De Beer, T., 2019. A multivariate approach to predict the volumetric and gravimetric feeding behavior of a low feed rate feeder based on raw material properties. International Journal of Pharmaceutics 557, 342–353. https://doi.org/10.1016/j.ijpharm.2018.12.066

Burcham, C.L., Florence, A.J., Johnson, M.D., 2018. Continuous Manufacturing in Pharmaceutical Process Development and Manufacturing. Annual Review of Chemical and Biomolecular Engineering 9, 253–281. https://doi.org/10.1146/annurev-chembioeng-060817-084355

Cogoni, G., 2021. A hybrid NIR-soft sensor method for real time in-process control during continuous direct compression manufacturing operations. International Journal of Pharmaceutics 10.

Dave, V.S., Saoji, S.D., Raut, N.A., Haware, R.V., 2015. Excipient Variability and Its Impact on Dosage Form Functionality. Journal of Pharmaceutical Sciences 104, 906–915. https://doi.org/10.1002/jps.24299

De Leersnyder, F., Peeters, E., Djalabi, H., Vanhoorne, V., Van Snick, B., Hong, K., Hammond, S., Liu, A.Y., Ziemons, E., Vervaet, C., De Beer, T., 2018. Development and validation of an in-line NIR spectroscopic method for continuous blend potency determination in

the feed frame of a tablet press. Journal of Pharmaceutical and Biomedical Analysis 151, 274–283. https://doi.org/10.1016/j.jpba.2018.01.032

Dun, J., Osei-Yeboah, F., Boulas, P., Lin, Y., Sun, C.C., 2020. A systematic evaluation of poloxamers as tablet lubricants. International Journal of Pharmaceutics 576, 118994. https://doi.org/10.1016/j.ijpharm.2019.118994

Engisch, W.E., Muzzio, F.J., 2015a. Feedrate deviations caused by hopper refill of loss-in-weight feeders. Powder Technology 283, 389–400. https://doi.org/10.1016/j.powtec.2015.06.001

Engisch, W.E., Muzzio, F.J., 2015b. Loss-in-Weight Feeding Trials Case Study: Pharmaceutical Formulation. Journal of Pharmaceutical Innovation 10, 56–75. https://doi.org/10.1007/s12247-014-9206-1

Engisch, W.E., Muzzio, F.J., 2012. Method for characterization of loss-in-weight feeder equipment. Powder Technology 228, 395–403. https://doi.org/10.1016/j.powtec.2012.05.058

Ervasti, T., 2015. Continuous manufacturing of extended release tablets via powder mixing and direct compression. International Journal of Pharmaceutics 12.

Escotet-Espinoza, M.S., Moghtadernejad, S., Scicolone, J., Wang, Y., Pereira, G., Schäfer, E., Vigh, T., Klingeleers, D., Ierapetritou, M., Muzzio, F.J., 2018a. Using a material property library to find surrogate materials for pharmaceutical process development. Powder Technology 339, 659–676. https://doi.org/10.1016/j.powtec.2018.08.042

Escotet-Espinoza, M.S., Vadodaria, S., Singh, R., Muzzio, F.J., Ierapetritou, M.G., 2018b. Modeling the effects of material properties on tablet compaction: A building block for controlling both batch and continuous pharmaceutical manufacturing processes. International Journal of Pharmaceutics 543, 274–287. https://doi.org/10.1016/j.ijpharm.2018.03.036

Fisher, A.C., 2022. An Audit of Pharmaceutical Continuous Manufacturing Regulatory Submissions and Outcomes in the US 25.

Fonteyne, M., Correia, A., De Plecker, S., Vercruysse, J., Ilić, I., Zhou, Q., Vervaet, C., Remon, J.P., Onofre, F., Bulone, V., De Beer, T., 2015. Impact of microcrystalline cellulose material attributes: A case study on continuous twin screw granulation. International Journal of Pharmaceutics 478, 705–717. https://doi.org/10.1016/j.ijpharm.2014.11.070

Fonteyne, M., Wickström, H., Peeters, E., Vercruysse, J., Ehlers, H., Peters, B.-H., Remon, J.P., Vervaet, C., Ketolainen, J., Sandler, N., Rantanen, J., Naelapää, K., Beer, T.D., 2014. Influence of raw material properties upon critical quality attributes of continuously produced granules and tablets. European Journal of Pharmaceutics and Biopharmaceutics 87, 252–263. https://doi.org/10.1016/j.ejpb.2014.02.011

Freeman, R., 2007. Measuring the flow properties of consolidated, conditioned and aerated powders — A comparative study using a powder rheometer and a rotational shear cell. Powder Technology 174, 25–33. https://doi.org/10.1016/j.powtec.2006.10.016

Freeman, R.E., Cooke, J.R., Schneider, L.C.R., 2009. Measuring shear properties and normal stresses generated within a rotational shear cell for consolidated and non-consolidated powders. Powder Technology 190, 65–69. https://doi.org/10.1016/j.powtec.2008.04.084

Freeman Technology, Instruction documents: W7008 Compressibility, 2007.

Freeman Technology, Instruction documents: W7012 Variable Flow Rate, 2007.

Freeman Technology, Instruction documents: W7013 Stability and Variable Flow Rate, 2007.

Freeman Technology, Instruction documents: W7018 Shear Cell, 2007.

Freeman Technology, Instruction documents: W7030 Basic Flowability Energy, 2007.

Freeman Technology, Instruction documents: W7050 1ml Shear Cell, 2007.

Furukawa, R., 2020. Effect of material properties on the residence time distribution (RTD) of a tablet press feed frame. International Journal of Pharmaceutics 10.

Gao, Y., Muzzio, F., Ierapetritou, M., 2011a. Characterization of feeder effects on continuous solid mixing using fourier series analysis. AIChE Journal 57, 1144–1153. https://doi.org/10.1002/aic.12348

Gao, Y., Vanarase, A., Muzzio, F., Ierapetritou, M., 2011b. Characterizing continuous powder mixing using residence time distribution. Chemical Engineering Science 66, 417–425. https://doi.org/10.1016/j.ces.2010.10.045

GEA Operating and Maintenance Manual for a "Modul P," 2018.

Goh, H.P., Heng, P.W.S., Liew, C.V., 2018. Comparative evaluation of powder flow parameters with reference to particle size and shape. International Journal of Pharmaceutics 547, 133–141. https://doi.org/10.1016/j.ijpharm.2018.05.059

Hagelstein, V., Gerhart, M., Wagner, K.G., 2018. Tricalcium citrate – a new brittle tableting excipient for direct compression and dry granulation with enormous hardness yield. Drug Development and Industrial Pharmacy 44, 1631–1641. https://doi.org/10.1080/03639045.2018.1483389

Hanson, J., 2018. Control of a system of loss-in-weight feeders for drug product continuous manufacturing. Powder Technology 331, 236–243. https://doi.org/10.1016/j.powtec.2018.03.027

Haware, R.V., Bauer-Brandl, A., Tho, I., 2010. Comparative evaluation of the powder and compression properties of various grades and brands of micr 12.

Hopkins, M., 2006. Loss in Weight Feeder Systems. Measurement and Control 39, 237–240. https://doi.org/10.1177/002029400603900801

Hsiao, W.-K., Hörmann, T.R., Toson, P., Paudel, A., Ghiotti, P., Stauffer, F., Bauer, F., Lakio, S., Behrend, O., Maurer, R., Holman, J., Khinast, J., 2020. Feeding of particle-based materials in continuous solid dosage manufacturing: a material science perspective. Drug Discovery Today 25, 800–806. https://doi.org/10.1016/j.drudis.2020.01.013

ICH, 2009. International Conference on Harmonisation of Technical Requirements for Registration of Pharmaceuticals for Human Use. ICH Harmonised Tripartite Guideline: Pharmaceutical Development Q8(R2). URL https://www.ich.org/page/quality-guidelines

Järvinen, M.A., Paaso, J., Paavola, M., Leiviskä, K., Juuti, M., Muzzio, F., Järvinen, K., 2013. Continuous direct tablet compression: effects of impeller rotation rate, total feed rate and drug content on the tablet properties and drug release. Drug Development and Industrial Pharmacy 39, 1802–1808. https://doi.org/10.3109/03639045.2012.738681

Johansson, M.E., 1984. Granular magnesium stearate as a lubricant in tablet formulations. International Journal of Pharmaceutics 21, 307–315. https://doi.org/10.1016/0378-5173(84)90189-3

Kamyar, R., 2021. Soft sensor for real-time estimation of tablet potency in continuous direct compression manufacturing operation. International Journal of Pharmaceutics 13.

Ketterhagen, W.R., Mullarney, M.P., Kresevic, J., Blackwood, D., 2018. Computational approaches to predict the effect of shear during processing of lubricated pharmaceutical blends. Powder Technology 335, 427–439. https://doi.org/10.1016/j.powtec.2018.05.023

Knight, P.., Seville, J.P.., Wellm, A.., Instone, T., 2001. Prediction of impeller torque in high shear powder mixers. Chemical Engineering Science 56, 4457–4471. https://doi.org/10.1016/S0009-2509(01)00114-2

Kushner, J., 2012. Incorporating Turbula mixers into a blending scale-up model for evaluating the effect of magnesium stearate on tablet tensile strength and bulk specific volume. International Journal of Pharmaceutics 429, 1–11. https://doi.org/10.1016/j.ijpharm.2012.02.040

Kushner, J., Moore, F., 2010. Scale-up model describing the impact of lubrication on tablet tensile strength. International Journal of Pharmaceutics 399, 19–30. https://doi.org/10.1016/j.ijpharm.2010.07.033

Kushner, J., Schlack, H., 2014. Commercial scale validation of a process scale-up model for lubricant blending of pharmaceutical powders. International Journal of Pharmaceutics 475, 147–155. https://doi.org/10.1016/j.ijpharm.2014.08.036

Landín, M., González, M.P., Souto, C., Concheiro, A., Gómez-Amoza, J.L., Martínez-Pacheco, R., 1993. Comparison of two Varieties of Microcrystalline Cellulose as Filler-Binders II. Hydrochlorothiazide Tablets. null 19, 1211–1220. https://doi.org/10.3109/03639049309063013

Lee, K.T., Kimber, J.A., Cogoni, G., Brandon, J.K., Wilsdon, D., Verrier, H.M., Grieb, S., Blackwood, D.O., Jain, A.C., Doshi, P., 2021. Continuous Mixing Technology: Characterization of a Vertical Mixer Using Residence Time Distribution. Journal of Pharmaceutical Sciences. https://doi.org/10.1016/j.xphs.2021.01.035

Lee, S.L., O'Connor, T.F., Yang, X., Cruz, C.N., Chatterjee, S., Madurawe, R.D., Moore, C.M.V., Yu, L.X., Woodcock, J., 2015. Modernizing Pharmaceutical Manufacturing: from Batch to Continuous Production. Journal of Pharmaceutical Innovation 10, 191–199. https://doi.org/10.1007/s12247-015-9215-8

Leuenberger, H., 2001. New trends in the production of pharmaceutical granules: batch versus continuous processing. European Journal of Pharmaceutics and Biopharmaceutics 52, 289–296. https://doi.org/10.1016/S0939-6411(01)00199-0

Llusa, M., Faulhammer, E., Biserni, S., Calzolari, V., Lawrence, S., Bresciani, M., Khinast, J., 2014. The effects of powder compressibility, speed of capsule filling and pre-compression on plug densification. International Journal of Pharmaceutics 471, 182–188. https://doi.org/10.1016/j.ijpharm.2014.04.073

Louw, R., 2003. Evaluation and comparison of magnesium stearate and sodium stearyl fumarate (Pruv) as lubricants in directly compressible tablet formulations : their effect on tablet properties and drug dissolution (Master Thesis). North-West University, Potchefstroom Campus.

Madian, A., Leturia, M., Ablitzer, C., Matheron, P., Bernard-Granger, G., Saleh, K., 2020. Impact of fine particles on the rheological properties of uranium dioxide powders. Nuclear Engineering and Technology 52, 1714–1723. https://doi.org/10.1016/j.net.2020.01.012

Mangal, S., Gengenbach, T., Millington-Smith, D., Armstrong, B., Morton, D.A.V., Larson, I., 2016. Relationship between the cohesion of guest particles on the flow behaviour of interactive mixtures. European Journal of Pharmaceutics and Biopharmaceutics 102, 168–177. https://doi.org/10.1016/j.ejpb.2016.03.012

Marikh, K., Berthiaux, H., Gatumel, C., Mizonov, V., Barantseva, E., 2008. Influence of stirrer type on mixture homogeneity in continuous powder mixing: A model case and a pharmaceutical case. Chemical Engineering Research and Design 86, 1027–1037. https://doi.org/10.1016/j.cherd.2008.04.001

Megarry, A.J., 2019. A big data approach to pharmaceutical flow properties. International Journal of Pharmaceutics 9.

Mehrotra, A., Llusa, M., Faqih, A., Levin, M., Muzzio, F.J., 2007. Influence of shear intensity and total shear on properties of blends and tablets of lactose and cellulose lubricated with magnesium stearate. International Journal of Pharmaceutics 336, 284–291. https://doi.org/10.1016/j.ijpharm.2006.12.013

Meier, R., Thommes, M., Rasenack, N., 2016. Granule size distributions after twin-screw granulation – Do not forget the feeding systems. European Journal of Pharmaceutics and Biopharmaceutics 11.

Michalson, E.T., 2007. High potency active pharmaceutical ingredients. chimica oggi 25, 4.

Moghtadernejad, S., Escotet-Espinoza, M.S., Oka, S., Singh, R., Liu, Z., Román-Ospino, A.D., Li, T., Razavi, S., Panikar, S., Scicolone, J., Callegari, G., Hausner, D., Muzzio, F., 2018. A Training on: Continuous Manufacturing (Direct Compaction) of Solid Dose Pharmaceutical Products. Journal of Pharmaceutical Innovation 13, 155–187. https://doi.org/10.1007/s12247-018-9313-5

Morin, G., Briens, L., 2013. The Effect of Lubricants on Powder Flowability for Pharmaceutical Application. AAPS PharmSciTech 14, 1158–1168. https://doi.org/10.1208/s12249-013-0007-5

Mukaka, M.M., 2012. Statistics Corner: A guide to appropriate use of Correlation coefficient in medical research 3.

Nowak, S., 2016. Three ways to improve continuous loss-in-weight feeding accuracy 4.

Osorio, J.G., Muzzio, F.J., 2013. Effects of powder flow properties on capsule filling weight uniformity. Drug Development and Industrial Pharmacy 39, 1464–1475. https://doi.org/10.3109/03639045.2012.728227

Peeters, E., 2014. Investigation of the tableting process in continuous production: Influence of feeding and extended dwell time during compression on dependent process variables and tablet properties. Ghent Univeristy, Ghent.

Peeters, M., Peeters, E., Van Hauwermeiren, D., Cogoni, G., Liu, A.Y., De Beer, T., 2021. Determination and understanding of lead-lag between in-line NIR tablet press feed frame and off-line NIR tablet measurements. Submitted to International Journal of Pharmaceutics.

Pitt, K.G., Newton, J.M., Stanley, P., 1988. Tensile fracture of doubly-convex cylindrical discs under diametral loading. Journal of Materials Science 23, 2723–2728. https://doi.org/10.1007/BF00547442

Portillo, P.M., Ierapetritou, M.G., Muzzio, F.J., 2008. Characterization of continuous convective powder mixing processes. Powder Technology 182, 368–378. https://doi.org/10.1016/j.powtec.2007.06.024

Razavi, S.M., Gonzalez, M., Cuitiño, A.M., 2018. Quantification of lubrication and particle size distribution effects on tensile strength and stiffness of tablets. Powder Technology 336, 360–374. https://doi.org/10.1016/j.powtec.2018.06.001

Roggo, Y., Pauli, V., Jelsch, M., Pellegatti, L., Elbaz, F., Ensslin, S., Kleinebudde, P., Krumme, M., 2020. Continuous manufacturing process monitoring of pharmaceutical solid dosage form: A case study. Journal of Pharmaceutical and Biomedical Analysis 179, 112971. https://doi.org/10.1016/j.jpba.2019.112971

Santana, H.H.S., Maier, G., Ródenas, J., 2011. Flowability analysis of uranium dioxide powder at different temperatures containing different lubricants. Applied Radiation and Isotopes 69, 1162–1164. https://doi.org/10.1016/j.apradiso.2010.10.017

Shah, N.H., Stiel, D., Weiss, M., Infeld, M.H., Malick, A.W., 1986. Evaluation of Two New Tablet Lubricants -Sodium Stearyl Fumarate and Glyceryl Behenate. Measurement 19.

Shotton, E., Ganderton, D., 2011. The Strength of Compressed Tablets: Part I. The Measurement of Tablet Strength and its Relation to Compression Forces. Journal of Pharmacy and Pharmacology 12, 87T-92T. https://doi.org/10.1111/j.2042-7158.1960.tb10458.x

Sierra-Vega, N.O., Román-Ospino, A., Scicolone, J., Muzzio, F.J., Romañach, R.J., Méndez, R., 2019. Assessment of blend uniformity in a continuous tablet manufacturing process. International Journal of Pharmaceutics 560, 322–333. https://doi.org/10.1016/j.ijpharm.2019.01.073

Snick, B.V., 2017a. Continuous direct compression as manufacturing platform for sustained release tablets. International Journal of Pharmaceutics 18.

Snick, B.V., 2017b. Development of a continuous direct compression platform for low-dose drug products. International Journal of Pharmaceutics 18.

Stauffer, F., Vanhoorne, V., Pilcer, G., Chavez, P.-F., Rome, S., Schubert, M.A., Aerts, L., De Beer, T., 2018. Raw material variability of an active pharmaceutical ingredient and its relevance for processability in secondary continuous pharmaceutical manufacturing. European Journal of Pharmaceutics and Biopharmaceutics 127, 92–103. https://doi.org/10.1016/j.ejpb.2018.02.017

Sun, C., Grant, D.J.., 2001. Effects of initial particle size on the tableting properties of l-lysine monohydrochloride dihydrate powder. International Journal of Pharmaceutics 215, 221–228. https://doi.org/10.1016/S0378-5173(00)00701-8

Swaminathan, V., Kildsig, D.O., 2002. Effect of magnesium stearate on the content uniformity of active ingredient in pharmaceutical powder mixtures 5.

Tahir, F., Palmer, J., Khoo, J., Holman, J., Yadav, I.K., Reynolds, G., Meehan, E., Mitchell, A., Bajwa, G., 2020. Development of feed factor prediction models for loss-in-weight powder feeders. Powder Technology 364, 1025–1038. https://doi.org/10.1016/j.powtec.2019.09.071

Toson, P., Siegmann, E., Trogrlic, M., Kureck, H., Khinast, J., Jajcevic, D., Doshi, P., Blackwood, D., Bonnassieux, A., Daugherity, P.D., am Ende, M.T., 2018. Detailed modeling and process design of an advanced continuous powder mixer. International Journal of Pharmaceutics 552, 288–300. https://doi.org/10.1016/j.ijpharm.2018.09.032

Uzondu, B., Leung, L.Y., Mao, C., Yang, C.-Y., 2018. A mechanistic study on tablet ejection force and its sensitivity to lubrication for pharmaceutical powders. International Journal of Pharmaceutics 543, 234–244. https://doi.org/10.1016/j.ijpharm.2018.03.064

Van Hauwermeiren, D., Peeters, M., Peeters, E., Cogoni, G., Liu, A.Y., De Beer, T., 2021. Development of a tablet press feed frame lead lag determination model using in-line and off-line NIR measurements. Submitted to Computers and Chemical Engineering.

Vanarase, A.U., Alcalà, M., Jerez Rozo, J.I., Muzzio, F.J., Romañach, R.J., 2010. Real-time monitoring of drug concentration in a continuous powder mixing process using NIR spectroscopy. Chemical Engineering Science 65, 5728–5733. https://doi.org/10.1016/j.ces.2010.01.036

Wang, J., Wen, H., Desai, D., 2010. Lubrication in tablet formulations. European Journal of Pharmaceutics and Biopharmaceutics 75, 1–15. https://doi.org/10.1016/j.ejpb.2010.01.007

Wang, W., Lu, Y., 2018. Analysis of the Mean Absolute Error (MAE) and the Root Mean Square Error (RMSE) in Assessing Rounding Model 11.

Wang, Y., Koynov, S., Glasser, B.J., Muzzio, F.J., 2016. A method to analyze shear cell data of powders measured under different initial consolidation stresses. Powder Technology 294, 105–112. https://doi.org/10.1016/j.powtec.2016.02.027

Wang, Y., Li, T., Muzzio, F.J., Glasser, B.J., 2017. Predicting feeder performance based on material flow properties. Powder Technology 308, 135–148. https://doi.org/10.1016/j.powtec.2016.12.010

Xie, X., Puri, V.M., 2006. Uniformity of Powder Die Filling Using a Feed Shoe: A Review. Particulate Science and Technology 24, 411–426. https://doi.org/10.1080/02726350600934663

Yadav, I.K., Holman, J., Meehan, E., Tahir, F., Khoo, J., Taylor, J., Benedetti, A., Aderinto, O., Bajwa, G., 2019. Influence of material properties and equipment configuration on loss-in-weight feeder performance for drug product continuous manufacture. Powder Technology 348, 126–137. https://doi.org/10.1016/j.powtec.2019.01.071

Zegzulka, J., 2020. Characterization and flowability methods for metal powders. Scientific Reports 19.

A Appendix

A.1 Chapter 6

A.1.1 Material Attributes of the Blends

Table A 1 Material attributes of MCC-SiO_2 mixtures obtained by the compressibility method using the FT4.

Blend No.	CBD [g/ml]	Compressibility at 15 kPa [%]
1	0.372 ± 0.008	8.33 ± 0.39
2	0.384 ± 0.011	6.70 ± 0.78
3	0.386 ± 0.008	6.89 ± 0.37
4	0.385 ± 0.008	6.62 ± 0.04
5	0.394 ± 0.014	5.95 ± 0.61
6	0.382 ± 0.004	6.31 ± 0.11
7	0.374 ± 0.003	6.94 ± 0.05
8	0.367 ± 0.005	7.66 ± 0.09
9	0.391 ± 0.006	6.50 ± 0.26
10	0.392 ± 0.003	5.74 ± 0.12
11	0.381 ± 0.004	6.67 ± 0.34
12	0.376 ± 0.001	7.26 ± 0.04

A.1.2 Y_M, Y_0 and k Obtained by MODDE

A.1.2.1 Fit Statistics: Y_M

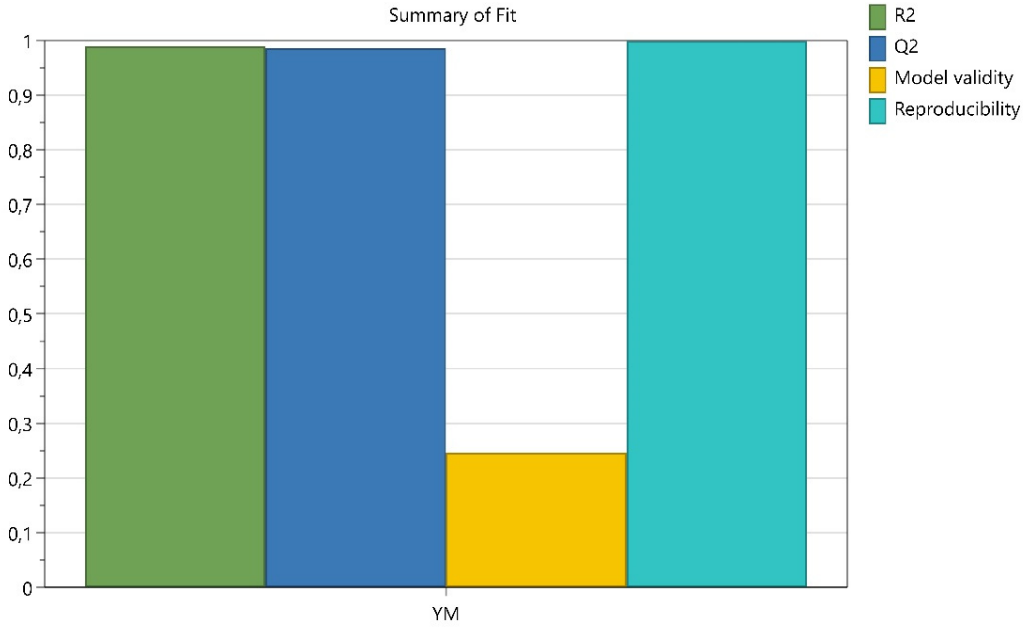

Figure A 1 Y_M - Summary of Fit.

According to MODDE the model validity can be low in very good models (Q^2 >0.9).

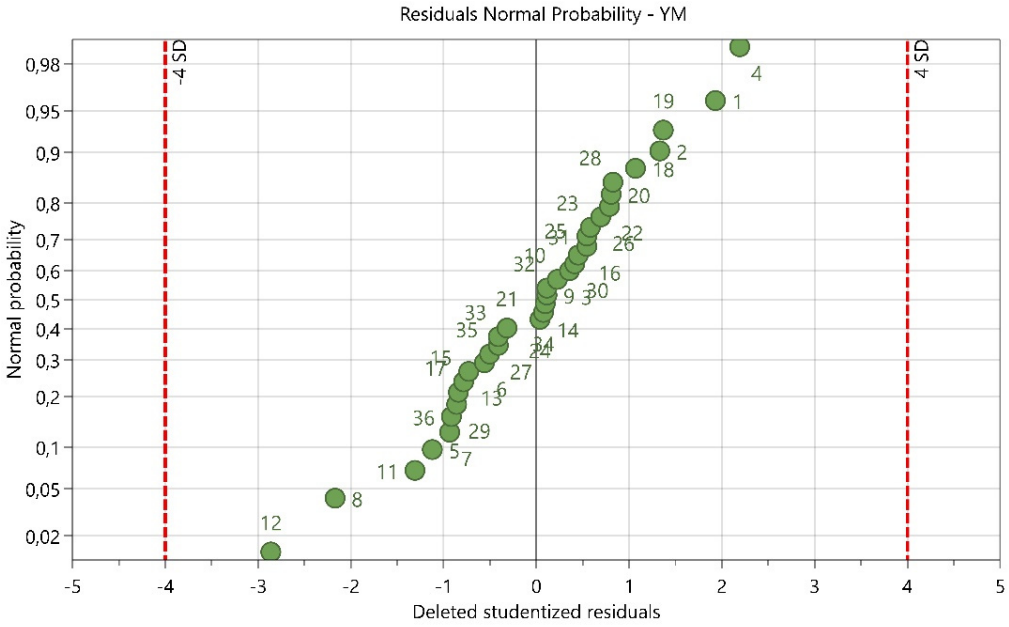

Figure A 2 Y_M - Residuals Normal Probability.

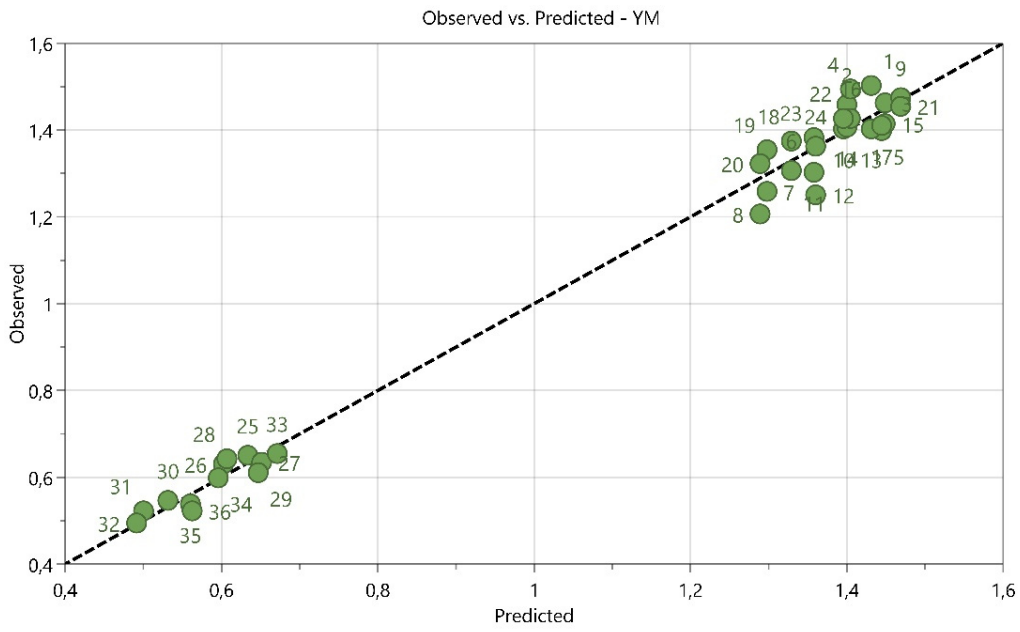

Figure A 3 Y_M - Observed vs. predicted.

A.1.2.2 **Fit Statistics: Y_0**

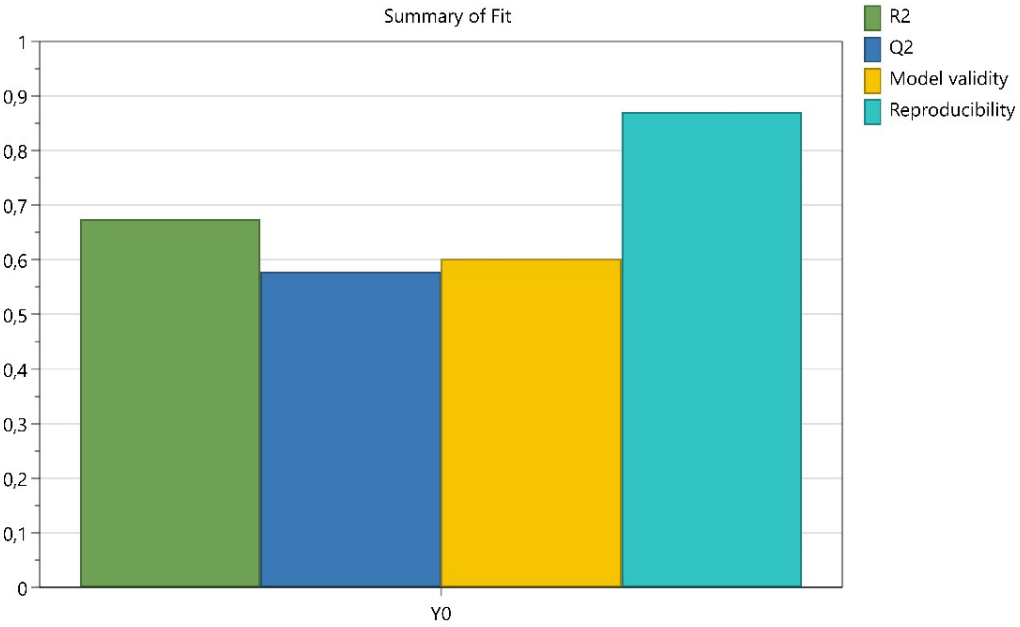

Figure A 4 Y_0 - Summary of Fit.

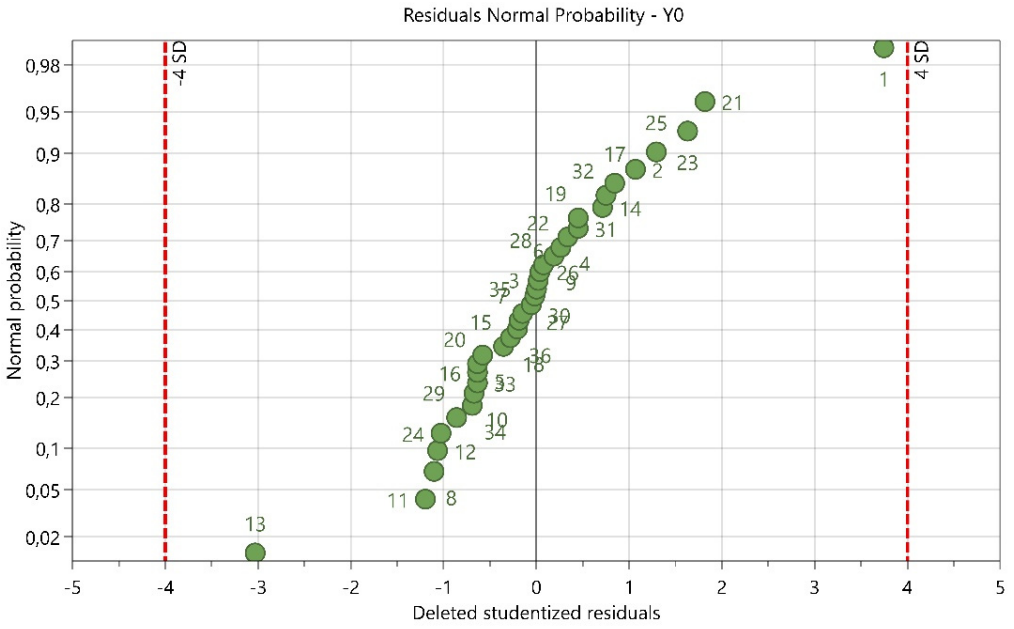

Figure A 5 Y_0 - Residuals Normal Probability.

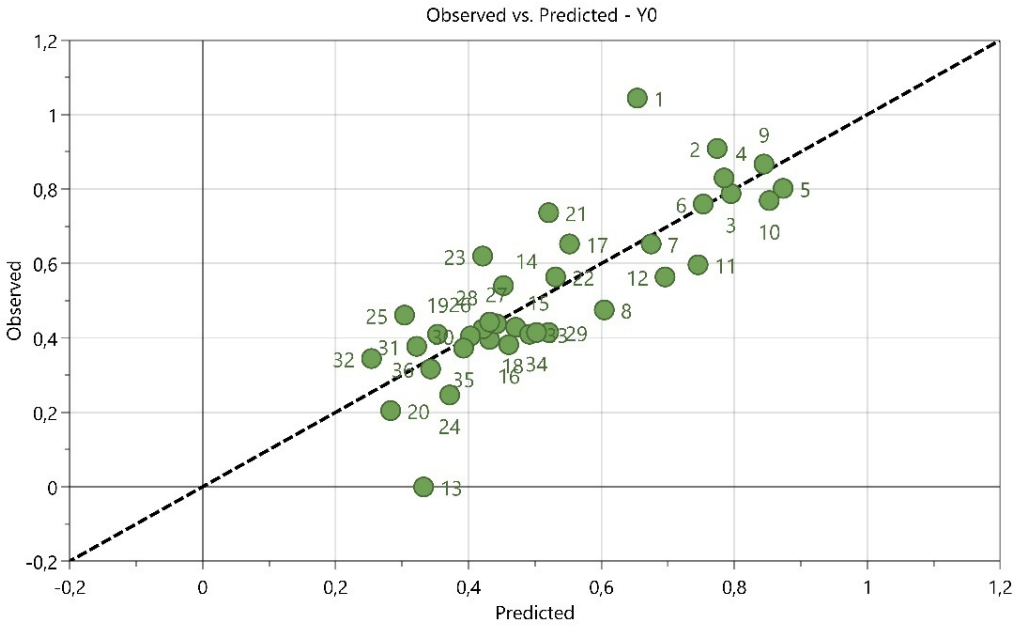

Figure A 6 Y_0 - Observed vs. Predicted.

A.1.2.3 **Fit Statistics: k**

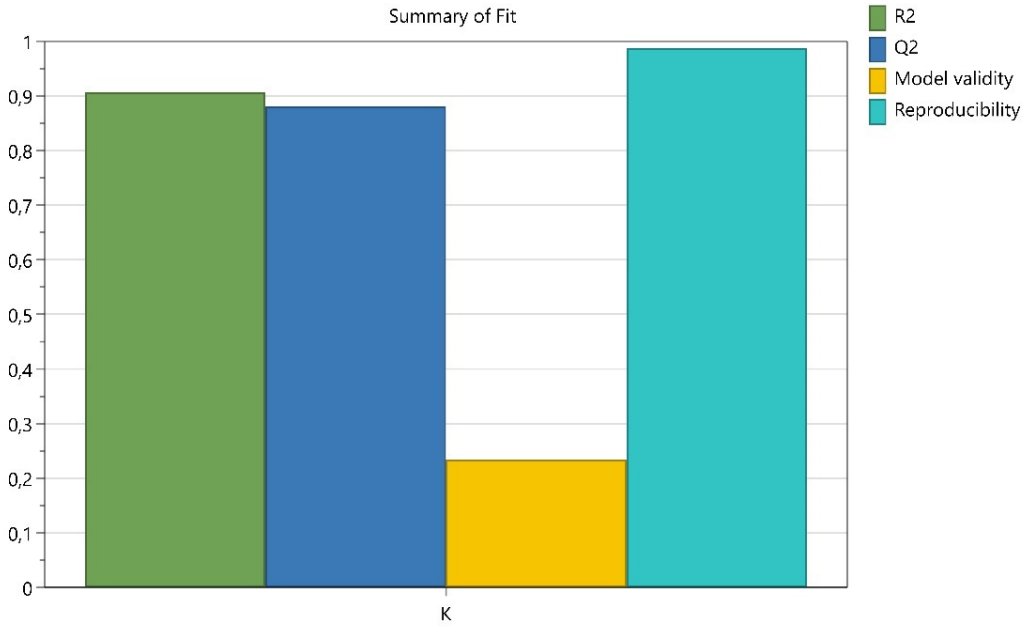

Figure A 7 k - Summary of Fit.

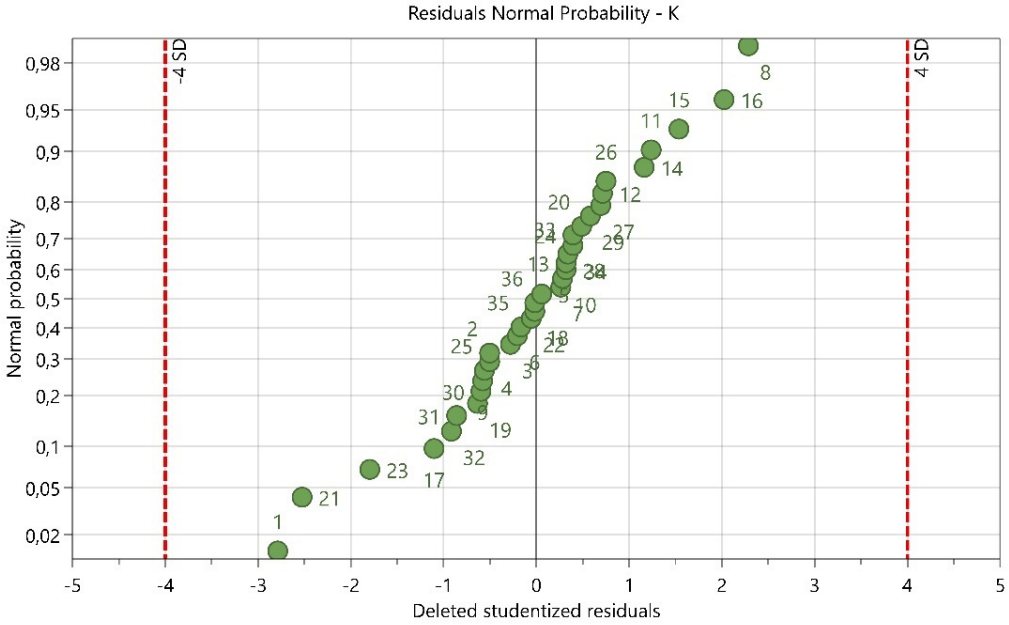

Figure A 8 k - Residuals Normal Probability

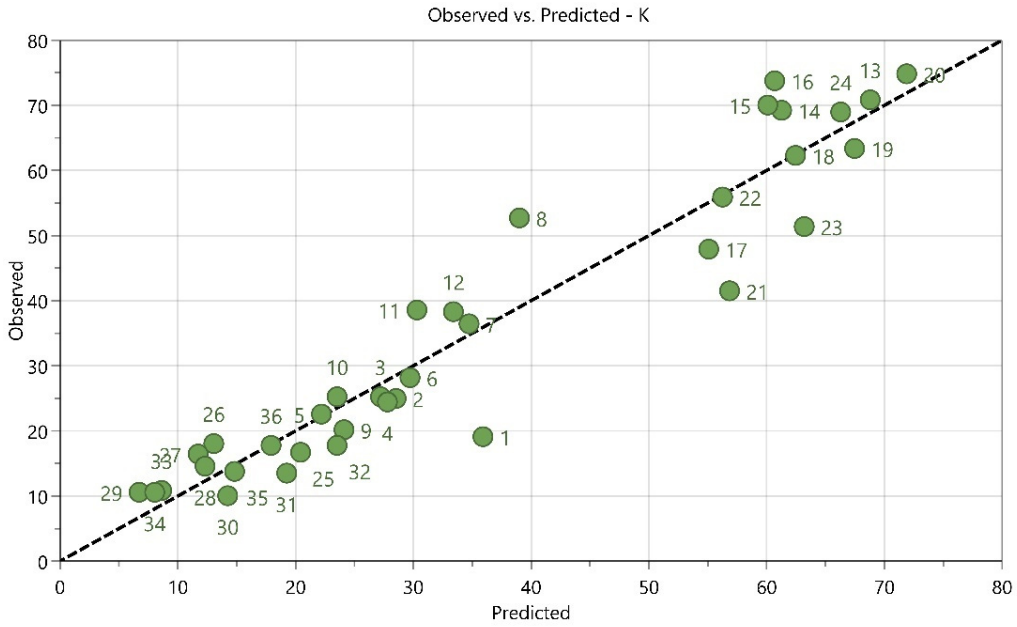

Figure A 9 k - Observed vs. Predicted.

A.1.3 Overview of Feed Factor Predictions at 20 mm Screw Pitches

a. 5 kg/h

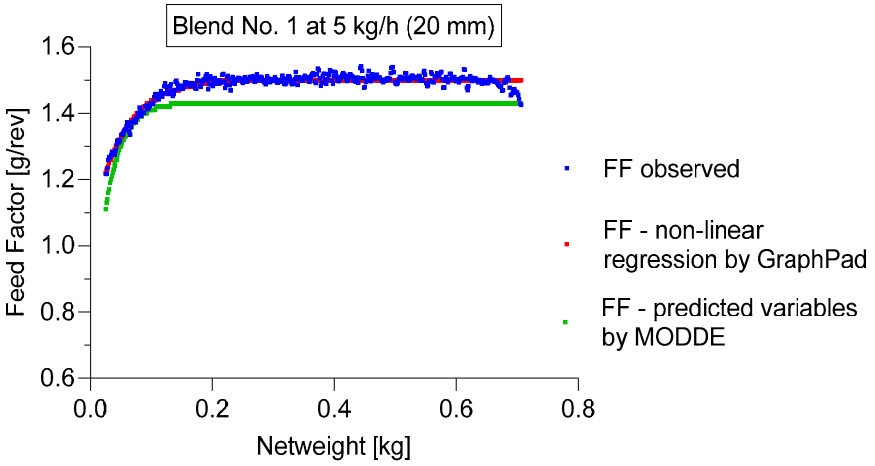

Figure A 10 Blend 1 at 5 kg/h and 20 mm ScP.

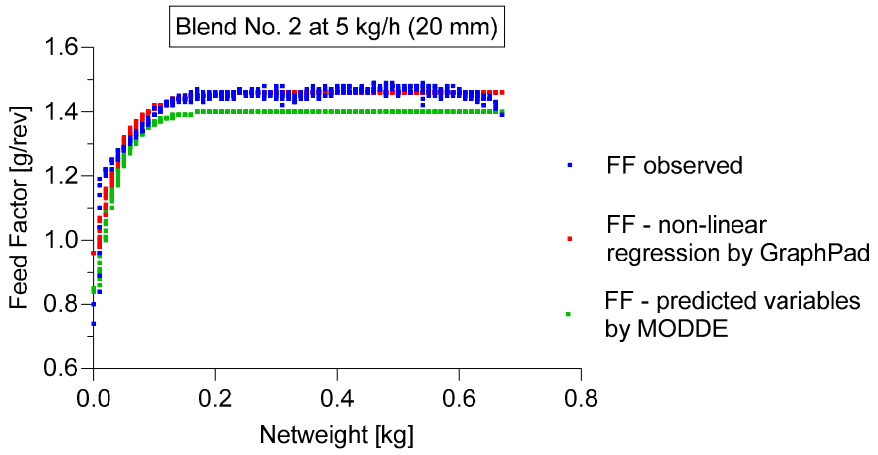

Figure A 11 Blend 2 at 5 kg/h and 20 mm ScP.

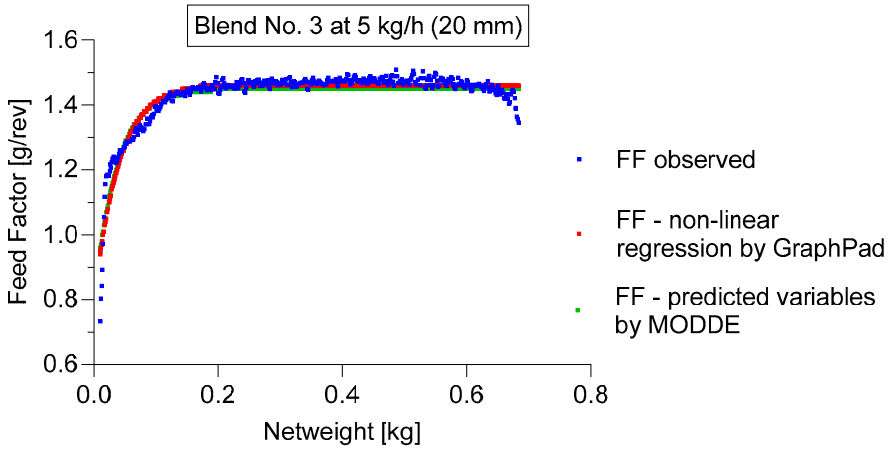

Figure A 12 Blend 3 at 5 kg/h and 20 mm ScP.

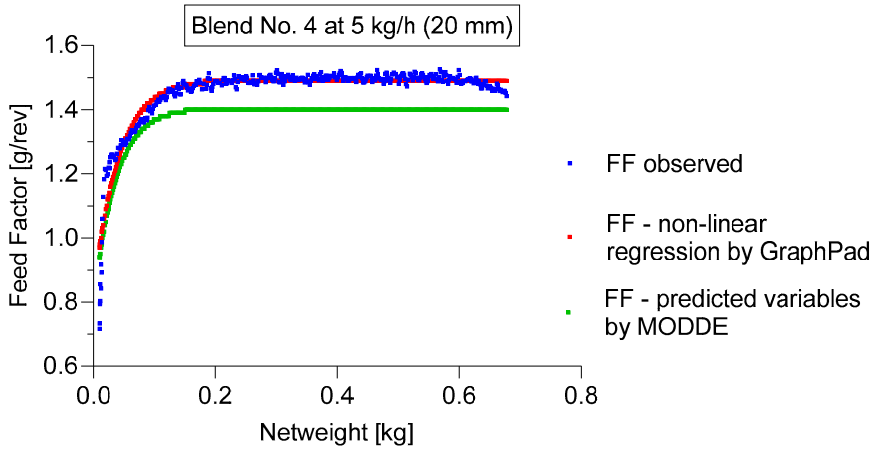

Figure A 13 Blend 4 at 5 kg/h and 20 mm ScP.

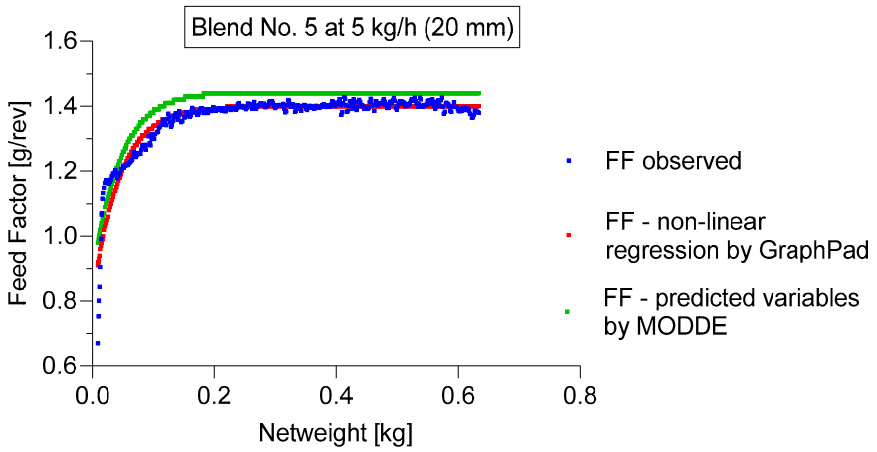

Figure A 14 Blend 5 at 5 kg/h and 20 mm ScP.

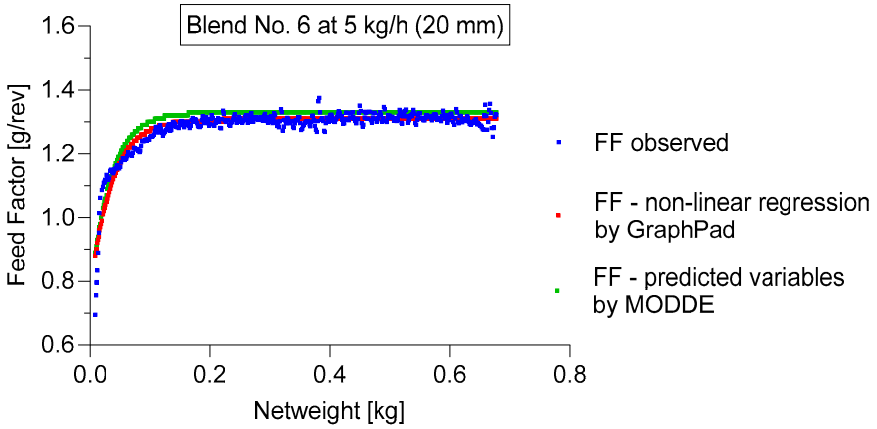

Figure A 15 Blend 6 at 5 kg/h and 20 mm ScP.

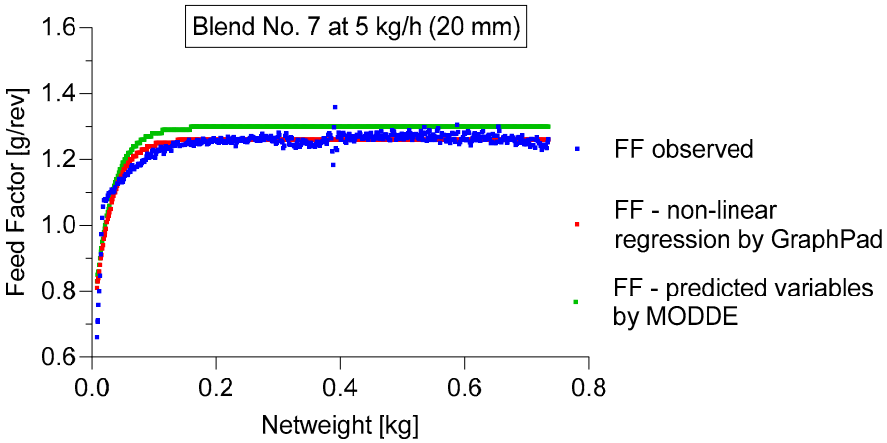

Figure A 16 Blend 7 at 5 kg/h and 20 mm ScP.

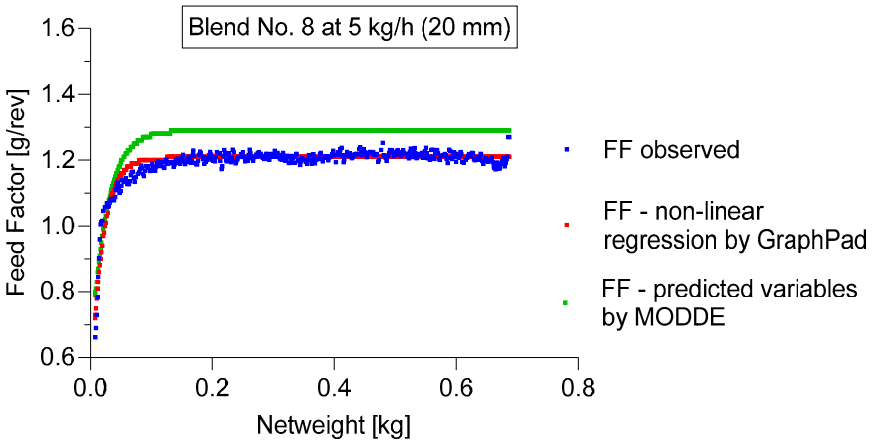

Figure A 17 Blend 8 at 5 kg/h and 20 mm ScP.

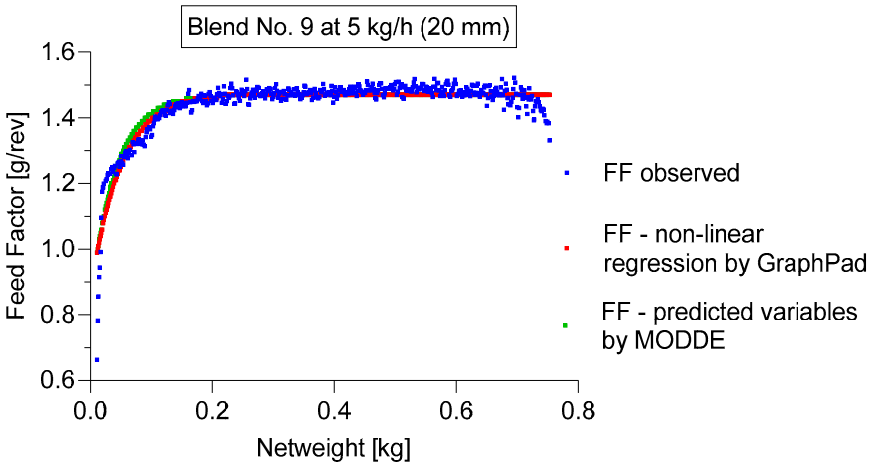

Figure A 18 Blend 9 at 5 kg/h and 20 mm ScP.

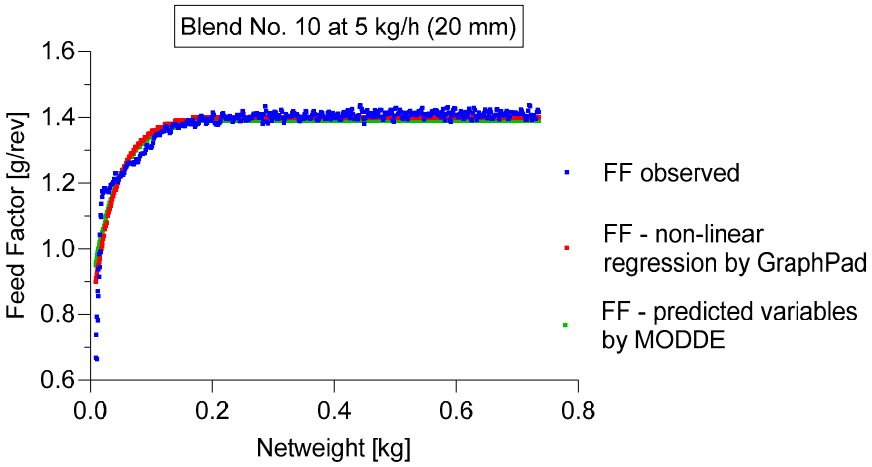

Figure A 19 Blend 10 at 5 kg/h and 20 mm ScP.

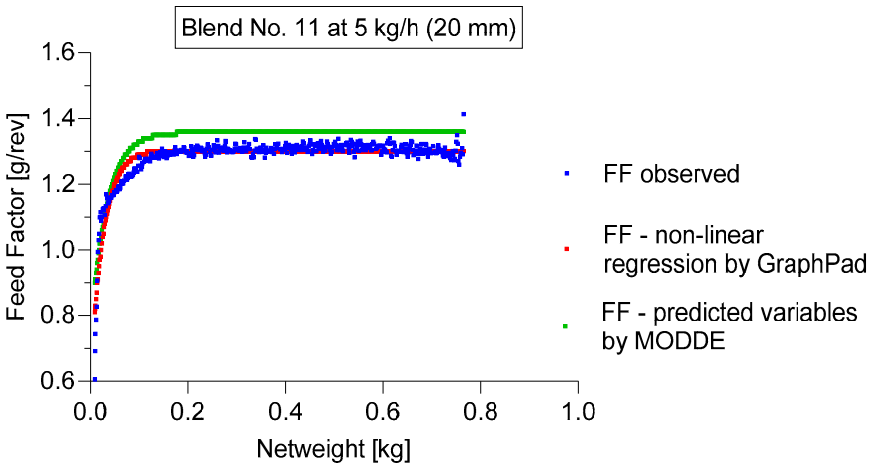

Figure A 20 Blend 11 at 5 kg/h and 20 mm ScP.

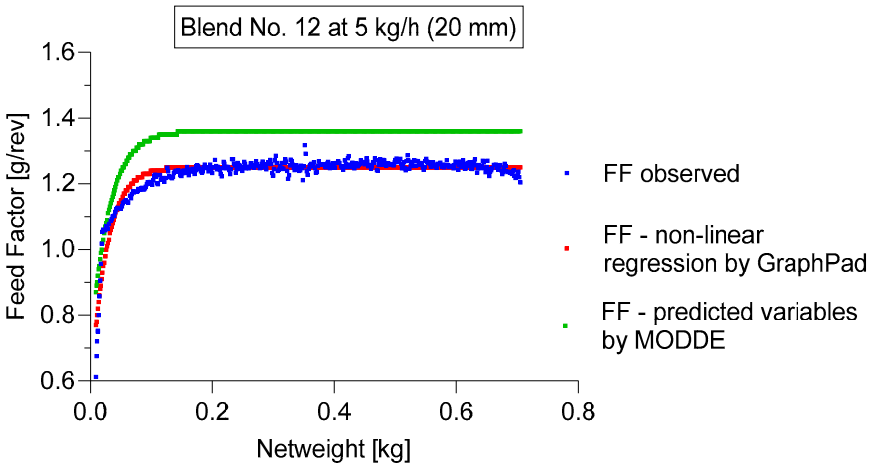

Figure A 21 Blend 12 at 5 kg/h and 20 mm ScP.

b. 10 kg/h

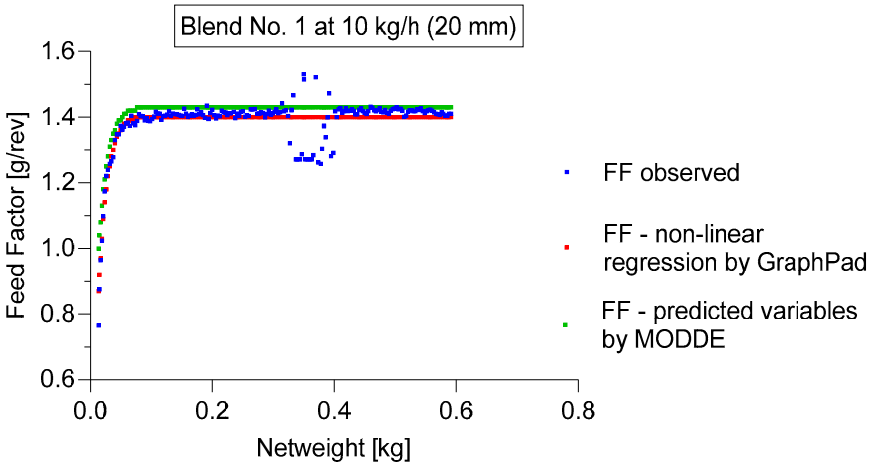

Figure A 22 Blend 1 at 10 kg/h and 20 mm ScP.

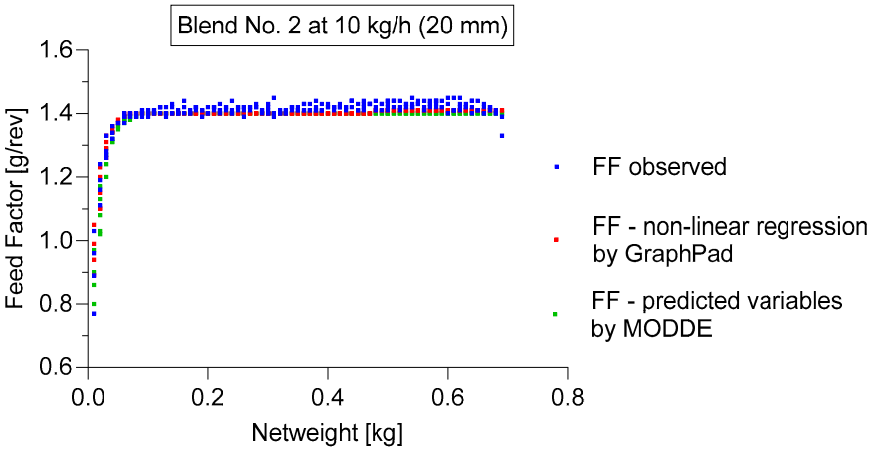

Figure A 23 Blend 2 at 10 kg/h and 20 mm ScP.

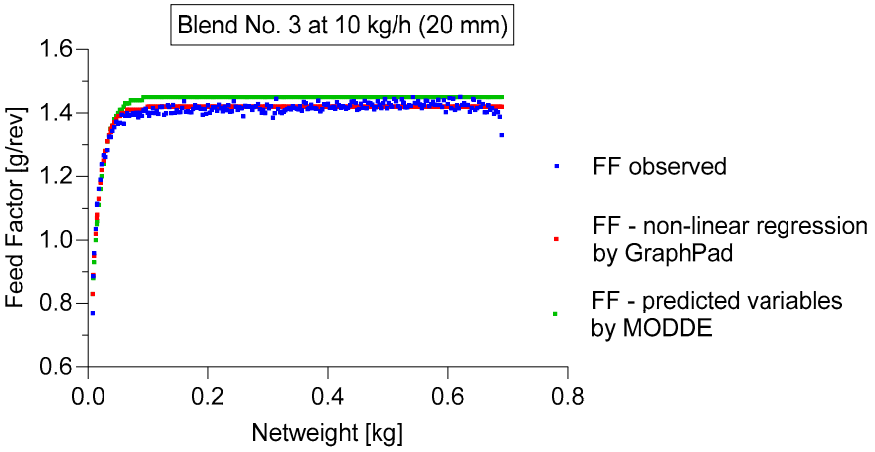

Figure A 24 Blend 3 at 10 kg/h and 20 mm ScP.

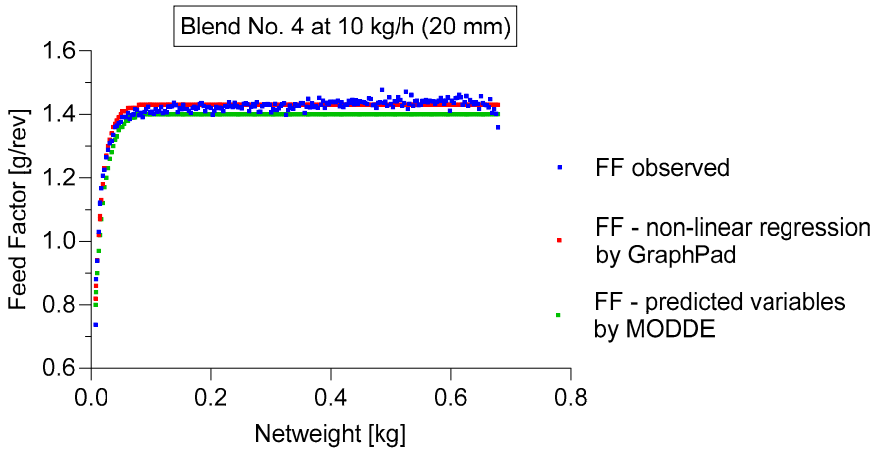

Figure A 25 Blend 4 at 10 kg/h and 20 mm ScP.

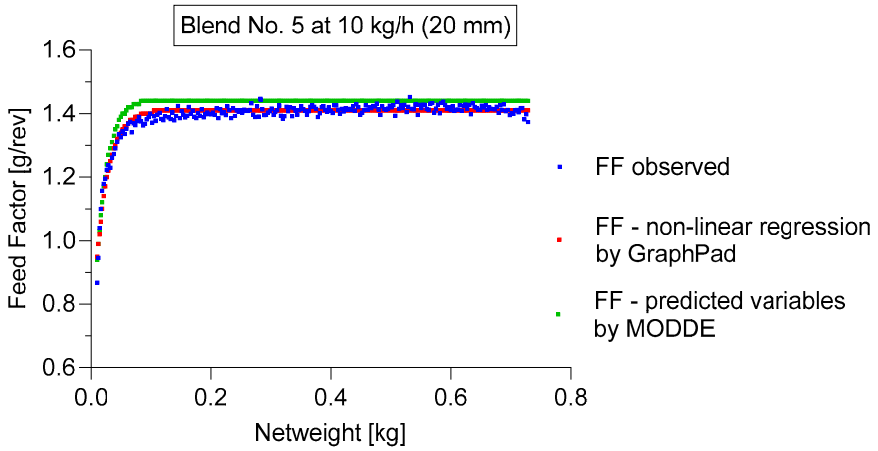

Figure A 26 Blend 5 at 10 kg/h and 20 mm ScP.

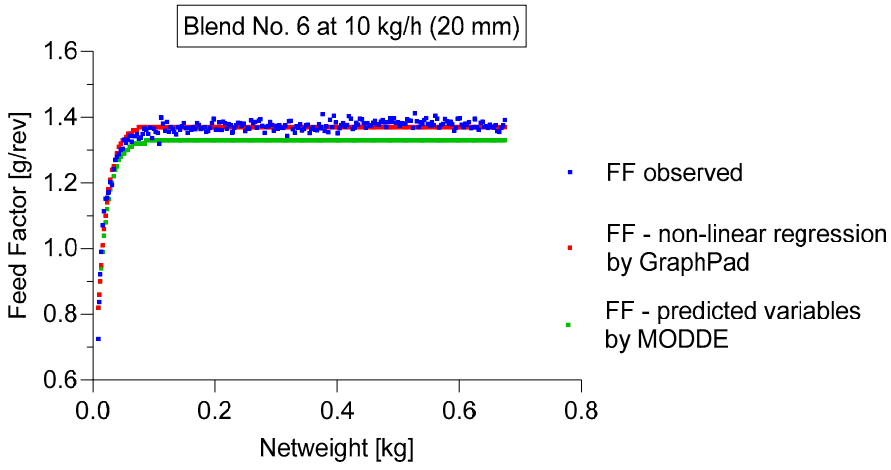

Figure A 27 Blend 6 at 10 kg/h and 20 mm ScP.

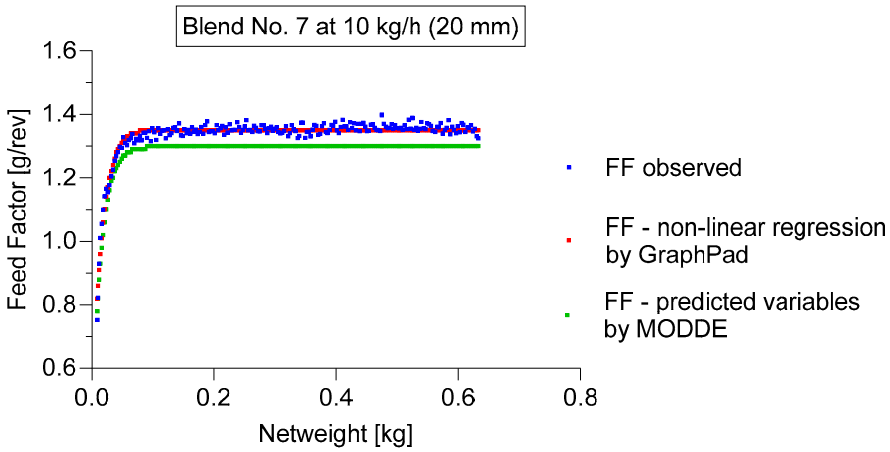

Figure A 28 Blend 7 at 10 kg/h and 20 mm ScP.

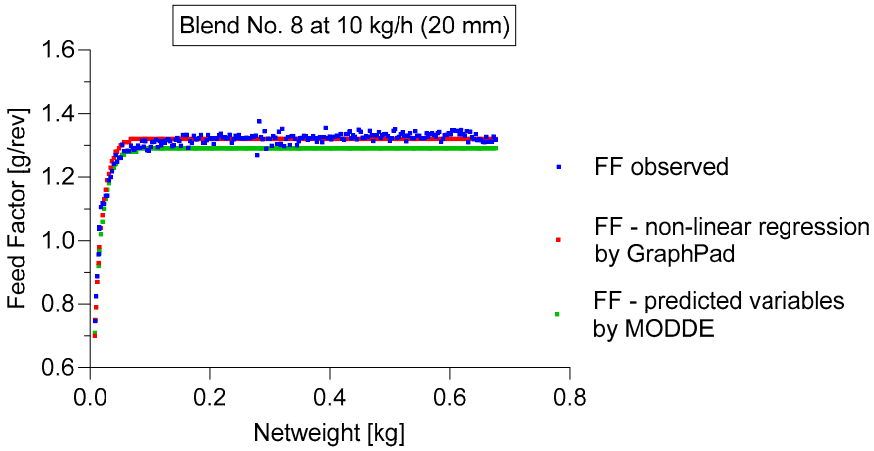

Figure A 29 Blend 8 at 10 kg/h and 20 mm ScP.

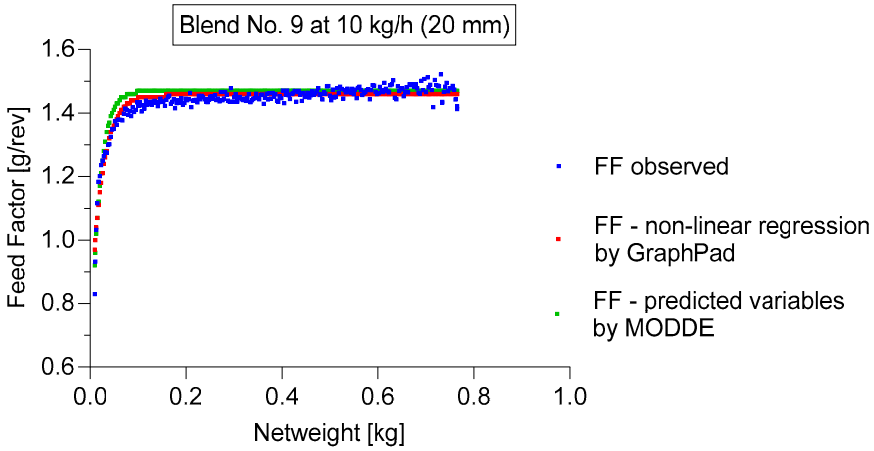

Figure A 30 Blend 9 at 10 kg/h and 20 mm ScP.

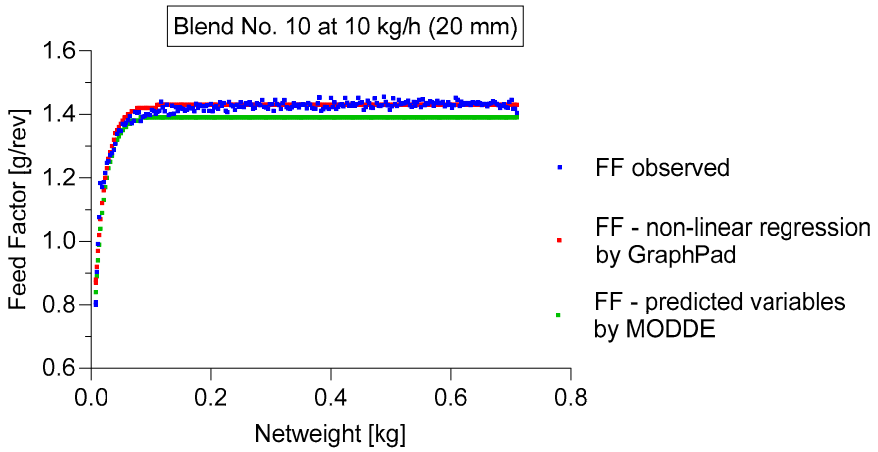

Figure A 31 Blend 10 at 10 kg/h and 20 mm ScP.

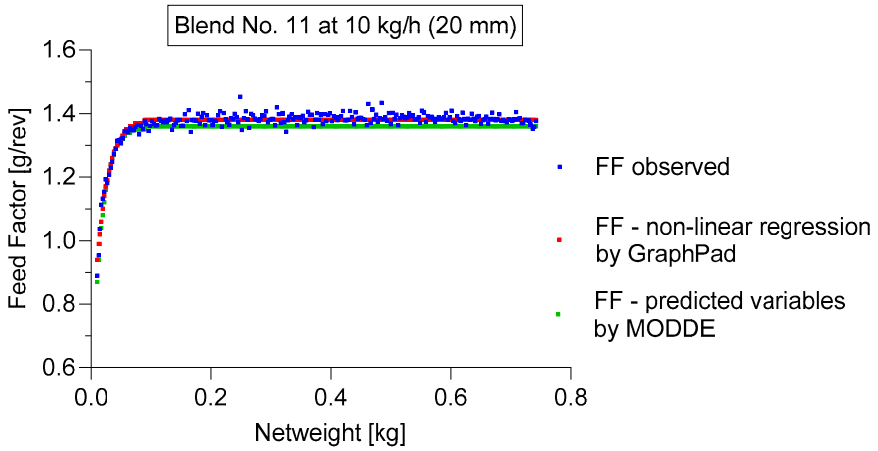

Figure A 32 Blend 11 at 10 kg/h and 20 mm ScP.

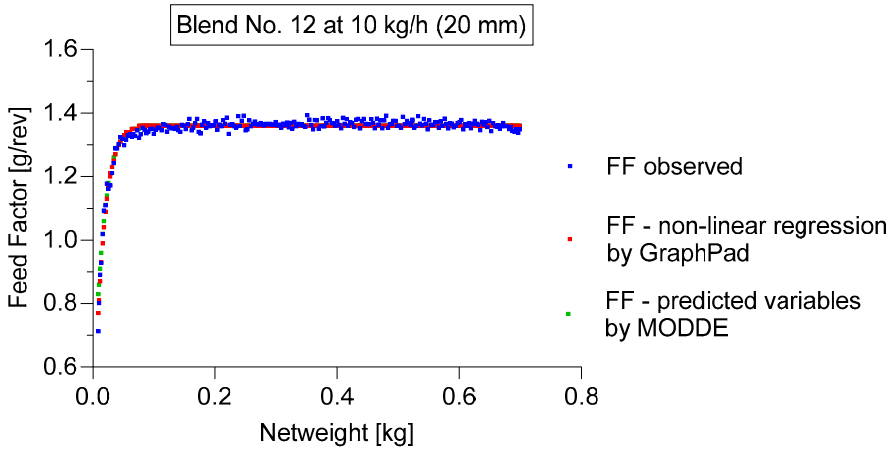

Figure A 33 Blend 12 at 10 kg/h and 20 mm ScP.

A.1.4 **Overview of Feed Factor Predictions at 10 mm Screw Pitches**

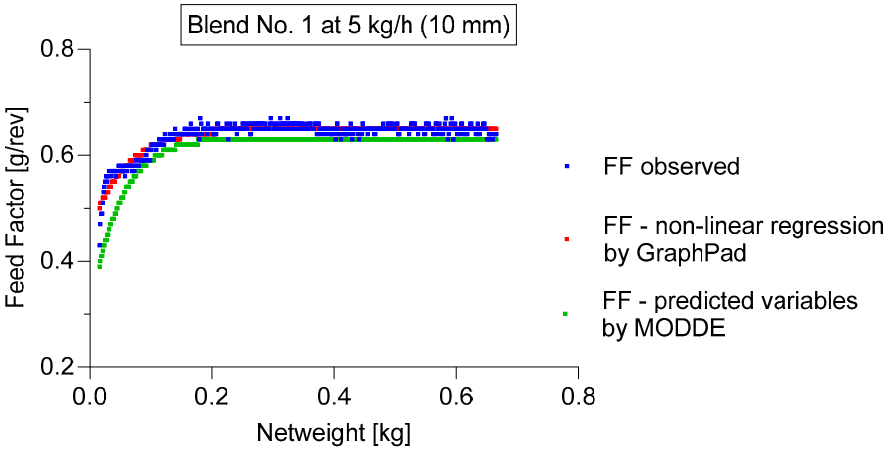

Figure A 34 Blend 1 at 5 kg/h and 10 mm ScP.

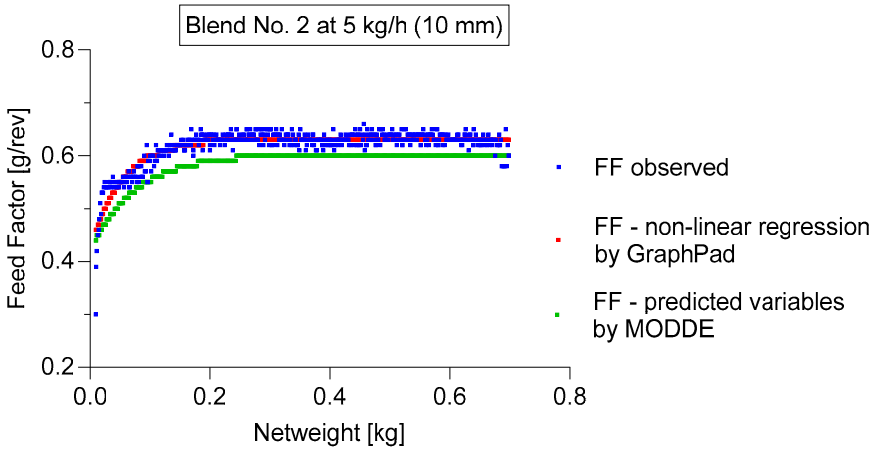

Figure A 35 Blend 2 at 5 kg/h and 10 mm ScP.

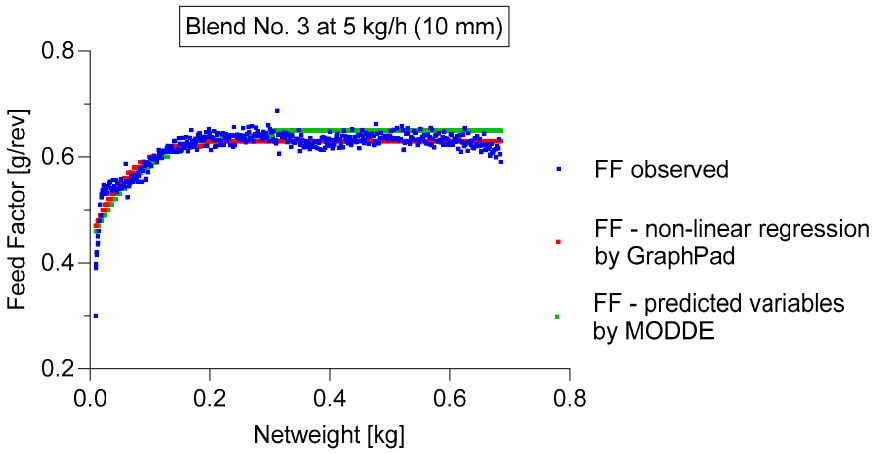

Figure A 36 Blend 3 at 5 kg/h and 10 mm ScP.

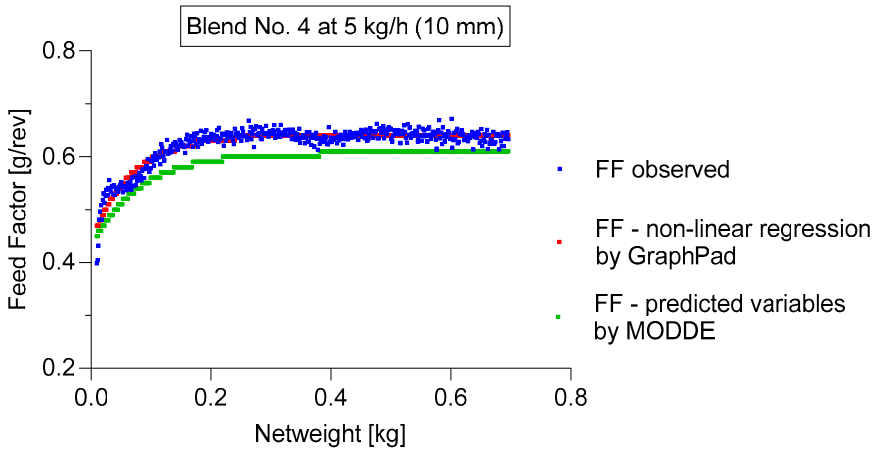

Figure A 37 Blend 4 at 5 kg/h and 10 mm ScP.

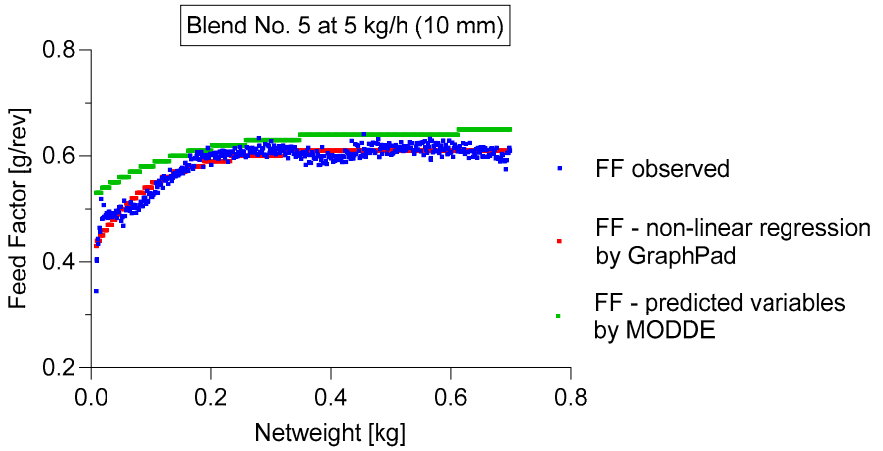

Figure A 38 Blend 5 at 5 kg/h and 10 mm ScP.

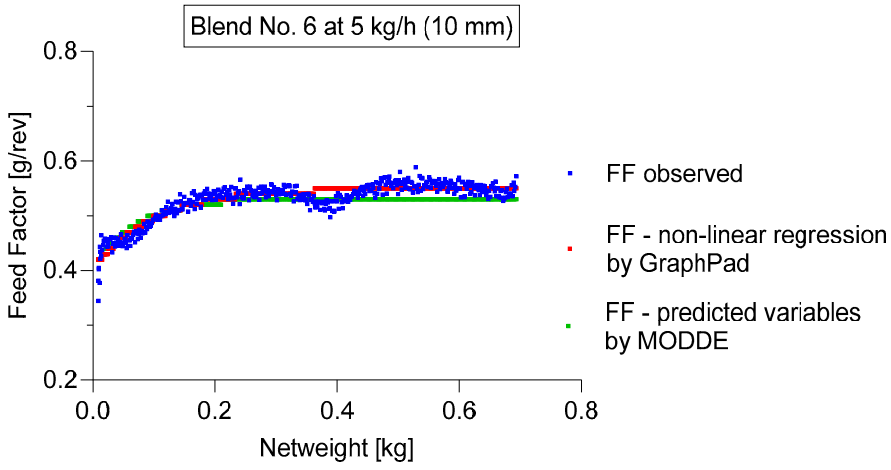

Figure A 39 Blend 6 at 5 kg/h and 10 mm ScP.

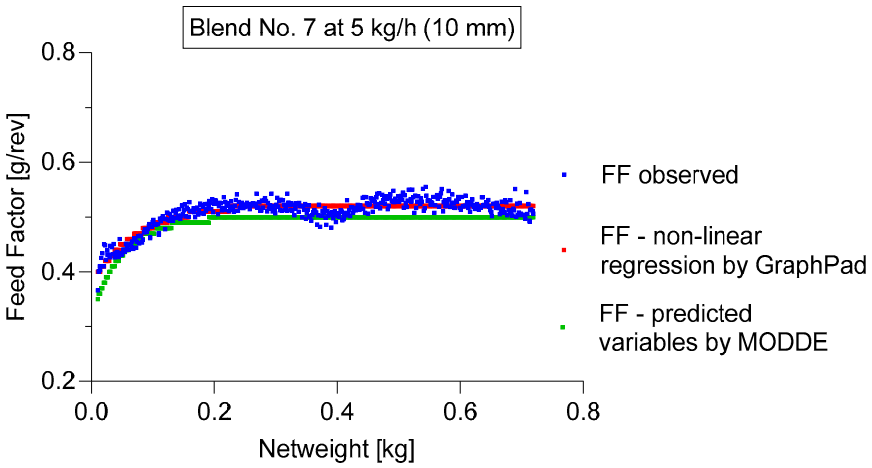

Figure A 40 Blend 7 at 5 kg/h and 10 mm ScP.

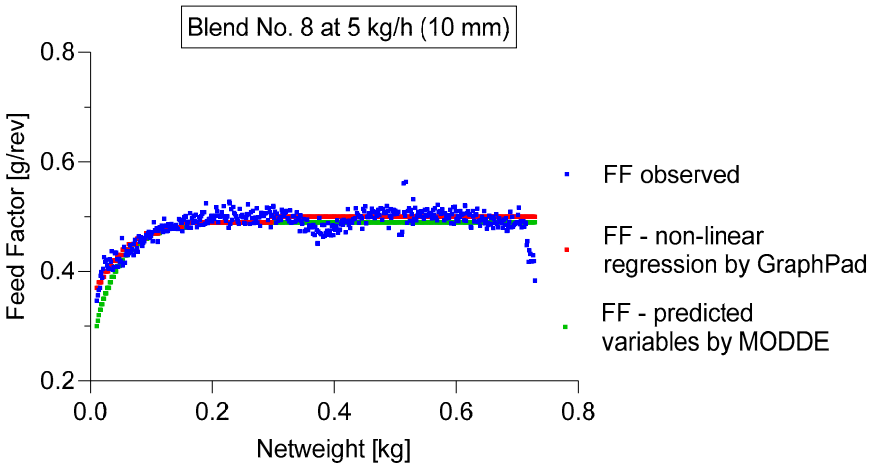

Figure A 41 Blend 8 at 5 kg/h and 10 mm ScP.

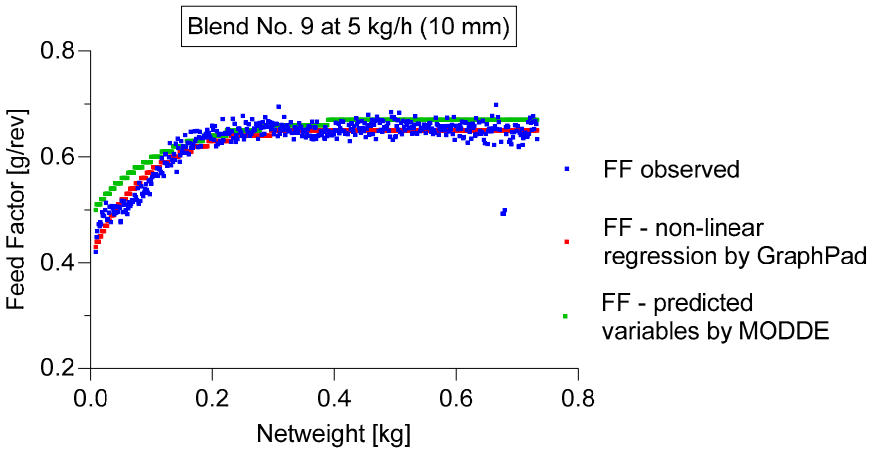

Figure A 42 Blend 9 at 5 kg/h and 10 mm ScP.

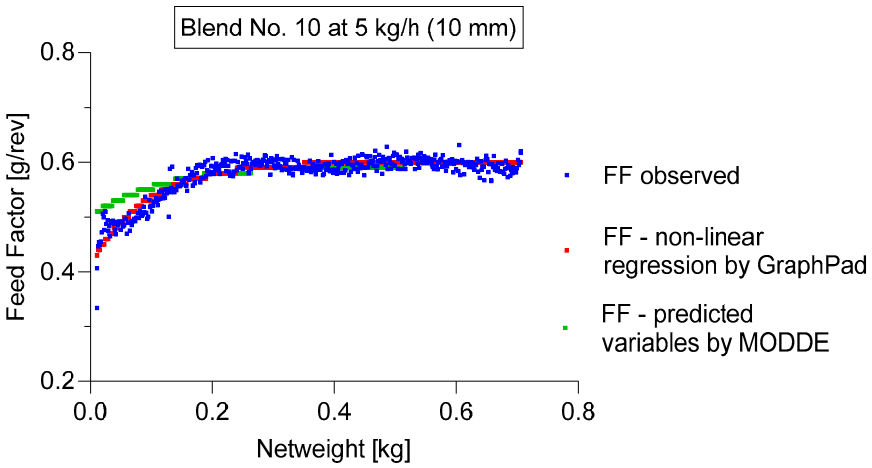

Figure A 43 Blend 10 at 5 kg/h and 10 mm ScP.

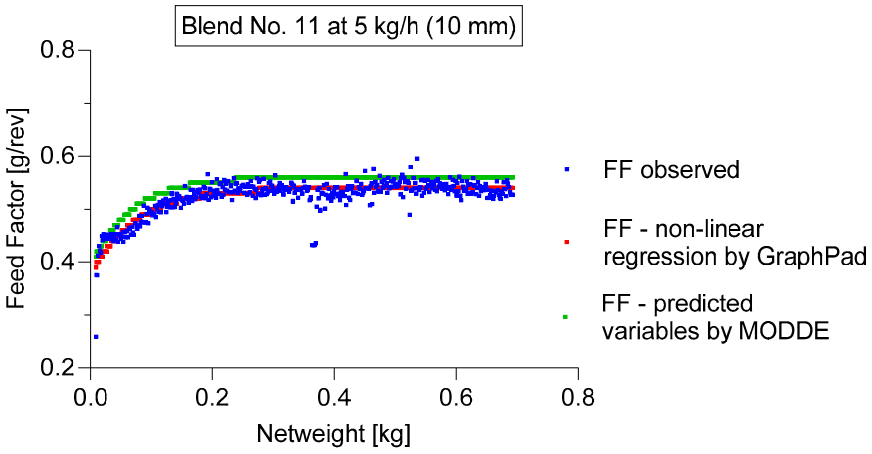

Figure A 44 Blend 11 at 5 kg/h and 10 mm ScP.

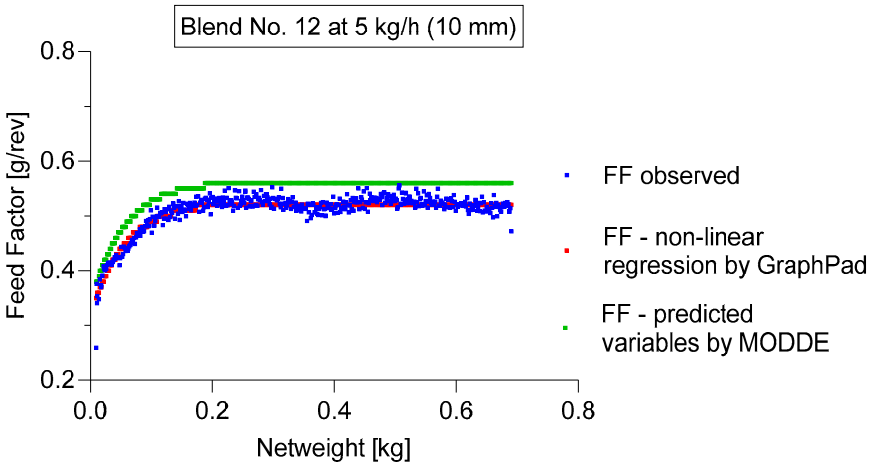

Figure A 45 Blend 12 at 5 kg/h and 10 mm ScP.

A.2 **Chapter 7**

A.2.1 **Ejection Force**

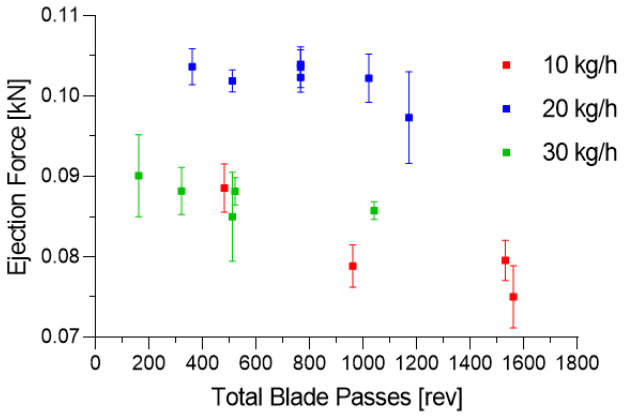

Figure A 46 Ejection force as function of TBP.

Regarding TBP and ejection force, curiously, the values at 20 kg/h were higher than at 10 and 30 kg/h. Considered individually, the correlation between TBP and the values at 20 kg/h are not significant (-0,658 p=0,108). Contrary, values at 10 kg/h and 30 kg/h combined showed a highly significant and strong correlation (-0.911 p=0.0002), where higher TBP and higher lubrication respectively resulted in lower ejection forces. Why only the data at 20 kg/h were higher could not be explained by the available data. The same phenomena could be observed at ejection force in dependency of particle size (d_{10}), where only data regarding 10 kg/h & 30 kg/h showed a correlation (-0.789 p=0.007).[20 kg/h (0,313 p=0,494)]

The influence of particle size on ejection force can be traced back again on the lubrication described previously.

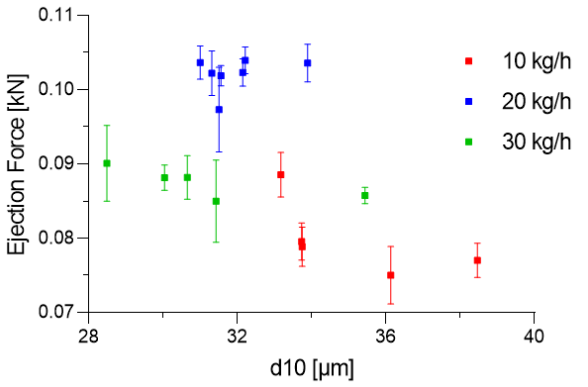

Figure A 47 Ejection force as function of particle size (d_{10}).

A.2.2 **Correlation Matrix**

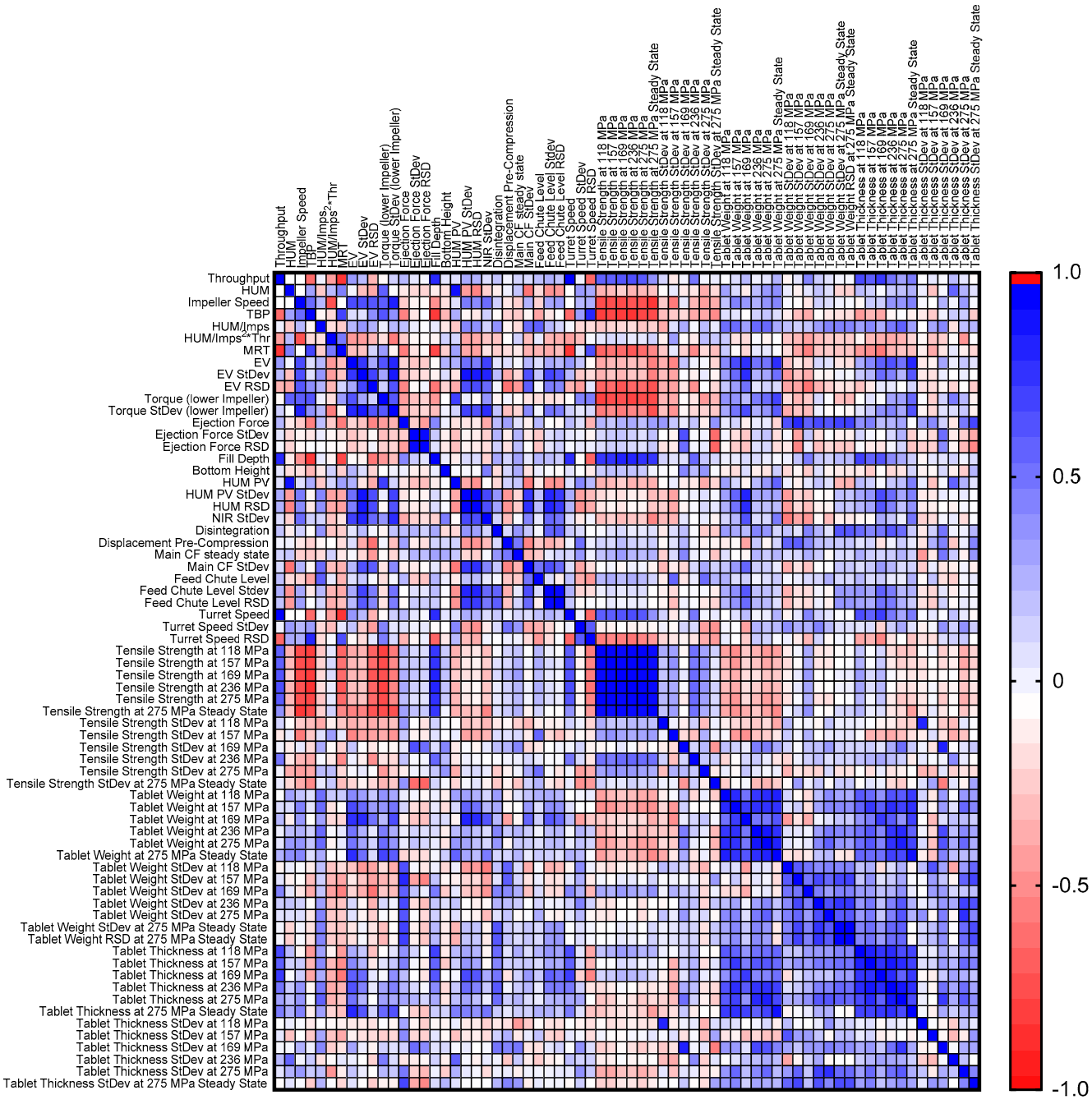

Figure A 48 Correlation matrix of the input parameters and responses considered in this chapter.

A.3 **Chapter 10**

A.3.1 **Model Settings Regarding EV, CBD and FD**

Table A 2 Model settings to assess the CBD, EV and FD based on THR, IMP, HUM and CBD_i.

Experiment No.	**THR [kg/h]**	**IMP [rpm]**	**HUM [g]**	**CBDi [g/ml]**
1	30	550	800	0.472
2	30	550	800	0.500
3	10	200	800	0.472
4	10	550	800	0.472
5	30	200	800	0.472
6	10	200	800	0.486
7	10	550	800	0.486
8	20	375	800	0.486
9	30	200	800	0.486
10	20	375	800	0.486
11	30	550	800	0.486
12	20	375	800	0.486
13	10	200	800	0.500
14	10	550	800	0.500
15	30	200	800	0.500
16	20	375	800	0.477
17	20	375	800	0.512
18	20	375	800	0.521
19	10	200	400	0.557
20	10	650	400	0.557
21	10	425	600	0.557
22	10	200	800	0.557
23	10	650	800	0.557
24	20	425	400	0.557
25	20	425	600	0.557
26	20	200	600	0.557
27	20	425	600	0.557
28	20	425	800	0.557
29	20	425	600	0.557
30	20	650	600	0.557
31	30	200	400	0.557
32	30	650	400	0.557
33	30	425	600	0.557
34	30	650	800	0.557
35	30	200	800	0.557

A.3.2 **Model Settings Regarding TS**

Table A 3 Model settings to assess the TS based on THR, IMP, HUM, CBD_i and CP.

Experiment No.	THR [kg/h]	IMP [rpm]	HUM [g]	CBDi [g/ml]	CP [MPa]
1	30	550	800	0.472	275
2	30	550	800	0.500	275
3	10	200	800	0.472	275
4	10	550	800	0.472	275
5	30	200	800	0.472	275
6	10	200	800	0.486	275
7	10	550	800	0.486	275
8	20	375	800	0.486	275
9	30	200	800	0.486	275
10	20	375	800	0.486	275
11	30	550	800	0.486	275
12	20	375	800	0.486	275
13	10	200	800	0.500	275
14	10	550	800	0.500	275
15	30	200	800	0.500	275
16	20	375	800	0.477	275
17	20	375	800	0.512	275
18	20	375	800	0.521	275
19	10	200	400	0.557	275
20	10	650	400	0.557	275
21	10	425	600	0.557	275
22	10	200	800	0.557	275
23	10	650	800	0.557	275
24	20	425	400	0.557	275
25	20	425	600	0.557	275
26	20	200	600	0.557	275
27	20	425	600	0.557	275
28	20	425	800	0.557	275
29	20	425	600	0.557	275
30	20	650	600	0.557	275
31	30	200	400	0.557	275
32	30	650	400	0.557	275
33	30	425	600	0.557	275
34	30	650	800	0.557	275
35	30	200	800	0.557	275
36	10	200	400	0.557	275
37	10	650	400	0.557	275

38	10	425	600	0.557	275
39	10	200	800	0.557	275
40	10	650	800	0.557	275
41	20	425	400	0.557	275
42	20	425	600	0.557	275
43	20	200	600	0.557	275
44	20	425	600	0.557	275
45	20	425	800	0.557	275
46	20	425	600	0.557	275
47	20	650	600	0.557	275
48	30	200	400	0.557	275
49	30	650	400	0.557	275
50	30	425	600	0.557	275
51	30	200	800	0.557	275
52	10	200	400	0.557	118
53	10	650	400	0.557	118
54	10	425	600	0.557	118
55	10	200	800	0.557	118
56	10	650	800	0.557	118
57	20	425	400	0.557	118
58	20	425	600	0.557	118
59	20	200	600	0.557	118
60	20	425	600	0.557	118
61	20	425	800	0.557	118
62	20	425	600	0.557	118
63	20	650	600	0.557	118
64	30	200	400	0.557	118
65	30	650	400	0.557	118
66	30	425	600	0.557	118
67	30	200	800	0.557	118
68	10	200	400	0.557	157
69	10	650	400	0.557	157
70	10	425	600	0.557	157
71	10	200	800	0.557	157
72	10	650	800	0.557	157
73	20	425	400	0.557	157
74	20	425	600	0.557	157
75	20	200	600	0.557	157
76	20	425	600	0.557	157
77	20	425	800	0.557	157
78	20	425	600	0.557	157
79	20	650	600	0.557	157

80	30	200	400	0.557	157
81	30	650	400	0.557	157
82	30	425	600	0.557	157
83	30	200	800	0.557	157
84	10	200	400	0.557	169
85	10	650	400	0.557	169
86	10	425	600	0.557	169
87	10	200	800	0.557	169
88	10	650	800	0.557	169
89	20	425	400	0.557	169
90	20	425	600	0.557	169
91	20	200	600	0.557	169
92	20	425	600	0.557	169
93	20	425	800	0.557	169
94	20	425	600	0.557	169
95	20	650	600	0.557	169
96	30	200	400	0.557	169
97	30	650	400	0.557	169
98	30	425	600	0.557	169
99	30	200	800	0.557	169
100	10	200	400	0.557	236
101	10	650	400	0.557	236
102	10	425	600	0.557	236
103	10	200	800	0.557	236
104	10	650	800	0.557	236
105	20	425	400	0.557	236
106	20	425	600	0.557	236
107	20	200	600	0.557	236
108	20	425	600	0.557	236
109	20	425	800	0.557	236
110	20	425	600	0.557	236
111	20	650	600	0.557	236
112	30	200	400	0.557	236
113	30	650	400	0.557	236
114	30	425	600	0.557	236
115	30	200	800	0.557	236